THE EFFECT OF DETACHMENT SLIDING ON SURFACE WASH EROSION IN THE CONTINUOUS PERMAFROST ZONE, HOT WEATHER CREEK, FOSHEIM PENINSULA, ELLESMERE ISLAND, N.W.T.

by

© Steve Kokelj

A thesis submitted in conformity with the requirements
for the degree of Master of Arts
Graduate Department of Geography
University of Ottawa

0-612-36709-6

Abstract

An experimental design was developed to evaluate the effect of active-layer detachment sliding on surface wash erosion. Specifically, the aim was to examine to what extent the disturbance of vegetation cover, changes in hydrological conditions due to topographic modification by detachment sliding and the formation of a fresh active layer affect rates of surface wash erosion.

Detachment slides generally accumulated more snow than adjacent slopes and yielded greater amounts of surface runoff than vegetated slopes with similar snow covers. Surface drainage was inhibited on well-vegetated hummocky slopes where lags between radiation inputs and discharge responses were greater than at the rilled detachment slide plots. During rainfall events following snowmelt, plot response was affected by antecedent moisture conditions and the vegetation cover: surface flow was generated only in detachment slide scars and at the mixed plots but not on vegetated undisturbed slopes or on the bare undisturbed slope.

Suspended sediment concentrations at the fresh detachment slide scars are two orders of magnitude greater than on vegetated slopes. At disturbed slopes suspended sediment removal exceeds solute erosion by over one order of magnitude. The highest solute concentrations (> 12700 mg/L) were measured at the fresh detachment slide scar in marine sediments. Soil solute concentrations in the fresh active layer were two orders of magnitude greater than on adjacent undisturbed slopes. The removal of the active layer allows the underlying permafrost to thaw in subsequent years. New flow paths over and through this soil develop, and if in marine deposits, salts which have been held in place by freezing, can be released.

Greater amounts of surface runoff production at fresh scars and the removal of vegetation result in high rates of surface erosion and high sediment yields (1560 g/m^2) at fresh detachment slide scars. Abiotic conditions at the scar (rapid removal of meltwater, high rates of erosion, elevated salt concentrations in fresh active layers if sliding occurs in marine sediments) may inhibit recolonization by plants, prolonging high rates of suspended sediment erosion. Elevated amounts of suspended sediment erosion at the pre-1950 scars (>260 g/m^2) suggest that detachment sliding affects surface wash erosion rates for years to decades.

Acknowledgments

Several people and organizations deserve thanks as without them the completion of this thesis would not have been possible.

First and foremost, I would like to thank my supervisor and friend Dr. Antoni Lewkowicz for taking me on as a graduate student and introducing me to the field of permafrost research. His support, guidance and patience were invaluable through all stages of this thesis. I would also like to thank Dr. Peter Johnson for pointing me towards the road on which I now travel and to Dr. Konrad Gajewski for his enthusiastic support.

Shawne Clarke was the hardest working field assistant I will ever have. Her help in the field and the companionship and support she has provided throughout the past two years have tremendously improved the quality of this thesis. Thank you for everything Shawne.

Thanks to Caroline Duschene for her assistance with laboratory analyses and to Bruce Robin for his help with computers. I would also like to thank my friends for their encouragement and support. Dave Bajurny who has endured hours of conversation related to permafrost slope processes (a true friend), Mark Wacyk whose cabin in the woods was a place for timely retreats throughout the past two years and Dan Fratnik who provided frequent and inexpensive computer support during times of trouble all deserve special thanks.

This research was supported financially by funds from the Natural Sciences and Engineering Research Council and from the Northern Training Grant Program of Indian Affairs and Northern Development Canada. Essential logistical support was given by the Polar Continental Shelf Project, Natural Resources Canada. Field assistance given by Lianne Bellisario and Helen Taylor in 1993, is gratefully acknowledged. Thanks is also extended to Boyce Partridge and the Canadian Military personal at Eureka (Oh Canada!) for the unexpected support which they provided.

Financial support during 1996-98 was provided by Department of Geography, University of Ottawa teaching assistantships and research assistantships from Dr. A. G. Lewkowicz.

Finally, I would like to thank my family, Julia, Tilley Chopiany and particularly my mother and father, Leslie and Victor Kokelj whose unconditional love and support have made my endeavours possible.

Table of Contents

List of Figures

List of Tables

List of Appendices

Chapter 1 - Introduction

1.1 – Background and Aims

Slopewash processes may be of significance in the evolution of periglacial landscapes (French, 1996; Lewkowicz et al., 1978; Rudberg, 1969; Washburn, 1980). However, very few studies have quantified rates of surface wash in permafrost environments, and hypotheses relating to the efficacy of the process remain largely speculative. This suggests the need for further investigation of slopewash processes in areas underlain by continuous permafrost, focusing on variables such as amounts and distribution of snow cover, rates and distribution of snowmelt runoff and the influence of vegetation cover (Lewkowicz, 1983).

Several researchers have documented terrain disturbance in the continuous permafrost zone. The development of thermokarst terrain is reported from numerous locations (French and Egginton, 1973; Mackay and Mathews, 1983; Sharpe, 1985). Ground ice slumps, (e.g. Lewkowicz, 1987; Mackay, 1966; McRoberts and Morgestern, 1974) and active layer detachment slides (e.g. Hodgson, 1977; Lewkowicz, 1992; Mathewson and Mayer-Cole, 1984; Stangl et al., 1982), have been described throughout the high arctic, but the impacts of slope disturbances on surface wash erosion in the continuous permafrost zone have not been investigated.

This research was conducted at Hot Weather Creek, Fosheim Peninsula, Ellesmere Island. Detachment sliding is one of the most important mass movement processes on the Fosheim Peninsula (Lewkowicz, 1992). This study measures rates of surface wash on detachment scars of varying age, and on undisturbed vegetated and non-vegetated slopes to determine the influence of detachment sliding on surface runoff and on surface wash erosion. Specifically, the aims are to examine the effect of: (1) detachment sliding on surface runoff production, and (2) removal of vegetation and the formation of a fresh active layer on rates of suspended sediment and solute erosion.

1.2 - Literature Review

Permafrost slope hydrology has been investigated by several researchers, however there are few studies in which surface or subsurface runoff were measured in areas of continuous permafrost (Table 1-1). Closely related to permafrost slope hydrology are processes of permafrost slope erosion. Very few studies are known in which sediment or solute concentrations in surface or subsurface wash have been quantified. Only the studies by Bellisario (1992), Lewkowicz et al., (1978), Lewkowicz and French (1982b), and Lewkowicz (1983) have involved research on both discharge and sediment and solute concentrations, or in other words, slopewash.

Table 1-1: Studies in permafrost slope hydrology measuring surface and/or subsurface discharge.

Study Location	Author(s)	Comments
Radstock Bay and Resolute	Wilkinson and Bunting (1975)	- measured rill flow and sediment transport
Devon Island ($0.12\ km^2$ basin)	Ryden (1977)	- measured stream runoff in a wetland area
Cornwallis Island (smallest basin $.5km^2$)	Marsh and Woo (1979)	- measured runoff from four small basins - smallest basin consisted of a large wetland area, retarding streamflow and increasing rates of evaporation
Cornwallis Island	Woo and Steer (1982)	- measured surface flow - observed relationships between slope topography, the changing active layer storage capacity and the various hydrological processes acting on the slope
Banks Island (4 study plots)	Lewkowicz and French (1982a)	- measured surface and subsurface flow - identified the importance of sub-surface flow, particularly at interfluve sites - found that surface flow was most significant during early melt, at snowbank sites
Cornwallis Island ($26400\ m^2$ plot)	Steer and Woo (1983)	- measured surface and subsurface flow - found that surface flow was 2.5 times greater than subsurface flow
Imnaviat Creek Alaska (4, $89m^2$ plots)	Kane and Hinzman (1988)	- measured surface and subsurface flow - identified runoff as the dominant hydrological process during snowmelt
Melville Island (perennial snowbank)	Young and Lewkowicz (1988)	- measured outflow from a perennial snowbank with basal ice
Melville Island ($.08\ km^2$ catchment)	Lewkowicz and Young (1990)	- measured stream runoff of a perennial snowbank - observed discharge regime with proglacial character

1.2.1 – Permafrost Slope Hydrology

Woo and Steer (1986) identified three broad periods of permafrost hydrologic activity, based on supplies of water and energy: winter, spring and summer.

The winter period is characterised by very low energy and moisture availability. Snowfall in the high arctic is minimal, and much of the thin snow cover is redistributed by winter winds. Areas of snow accumulation are topographically controlled. Ridge tops and steep slopes tend to have thin snow covers, while concave slopes, valley bottoms and lee slopes are generally areas of greater accumulation (Woo, 1993). Sediment incorporated into the snowpack by aeolian activity is significant in lowering the surface albedo. This may result in more rapid ablation and snowmelt runoff (Woo et al., 1990).

When atmospheric conditions are conducive to melt and the snow surface reaches 0°C, meltwater percolates through the cold snowpack by downward diffusion or along flow fingers (Woo, 1982). During early snowmelt, latent heat is released by the refreezing of meltwater within the snowpack (Marsh and Woo, 1984). Once the wetting front reaches the base of the snow cover, there is an initial infiltration of water into the ground. Meltwater infiltrates via pore spaces formed by moisture movement during the winter. The meltwater then refreezes, releasing latent heat into the ground and impounding meltwater to saturate the snow immediately above the underlying soil (Marsh and Woo, 1984). Basal ice forms, releasing additional latent heat into the warming snowpack. Throughout the early snowmelt period there is a considerable redistribution of mass within the snowpack (Woo, 1982). As the snow continues to ripen, surface melt increases and runoff eventually occurs.

The abundance of water and energy makes the spring melt period the most significant part of the hydrological year (Woo and Steer, 1986). Once an area is free of snow, two very important hydrologic processes begin: runoff and thawing of the active layer. For overland flow to commence, the slope's depression storage, dependent on the microtopography, must first be satisfied (Woo and Steer, 1982). During early melt the active layer is very thin, so initially most of the runoff occurs as overland flow (Woo and Steer, 1982). Throughout early spring, surface runoff follows diurnal cycles, reflecting snowmelt rhythms (Lewkowicz and French, 1982a). As spring melt progresses, the snowbanks become thinner, and the lag times between energy inputs and peak discharge decrease (Lewkowicz and Young, 1990). As snow cover depletes and the frost table continues to drop, the thawing active layer permits more water to move downslope as subsurface flow (Woo and Steer, 1982). During late spring, the supply of energy remains high, but the moisture supply limits hydrologic activity to subsurface flow.

For the remainder of the summer, hydrologic activity is limited to subsurface flow, with the exception of rainfall recharge events (Lewkowicz and French, 1982a). Spatial and temporal variation in recharge responses are related to antecedent slope conditions (Lewkowicz and French, 1982a). Although the relative importance (Figure 1-1) of subsurface flow during the summer season may be significant (Lewkowicz and French, 1982a) several studies demonstrate the overall importance of surface flow during the melt season, particularly at snowbank locations (Lewkowicz and French, 1982a; Lewkowicz, 1983; Woo and Steer, 1982).

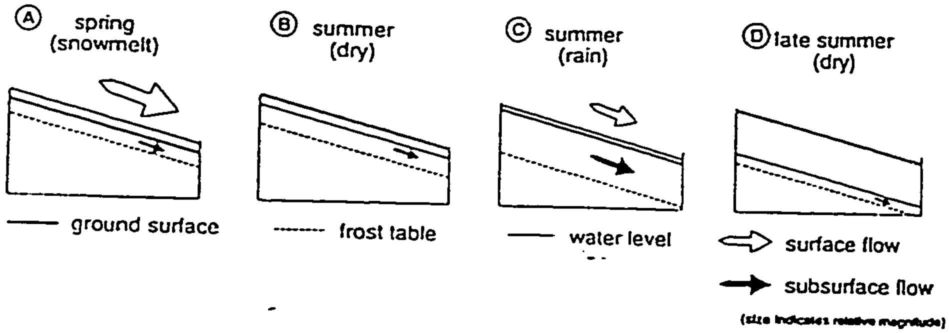

Figure 1-1: Schematic profiles showing relative positions of the water table and permafrost table during the hydrologic periods (Woo and Xia, 1995).

1.2.2 - Surface Wash

Slopewash in the high arctic consists of two sets of processes: a) surface wash, the downslope transport of weathered material over the ground surface by running water and b) subsurface wash, the group of processes associated with water moving within regolith (Lewkowicz et al., 1978). In the continuous permafrost zone, slopewash processes in the thin active layer may be a significant geomorphic process. The presence of an impermeable permafrost table is conducive to overland flow production during the melt season and hence the erosion of unvegetated slopes (Washburn, 1980). However, the overall efficacy of surface wash as an agent of erosion in permafrost environments remains a subject of speculation.

Lewkowicz's (1983) study of surface wash on Banks Island was undertaken in an area transitional between the tundra regions to the south and the polar desert and semi-desert to the north. The following hypotheses concerning the spatial variability of overland flow erosion in permafrost areas were proposed (Figure 1-2). The importance of solute removal at interfluve sites was significant at Banks Island, but is believed to decrease between the tundra zones and the polar desert and semi-desert zones due to lower amounts of overland flow runoff, flow temperature and biogenic CO_2 production (Lewkowicz, 1983). A similar response is hypothesised for removal by solution at snowbank sites. On the other hand, suspended sediment removal by surface wash at snowbank sites may increase northward from the tree line with maximum erosion rates occur in the polar desert zone. This is because the positive erosional effects of vegetation decline outweigh the negative effects of lower runoff.

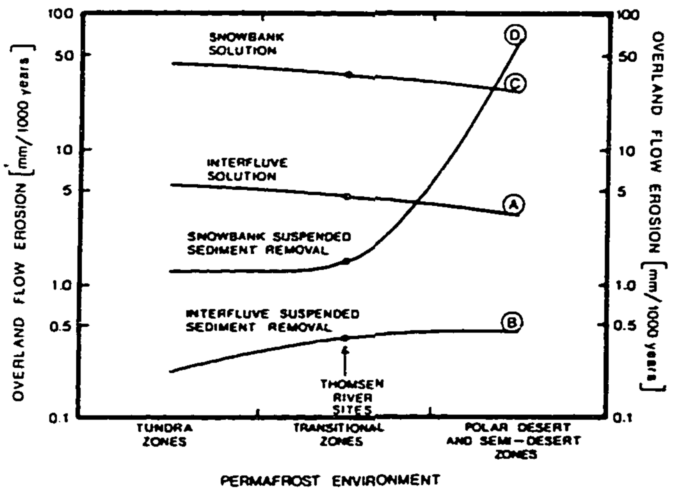

Figure 1-2: Inferred variation of overland flow erosion in areas of continuous permafrost (Lewkowicz, 1983).

The studies which have attempted to measure suspended sediment and solute concentrations by overland flow will be discussed (Table 6-5). The findings of these investigations may be considered within the spatial framework proposed in Lewkowicz (1983).

Wilkinson and Bunting (1975) measured sediment and solute transport on a low angled slope within a network of rills at Radstock Bay. Using sediment traps, the "sediment discharge recorded" was obtained for several rills on the study slope. Concentrations of up to 1700 mg L^{-1} were measured, but as flow velocities decreased downslope, so too did the measured suspended sediment concentrations. The authors found that snow patches with trapped aeolian material provided late melt recharges in sediment load without increases in flow velocities. However, they were not able to define the total amount of material transported during the runoff period.

Lewkowicz (1983) measured rates of overland flow erosion at four small plots on Banks Island. Sediment removal by solution was more important than removal by suspension, and denudation was 8-30 times greater for this process (2.0 to 74.1 mm per 1000 years) (Lewkowicz, 1983). Low suspended sediment concentrations appeared to be related to the limited availability of sediment, as little or no relationship between sediment transportation and diurnal fluctuations in surface flow were noted (Lewkowicz, 1983). It was also suggested that vegetation cover plays a significant role in reducing the rates of surface wash erosion (Lewkowicz, 1983).

In a study of slopewash on unvegetated slopes on Spitsbergen, Jahn used sediment traps to measure suspended sediment transport by surface wash (Jahn, 1961). Meltwater was responsible for most of the sediment transport throughout the season. However, neither discharge nor removal by solution were measured. Net denudation values of at least 16 g m^2 yr^{-1} were calculated at a snowbank location with abundant runoff (Jahn, 1961). Jahn's denudation values of 7 mm per 1000 yrs (Lewkowicz, 1988), are similar to Lewkowicz's values for poorly vegetated slopes on Banks Island.

These results suggest that due to low suspended sediment concentrations, rapid modification of landscape by surface wash is unlikely. A more recent study conducted by Bellisario (1993) on the Fosheim Peninsula, near Eureka, showed that substantial amounts of material may be moved down slopes with low vegetation covers during the melt period by rillwash and gullying. Denudation values of 200 g m^{-2} yr^{-1} were obtained by Bellisario. Unlike earlier studies, Bellisario's research indicates that surface wash can be a significant geomorphic process in a polar desert.

This review of literature supports the hypothesis of Lewkowicz (1983), but this is based on results of only four local studies distributed over a vast geographical area. Apart from Lewkowicz's studies, only Bellisario's work attempted to measure discharge and sediment removal. The paucity of data concerning the role of surface wash as a geomorphic agent in the permafrost environment, and the difficulty of comparing the few existing studies, clearly limit our understanding of its spatial and temporal variation.

1.3 - Aims, Hypotheses and Methodology

The study examines to what extent the disturbance of vegetation cover and changes in snow accumulation due to topographic alteration by detachment sliding affect rates of erosion.

The four main objectives of the research are:

(1) To measure rates of surface wash erosion in the high Arctic.

(2) To determine the influence of detachment sliding on surface hydrology.

(3) To determine the influence of vegetation on surface wash rates.

(4) To determine the influence of detachment sliding on surface wash rates.

Prior to melt in 1996, nine study plots were established at Hot Weather Creek, to evaluate the influence of detachment sliding on the rates of surface wash erosion. Inter-annual variation was examined using data for two plots (A1 and A3) from 1993 (collected by A. G. Lewkowicz). The main research hypothesis is:

1) Slopes affected by detachment sliding experience increased rates of surface wash erosion.

The research design was implemented to investigate the main hypothesis. Nine plots ranging in size from 250 m^2 to 16000 m^2 were set up on: (1) an undisturbed unvegetated slope, (2) two disturbed unvegetated slopes (fresh detachment slide scars)(Figure 1-3), (3) two moderately vegetated slopes (old detachment slide scars), (4) three well-vegetated slopes (Figure 1-4) , and (5) a large section of a slope which included undisturbed areas as well as young and old detachment slide scars. Runoff from each plot was measured with a flume equipped with an electronic stage recorder, and water samples were collected at regular intervals to establish the relationship between suspended sediment concentration and discharge at each site, so that sediment loads could be evaluated. Conductivity probes at each flume continuously measured the effect of solute concentrations in the runoff. Regular conductivity measurements were also taken at each flume using a YSI salinity-conductivity-temperature meter in order to calibrate the conductivity probes.

Figure 1-3: A1, fresh detachment slide scar

Figure 1-4: B3, well-vegetated study plot.

Nine sub-hypotheses were formulated to facilitate testing of the main hypothesis:

1a. Surface runoff production is increased on slopes where the organic layer has been removed by detachment sliding.

Snowmelt runoff coefficients from fresh and old detachment slide scars can be compared with those from mixed plots and vegetated undisturbed slopes. Testing of this hypothesis can also utilize data from ring infiltrometer experiments and by soil moisture samples collected from several slopes (vegetated slopes and detachment slide scars) after a major rain-storm in 1997.

1b. Rates of surface wash erosion are dependent on the percentage of vegetation cover on a slope.

After the runoff period, a vegetation survey was conducted at each study plot. Percentage vegetation cover, and the distribution of cover were determined. The stabilizing effect of vegetation should result in low rates of erosion on well-vegetated undisturbed plots. Sites with low vegetation cover are susceptible to much higher rates of surface wash erosion. Hypothesis 1b can be tested by comparing the rates of surface wash erosion the study plots.

1c. Suspended sediment removal from slopes is dependent on the distribution of vegetation cover, and on the nature of the slope drainage network.

This hypothesis can be tested by comparing the sediment yields at B3 (mixed plot with detachment slide on upper part of the slope – vegetated/non-channelized lower slope) with the sediment yields at A3 (mixed plot with several detachment slides on central part of the slope – channelized drainage). Similar comparisons can also be made between suspended sediment yields and the distribution of vegetation cover at the other plots.

1d. Greater amounts of snow accumulation on bare detachment slide slopes result in hydrologic conditions which are different from those on bare slopes unaffected by sliding.

Snow surveys were conducted on all study plots prior to the onset of ablation. Most unvegetated undisturbed slopes are exposed areas which do not favour snow accumulation. The topographic depressions characteristic of detachment slide scars should increase the accumulation of snow reworked by winter winds, resulting in greater amounts of snowmelt runoff. Hypothesis 1d can be tested by comparing the water equivalent of snow on plots recently affected by detachment sliding with that on bare slopes unaffected by sliding.

1e. Detachment scars are more susceptible to erosion by surface wash than other unvegetated areas due to changed hydrological conditions.

Hypothesis 1e can be tested by comparing the snowmelt runoff and erosion on four plots affected by detachment sliding, with the one undisturbed, unvegetated study plot.

1f. Detachment slides in Holocene marine sediments result in the formation of a fresh active layer with high salt concentrations.

This hypothesis can be tested by comparing soil geochemistry, solute concentrations and water geochemistry among the study plots.

1g. High salt concentrations in the fresh active layer inhibit revegetation of the scar zone.

Na^+ concentrations measured in the fresh active layer can be compared to concentrations on adjacent undisturbed slopes. These values can be compared with the salt tolerances of arctic halophytes (Srivastava and Jefferies, 1995a). In addition, the revegetation of the fresh detachment slide scar in marine sediments and the fresh scar in non-marine deposits can be compared.

1h. The revegetation of detachment scars reduces the rate of suspended sediment erosion by surface wash.

1i. The revegetation and restabilization of detachment scars is a slow process (decades to centuries).

Two study plots were established on old detachment slide scars (pre-1950) and two on fresh detachment slide scars (1988). A comparison of the rates of surface wash erosion on the young and old detachment slide scars and the vegetation cover on the respective plots provides a framework to test hypothesis 1h. In addition, these surface wash rates can be compared to the rates of erosion on three well-vegetated undisturbed slopes. Comparing the relationships between surface wash rates and vegetation cover on variously aged detachment slide scars (young 1988, old, pre-1950) and on undisturbed slopes will provide a measure of the spatial variability of surface wash erosion, and insight into the temporal scale of slope restabilization (hypothesis 1i). The average amount of solute removal for 1993 and 1996 can be compared with the total sodium in the soil at the fresh detachment slide in marine sediments (A1), and at undisturbed slopes, in order to estimate the time required for sodium levels to reach residual values following detachment sliding. This can provide a temporal perspective on the ecological and geomorphic impact of detachment sliding in marine deposits.

1.4 – Site Selection and Plot Descriptions

Two groups of study plots were established on slopes in the lower portion of the Hot Weather Creek valley (79^0 58' N. 89^0 23'W). A series of 1950 and 1990 air photos of the Hot Weather Creek area were used in conjunction with Lewkowicz's (1992) map of detachment slides in the lower valley of Hot Weather Creek to establish tentative study plots, and to create a detailed map of the proposed study area. Upon arrival in the field some modifications to the initial site plan were required. Nine study plots, ranging in size from 250 m^2 to 16000 m^2, were established on disturbed and undisturbed sites with varying vegetation covers (Table 1-2 and Figure 1-5). Plot topography and the distribution of vegetation by transect are presented in Figures 1-6 to 1-14.

Table 1-2: Description of surface wash plots.

Plot	Description	Size m^2	Slope angle	Orientation	Vegetation cover
A1	- fresh detachment scar, 1988	475 m^2	11^0	East	- 8% - lower slope 0%
A2	- old detachment scar, pre – 1950	440 m^2	7^0	Southeast	- 8%
A3	- various aged detachment scars, bare and vegetated undisturbed slopes	15680 m^2	7^0	East and North	- 17%
A4	- undisturbed slope	1150 m^2	5^0	East	- 28%
A5	- undisturbed slope	440 m^2	8^0	East	- 4%
B1	- fresh detachment scar, 1988	420 m^2	28^0	Northwest	- 8%
B2	- old detachment scar, pre – 1950	605 m^2	6^0	Northwest	- 13%
B3	- various aged detachment scars, bare and well vegetated slopes	1270 m^2	18^0	Northwest	- 30% overall - lower slope 50%
B4	- undisturbed slope	95 m^2	26^0	West	- 15% overall - lower slope 40%

Figure 1-5: Study area location map. A-Queen Elizabeth Islands; B-Fosheim Peninsula, Ellesmere Island; C- Valley of Hot Weather Creek in the vicinity of former Geological Survey of Canada Camp; D-Site A; E-Site B.

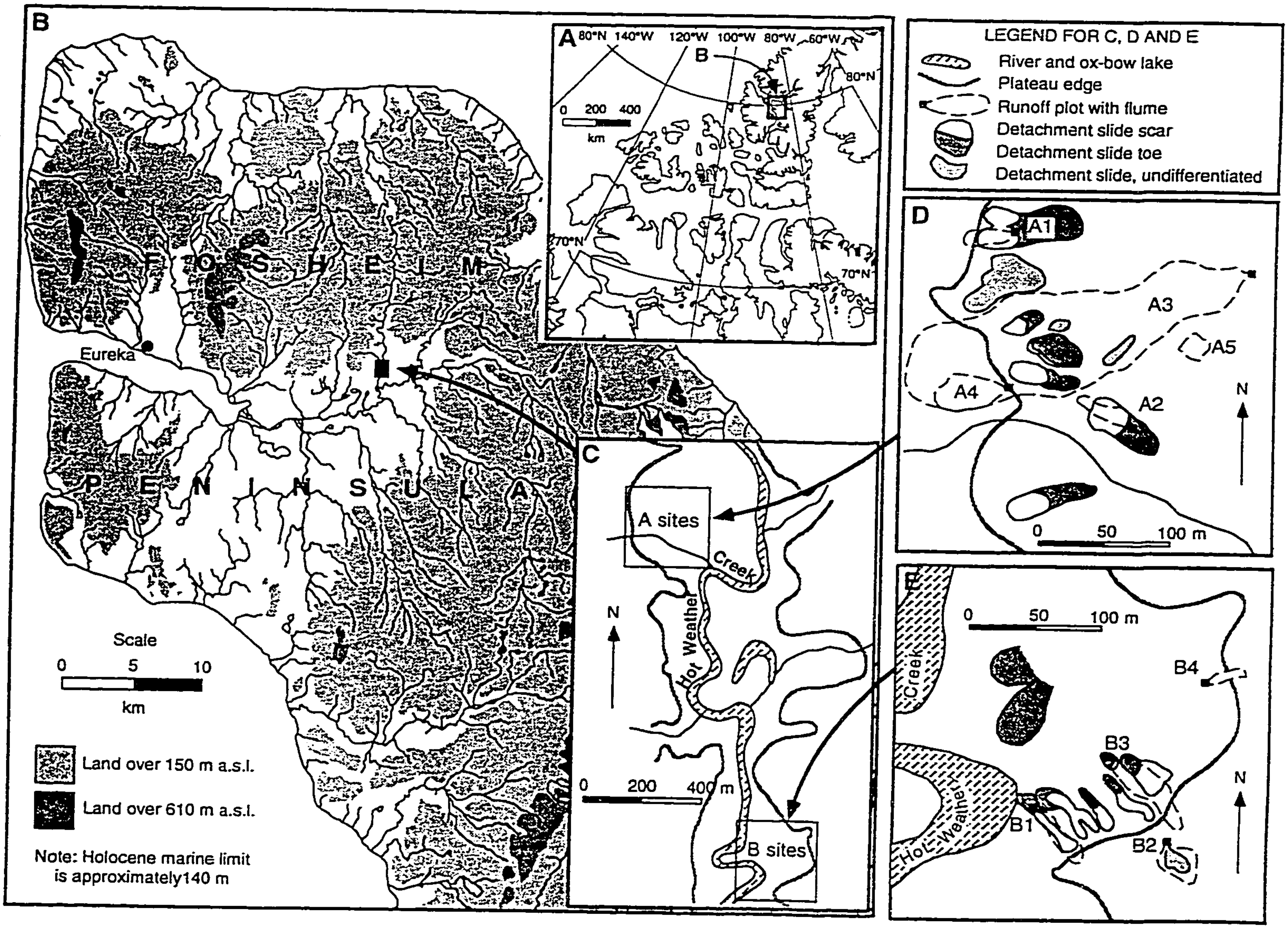

Figure 1-6: A1, plot topography and vegetation cover by transect

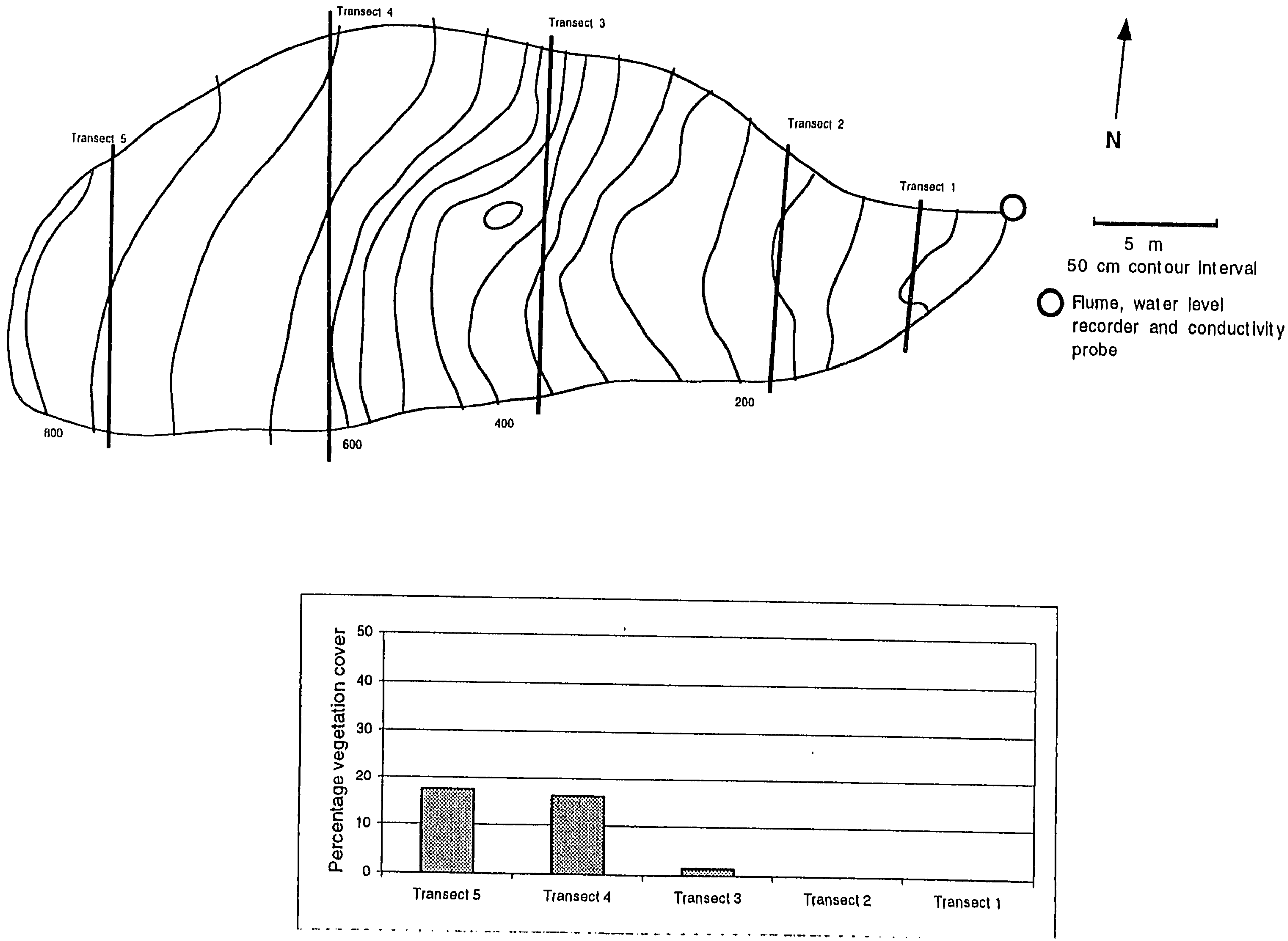

Figure 1-7: A2, plot topography and vegetation cover by transect

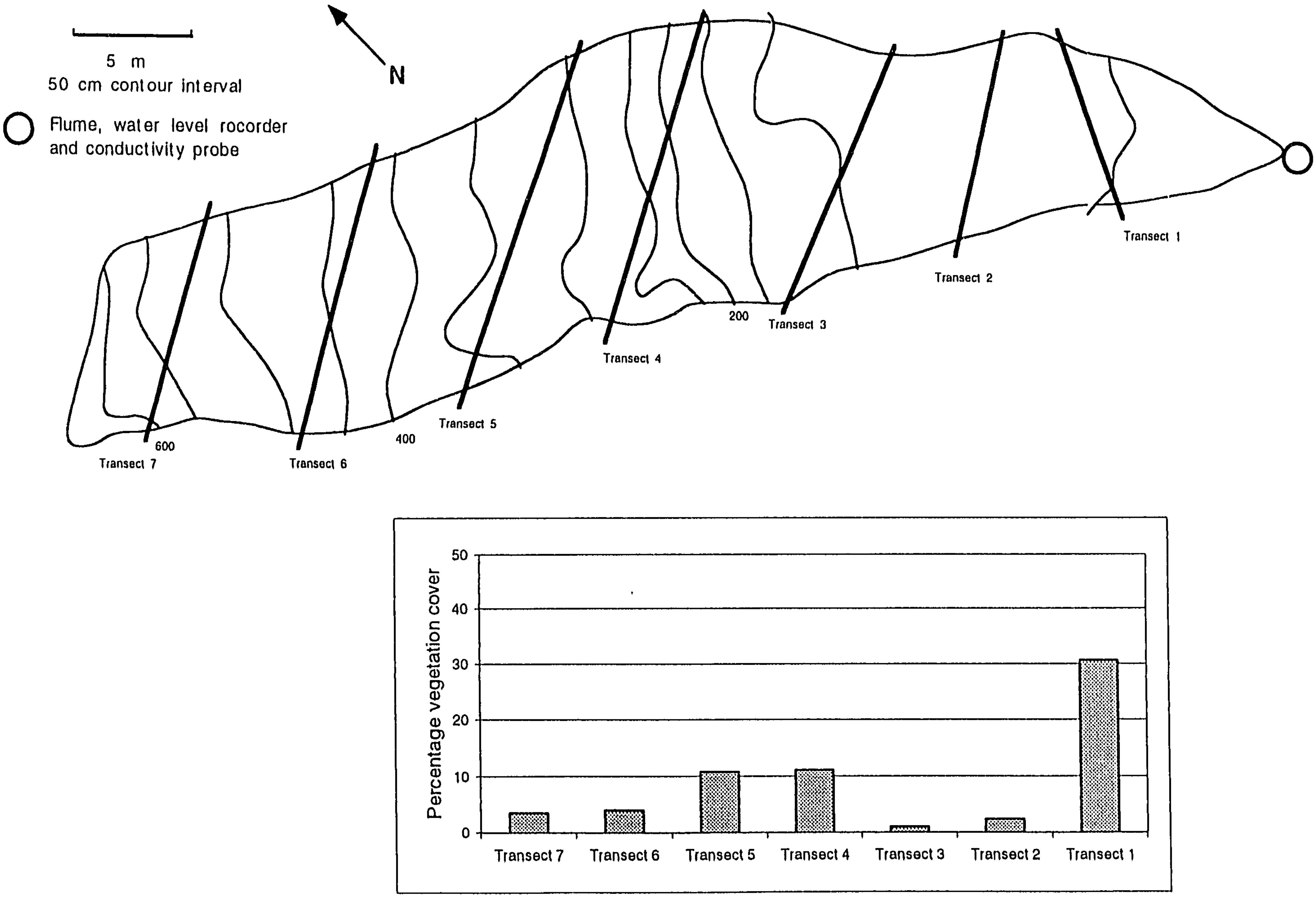

Figure 1-8: A3, vegetation cover by transect.
Note: A topographic survey was not conducted due to the large size of the plot.

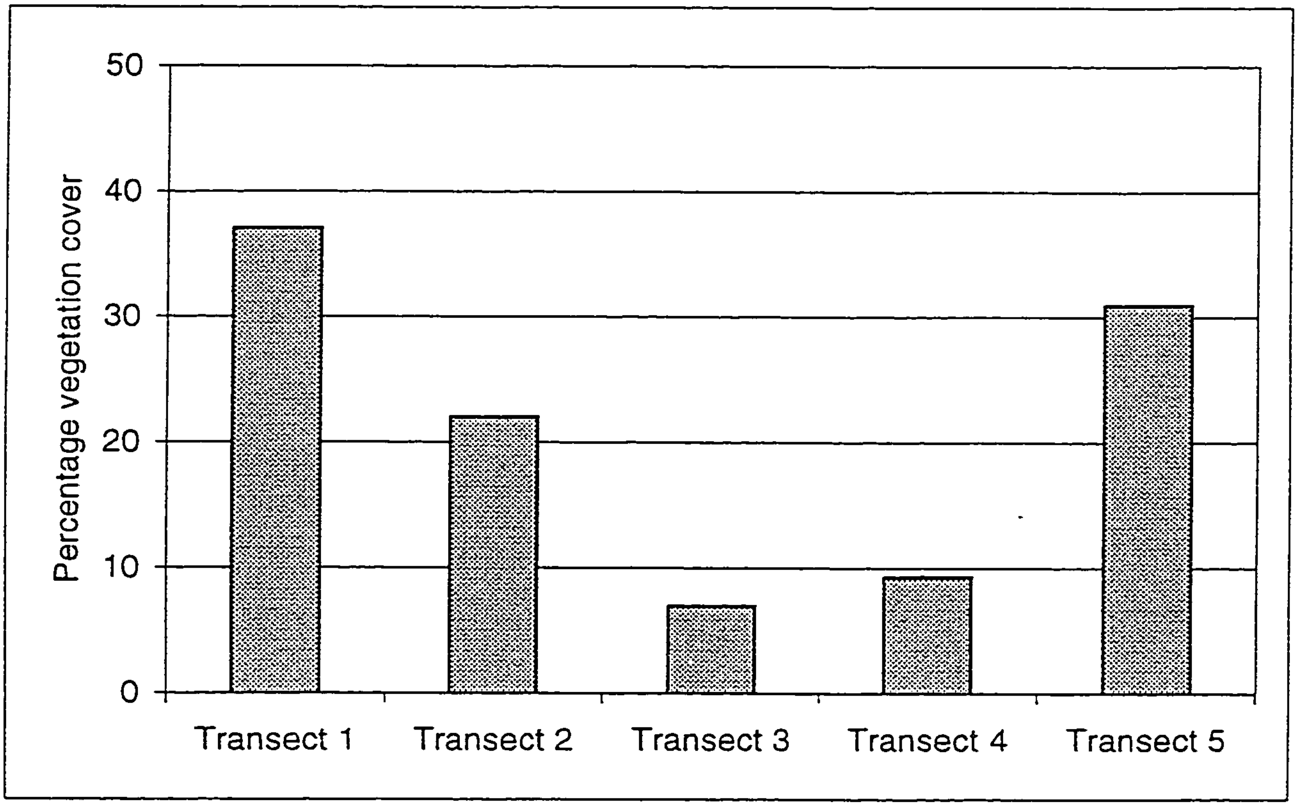

Figure 1-9: A4, plot topography and vegetation cover by transect

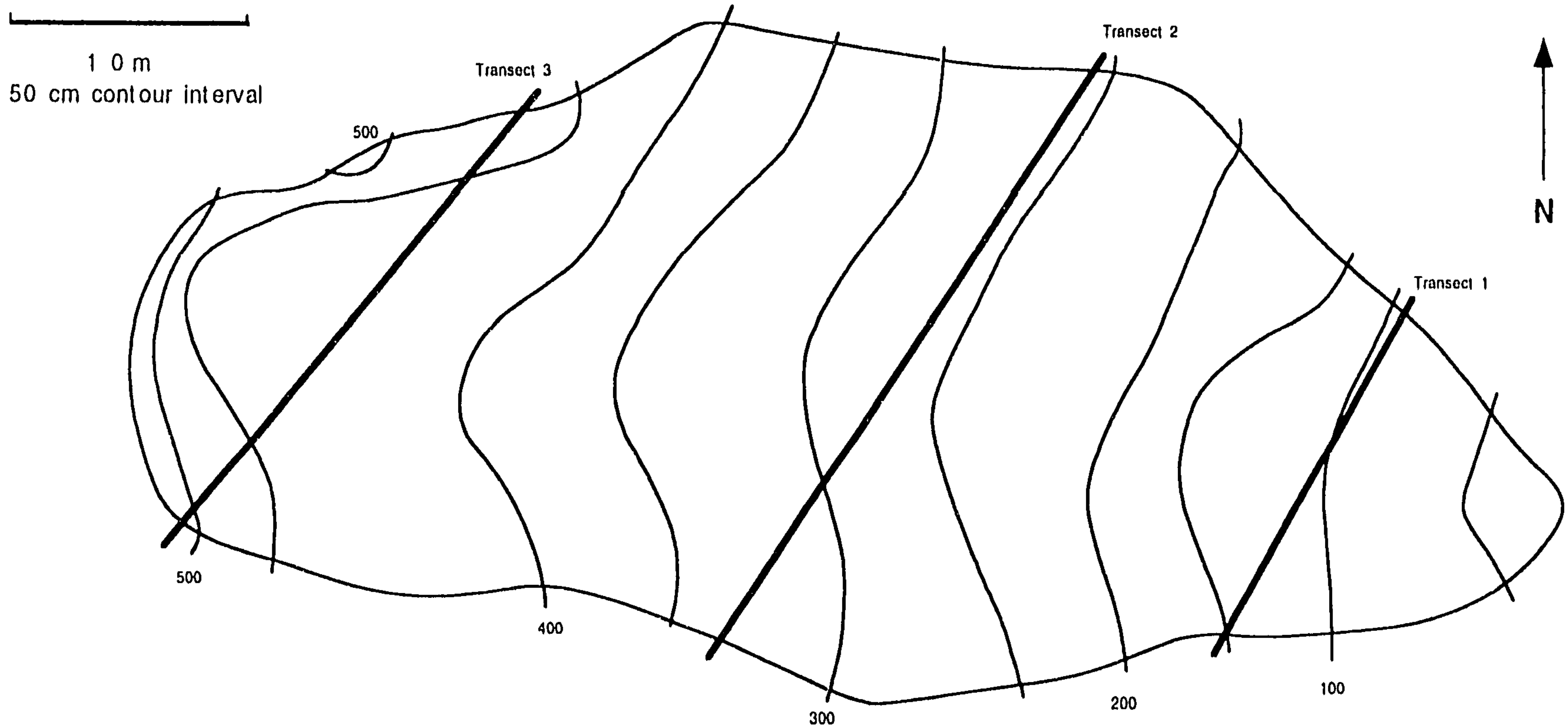

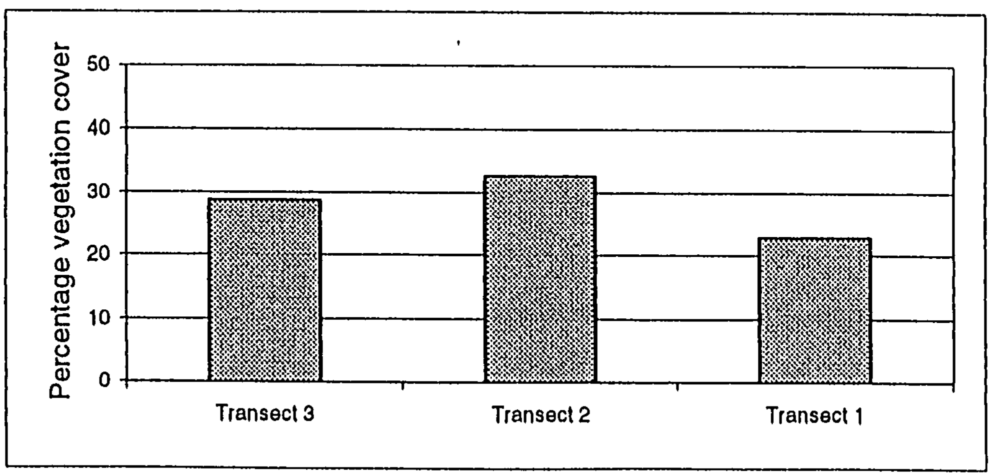

Figure 1-10: A5, plot topography and vegetation cover by transect

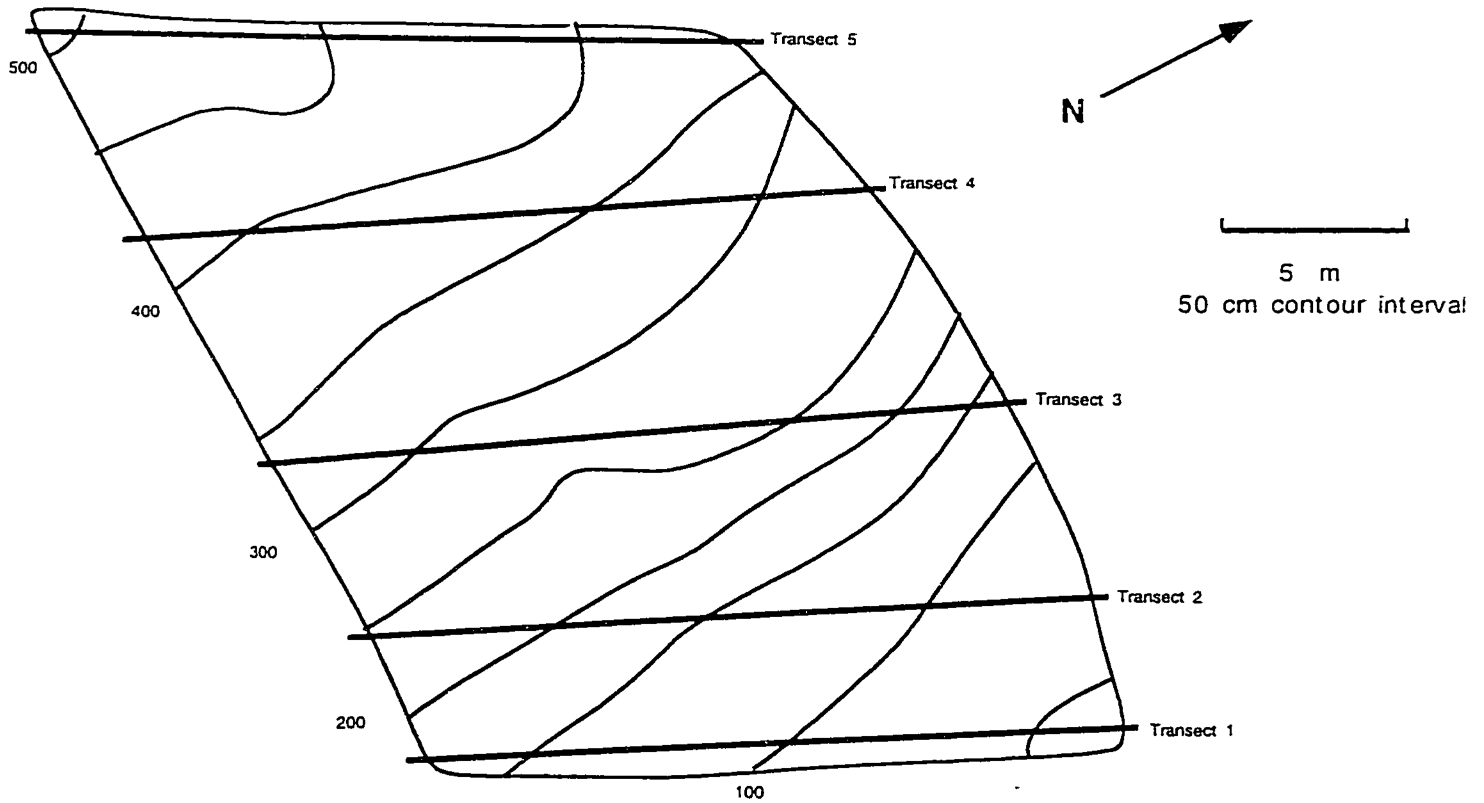

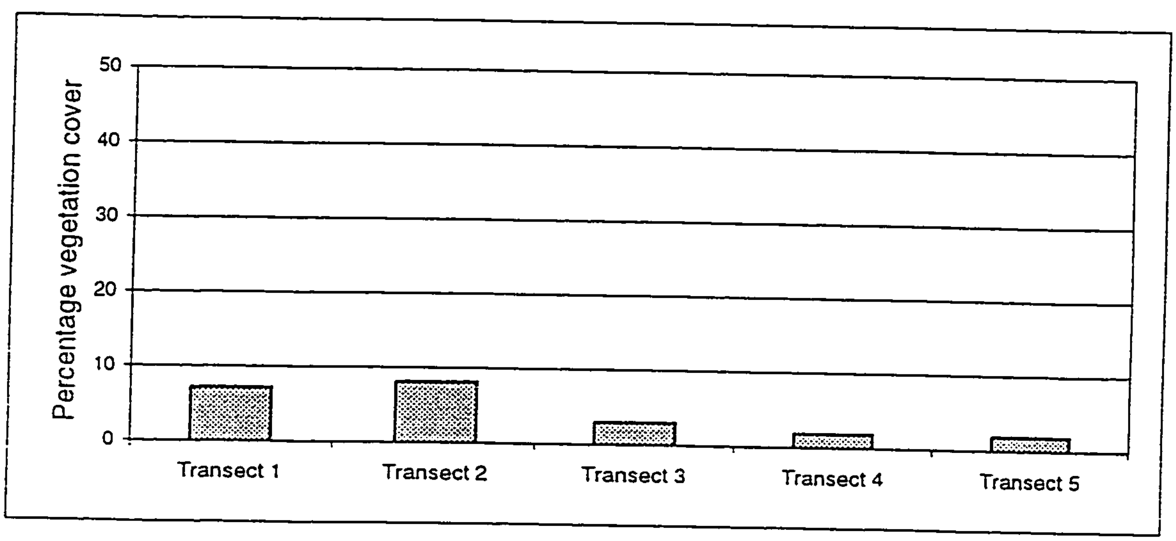

Figure 1-11: B1, plot topography and vegetation cover by transect

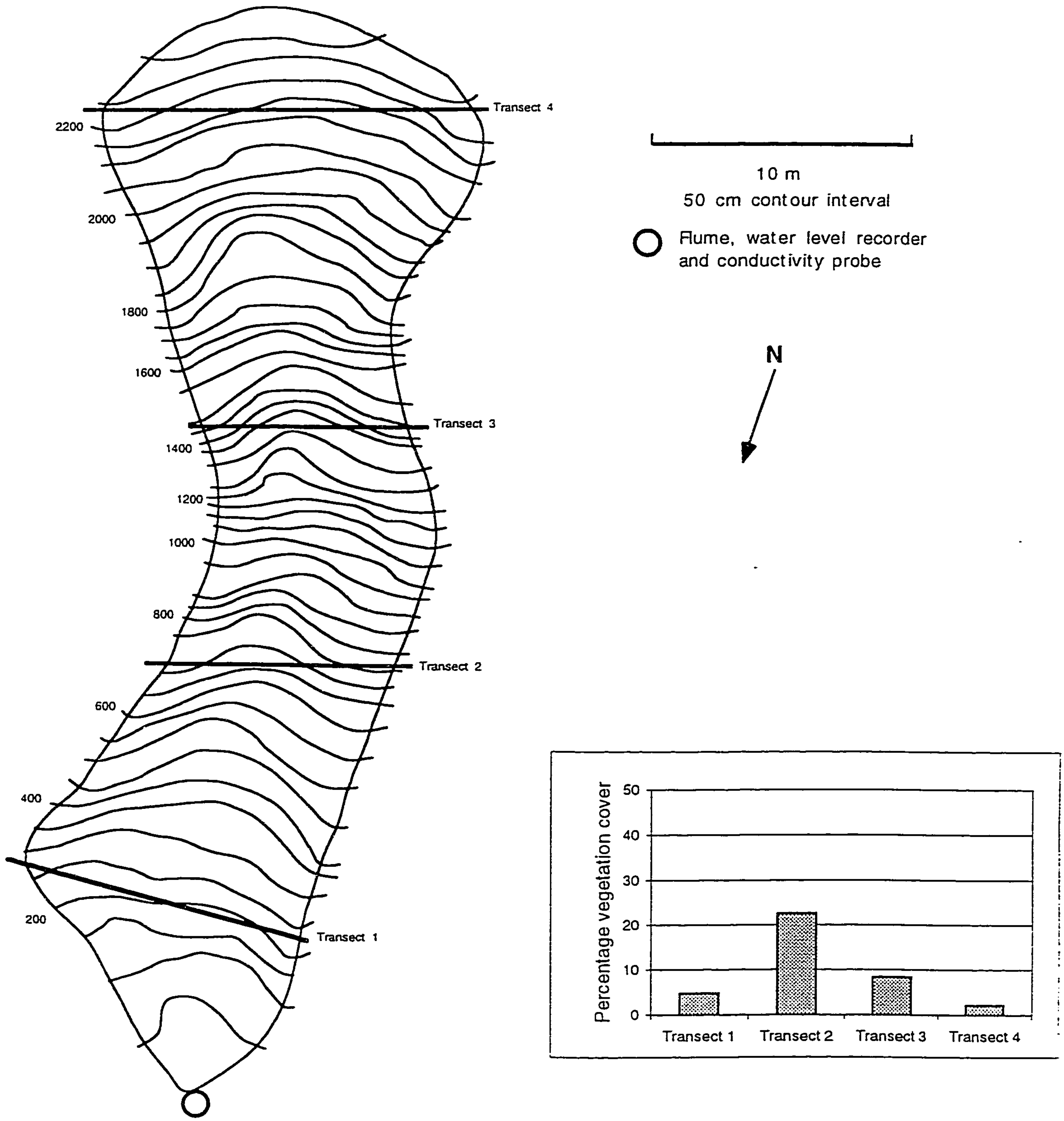

Figure 1-12: B2, plot topography and vegetation cover by transect

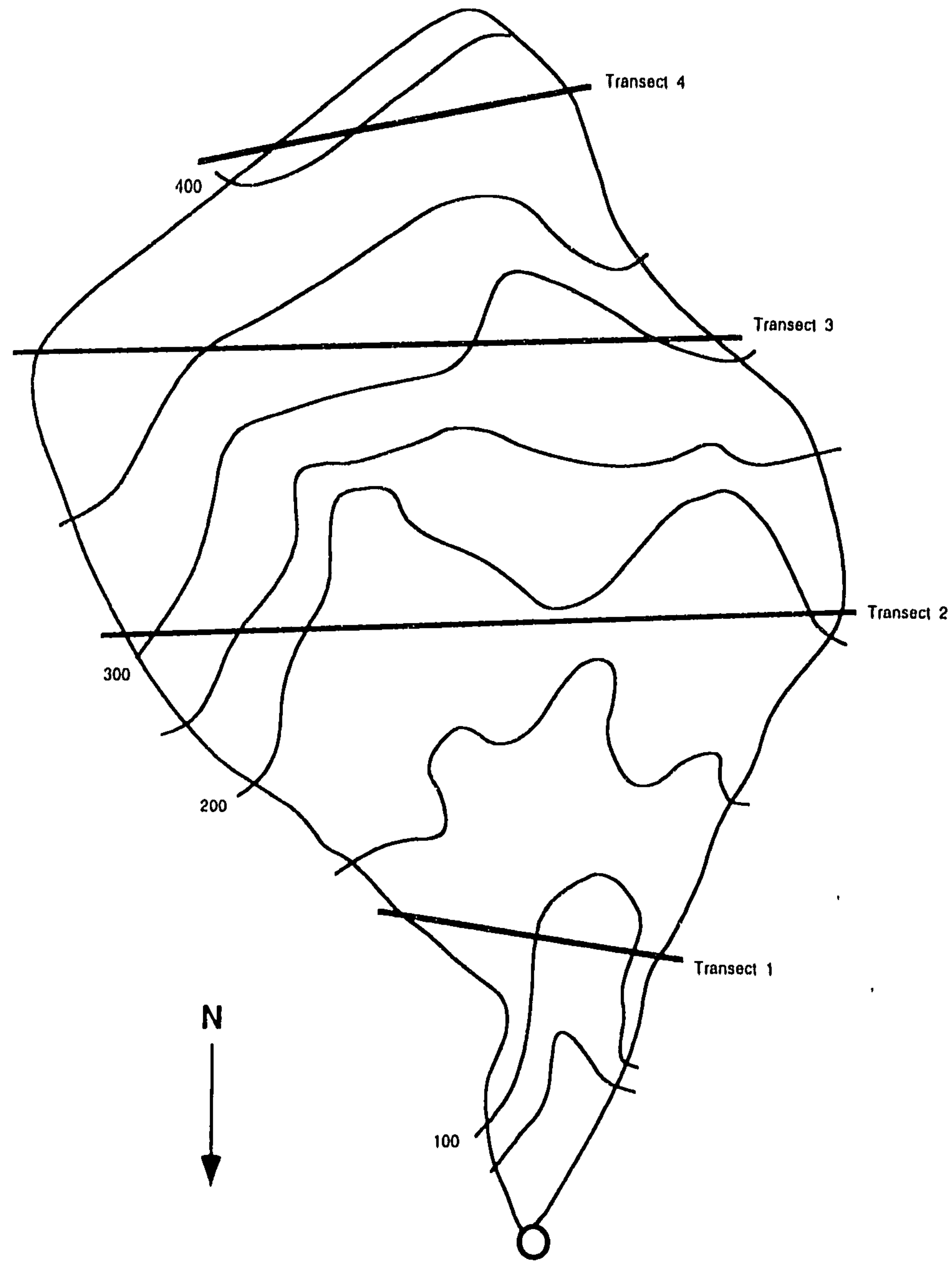

1 0 m
50 cm contour interval

O Flume, water level recorder and conductivity probe

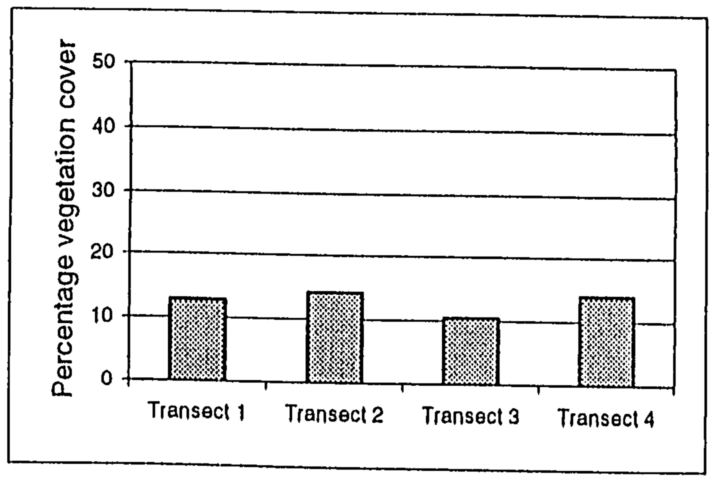

Figure 1-13: B3, plot topography and vegetation cover by transect

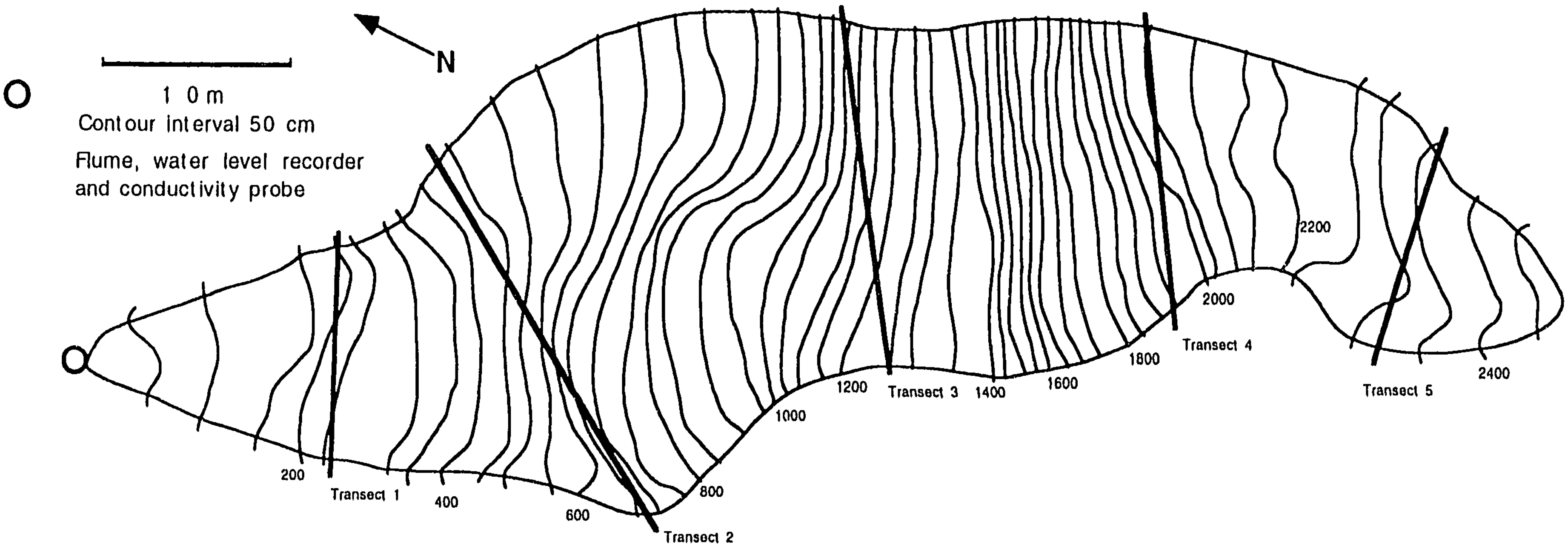

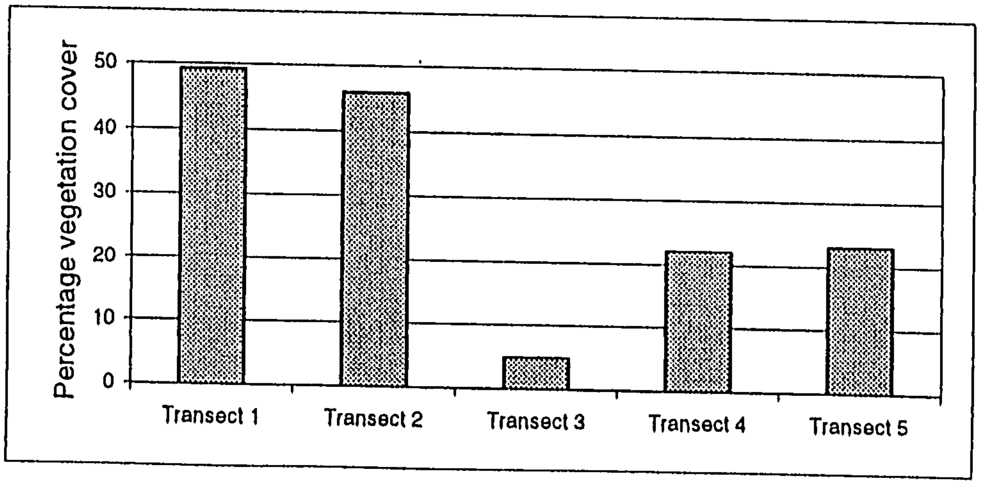

Figure 1-14: B4, plot topography and vegetation cover by transect

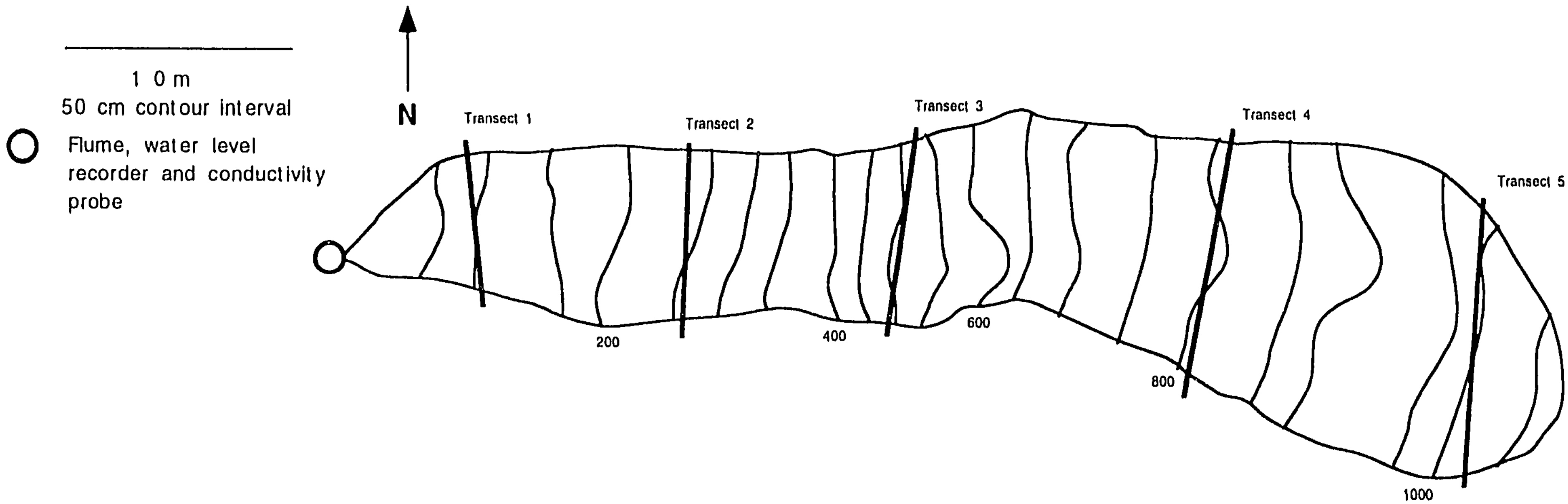

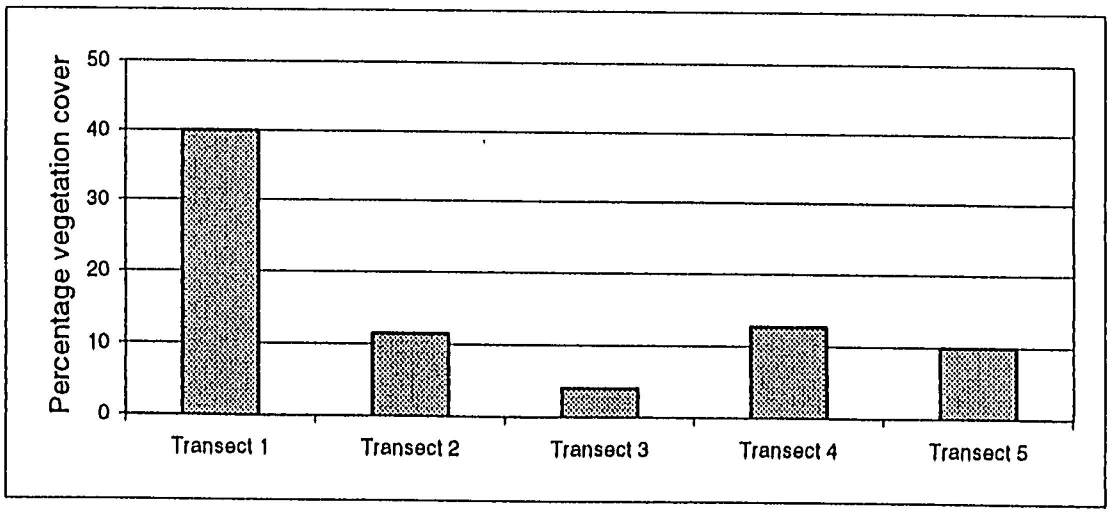

Chapter 2 - Study Area

2.1 – Physiography, Geology and Geomorphology

The study area is located in the Hot Weather Creek basin about 25 km east of Eureka, on the Fosheim Peninsula, Ellesmere Island (see Figure 1-5). Hot Weather Creek is a 22 km long tributary of the Slidre river. The 155 km^2 basin consists of a broad, rolling, well-vegetated lowland with a maximum elevation of 300 m a.s.l. In the vicinity of the study slopes, Hot Weather Creek is characterized by a meandering morphology, within a valley incised about 25 to 50 m below the surrounding plateau (Lewkowicz and Wolfe, 1994). The basin is underlain by continuous permafrost. Borehole measurements indicate that the permafrost is about 500 m thick (Taylor et al., 1982). Active layer depths range from 40-90 cm depending on vegetation cover and substrate.

The watershed is underlain by poorly consolidated sandstone and subordinate shale and coal of the Upper Cretaceous, Lower Tertiary Eureka Sound Group (Hodgson et al. 1991). Weathered and colluviated materials dominate the surface deposits in the basin (Hodgson et al., 1991). The Quaternary history of the Fosheim Peninsula is not entirely understood, however it is believed that the Hot Weather Creek basin has not been glaciated since at least the late Wisconsinan (Hodgson, 1989; Bell, 1996). Since 9 ka the Peninsula has undergone more than 140 m of emergence (Hodgson et al., 1991; Bell, 1996). The sediments associated with the higher sea levels consist of marine, estuarine and deltaic deposits composed of medium-fine grained sand, silt and clays (Hodgson et al., 1991). Such deposits are present in the southern part of the basin. The fine grained marine deposits favor the development of ground ice (Hodgson et al., 1991), but in fact ice wedges and ground ice are present in materials throughout the basin.

According to Hodgson's (1991) interpretation of surficial deposits in the Hot Weather Creek basin, the slopewash study plots are within the surficial unit identified as "Marine washed bedrock". At both study sites, a veneer of weathered bedrock, till and colluviated marine silts and clays covers bedrock on the fluvially incised slopes.

Typical slope processes active in the basin include slopewash and solifluction. Retrogressive thaw slumps are present in massive ice about 1 km north of the study site and slumping has occurred in several locations where streambank erosion has exposed icy sediments or massive ground ice. The lack of complete winter snow cover can lead to deflation of bare patches resulting in the redistribution of sediment by winter winds (Edlund and Woo, 1991; Lewkowicz, 1998). The most common rapid mass movements in the study area are active layer detachment slides. Lewkowicz (1990) mapped more than 500 detachment slides in three areas on the Fosheim Peninsula. The average rate of activity in an area of 5.3 km^2 in the valley of lower Black Top Creek is 3.5 failures per year, however 75 slides were initiated within the study area during July and August 1988 (Lewkowicz, 1992). The late summer warm spell in 1988 produced a similar response on the slopes of Hot Weather Creek where over 40 detachment slides occurred in a 2 km stretch of valley immediately downstream of Hot Weather Creek base camp. This single event increased the total number of slides in the area by 32% (Lewkowicz, 1992). The relatively high summer temperatures and low cloud cover on the Fosheim Peninsula likely cause active layer detachment slides to be more common there than in other areas of the high arctic (Lewkowicz, 1992).

2.2 - Climate

Compared to most of the high arctic archipelago, summer temperatures in the Hot Weather Creek basin are anomalously warm due to the surrounding fiords, and mountain ranges of Ellesmere and Axel Heiberg Islands (Edlund and Alt, 1989). These tend to block or dissipate slow moving disturbances from the Arctic Ocean and from Baffin Bay (Edlund and Alt, 1989). Eureka, located on the north shore of Slidre Fiord has a mean annual precipitation of only 64 mm, but this value is unreliable because snowfall may be significantly underestimated (Woo et al., 1983). Due to its inland location Hot Weather Creek experiences temperatures which consistently exceed those at Eureka. Several studies conducted at Hot Weather Creek (Edlund et al., 1989; Edlund et al., 1990; Lewkowicz and Wolf, 1994) show that summer temperature and precipitation consistently exceed those at Eureka (Tables 2-1 and 2-2).

At Eureka the greatest amount of precipitation is recorded during the months of July and August, most of which falls as rain. During the period from September to May most of the precipitation falls as snow. In the Hot Weather Creek basin, the redistribution of snow by prevailing southerly winds throughout much of the winter, results in greater snow accumulations on north-facing slopes (Woo et al., 1990). Topographic depressions also favor the accumulation of snow reworked by winter wind action (Woo, 1982).

Table 2-1: **Average Monthly Temperature (°C)**

	May		June		July		August	
	Eureka	HWC	Eureka	HWC	Eureka	HWC	Eureka	HWC
1950-80[a]	-10.7	N.A.	1.8	N.A.	5.4	N.A.	3.3	N.A.
1988	-7.0	N.A.	3.1*	7.2*	7.2	12.7	7.2**	10.6**
1990[b]	-5.0	-3.8	4.5	7.5	5.6	8.6	5.3	7.6
1991[b]	-4.3	-4.1	3.1	5.5	6.3	10.3	4.0	5.7

[a] Atmospheric Environment Service (1984); [b] Eureka Weather Station Records and HWC Automatic Weather Station
* Mean temperature from June 15-30
** Mean temperature from August 1-18
1988 from Edlund et al. (1989), 1990-91 from Lewkowicz and Wolfe (1994)

Table 2-2: **Total Precipitation (mm)**

June-August

	Eureka	HWC
1950-80[a]	29	N.A.
1990[b]	13	16
1991[b]	49	62

[a] Atmospheric Environment Service (1984); [b] Eureka Weather Station Records and HWC Automatic Weather Station
(Lewkowicz and Wolfe, 1994),

2.3 - Vegetation

Vegetation in the study area is strongly influenced by moisture supply. Precipitation and ground ice thaw are two sources of soil moisture in this region, enabling a denser tundra and wet meadow vegetation to grow (Figure 2-1) in areas where sparse polar desert and barrens vegetation would be expected (Edlund et al., 1989). One hundred and forty vascular plant species occur in the Hot Weather Creek area, compared with less than thirty five which generally occur on similar materials in the western and central Queen Elizabeth Islands (Edlund et al., 1990). Vegetation communities in the Hot Weather Creek basin are summarized in Edlund et al. (1989).

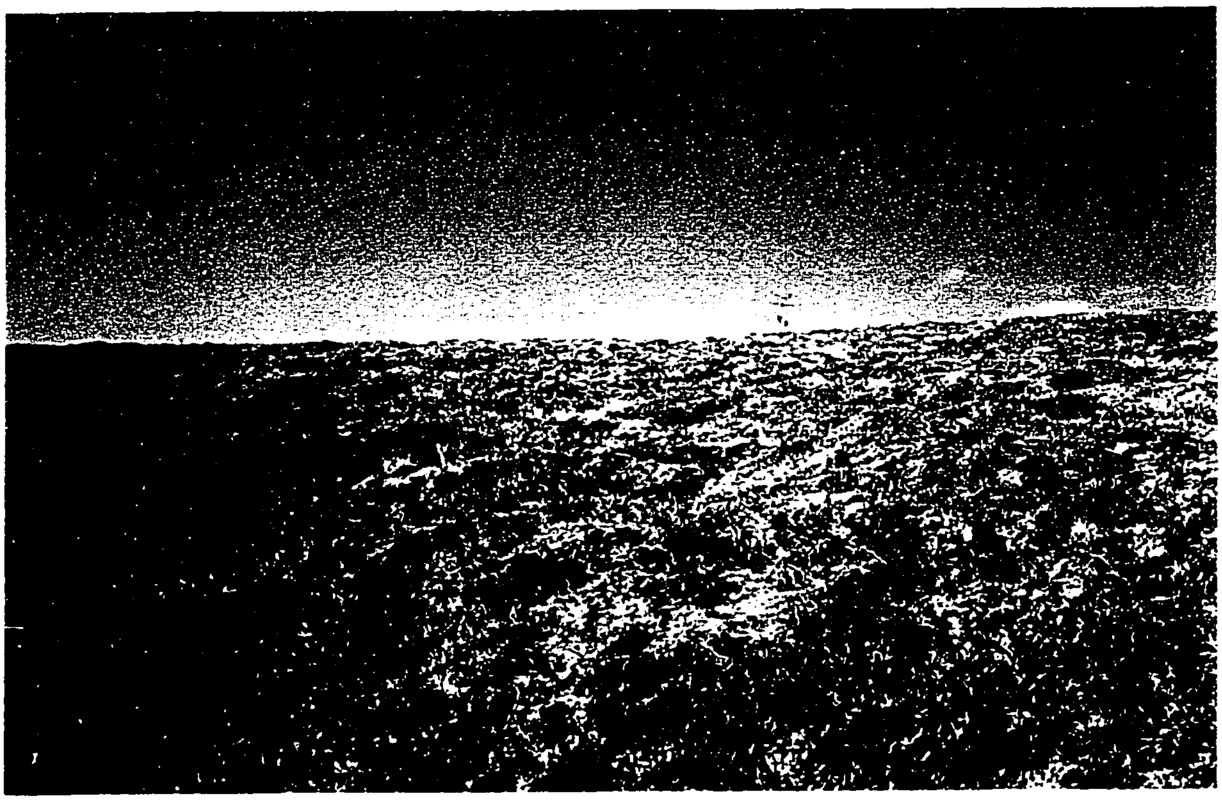

Figure 2-1: Well-vegetated hummocky slopes in the study area are dominated by *Salix arctica and Dryas integrifolia.*

Most of the well-vegetated plots in the study area are covered by hummocky tundra. The hummocky tundra vegetation community comprises the largest vegetation community in the Hot Weather Creek area (Edlund, 1989). This community dominated by *Salix arctica* and *Dryas integrifolia* is found on almost all moderately drained, neutral to moderately alkaline soils of the silty lowland surfaces, and may provide up to 50 percent vegetation cover (Edlund et al., 1989). The barren community is the most common on drier more exposed sites (Edlund et al., 1989). *Dryas integrifolia* and *Salix arctica* still dominate but provide generally less than 20 percent cover. Recent detachment scars are largely free of vegetation, while the older scars contain only sparse grasses and a few other colonizers.

Chapter 3 – Research Techniques

3.1 – Meteorological Measurements

3.1.1 – Snow Cover and Precipitation

Snow surveys were conducted prior to the spring melt. The average depth and distribution of snow cover on the study slopes was estimated by taking snow depth measurements in three to five transects (depending on plot size) across the slope. A steel snow probe was used to measure snow depths at 2 m intervals, except at the much larger site A3, where measurements were made every 5 meters. A total of 16 snow cores were taken along transects to determine snow-water equivalents and to measure the amounts of aeolian sediment contained in the snowpack. At least one core sample was collected from each plot. The samples were melted in the field and their water volumes were recorded so that water equivalents could be calculated (Appendix A-1). Snow water equivalents for the plots were determined by multiplying the average snow depth of each plot by the plot area and then multiplying by the average snow density (0.32 Mg/m^3) determined in Appendix A-1.

The methods for determining sediment and solute concentrations in the snowpack were identical to the methods used for slopewash samples and are explained in sections 3.3.1 and 3.3.2.

A Weathermeasure tipping bucket rain gauge installed near the base of study site B and was connected to a Campbell scientific 21x data logger for instantaneous records. The rain gauge recorded precipitation with a resolution of 0.25 mm.

3.1.2 – Ablation and Net Radiation

Soon after arrival on May 26, 1996, two Hobo temperature recorders with thermistors enclosed in gill shields at standard screen height were erected on the slopes of sites A and B. Air temperature was sampled every 12 minutes at both locations throughout the study period, however due to equipment failure no temperature record was recovered for site A. A Middleton net radiometer and two ablatometers (Lewkowicz, 1985) connected to the Campbell Scientific 21X logger were set up at site A to measure net radiation and rates of snow ablation.

3.2 - Discharge

3.2.1 – Data Collection

Surface wash discharge from each plot was measured using a trapezoidal flume (Bos et. al., 1984) equipped with a stilling well and an electronic water-level recorder (Figure 3-1). Seven of these flumes could accommodate discharges of 1.5 L/s while the flume at site A3 could accommodate discharges of up to 4.3 L/s. Each potentiometeric water level recorder was linked by a long wire to one of the 21X data loggers, providing continuous stage measurements. Stage-discharge relationships were established at each site by taking frequent (at least daily) manual discharge measurements.

Manual discharges were determined by averaging five consecutive discharge measurements. Discharges were derived by collecting the water leaving the flume over timed intervals. Depending on the discharge, water was collected for between 5 and 10 seconds, except during peak flows at site A3 when the largest collector would fill in under 5 seconds. The standard deviation of the five samples was low, e.g. 1% at 36.6 mL/s at plot B3 and 1.5% at 1286 mL/s at A3.

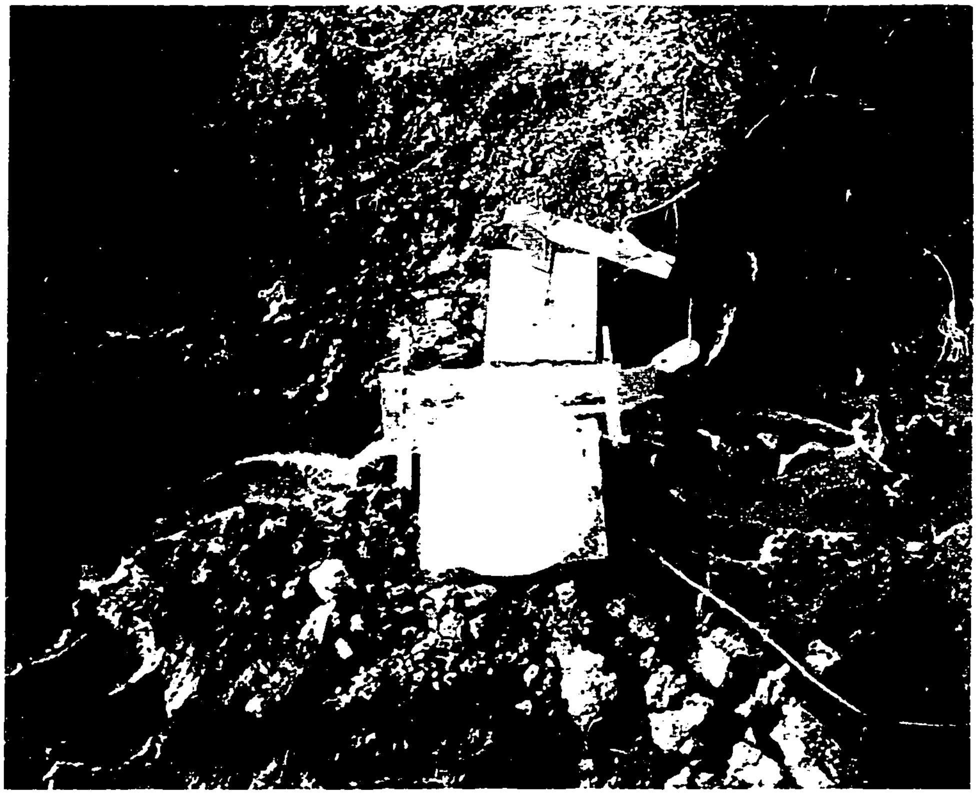

Figure 3-1: Flume and stilling well, site B2.

Tests of the potentiometeric water level recorders in the laboratory prior to fieldwork indicated a slight hysteretic effect. Hysteresis can be attributed to friction in the potentiometer, and to systematic float error, resulting in rising water levels being registered too low, and falling water levels being registered too high (Bos et al., 1984). These errors were partially overcome by enlarging the float diameter to decrease float error, and increasing the radius of the float wheel to reduce friction. In laboratory tests, the potentiometeric water level recorders recorded stage fluctuations to a precision of better than 0.5 mm. Hysteresis was observed, but maximum float lags were certainly < 2 mm. According to the stage discharge relationships for the 1.5 L/s sized flume, a 0.5 mm change in water level represents a 4.9 ml/s change in discharge at low flow, and a 29 ml/s change in discharge at maximum flow (Bos et al., 1984). The systematic error related to this hysteresis should not have a significant influence on the final hydrographs.

During early melt, icing of the flume resulted in some anomalous data-logger readings. Times of flow cessation and recharge were carefully documented. The removal of ice from both the flume and stilling well prior to morning recharge, ensured that correct stage values were recorded when flow resumed. Lags in stage fluctuations could also be due to sedimentation of flumes. The removal of sediment from flumes (particularly at fresh detachment scar sites) was a concern throughout the runoff season. Significant changes in stage discharge relationships during the melt season were noted at some sites. This is probably due to settlement of the ground underlying the flume-stilling well apparatus. All of these events were thoroughly documented and referred to when establishing the stage-discharge relationships and during construction of the discharge hydrographs.

A maximum of four separate stage-discharge relationships were established for each study plot. Anomalous data points (indicated for example, by a sudden rise in stage at 0100h) due to icing or sedimentation of the flume, or due to the plugging of the conduit connecting the stilling well and the flume, were discarded from the stage-discharge relationships. The graphs and regression summaries are presented in Appendix A-2. Because polynomial equations were used to describe the relationships, extremely low stage values would result in the predicted rise in discharge. Consequently, predicted flows that increased under decreasing stage levels were assumed to be 0 mL/s. If this applied to a particular stage-discharge relationship, the stage value below which zero discharge was assumed is noted in Appendix A-2.

3.2.2 – Surface Flow Hydrographs

Using the continuous stage records and the stage-discharge relationships described in the previous section, continuous records of surface flow discharge were developed for each of the plots. Hydrograph fluctuations were compared with those of nearby plots and carefully analyzed with reference to net radiation over snow, temperature, precipitation and field notes to identify anomalous stage readings. Some examples of hydrograph corrections are given in Appendix A-3. In cases where the stage was incorrect due to sedimentation or icing of the flume the discharge was interpolated between two known (manually measured) data points (see Appendix A-3). During flow recession the occasional sticking of potentiometeric water level recorders would result in anomalous hydrographs. Under such circumstances the discharges were again corrected by connecting two known data points. The modification of hydrographs in these situations probably resulted in the underprediction of discharge.

Rainfall recharge data for A2 and B1 are incomplete due to sedimentation of these flumes. Solely for the purpose of determining sediment loads, runoff was estimated by establishing a relationship between instantaneous samples at these two sites with values from nearby sites, A3 or B2 respectively (Appendix A-4). The continuous discharge record at the nearby site was then used to predict runoff during the rainfall events.

3.3 – Sediment Measurement Techniques

3.3.1 – Suspended Sediment

Samples for suspended sediment were collected between two to six times daily in order to establish site-specific relationships between suspended sediment concentration and discharge so that sediment loads could be predicted. The sample size ranged between 150 and 300 ml. During peak sediment periods at plots with higher suspended sediment concentrations, smaller samples were collected as the quantity of sediment exceeded the capacity of the filtering method.

The procedure for analyzing the suspended sediment and solute concentrations of the melted snow and surface wash samples were identical. Samples containing high concentrations of suspended sediment were first filtered through a pre-weighed (in the laboratory) 125 mmØ Whatman Qualitative filters using an Østrem filter pump. Each sample was then emptied into a Gelman filtering apparatus, and filtered through pre-weighed (in the laboratory) 2.7 μm Whatman GF/D then 1.2 μm Whatman GF/C glass fiber filters, using a Nalgene hand vacuum pump. All particles which passed through the 1.2 μm filter were assumed to be in solution. These filters were placed in petri dishes, labeled and packaged, for laboratory analysis at the University of Ottawa. The filtrate was then emptied into a graduated cylinder, and its volume recorded.

Upon return to Ottawa, sediment samples were placed in a freezer until analysis of suspended sediment could be conducted. Each sediment sample was placed in a pre-weighed foil boat, and dried for six hours in a gravimeteric oven at 105 ^{0}C. After being removed from the oven, samples were immediately placed in a desiccator and weighed on a Mettler AB 204 precision scale accurate to four decimal places.

Suspended sediment concentrations were calculated by dividing the total weight of sediment in each sample by the volume of the filtrate.

SSC = [(dry weight + foil boats) – filter weight – foil boats] / sample volume

Potential error associated with this methodology involves changes in the volume of the pre-filtered sample to that of the filtrate. Volumetric change may occur due to water retention by the filter. However, water loss is minimal because this process involves water being drawn through the filter under vacuum. The removal of sediment from the sample could reduce the volume of the filtrate. The average amount of sediment is 0.97 g per 100 ml sample for site B1. Assuming that the sediment has a density of 2.5 g/cm^3, the volume of the filtrate would be reduced by 0.39 %. The largest volumetric decrease calculated for site B1 is 3.2%. The sediment concentrations at vegetated sites are two orders of magnitude less than those at site B1. The removal of sediment from the pre-filtered samples would not yield a detectable change in the volume of the filtrate.

3.3.2 - Predicting Suspended Sediment Loads

The determination of suspended sediment loads required that relationships be established between discharge and suspended sediment concentrations. The graph of concentration versus discharge usually plots as a straight line on logarithmic coordinates and therefore conforms to the equation $C = aQ^b$ (Gregory and Walling, 1973). Given the large degree of seasonal variability in sediment production (see Section 5.1.1.2), an accurate estimate of suspended sediment load required a breakdown of the runoff season at each plot into separate flow periods (see Section 5.1.3 and for regression summaries Appendix C-4). The flow season was separated into a maximum of four different periods of transport: early melt, main melt, recession flow, and rainfall. The "early melt" and "late melt" periods were restricted to times prior to and after main melt (peak discharge period) where peak diurnal discharges were half of the peak discharge during main melt. If the r^2 value was not significantly improved by separating the flow season, then two or more consecutive flow periods were combined together.

Linear relationships were initially established but were replaced by polynomial functions if the r^2 value improved by better than 0.05. Where polynomial equations were used to describe the discharge-suspended sediment relationships ("rain" at A3, "early main" at B1 and the entire runoff period at B3), extremely low flows often resulted in a predicted increase in suspended sediment concentrations. The discharge at which minimum predicted suspended sediment concentration occurred was established and then a constant minimum suspended sediment concentration was applied to any lower discharges. The total amount of sediment transported at these low discharges is negligible.

3.3.3 – Niveo-Aeolian Inputs

Average sediment and solute concentrations were combined and multiplied by the total water equivalents of each plot to determine niveo-aeolian inputs. For the niveo-aeolian concentrations see Appendix C-5.

3.3.4 - Dissolved Solids

Dissolved solid concentrations are directly related to electrical conductivity measurements (Gregory and Walling, 1973; Stone et al., 1993). Conductivity probes constructed using the design of Stone et al. (1993) were installed immediately upslope of the flumes. The probes were connected to the data loggers, thus providing a continuous record of surface wash conductivity. Conductivity probe pools were carefully monitored and frequently dredged to prevent burial of the stainless steel pins. Conductivity and water temperature measurements using a hand held digital YSI conductivity probe (Model 30) were taken at regular intervals to calibrate the individual conductivity probes. The filtrate conductivity of suspended sediment samples was also measured. The temperature (^{0}C) and conductivity (μS/cm) of the filtrate were measured using the YSI conductivity meter. Three samples of filtrate were kept from each site: one from the early melt period, one from the peak melt period and one from late melt. One third of each sample was used to calculate the conductivity correction factor (see Step 1, this section). One third was evaporated so that total dissolved solid concentrations could be determined and a relationship could be established between dissolved load and conductivity (see Step 7 and Section 5.2) so that dissolved load could be predicted. The last third of each sample was sent for basic water chemistry analyses.

In the field the YSI conductivity probe provided the measurement of water temperature and conductivity corrected to 25°C using a built-in temperature correction factor (*a* constant) of 1.91%/°C. This posed some difficulties as the required measurements of the filtered samples were water temperature and conductivity at the sampled temperature, with the intention of correcting conductivity to 25°C with the *a* constant derived in the lab using the water samples returned from the field. As a result several steps were required to correct the values measured in the field so that the conductivity probes could be calibrated.

Establishing a relationship between data logger conductivity values and on site conductivity required that the latter be converted to conductivity at site temperature. To achieve this the conductivity of the filtrate was converted to conductivity at site temperature using laboratory calculated a values. This required undertaking the following steps which are described in detail below and can be followed along in Table 3-1: (1) The calculation of an a constant for each site (Appendix A-5), (2) the conversion of the filtrate conductivity at 25°C to the conductivity at the sampled temperature, (3) the development of a continuous runoff water temperature record (Figure 3-2 and Appendix A-6) so that (4) the conductivity at sampled temperature could be converted to the conductivity at site temperature using the calculated a value (1), and (5) the establishment of a relationship between conductivity at site temperature and data logger conductivity probe values so that a continuous record of non-temperature corrected conductivity could be developed (Figure 3-3 and Appendix A-7). After this the continuous conductivity was corrected to 25°C (6) using the calculated a values (1) and the continuous temperature record (3), and (7) finally the relationship established between dissolved solid concentrations and conductivity (see Section 5.2) was applied to the temperature corrected conductivity so that solute concentrations could be predicted.

Table 3-1: Conductivity conversions for site B2.

	Sample	filtered sample at 25 °C (LR)	temperature at the time of sampling (°C) (t)	Conductivity at the sampled temperature (see Step 2) Lst = LR*(1+1.91(t-R))	On site water temperature (see Step 3 and Fig. 3-2) (°C)	Air temperature (°C) (t2)	Predicted and measured on site water temperature (°C) (R2)	Conductivity corrected to on site water temperature using calculated a value (see Step 4) Lst2=Lst*(1+a(t2-R2))	Data logger values (see Step 5 and Fig. 3-3)
1	6091315	244.1	4.1	146.7			2.2	141.9207	64
2	1820	320.6	4.6	195.7			1.85	186.5333	30.72
3	6101200	556	7.2	367.0	2.3	0.98	2.3	336.4024	20.96
4	1702	386.5	7.2	255.1			2.4	234.2818	52.42
5	1919	294.7	6.5	190.6	3.02	0.17	3.02	179.3018	54.58
6	6110001	294.5	3.1	171.3			1.3	166.0714	60.72
7	845	438.6	6.2	281.1			1.27	257.5479	48.69
8	1645	451.6	4.9	278.2			1.45	261.9083	46.52
9	2206	526	3.2	307.0	0.7	-1.46	0.7	293.9373	48.91
10	6121047	413.8	6.8	270.0			1.63	246.2285	41.07
11	1714	422.9	6.3	271.9			1.8	251.0561	45.5
12	1935	420.5	6.8	274.3			1.7	250.5417	45.51
13	6130020	421.2	4.4	255.5	0.4	-2.1	0.4	238.1024	55.56
14	1115	412.3	7.1	271.3	3.6	0.98	3.6	255.1941	42.62
15	1232	488.7	6.5	316.0			2.1	292.3797	45.85
16	1608	400.6	3.4	235.3			1.9	229.3276	55.66
17	2042	416.4	5.1	258.1	1.5	0.17	1.5	242.3329	49.32
18	2123	509	4.8	312.6			1.79	296.621	49.87
19	6141112	419	6.6	271.7			2.7	253.7298	43.43
20	1301	486.4	6	309.9			2.85	293.2911	46.84
21	1746	390.6	6.3	251.1			2.9	236.5764	60.2
22	2010	367.1	7.4	243.7	1.9	2.59	1.9	220.9101	61.62
23	2310	394.2	8.6	270.7			3	244.9482	58.24
24	6150035	359.4	8.6	246.8			2.7	222.0653	59.66

	Sample	filtered sample at 25 °C	temperature at the time of sampling (°C)	Conductivity at the sampled temperature (see Step 2)	On site water temperature (see Step 3 and Fig. 3.1-2) (°C)	Air temperature (°C)	Predicted and measured on site water temperature (°C)	Conductivity corrected to on site water temperature using calculated a value	Data logger values (see Step 5)
		(LR)	(t)	Lst = LR*(1+1.91(t-R))		(t2)	(R2)	Lst2=Lst*(1+a(t2-R2))	
25	757	361.6	8.4	247.0			3.3	225.5404	49.65
26	931	390.1	7.2	257.5			4.1	243.9049	48.23
27	1721	308.9	6.4	199.2			4.7	193.4045	72.6
28	1925	359.9	8.5	246.5			3.8	226.784	66.71
29	6161149	395.5	8.3	269.3	3.7	4.14	3.7	248.2844	59.79
30	1654	405.9	6.3	260.9			4.1	251.1661	48.43
31	2223	646	6.6	419.0	1.8	2.59	1.8	384.7818	36.22
32	6170749	307.9	10.5	222.6			2.9	193.8637	56.01
33	1526	352.4	10	251.4	5.2	6.04	5.2	230.9201	49.16
34	2034	392.8	8.1	266.0			7.2	261.9382	42.14
35	6180020	437.8	11.8	327.4	3.8	4.89	3.8	282.8925	41.09
36	1134	560	11.8	418.8	7.2	6.39	7.2	386.0616	34.03
37	1741	476.9	10.8	347.6			8.8	335.7383	34.46
38	2045	559	8.8	386.0	7.5	6.78	7.5	377.5029	29.25
39	6190250	757	10.2	543.0	5.1	4.14	5.1	495.9322	29.55
40	1358	1250	11.5	927.7			8.7	883.5296	19.47
41	1815	1392	9.4	977.2	9.9	7.9	9.9	985.5462	16.06
42	6241155	3230	8.1	2187.4	4.4	4.53	4.4	2049.802	8.42
43	1627	3771	6.5	2438.5			5.4	2392.917	7.36
44	6251155	3952	3.9	2359.3	3.9	2.59	3.9	2359.304	8.39
45	1555	4200	4.2	2531.4	4.8	1.38	4.8	2557.245	7.25
46	6272230	3814	5.8	2415.3			4.2	2349.633	7.5

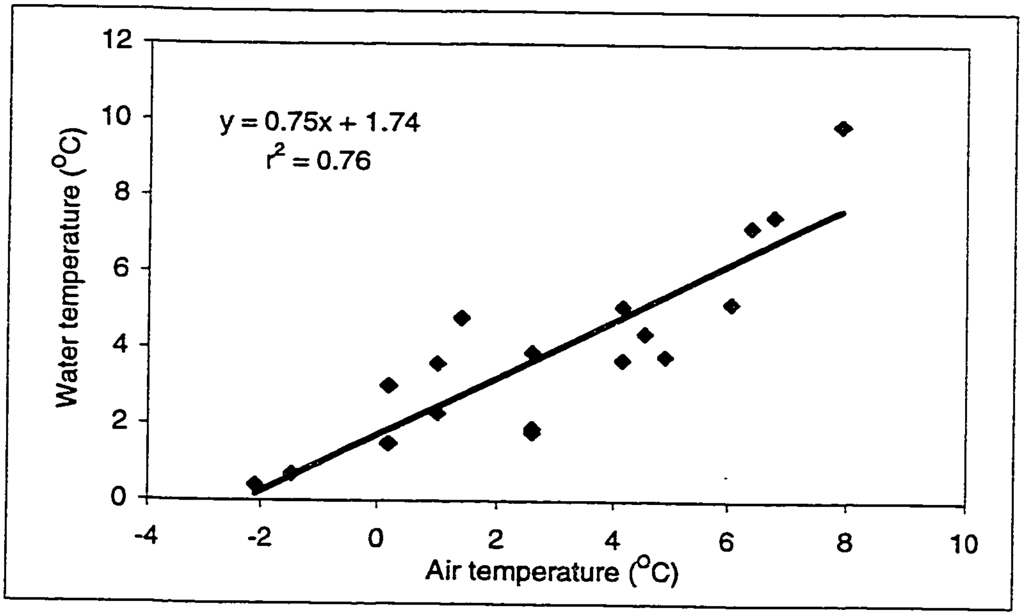

Figure 3-2: Air temperature - on site water temperature relationship.

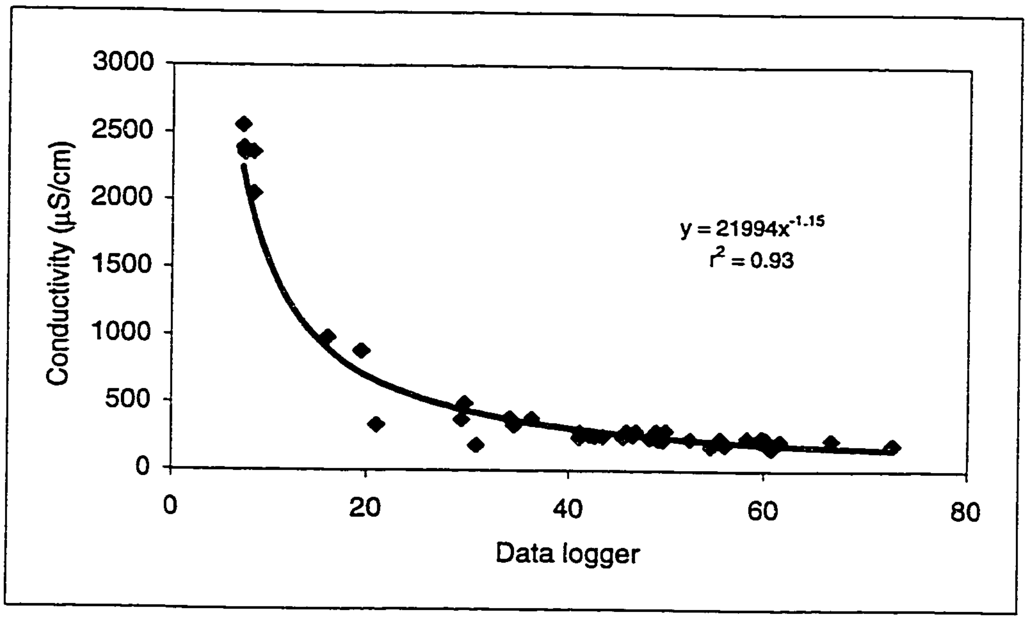

Figure 3-3: Relationship between data logger values and temperature corrected on site conductivity.

Step 1.

Rather than using the YSI a value of 1.91%/°C, a temperature coefficient was derived for each site. In the laboratory at the University of Ottawa, the three 20 ml samples of filtrate from each site were cooled and then warmed to 25 ^{0}C with the temperature and conductivity read at frequent intervals. The temperature coefficient a was calculated using the following equation (Gardiner and Dackombe, 1983):

$$a = (Lt2 - Lt1) / ((Lt1(t2-R) - Lt2(t1-R))$$

where:

$Lt1$ is the conductivity at temperature 1 $(t1)$

$Lt2$ is the conductivity at the temperature 2 $(t2)$ which is determined during the experiment

R is the reference temperature of 25 ^{0}C.

An average a value was determined for three samples from each site (Appendix A-5).

Step 2.

Using the programmed YSI temperature coefficient (1.91%/°C) the temperature corrected conductivity measurements made in the field were converted to the conductivity at the sampled temperature using:

$$Ls_t = LR * (1+(a/100))(t - R)$$

where:

Ls_t = conductivity at sampled temperature

LR = conductivity at reference temperature (25 ^{0}C)

t = sample temperature

a = YSI temperature coefficient (1.91)

R = reference temperature

Step 3.

The next step required that the conductivity at sampled temperature (Ls_t) be converted to the conductivity at site temperature using the a coefficients calculated for individual sites (see Step 1). A continuous record of water temperatures had to be developed for each plot so that on-site water temperatures at the time of sampling could be predicted. Several on-site water temperature measurements were made during the runoff season. Linear relationships were established between air temperature or net radiation and water temperature measurements (Figure 3-2 and Appendix A-6). Rapid fluctuations in temperature or net radiation are not closely mirrored by water temperatures and occasionally result in highly anamolous data points. A few extreme outliers were omitted from the relationships. The continuous air temperature or net radiation records were then used to predict water temperatures.

Step 4.

Ls_t was converted to the conductivity at the site temperature using the calculated a values and the measured or predicted site temperatures using:

$$Lst2 = Lst * (1 + (a/100))\ (t - R)$$

where:

$Lst2$ = conductivity at site temperature

Lst = conductivity at sampled temperature

a = temperature coefficient (see Step 1)

t = predicted or measured (if available) on site water temperature

R = reference temperature – sample temperate (see Step 3)

Step 5.

The conductivities converted to site temperature were plotted against the data logger conductivity values. The relationships between data logger values and on site conductivity measurements are best described by power functions (see Figure 3-3) (Appendix A-7). These equations were applied to the continuous conductivity records so that continuous records of non-temperature corrected conductivity could be developed.

Step 6.

The continuous conductivity records were standardized to 25°C using:

$$LR = LT / [1 + (a/100))(t - R))]$$

where:

LR = the conductivity at the reference temperature,

LT = the conductivity at the sample temperature,

a = temperature coefficient (see Step 1)

t = predicted on site water temperature (see Step 3)

R = reference temperature (25^0C)

Step 7.

To convert conductivity in µS/cm to a concentration in mg/L, 30 to 50 mL of each water sample was evaporated, and the precipitate weighed after cooling. A linear regression through the origin was established by plotting the sample conductivity at 25°C vs. the dry weight of the precipitate (mg/L). This yielded the equation:

$y = 0.60x$ (see Section 5.2 and Figure 5-36)

The equation was then applied to the temperature corrected continuous conductivity records so that solute concentrations could be predicted and the total dissolved load could be determined.

Major chemical components present in surface wash at each plot were determined by analyzing the remaining sample. The analyses were performed by John Loop at the Ottawa Carleton Geoscience Centre Geochemistry Laboratory. Using a Atomscan 25 Inductively coupled plasma – atomic emission spectrometer water samples were tested for anions (F^-, Cl^-, NO_2^-, Br^-, NO_3^-, HPO_4^{--}, SO_4^{--}) and cations (Al^{+++}, Ba^{++}, Ca^{++}, Fe^{++}, K^+, Li^+, Mg^{++}, Mn^{++}, Na^+, Sr^{++}). The three samples from each site were collected during the early, peak and late melt periods so that changes in the relative proportions of dissolved ionic constituents could be identified. Due to the small amount of sample, bicarbonates were determined by a balance equation, and alkalinity measurements were completely restricted.

3.3.5 - Sorbed Ions

The methodology used to investigate sorbed cations was derived from Lorrain and Souchez (1972). Several suspended sediment samples were retained after being processed. Suspended particles collected on the filters were treated with a 1N acetate ammonium solution (pH7). Each filter was soaked in the solution, then placed in the filtering apparatus and washed three times with a small volume of acetate ammonium. The solution was then refiltered through a 1.2 μm Whatman GF/C glass fiber filter, using a Nalgene hand vacuum pump. The volume of the solution was recorded and then poured into a clean polyethylene bottle and latter sent to the geochemistry lab for geochemical analysis.

The results from the lab were presented as cation concentrations (mg/L) in the exchanger solution and were converted into mg/sample volume so that the sorbed ion concentration could be compared to the suspended sediment concentrations of the respective samples.

3.3.6 - Sediment Yields and Denudation Rates

Suspended sediment loads were determined using the continuous discharge records, and the relationships established between suspended sediment concentrations and discharge. The total solute load was calculated using the continuous record of solute concentrations and the continuous discharge record. Surface lowering of the slopes was calculated by adding up total sediment loads and dividing the specific yield by the dry bulk density for surface sediments of 1.1 Mg/m^3 from Lewkowicz (1998).

3.4 – Grain-Size Analysis and Loss on Ignition

3.4.1 – Surface Samples

At least two surface grab sediment samples were collected from each plot for grain-size analysis. The samples were oven dried for 12 hours and weighed after cooling in a dessicator. Particle distributions were determined by wet sieving the sample through a stack that was nested from coarse to fine. The –1, 0, 1, 2, 3, and 4ϕ sieves were used for the wet sieving. The sediment retained on each sieve and in the bottom pan (<63 μm) were washed into separate pre-weighed beakers and placed in a VWR convection oven at

105 ^{0}C for 24 hours. The retained portion of the sample on each sieve was weighed on a Mettler AB 204 precision scale accurate to four decimal places. The weights were recorded and the cumulative weights calculated.

Any particles smaller than 4 ϕ (63 μm) were retained for further analysis using a Granulometre 820 Particle Size Analyzer (P.S.A.). The residual (<63μm) was rehydrated with deionized water and a dispersant ($Na_4P_2O_7$) was added. Each sample was placed in a mixer just prior to being run, and subsampled using a pipette. The subsample was added to a small pool of deionized water contained within the P.S.A.. The concentration of sample in the holding pool ranged between 50 and 400 PPM and was treated by ultrasound for 15 seconds prior to running the analysis. Each sample was run with the particle size analyzer set at range 1 to achieve highest resolution (to measure between .1 and 63 μm). The results were compiled as grain-size percentages and as cumulative percentages. The resolution of the analyzer decreases logarithmically towards the larger grain-sizes. Each sample was run a second time to verify the results which were presented as a summary table and a graph. The grain-size percentages were applied to the known weight of the residual (<63 μm) so that a distribution by weight could be determined. The P.S.A data was then combined with the wet sieving results and plotted on a cumulative curve.

Prior to the grain-size analysis, each sample was subsampled and loss on ignition was performed to evaluate coal proportions. Each subsample (about 5 g) was placed in a pre-weighed ceramic crucible, dried in the gravimeteric oven for 6 hours and then placed in a dessicator to cool. The samples were weighed and burned in a Pyradia furnace for 6 hours at 500°C. The samples were allowed to cool, placed in a desiccator and then reweighed on the Mettler AB 204 precision scale. The samples were then replaced in the furnace and burned at 500°C for an additional 2 hours after which time they were reweighed. There was no significant difference in the weights of the samples after the additional 2 hour bake so it was concluded that six hours in the furnace at 500°C was sufficient to remove coal from the sediment samples.

Loss on ignition was calculated by subtracting the final weight of the sample from the pre-burn weight and then dividing this value by the pre-burn weight to obtain a percentage value.

3.4.2 – Suspended Sediment Samples

The methodology for particle size analysis of suspended sediment samples was modified because qualitative observations suggested that a significant portion of the sediment load consisted of coal. Conventional methods involve filtration of sediment through ashless filter papers. The filters are later burned off so that grain-size analysis can be performed on the residual sediment. This technique was not appropriate for two reasons: (1) the ashless filter papers were very inefficient at filtering samples with large sediment loads, and (1) the process of ashing the filter paper would destroy the coal portion of the sample. An alternative method for grain-size analysis of suspended sediment samples with large coal proportions was developed.

The goals of the analysis are: (1) To determine particle size distributions so that suspended sediment and surface sample grain-size distributions can be compared, and (2) to determine the proportion and distribution of coal within the suspended sediment samples. The second goal is not central to the thesis, but could provide valuable information if an analysis of fluvial energy environments were to be pursued.

Due to the exploratory nature of the suspended sediment analysis, a limited number of samples (16) were processed. Suspended sediment samples collected to determine sediment concentrations were retained and used for the grain-size analysis. The 125 mmϕ Whatman Qualitative filters were soaked in deionized water, carefully sprayed with deionized water and then backfiltered through an Østrem filter pump. The GF/C and GF/D glass fibre filters were more delicate and had to be treated carefully to ensure that the filter fibre would not break apart and be washed in with the sediment. The filters were soaked and individually back washed through the Gelman filter apparatus using a Nalgene hand pump. All of the water and sediment was retained in a pre-weighed beaker. The samples were evaporated and weighed so that the proportion of the total sample retained could be determined. If the samples were large enough they were divided in two so that loss on ignition could be performed on one half and grain-size analysis could be performed on the other. The procedure for loss on ignition was identical to the methodology outlined for the surface sediment samples (3.4.1).

Only a very small amount of sample is required for particle size analysis using the P.S.A. The presence of larger coal clasts in the suspended sediment samples were probably beyond the resolution of the P.S.A. so if the sample was large enough, prior to analysis it was wet sieved through a 150 μm membrane to determine the proportion of larger grain-sizes. The sediment retained by the membrane was washed into a pre-weighed beaker, evaporated, weighed and then replaced into the sample. After all of the wet sieving was completed the samples were placed into labeled vials and a small amount of dispersing agent ($Na_4P_2O_7$) was added to the hydrate.

For the analysis of suspended sediment samples the P.S.A. was set at range 2 for the evaluation of particle sizes from 1 to 200 μm. After analysis the remaining sample was replaced into the vial and all samples were returned to the Geography Laboratory where they were centrifuged so that the dispersant could be extracted. The samples were dried and placed into pre-weighed crucibles, weighed, then baked in the furnace for 6 hours at 500°C to burn off the coal. After baking the samples were reweighed, hydrated and once again filtered to determine the portion of uncoaled sample > 150μm. The decoaled samples completely passed through the membrane. Dispersant was added to the samples and they were returned to the NRC where each sample was rerun through the P.S.A..

Using the cumulative curve and phi scale of grain sizes (Folk 1974), the graphical median, mean, standard deviation (sorting) and skewness of each distribution (surface and suspended sediment samples) was calculated. The graphical method was used such that:

(1) $M\phi = \phi_{50}$

(2) $M_Z\phi = (\phi_{16} + \phi_{50} + \phi_{84})/3$

(3) $\sigma_G\phi = [(\phi_{84} - \phi_{16})/4] + [(\phi_{95} - \phi_5)/6.6]$

(4) $SK_G = [\phi_{84} + \phi_{16} - 2*\phi_{50})/ 2(\phi_{84} - \phi_{16})] + [\phi_{95} + \phi_5 + 2*\phi_{50})/ 2(\phi_{95} - \phi_5)]$

where the subscripts are percentile values read from the cumulative frequency graph in phi units. $M\phi$ is the graphic median, $M_Z\phi$ is the graphic mean, $\sigma_G\phi$ is the graphic standard deviation (sorting), and SK_G is the inclusive graphic skewness.

3.5 - Soil Analysis

3.5.1 - Soil Geochemistry

In 1997 five soil pits were dug to compare soil geochemistry of the active layer at a fresh detachment slide scar (A1), an adjacent undisturbed slope (adjacent to A1), a pre-1950 detachment slide scar (B2) and on vegetated undisturbed slopes (A3, B3). Soil pits were described visually, and samples (about 100 g) were collected at 10 cm intervals. The samples were bagged, returned to Ottawa and placed in a freezer until the geochemical analysis could be performed.

The methodology by Kalra and Maynard (1991) was adopted to perform a cation exchange on soil samples collected in 1997. Each sample was dried for 12 hrs at 105^0C, and then 20 g subsamples (individual weights were recorded) were placed into Erlenmeyer flasks. 100 mL of 1N ammonium acetate solution with a pH of 7 was added to each flask. The flasks were placed in a shaker for 30 minutes then placed on a table allowing the sediment to settle. The solution was poured off and filtered through a 1.2 μm filter using a Gelman filter apparatus with a Nalgene hand held vacuum pump. The solution was retained and sent to the geochemistry lab for analysis.

The geochemistry results were presented as a concentration in the cation exchange solution. These results were converted into g of individual ion/kg of soil (Appendix C-6).

3.5.2 - Soil Moisture Samples

Moisture content samples were collected on five slopes (A1, an adjacent undisturbed slope, A3, B2 and B3) 48 hrs after a record rainfall in August 1997. Samples were obtained at 8 cm depth intervals using a soil moisture corer. Each sample was bagged and weighed in the field and then reweighed in the laboratory to determine the amount of moisture lost since the initial weighing. They were placed in preweighed crucibles, weighed and then dried for 12 hours at 105 ^{0}C. The samples were placed in a desiccator and allowed to cool, then each sample was reweighed and the weight recorded. Soil moisture contents were obtained with the following calculation:

$$\text{Moisture content} = \frac{(A-B) + (D-E)}{(E-C)} * 100$$

where A = initial sample weight in the field

B = reweigh of the sample in the laboratory

C = crucible weight

D = weight of sample in crucible before baking

E = weight of sample in crucible after baking

3.5.3 – Infiltration Experiments

Double ring infiltrometer experiments were conducted to compare rates of infiltration between the surface soils on fresh detachment slide scars and on adjacent vegetated slopes. The rates of infiltration were obtained by measuring the rate at which water had to be added to the inner ring of the infiltrometer to maintain a constant head of water. This was done while maintaining a constant head in between the inner and outer ring which acted as a buffer to prevent the lateral movement of soil water from the inner ring (Dingman, 1984).

3.7 – Vegetation and Topographic Survey

After runoff had ceased and the slopes had dried, vegetation surveys of the plots were conducted to evaluate percentage vegetation cover and vegetation type. Percentage cover was measured using line-transect and quadrat methods (Wein and Rencz, 1976). At each plot, four to six transects (depending upon plot size) were established parallel to the contours. The transects were numbered from the base of the slope to the top. Evaluation of percentage vegetation cover involved 50 cm by 50 cm quadrat inventories at 2 m intervals along each of the transects. Evaluations were based on a qualitative visual estimate of percentage of vegetation cover within the quadrat (Goldsmith and Harrison, 1976). At the same time, percentage cover by species was also evaluated using the same sampling technique. Species were keyed out using the text "Illustrated Flora of the Canadian Arctic Archipelago" by Porsild (1957). Later in the summer a Nikon NE-10LA Digital Theodolite was used to conduct detailed topographic surveys of each study plot. The location of snow and vegetation transects were also recorded to provide a spatial context in which to place these data.

Chapter 4 – Hydrology

4.1 – Snow Depths

Average snow depths among the plots varied from 4 cm at A5 (bare undisturbed slope) to 40 cm at A1 (1988 detachment slide scar) in 1996 (Figure 4-1). In detachment scars, snow thickness was generally greatest in the centre of the upper part of the scar, decreasing towards the perimeter and was very thin around the natural berms which demarcate the edge of the slide (Figure 4-2). The expected relationship between snow depths and freshness of scar was present at site A, with progressive decrease in snow depths and hence water equivalents from A1 to A2 to A4 to A5. This is due to the decreasing efficiency of the scar to trap snow as the sides become increasingly rounded. However, this pattern was not repeated at site B. In particular, overall accumulation at plot B4 was augmented by a large snowbank with thickness up to 125 cm which extended across the plot. As noted earlier, slopes facing N and NW in the area typically accumulate the greatest amounts of snow (Young et al., 1997). Consequently the snow water equivalent at this plot was greater than that of B1. Plot B3 had a variable snow cover, with an average thickness of 37 cm. At B3, maximum snow depths of 163 cm were measured on a fresh scar near the crest of the slope that was infilled by the same snowbank affecting B4. Both A3 and B3 had highly variable snow depths across their sites (see Figure 4-1), ranging from snowbanks to bare areas. At A3, the upper vegetated plateau had a relatively thin snow cover and some bare patches were present on the unvegetated, undisturbed sections of the main slope. Detachment slide scars, small gullies and a large vegetated north-facing slope were areas of snow accumulation. Despite lower snowfall in 1993, site A1 had an average snow depth of 35 cm.

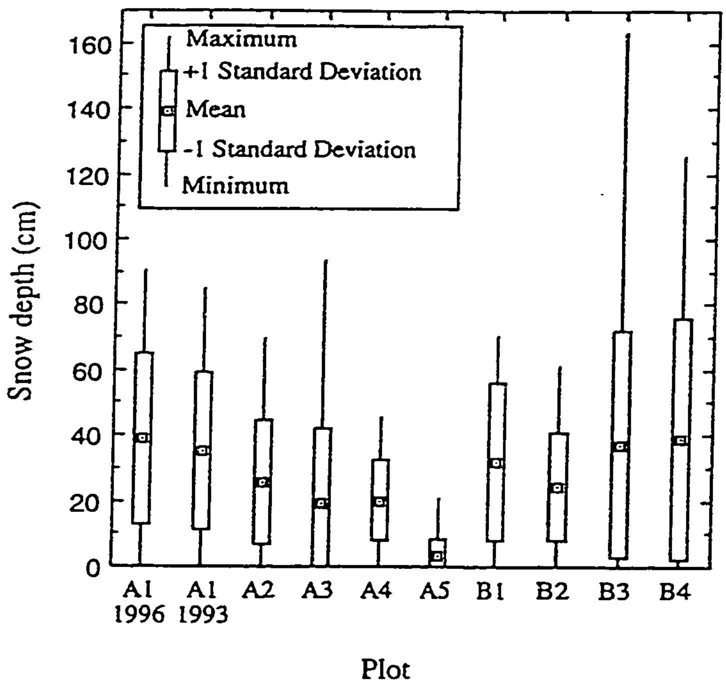

Figure 4-1: Snow depths at runoff plots.

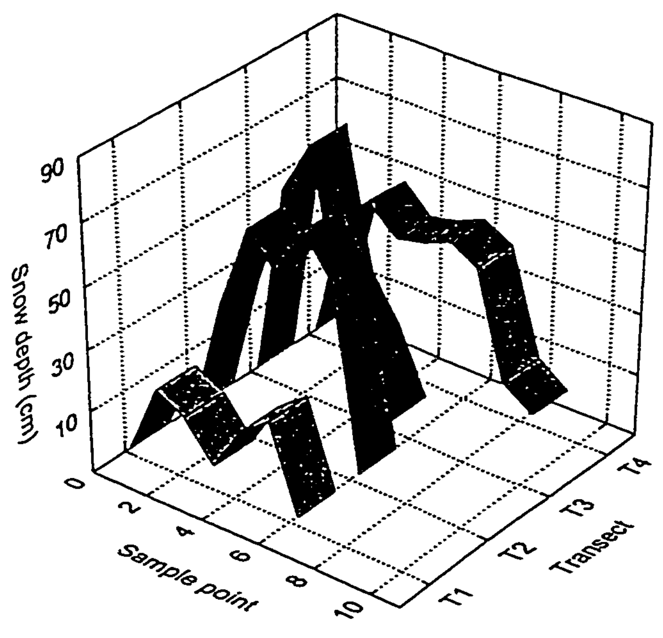

Figure 4-2: Snow depths at site B1.

4.2 – Surface Runoff

4.2.1 – Surface Flow During Snowmelt

Conditions at the runoff plots varied considerably in terms of orientation, snow surface angles, and aeolian dust concentrations. Consequently, the first plots to generate surface flow had one of the thinnest snow packs (A2) and one of the thickest (B4) (Figures 4-3 and 4-4). The last plot to generate flow, B2, did not do so until 6 days after A2. At other sites in the valley, overland flow was generated even earlier than at A2 (visual observations). These locations were all west-facing and exhibited substantial concentrations of aeolian particles. They generated runoff under clear skies at sub-zero temperatures. In 1993, flows were generated at plots A1 and A3 almost 10 days earlier than in 1996 due to warmer spring conditions (see Figure 4-3).

Snowmelt generated surface flow was sustained at the plots for 12-16 days. The pattern of flow during the melt season varied from plot to plot. At site A, plot A2 began to flow on June 5 (Julian day 157), and A1 began flowing on the following day (JD 158) (see Figure 4-3). Surface runoff was sustained for 10 days at A2 and 14 days at A1. Surface flow did not commence at plot A3 until June 9, however a small amount may have left the plot the previous day as throughflow. Snowmelt runoff was sustained at the plot for 16 days. Despite an average snow cover of 20 cm surface flow was not generated at site A4, however surface ponding and throughflow were observed. No flow occurred at site A5. At B sites surface flow commenced on June 06 (JD 158) at B4 where it was sustained for 10 days (Figure 4-4), however flow was limited to periods when solar inputs were intense and long enough in duration to allow water movement through the

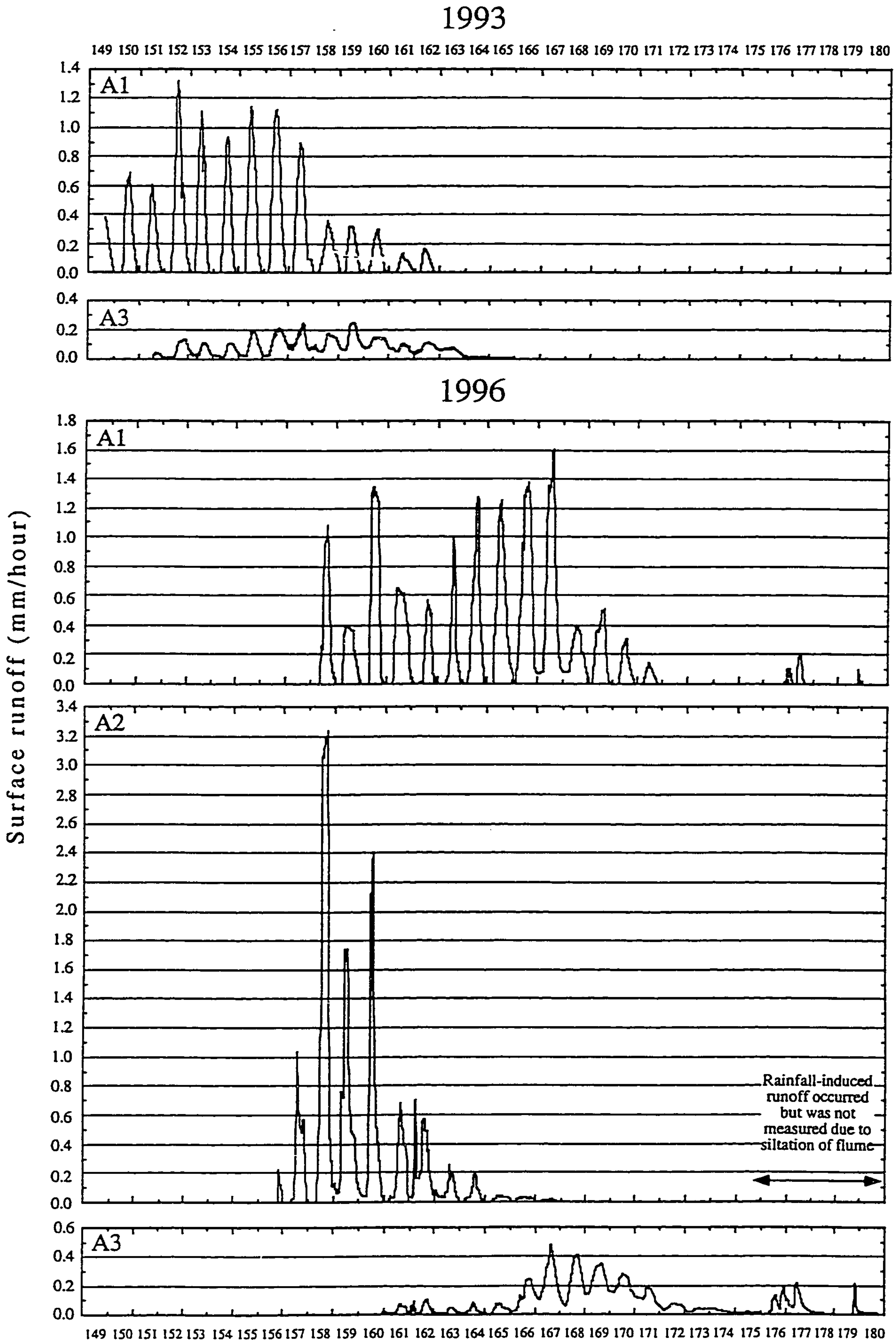

Figure 4-3: Surface runoff measured at site A runoff plots, 1993 and 1996.
Note: no runoff occurred at plots A4 and A5 in 1996.

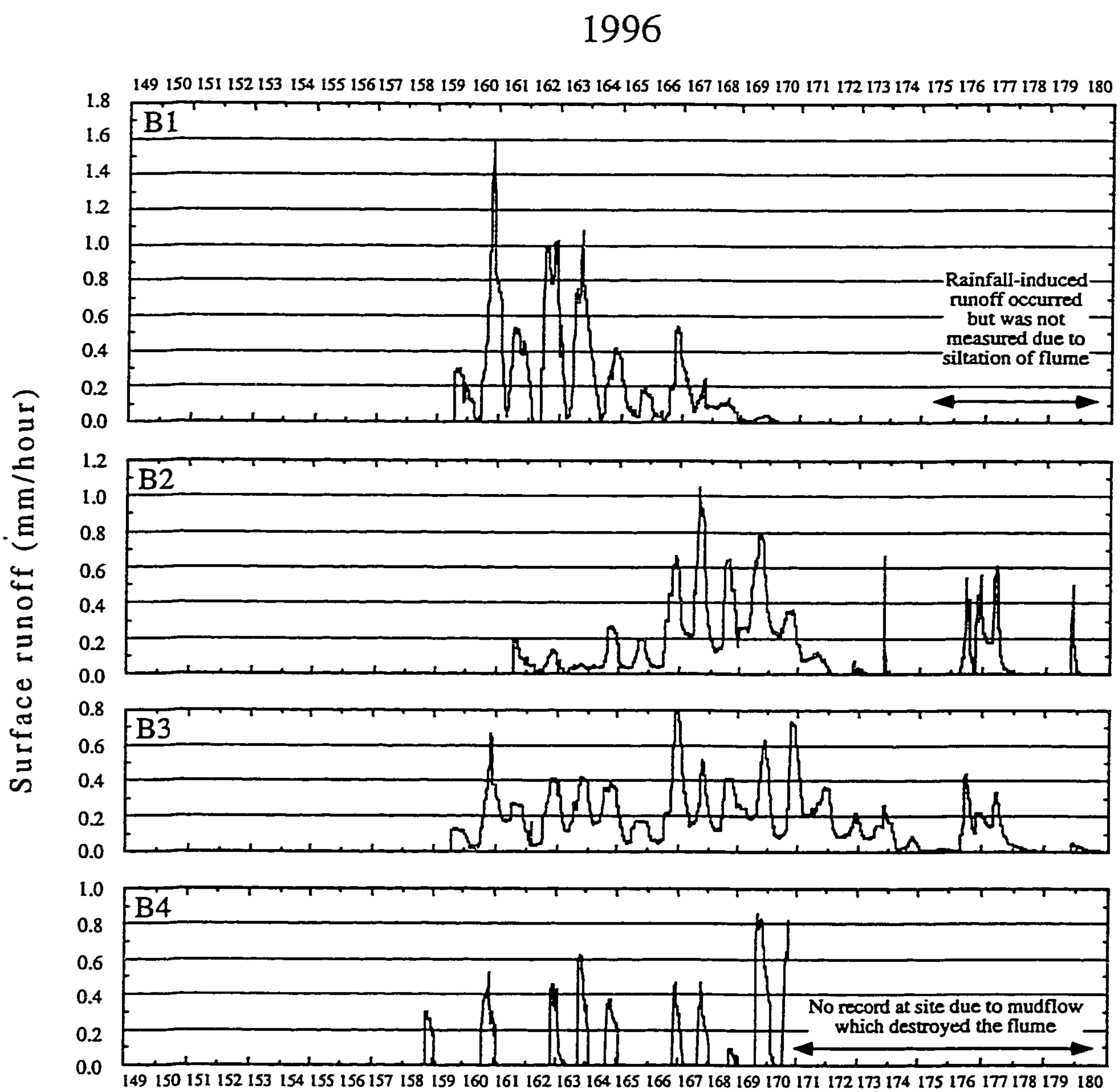

Figure 4-4: Surface runoff measured at site B runoff plots, 1996.

thick snow bank, and down the remainder of the vegetated slope. A mudflow destroyed the flume and stilling well on June 18 (JD 170) at which time only a small snow patch persisted on the plot. Surface flow began at plots B1 and B3 on June 07 (JD 159) and was sustained for 11 and 16 days (see Figures 4-4). At B2 snowmelt runoff commenced on June 10 (JD 162) and was sustained until June 20 (JD 172).

The pattern of flow during melt season varied from plot to plot. For example, a peak flow of 1.6 mm/hr at A1 was experienced 10 days after the start of flow (June 16, JD 168), while peak flow at B1 (1.6 mm/hr) occurred on the second day of flow (June 8, JD 160) after which time flows steadily decreased as the snowbank diminished (see Figures 4-3 and 4-4). Discharges at B3 peaked (0.68 mm/hr) on the seventh day of flow, however peaks of over 0.5 mm/hr were produced on at least four other days during snowmelt. At A3, the largest and most heterogeneous plot, surface flow generated by melt from thin snow in the upper part of the plot lasted for five days and was followed by melt from thicker snow in detachment slide scars and in north facing snowbanks located in the lower section, which produced peak seasonal discharges. The more complex seasonal hydrographs at the larger heterogeneous plots can be attributed to variable contributory areas with differing slope orientations and variable snow thickness that become isothermal at different times during the runoff period.

4.2.2 - Snowmelt Runoff Production

Surface flow was the dominant hydrological loss at the detachment slide plots and at the two mixed plots (Table 4-1). The plots with greater amounts of snow cover produced greater amounts of surface runoff (Figure 4-5). The observations show that in order to produce surface flow, much more snow must be present on vegetated slopes than on unvegetated or partially vegetated ones. A3, with 60 mm of snow produced 35 mm of runoff, while no surface flow occurred at A4 despite 64 mm of snow water equivalent, and B4 with 118 mm of snow produced only about 30 mm of surface runoff before a mudflow destroyed the plot. The runoff coefficient was at B4 was 25% and would have been only slightly greater if the remaining snowmelt had been measured.

A comparison between 1993 and 1996 indicates that snow accumulation and runoff at A1 and A3 were both lower in the earlier year (see Table 4-1). In 1996 plot A1 produced the greatest amount of runoff (102 mm) and had the highest runoff coefficient (81%) during snowmelt runoff (see Table 4-1). The same plot was monitored in 1993 and produced 74.4 mm of runoff with a runoff coefficient of 67%. The hydrographs at A1 followed a similar pattern during the melt season producing peak flows of 1.4 mm/hr in 1993 and 1.6 mm/hr in 1996. The large, heterogeneous plot A3 produced 35.1 mm of runoff with a coefficient of 58% in 1996, but only produced 26.8 mm of runoff in 1993. Peak flow at A3 in 1996 was almost double (0.5 mm/hr) that in 1993. Similarly the maximum rate of snow surface lowering measured with ablatometers was 14.8 mm/hr in 1996, while in 1993 it was 7.6 mm/hr, corresponding to approximately 7.4 and 3.8 mm/hr water equivalent, respectively.

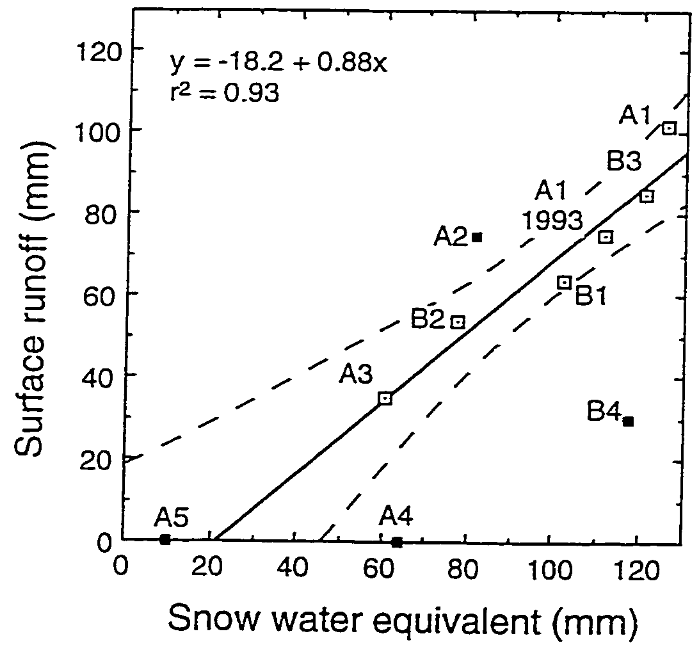

Figure 4-5: Comparison of snow water equivalent and plot surface runoff during snowmelt period. Least-squares regression line is used for detachment slide and mixed plots. Solid points (vegetated plots) not included in regression. A2 was also omitted because of problems defining plot area.

Table 4-1. Runoff Coefficients for Snowmelt.

Site	Snow-water equivalent (mm)	Total runoff (mm)	Runoff coefficient (%)
A1	126	102	81
A2	82	75	*92
A3	60	35	58
A4	64	0	0
A5	10	0	0
B1	102	64	63
B2	78	54	69
B3	120	83	69
B4	118	**30	**26
A1 (1993)	112	75	67
A3 (1993)		27	

* Area contributing runoff to flume varied during melt; potential error in runoff coefficient is estimated to be 10-15%

** B4 was monitored up to June 18 when a small mudslide destroyed the flume and stilling well; remaining snow is unlikely to have increased runoff coefficient by more than 2-3%

Young et al. (1997) measured surface runoff on nearby slopes in 1990. They recorded values of 0.6 $m^3m^{-1}h^{-1}$ on a 44 m long plot which had an average snow depth of 70 cm. This peak value is equivalent to 13.6 mm/hr which is one order of magnitude higher than flows measured for that plot on the following day (1.1 mm/hr) or peak flow values at their other site (1.8 mm/hr). The latter values fall into the range of measurements obtained in this study.

Surface flow hydrographs show diurnal fluctuations in discharge due to changes in snow ablation. Peak flows at site A plots with an easterly orientation typically occurred around 1300 to 1400 h local time. Northwesterly oriented plots at site B experienced peak flows around 2100 h. Discontinuous flow was common at sites A1, A2, B1 and B4 at the beginning of the season when melt rates were low and at the end of runoff when snow banks were reduced in size (see Figures 4-3 and 4-4).

Hydrograph rise and recessions are relatively steep for detachment slide plots (Figures 4-6). The elongated shape, uniform orientation and steeper slope angles of many of the detachment slide scars, create stronger diurnal changes in insolation onto the plot. Moreover, snow depths are more uniform so that high flux melt waves are likely to arrive simultaneously at the saturated zone at the base of the snow. Plots containing source areas of different orientations and terrain types such as A3 and B3 have greater variability in snow depths, and produce smoother hydrographs with lower peaks and gently rising and falling limbs (see Figure 4-6).

Hydrograph responses to small scale fluctuations in net radiation were compared at the B sites. Discharge responses to radiation spikes at B3 lagged behind both B1 and B2 by 15 minutes or more (Figure 4-7). Hydrograph response at B4 exhibited an even

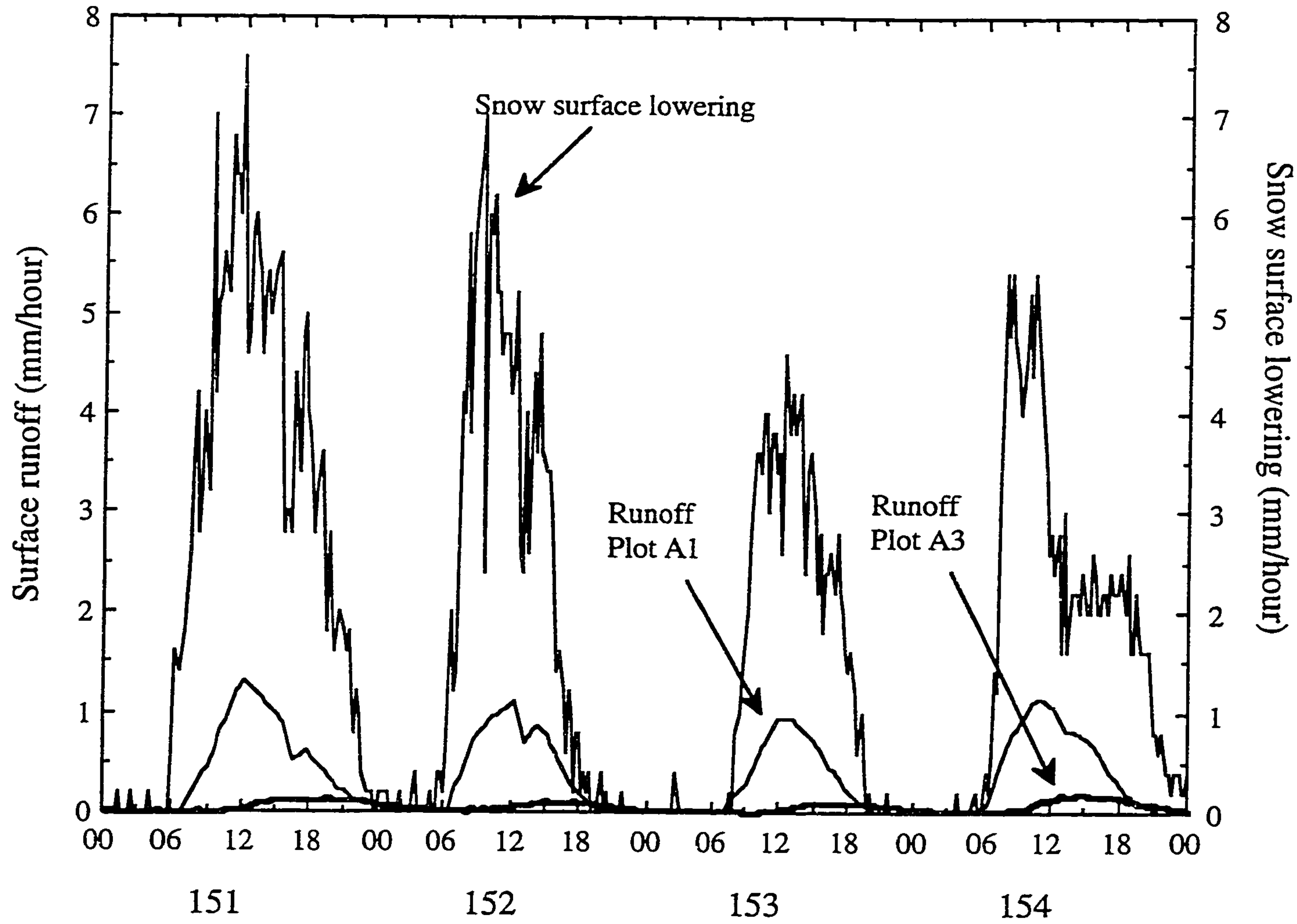

Figure 4-6: Snow surface lowering and runoff at plots A1 and A3, May 31-June 3, 1993. Lowering values are averages of 2 ablatometers. Near-surface snow densities were 0.5 Mg/m^3 during this period.

greater lag as meltwater first had to move through a very thick snowpack, then saturate a well-vegetated sandy slope before generating overland flow.

A trend for daily peak flow to occur earlier as the season progressed existed at plots B2, B4 and A3. This trend is associated with the thinning of snowbanks and the development of flowpaths through the snowpack as snowmelt progresses. This trend was not observed at B3. B3 also differed from the other plots in terms of the electrical conductivity, which increased as snowmelt progressed (see Section 5.2.1). This shows that at B3, residence times increased due to the development of subsurface pathways within the deepening active layer, and the vegetated hummocky microtopography inhibited rapid drainage as longer flow paths developed as the distance between the snowbank and flume increased. In contrast, the rilled detachment scar surfaces caused rapid passage of meltwater from the plots and the increasing distance from the snowbank edge upslope to the flume had little effect on lag times.

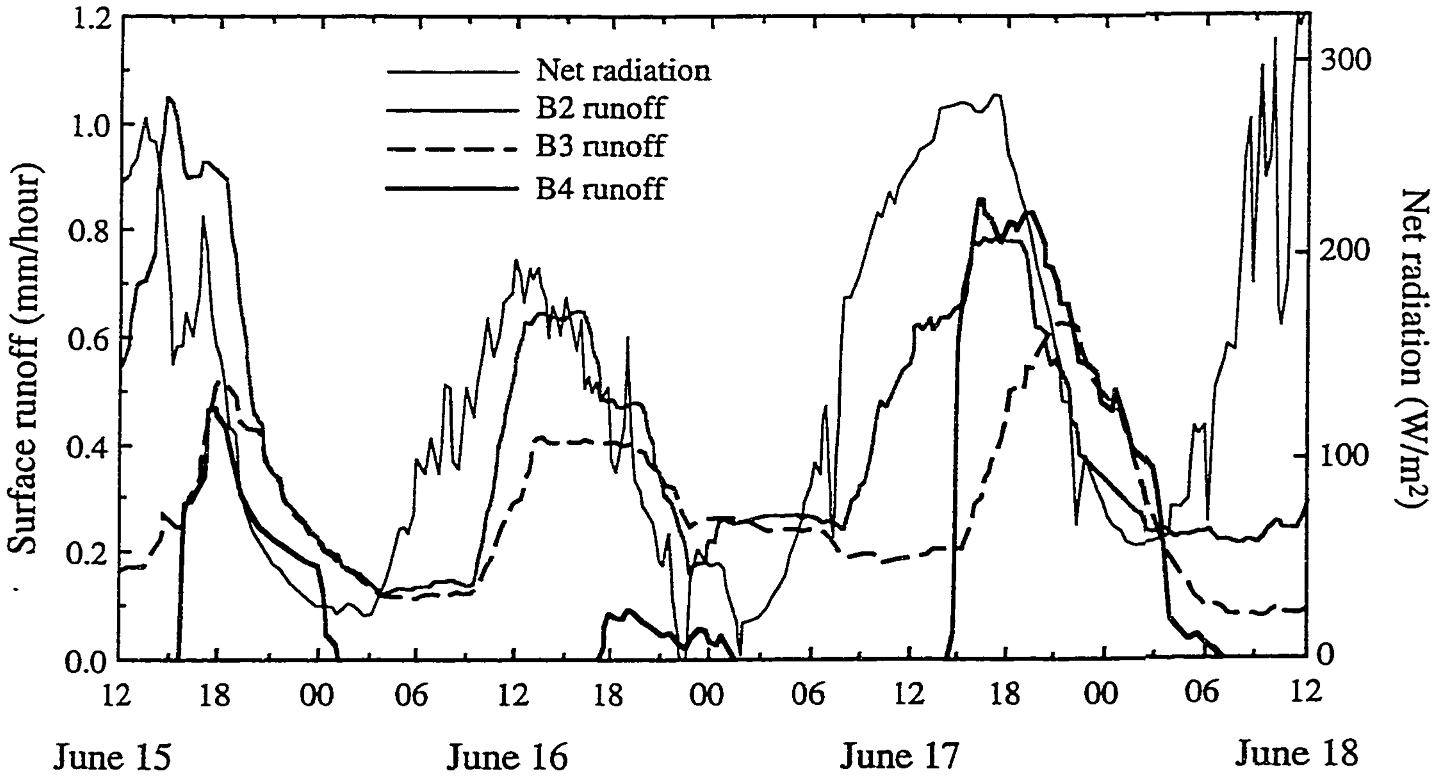

Figure 4-7: Response of plots at site B to net radiation, June 15-18, 1996.

4.2.3 – Surface Flow During Rainfall

Surface flow was generated several times during precipitation in 1996 (Table 4-2). No rainfall-induced runoff occurred in 1993. Overall, rainfall produced less than 15 % of the annual surface runoff at the plots. During the late snowmelt period, rain-on-snow events of 2.5 and 2.8 mm occurred on June 20 and 21 (JD 172 and JD 173) at sites A3 and B3 and caused discharges to increase (see Figures 4-3 and 4-4). Overland flow was also generated at B2 where small amounts of snow had persisted until two days previously. Surface flow did not develop at any of the other sites.

The largest storm of the summer (storm 3 in Table 4-2) occurred from June 24-25 (JD 176-177) during which time almost 20 mm of rain fell during three separate periods. Surface runoff was observed at all of the plots except the two vegetated sites A4 and B4, and A5 the unvegetated site. Excessive siltation of the flumes at A2 and B1 prevented its accurate assessment. Standard hydrograph separation techniques using recession curves were used to calculate individual runoff coefficients.

Table 4-2 shows that there was a steady increase in the plot runoff coefficients during storm 3, as antecedent moisture increased. Similarly, the highest coefficients (19%, 48%, 72%) were consistently observed at B3 which only became snow-free immediately prior to storm 3. A decrease in surface flow conductivity at B3 contrasts with sharp increases in conductivity associated with rainfall recharge at the other plots. Saturated slope conditions prevented infiltration, and rainfall was directly removed as overland flow as suggested for other permafrost areas (Slaughter and Kane, 1979; Lewkowicz and French, 1982). At A3, which also had been generating surface flow prior

Table 4-2. Runoff Coefficients for Rainfall.

Storm	Date	Duration (h)	Rainfall (mm)	A1 (%)	A3 (%)	B2 (%)	B3 (%)
1	June 20-21	6.25	2.5		*	8	*
2	June 21	2	2.8		*	9	*
3a	June 24	10	9.9		10	19	31
3b	June 24-25	6.5	5.6	8	27	48	55
3c	June 25	5.5	3.8	22	50	72	77
4	June 27	2.25	4.3	5	15	21	10

* Surface flow discharges increased during storm but cannot be separated from snowmelt.

to storm 3, snow had ablated from the upper part of the plot more than a week previously, and only a small section of the lower part of the plots was able to generate surface runoff at the start of the storm. A3 and B2 show more detailed discharge responses to fluctuations in rainfall (Figure 4-8). The B3 storm hydrographs show greater lag times in response to rainfall despite being on a much steeper slope than B2, and being much smaller in size than A3. Flow at all plots ceased by June 25 (JD 177).

On June 27 (JD, 179), another storm occurred and generated runoff at the same sites as on June 24 – 25 (Figure 4-9 and Table 4-2). There was a clear difference in the time of rise during this storm, with the vegetated plot, B3, responding after the unvegetated B2. Despite the lower amount of runoff at B3, surface flow continued for about 20 hours compared to 3 hours at B2 and about 10 hours at A3. This shows that the lack of an organic horizon and the presence of rills in the detachment scars allows more rapid runoff generation and hydrograph recession. Further evidence of this trend comes from soil moisture samples collected 48 h after a rainfall event of 20.8 mm at Eureka on July 30, 1997. These reveal higher moisture conditions in the near-surface on vegetated slopes (B3, A4 and the lower portion of A3) than on fresh (A1) and old (B2) detachment

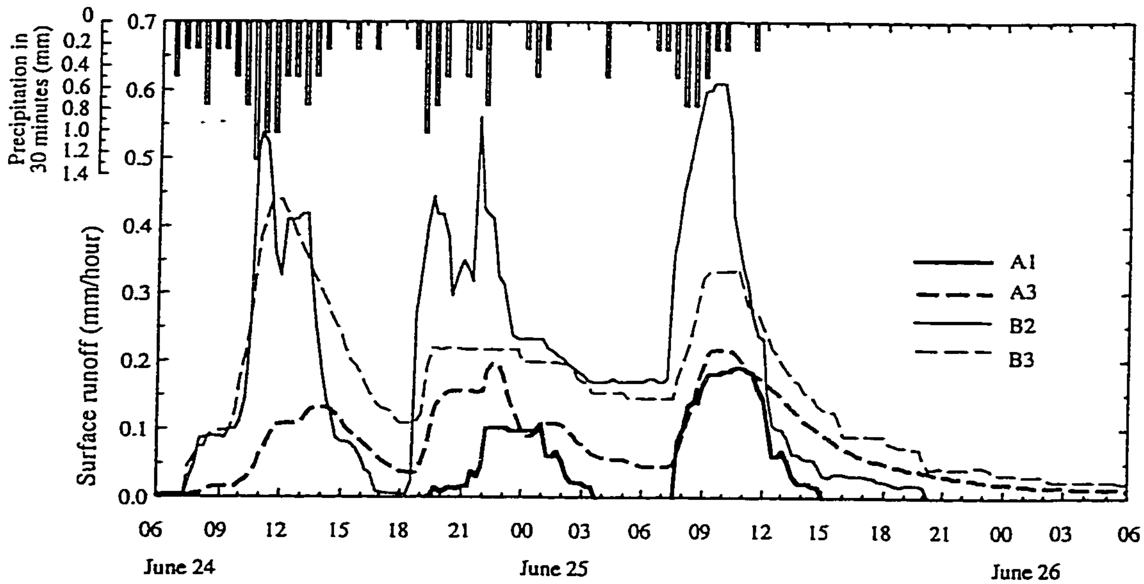

Figure 4-8: Response of plots A2, A3, B2 and B3 to rainfall, June 24-26, 1996.

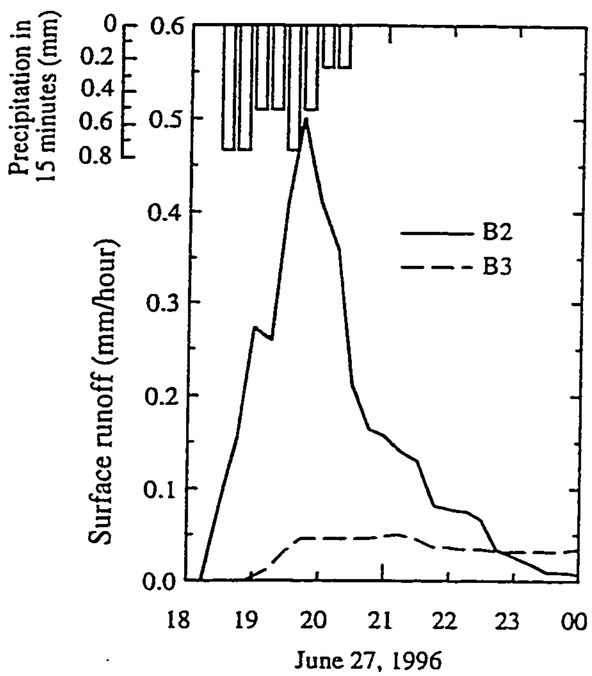

Figure 4-9: Response of plots B2 and B3 to rainfall, June 27, 1996.

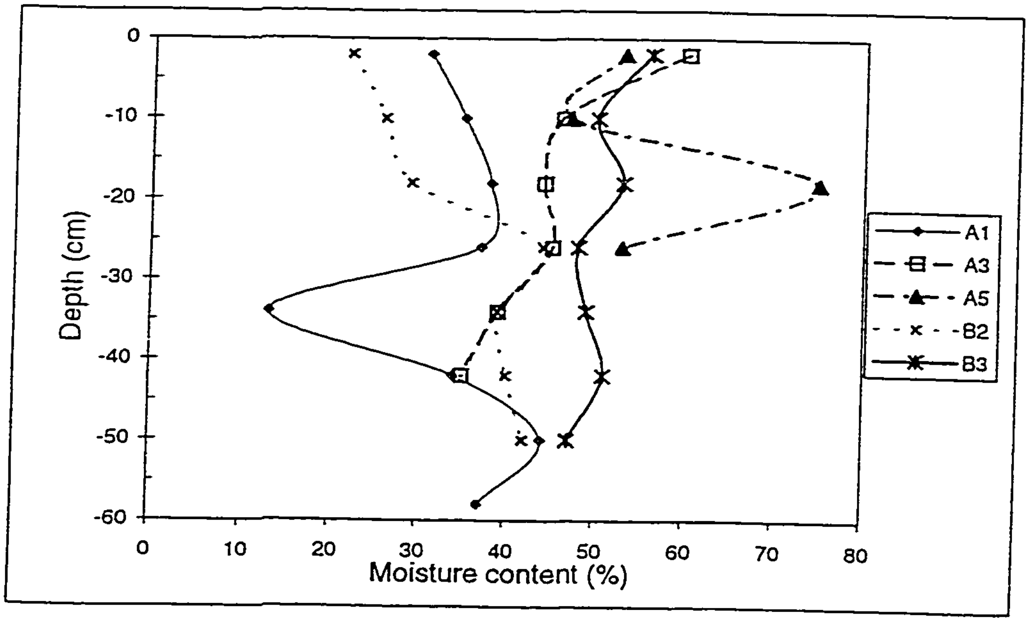

Figure 4-10: Runoff plot soil moisture profiles on August 1, 1997, 48 h after 21 mm storm at Eureka.

slide scars (Figure 4-10). Ring infiltrometer experiments showed that the infiltration capacity of the fresh scar at A1 was much lower than on the adjacent vegetated slope (Appendix B-1). After the June 27 storm in 1996, no further surface runoff was generated despite a wetter-than-average summer.

4.3 - Discussion (The Effect of Detachment Sliding on Slope Hydrology)

Because of redistribution of snow by winter winds, depressions such as detachment slide scars have the potential to increase snow accumulation at a site. The usual positive correlation between greater snow cover and vegetation cover (Bliss, 1990) is absent for detachment slide scars, so that more runoff is created than either on vegetated sites, or unvegetated undisturbed slopes which have very low snow covers. As a consequence of the greater amounts of snow and the higher runoff coefficients, surface flow was the dominant meltwater loss at four active layer detachment slide sites and two mixed plots. The minimum amount of end-of-the winter snow needed to generate overland flow at vegetated sites was much greater than that for unvegetated sites. Thus detachment sliding affected both inputs and outputs in the slope water balance during snowmelt.

The duration of snowmelt influences the probability of rainfall-induced surface runoff. Runoff response to rainfall can be attributed to antecedent moisture conditions, and to the presence of an organic horizon which has the potential to increase infiltration and moisture retention. Coarser surficial sediments at undisturbed slopes may also enhance the infiltration and moisture retention of the soil compared to the fine grained silts and clays at fresh detachment slide scars which swell when wetted to promote surface ponding and overland flow (Woo et al., 1990). Saturated slope conditions following surface runoff may be best sustained at vegetated plots, but their ability to absorb and store rainwater water decreases the chances of surface runoff production under drier conditions.

Detachment slides can modify the local cycling of water at the slope scale. The direct effects on streamflow are difficult to assess because of the wide range of runoff responses associated with site-specific conditions (snow cover, slope orientation, antecedent moisture conditions) and because of the variable hydraulic connections which can exist between the scars and the stream channel. Only in a basin where a large percentage of the area is affected by detachment slides are their hydrologic effects likely to be observable in stream discharge records.

Chapter 5 – Sediment Transport

5.1 - Suspended Sediment

5.1.1 – Suspended Sediment Concentrations

A total of 248 sediment samples were collected from the seven plots that produced surface runoff in 1996 (Appendix C-1). Suspended sediment concentrations varied between sites by up to two orders of magnitude (Figures 5-1 to 5-7). Inter-plot variability is largely due to the influence of vegetation cover and will be discussed in the following section (5.1.1.1). A positive relationship between suspended sediment and discharge existed at all of the plots (see Figures 5-1 to 5-7). However at each plot, samples obtained at similar discharges had suspended sediment concentrations which differed by more than one order of magnitude. The large amount of scatter can be attributed to several factors which influence sediment concentrations at both seasonal and diurnal time scales. These are discussed in detail in Sections 5.1.1.2 and 5.1.1.3.

5.1.1.1 – *The Influence of Vegetation Cover*

Summary suspended sediment concentrations for the plots and percentage vegetation cover are presented in Table 5-1. The averages of *sampled* concentrations presented are consistently higher than the mean *predicted* concentrations due to the disproportionate number of samples collected during higher flows with higher suspended sediment concentrations. Despite the inherent errors associated with using the predicted values, they better represent the true average of suspended sediment concentrations in surface wash and will be referred to below.

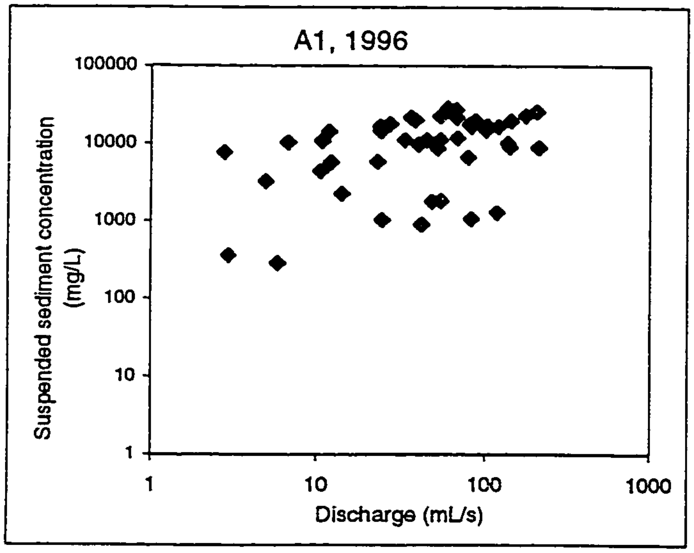

Figure 5-1

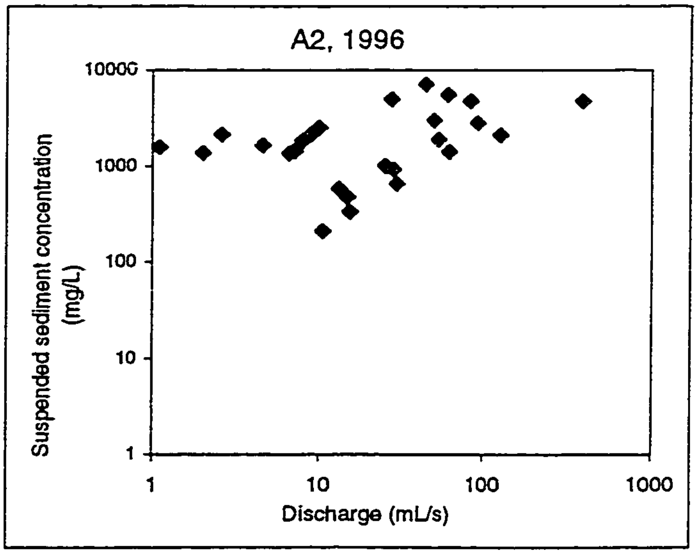

Figure 5-2

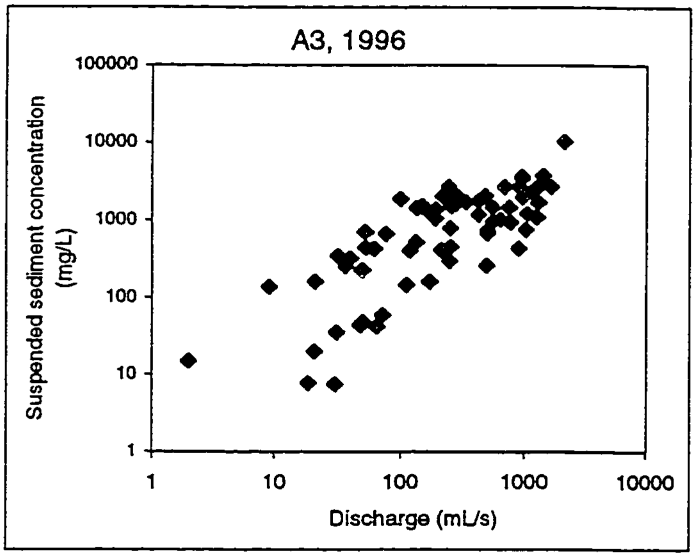

Figure 5-3

Figures 5-1 to 5-3: Discharge - suspended sediment relationships for site A.

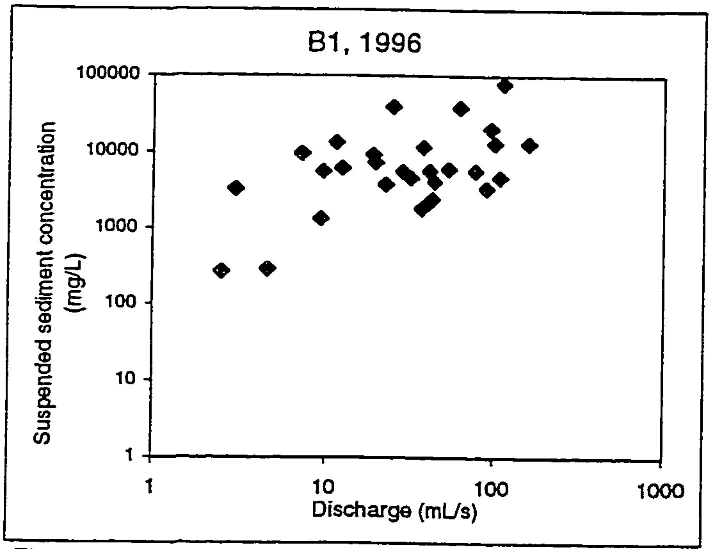

Figure 5-4

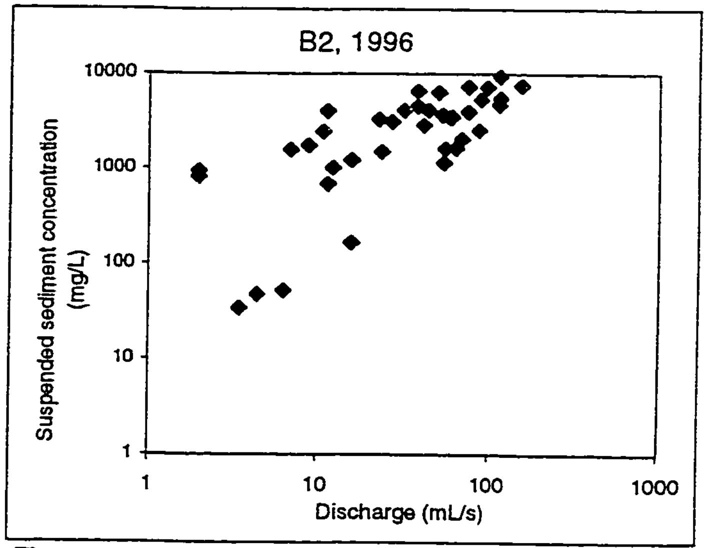

Figure 5-5

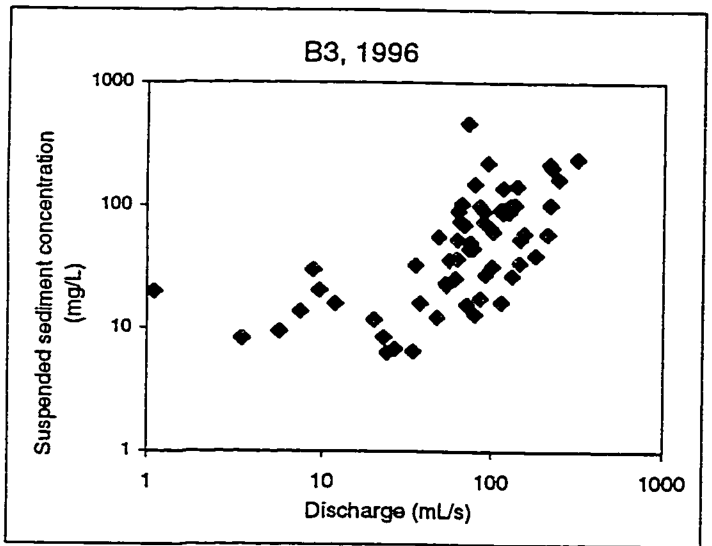

Figure 5-6

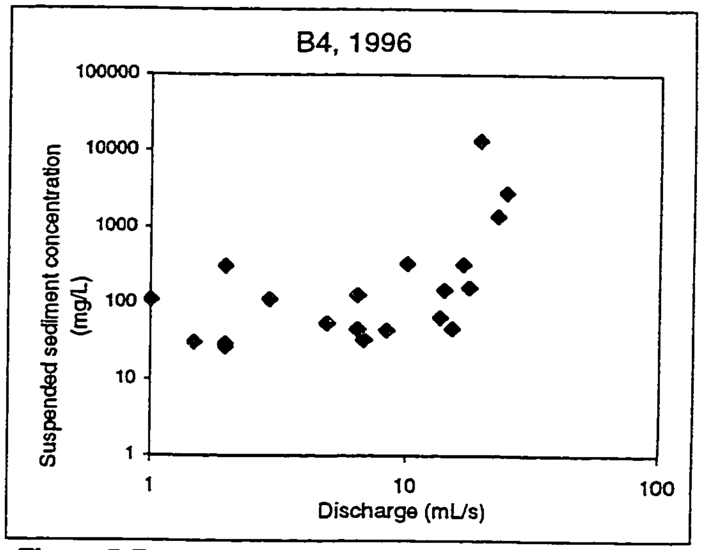

Figure 5-7

Figures 5-4 to 5-7: Discharge - suspended sediment relationships for site B.

Table 5-1: Suspended Sediment Concentrations in mg/L.

Plot	Vegetation cover (%)	Origin of the value	Number of Samples	Average Concentration (mg/L)	Maximum Concentration (mg/L)	Standard Deviation (mg/L)
A1 1996	8% overall 0% lower slope	Sampled Predicted*	42	11900 10500	28700	7980
A2	10% overall	Sampled Predicted*	32	2330 2040	7110	1740
A3 1996	15% overall	Sampled Predicted*	54	1260 882	10500	1510
B1	8% overall	Sampled Predicted*	28	11100 5520	78900	16100
B2	12% overall	Sampled Predicted*	38	3100 2570	9420	2330
B3	30% overall 50% lower slope	Sampled Predicted*	46	69.2 40.7	468	77.4
B4	15% overall 50% lower slope	Sampled Predicted*	23	998 405	13700	3060
A1 1993	8% overall 0% lower slope	Sampled Predicted*	29	11600 8110	21700	6000
A3 1996	15% overall	Sampled Predicted*	36	860 532	3100	700

* Predicted values are for the entire runoff period, calculated from sediment concentration-discharge relationships.

Maximum suspended sediment concentrations of 28 700 mg/L (A1) and 78 900 mg/L (B1) were measured at the fresh detachment slide scars (see Table 5-1). Total vegetation cover of these plots is less than 10%. Average suspended sediment concentrations for the entire runoff season were also the highest at A1 and B1 (10500 mg/L and 5520 mg/L respectively). The mean suspended sediment concentrations at the sparsely vegetated pre-1950 detachment slide scars (A2 and B2) were 2040 mg/L and 2570 mg/L. The mixed plot A3 had lower average suspended sediment concentrations (882 mg/L) than A2 and B2, but experienced a higher peak value (10500 mg/L). This peak suspended sediment concentration can be attributed to the brief, but high discharges generated from several unvegetated detachment slide scars on the upper part of the plot. Extensive vegetation cover (>50%) on the lower portions of B3 and B4 had a clear influence on suspended sediment concentrations. Mean predicted concentrations of 40.7 mg/L at B3 and 405 mg/L B4 are one to two orders of magnitude lower than at the fresh scars A1 and B1. The mean value at B4 is elevated due to high suspended sediment concentrations during late melt. At this time small mudflows that eventually destroyed the flume were initiated in the saturated sediments at the crest of the slope, and these caused increases in suspended sediment concentrations in surface flow.

5.1.1.2 – *Suspended Sediment Production (Seasonal Variation)*

Throughout the runoff period, the production of suspended sediment varied among the plots. The day of peak concentration ranged from June 10 (JD 162) at A2 and B1 to June 25 (JD 177) at B3. Peak suspended sediment concentrations occurred as early as the third day of runoff (at B1) and as late as the eighteenth day of runoff (at B3).

Peak concentrations were measured during snowmelt runoff at all plots except B3, but corresponded with peak measured discharge at only A3 (1993 and 1996) and B2. At A3, for example, at the time of peak discharge, much of the runoff was generated from several detachment slide scars on the middle part of the plot which resulted in higher suspended sediment concentrations. As melt progressed and discharge from the detachment scars declined, north-facing snowbanks in the lower well-vegetated section of the plot generated a greater proportion of the runoff (Figure 5-8). During this time the suspended sediment concentrations also declined despite equivalent discharges (Figure 5-9). At the very end of snowmelt, both discharge and suspended sediment concentrations were low as all of the runoff was derived from remnant snowpatches on the lower vegetated slope. During rainfall-induced runoff, suspended sediment concentrations were up to 7 times greater than concentrations measured under similar discharges during late snowmelt (Figure 5-9). This increase can be attributed to the expansion of contributory area and the change in slope conditions related to the thawing of the active layer. The concept of changing contributory areas at A3 is supported by conductivity and water geochemistry values (see Sections 5.2.1 and 5.2.2). At the same plot in 1993, a thinner snow cover and less runoff from the detachment slide scars resulted in lower average and peak sediment concentrations (see Table 5-1). Most of the runoff was generated by the

A B

Figure 5-8: A) The convergence of sediment rich runoff from the upper part of plot A3 (right channel) with sediment free runoff from the lower well-vegetated slope (left channel) and B) the convergence of flows from the two different contributory areas.

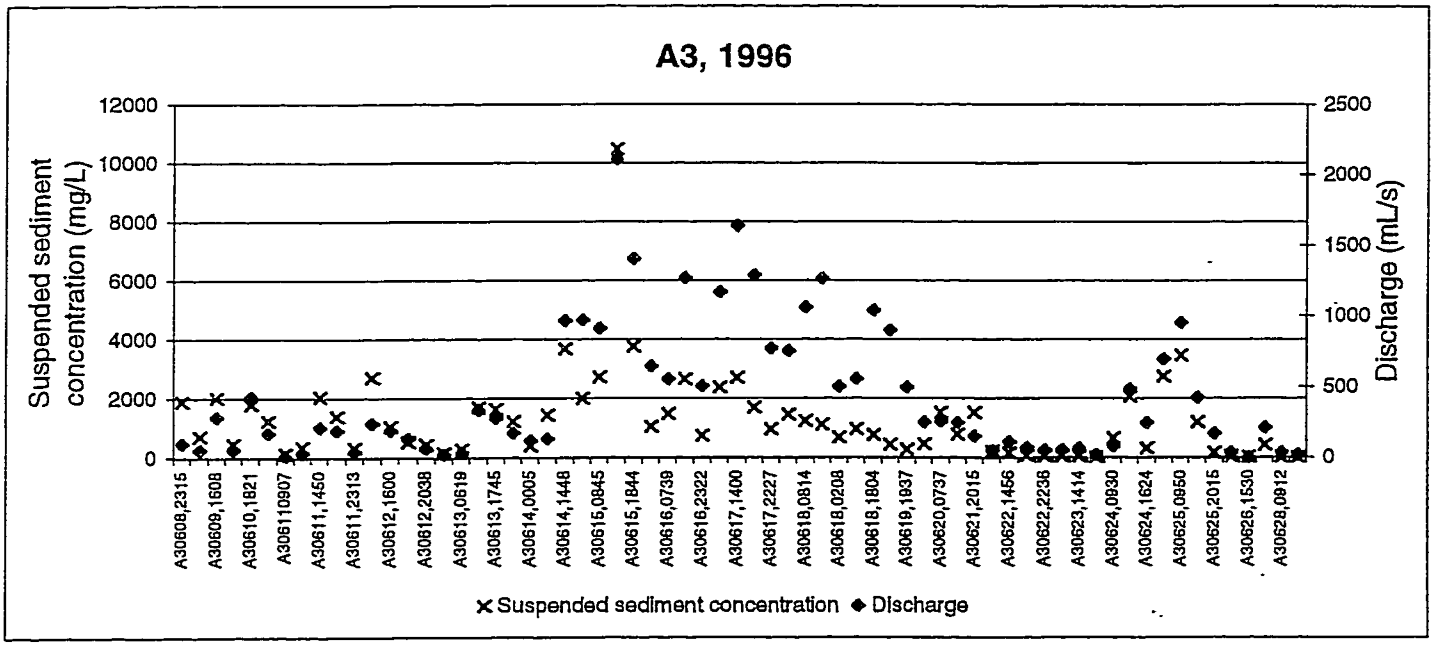

Figure 5-9: Comparison of sampled suspended sediment concentration and sampled plot discharge, A3,1996.
Note: Non-uniform sampling frequency.
Plot number, month, day and time are shown on the x-axis.

melt of a large snowbank on the lower vegetated portion of the plot (personal communication, A. G. Lewkowicz).

The correlation between peak discharge and peak suspended sediment concentration was not evident at other plots. At B3, for example, higher concentrations during late melt can be explained by snowbank recession resulting in surface wash over a fresh detachment slide scar on the upper part of the plot (Figure 5-10). When only a small snowbank remained at the crest of the slope, scar headwall collapse may have also contributed to higher sediment concentrations. Despite these factors the hummocky, vegetated lower portion of the slope acted to slow and disperse flows, promoting sediment deposition. The maximum suspended sediment concentration measured at the flume was only 468 mg/L. At B4, low suspended sediment concentrations between 26 mg/L and 164 mg/L were measured during early melt, until the snowbank receded to the steep, unvegetated crest of the slope. Then, under similar discharges, suspended sediment concentrations increased by two orders of magnitude (Figure 5-11). Within a day, small mudflows were initiated in saturated sediments at the crest of the slope. Air photos from 1990 show faint mudflow deposits on the vegetated slope suggesting that such phenomena had occurred previously, probably in years of high snow accumulation.

The seasonal variability of suspended sediment production at the above-mentioned plots can be attributed to snow distribution and snowmelt patterns over heterogeneous slopes. However, there is also a significant amount of scatter in the suspended sediment concentration - discharge relationships at homogeneous plots.

Increasing suspended sediment concentrations throughout melt are observed at the more homogeneous detachment slide scars. Plots A1 (1993 and 1996) (Figure 5-12

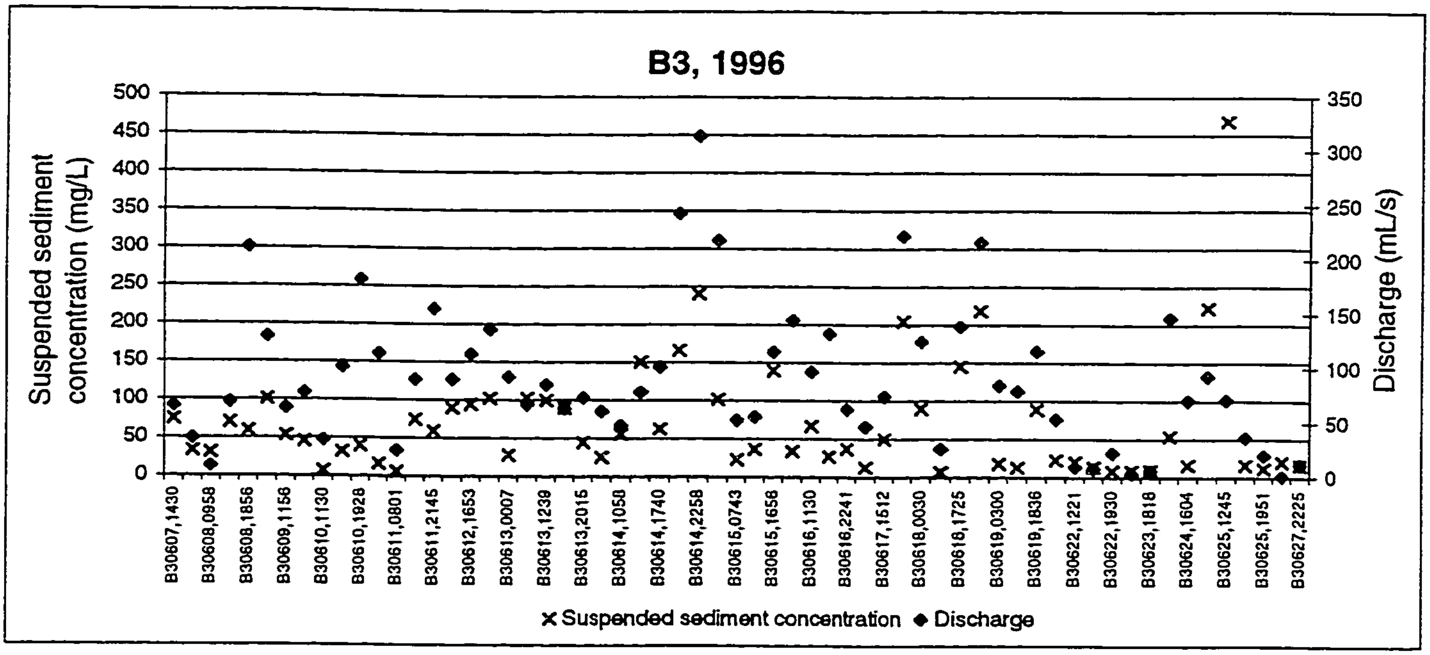

Figure 5-10: Comparison of sampled suspended sediment concentration and sampled plot discharge, B3, 1996.
Note: Non-uniform sampling frequency.

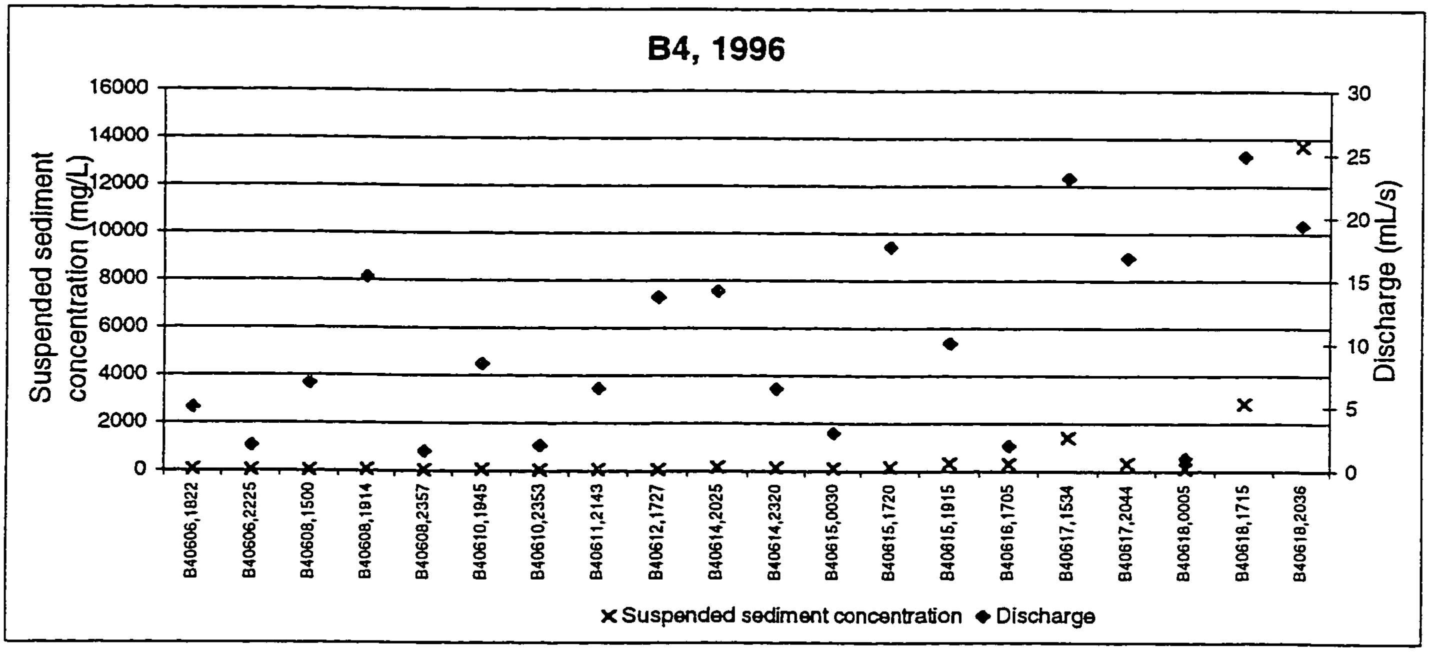

Figure 5-11: Comparison of sampled suspended sediment concentration and sampled plot discharge, B4, 1996.
Note: Non-uniform sampling frequency.

and 5-13) and A2 (Figure 5-14) show this trend in suspended sediment concentrations, and a relative increase with respect to discharge is noted at B1. The factors influencing these trends can be investigated through a more focused analysis. Plot A1, 1996 will be considered in detail due to the abundance of data.

Suspended sediment concentrations increased through the snowmelt period (Figure 5-13). For example on June 7 (JD 159) a suspended sediment concentration of 1800 mg/L was measured at a discharge of 50 mL/s. At similar discharges, sediment concentrations increased as follows: June 13 (JD 165) – 8785 mg/L, June 15 (JD 167) – 11256 mg/L, June 17 (JD 169) – 28754 mg/L, a change of more than one order of magnitude from early to late melt (see Figure 5-13). A similar trend is evident at the same plot in 1993, but extremes are not as marked (see Figure 5-12). It was hypothesized that low suspended sediment concentrations during the first few days of runoff in 1996 were due to the close proximity between the snowbank and flume (< 2 m). As the snowbank receded and the distance between snowbank and flume increased, there was a greater opportunity for sediment entrainment and for the addition of sediment from rill collapse. This hypothesis was tested by comparing the distance between the snowbank and flume with suspended sediment concentrations.

At plot A1, the distance between the edge of the snowbank and the flume was measured several times during snowmelt. The thinner snowcover on the lower portion of the plot ablated rapidly, but edge recession rates slowed when all that remained was the deeper snowpatch at the crest of the slope (Figure 5-15). A relationship was established between the measured distances and time of measurement so that the distance between snowbank and flume could be predicted throughout snowmelt. Using the predicted

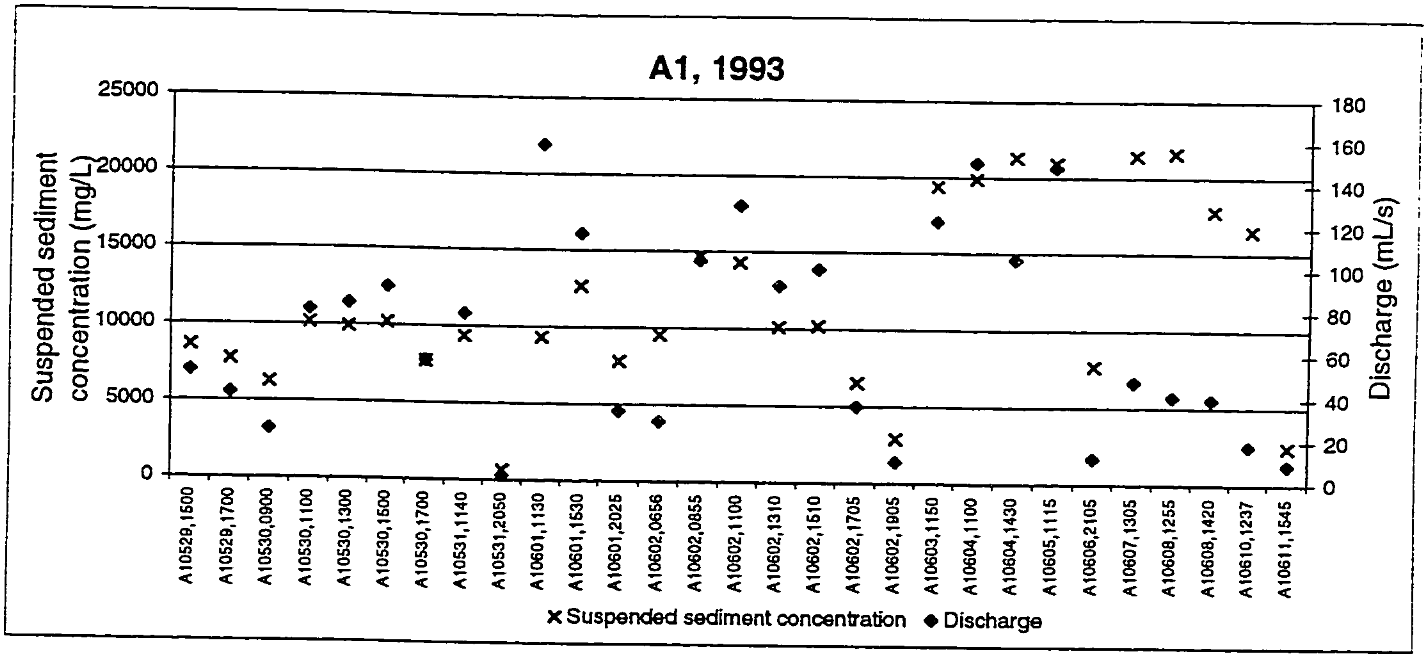

Figure 5-12: Comparison of sampled suspended sediment concentration and sampled plot discharge, A1, 1993.
Note: Non-uniform sampling frequency.

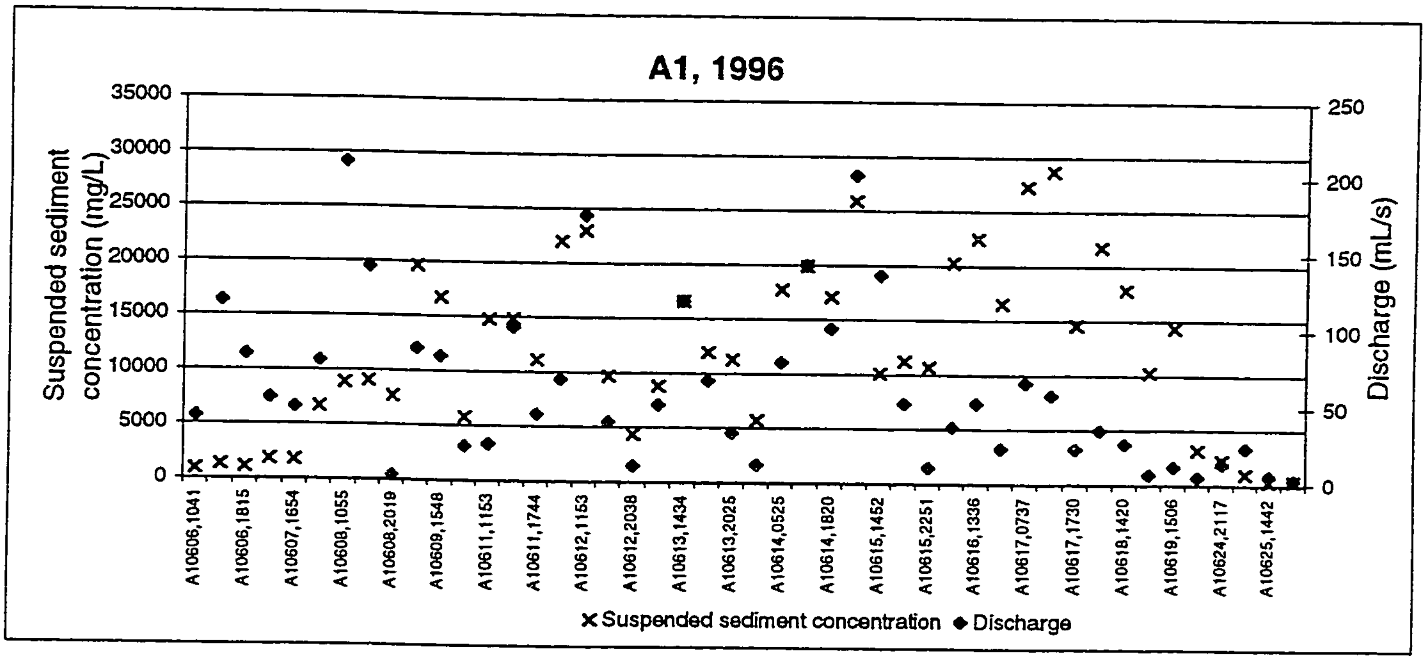

Figure 5-13: Comparison of sampled suspended sediment concentration and sampled plot discharge, A1, 1996.
Note: Non-uniform sampling frequency.

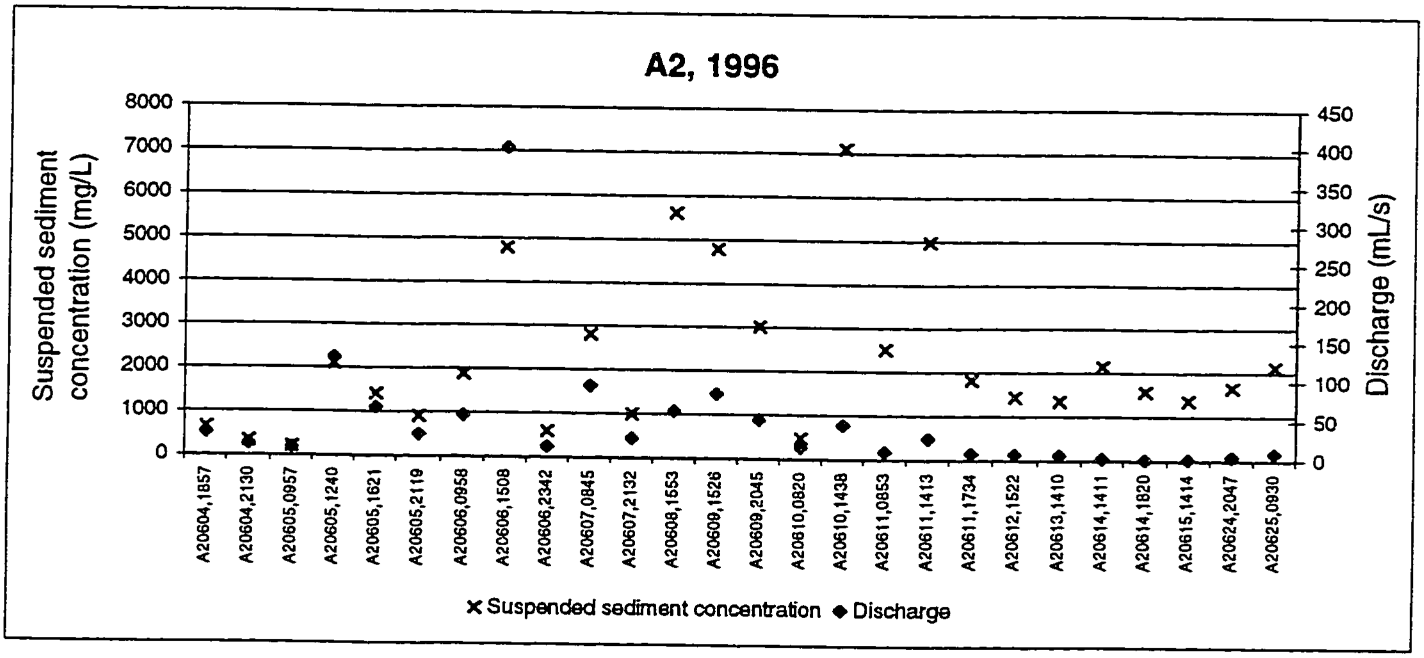

Figure 5-14: Comparison of sampled suspended sediment concentration and sampled plot discharge, A2, 1996.
Note: Non-uniform sampling frequency.

distance values, a relationship was then established between distance and peak daily suspended sediment concentration (Figure 5-16). The regression yielded an r^2 of 0.81. The general pattern of snowmelt was similar at A2 and B1 so this hypothesis may also explain the suspended sediment patterns at those plots. It must be noted that other factors which change uni-directionally with time, such as active-layer thaw, may have influenced suspended sediment production in rillwash but are effectively subsumed by the distance relationship.

5.1.1.3 – *Suspended Sediment Production (Diurnal Variation)*

Some of the scatter in the suspended sediment - discharge relationships can be attributed to diurnal variability. Inconsistent patterns of variability were observed at plots A1 (1993, 1996), A3, B2 and B3. No clear trends were observed at other plots largely due to the limited number of samples and the timing of their collection.

The direction of variability was inconsistent at plots A3 and B3. Diurnal variation of suspended sediment concentrations under similar discharge was estimated to be between 10% and 60%. The interpretation of diurnal suspended sediment patterns at these heterogeneous plots is difficult due to the low number of sample points and the influence of variables that operate on different time scales.

Only clockwise patterns were identified at site B2 which suggest that sediment concentrations were limited by the availability of erodible material. A1 also exhibited consistent trends. A1 was selected for detailed analysis because of the abundance and high quality of data and due to the homogeneity of the plot which decreases the number of variables that can influence suspended sediment production.

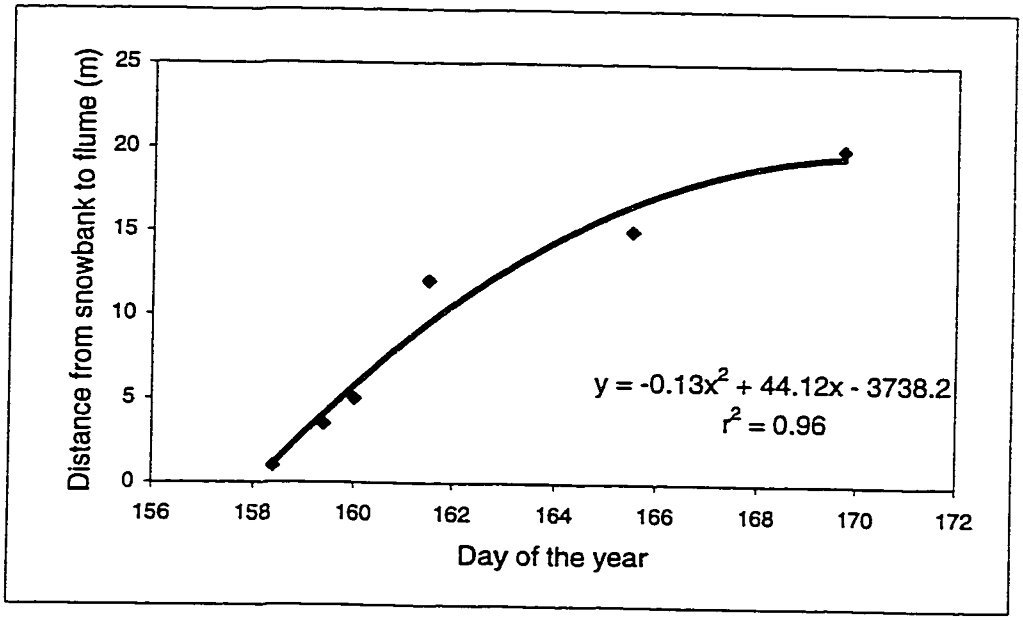

Figure 5-15: Time - distance from snowbank to flume rating curve, plot A1, 1996.

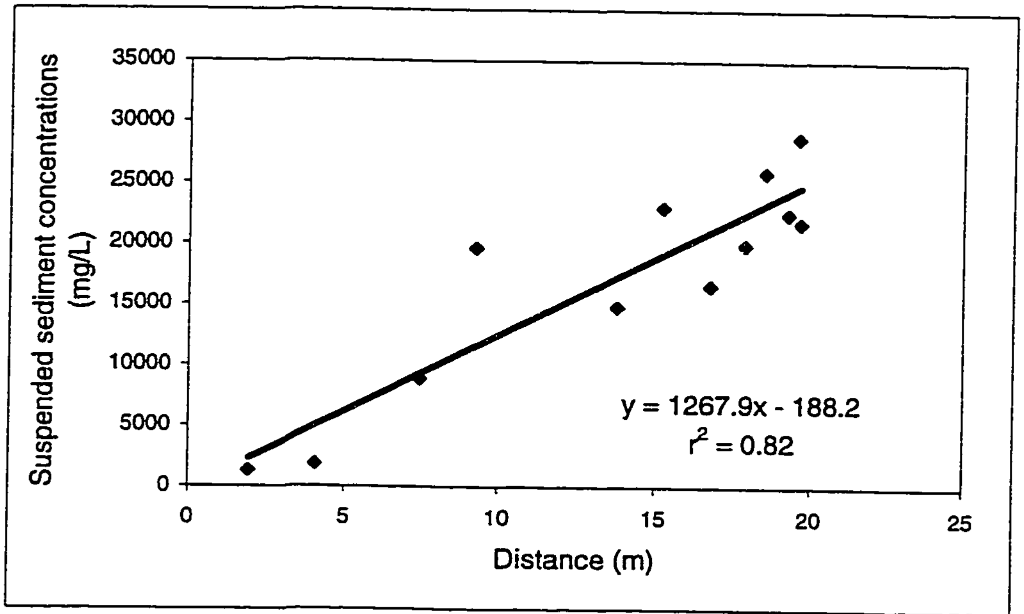

Figure 5-16: Distance from snowbank to flume - peak daily suspended sediment relationship, plot A1, 1996

Note: The peak daily suspended sediment concentration for the last day of snowmelt runoff (June 19) was discarded from the relationship due to the low peak concentration reflective of the very low surface discharges on that day.

Regression line constrained through zero.

Variability could not be examined when fewer than three samples were collected in a single diurnal cycle or when all samples were collected during hydrograph rise or recession. This restricted the identification of patterns to nine of the fourteen days of surface runoff. During early melt, counterclockwise trends were present for two diurnal cycles, indicating that suspended sediment concentrations were higher on the falling limb of diurnal hydrographs. During early runoff, the short distance between snowbank and flume can double within a day (see Figure 5-15). As shown above (see Figure 5-16) there is a strong relationship between suspended sediment concentrations and distance between the snowbank and flume, with suspended sediment concentrations increasing as the flow distance increases. The counterclockwise patterns suggest that during early melt, the large proportional increase in flow path length from the time of hydrograph rise to hydrograph recession can influence sediment transport on a diurnal time scale.

Clockwise patterns were identified for 7 of 14 days during snowmelt runoff (Figure 5-17). Estimated differences in the suspended sediment concentrations between rising and falling limbs of diurnal hydrographs at a 40 mL/s discharge range from about 10% to almost 60%. Fluvial undercutting, wetting and drying and freeze-thaw can all result in rill collapse which will supply sediment to the rill system. It is hypothesized that low discharges are not competent to remove the sediment input during overnight low flow. These additional inputs are flushed by rising flows on the following day. The inputs are exhausted by the time of peak discharge and lower suspended sediment concentrations are experienced during hydrograph recession. Despite the lack of vegetation cover and overall very high suspended sediment concentrations at A1, the clockwise patterns indicate a system which is limited by sediment supply.

Estimates based on diurnal patterns at A1, A3, B2 and B3 suggest that diurnal variability of suspended sediment concentrations under equal discharges can be as high as 60%. These differences will contribute to scatter in suspended sediment - discharge relationships, but are not as significant as the seasonal differences in suspended sediment concentrations under similar discharges which can vary by up to two orders of magnitude (see Section 5.1.1.2).

5.1.1.4 – *Discussion (Temporal Variability in Suspended Sediment Production)*

Several factors influence the temporal variability of suspended sediment concentrations. During melt, snow-covered slopes are protected from surface wash erosion. On heterogeneous slopes, differential patterns of snowmelt alter contributory areas which affect suspended sediment concentrations over time (see Section 5.1.1.2). Inter-annual variability in snow distribution and snowmelt patterns influence yearly differences in the absolute amount of sediment removal (see Section 5.1.3).

Variability in suspended sediment concentrations is also evident at homogeneous plots. The increasing distance between snowbank and flume explained much of the rising trend in suspended sediment concentrations over time at A1, and may be the cause of similar trends at the other homogeneous detachment slide slopes. The distance relationship (see Figure 5-16) suggests that a deeper snow cover at the top of the scar is more conducive to high amounts of suspended sediment erosion than an equivalent snowpack uniformly distributed over the scar, or concentrated near the base of the scar.

The thaw of surface sediments may act to strengthen the above-mentioned relationship. In early melt, fluvial undercutting along rill channels is limited by the

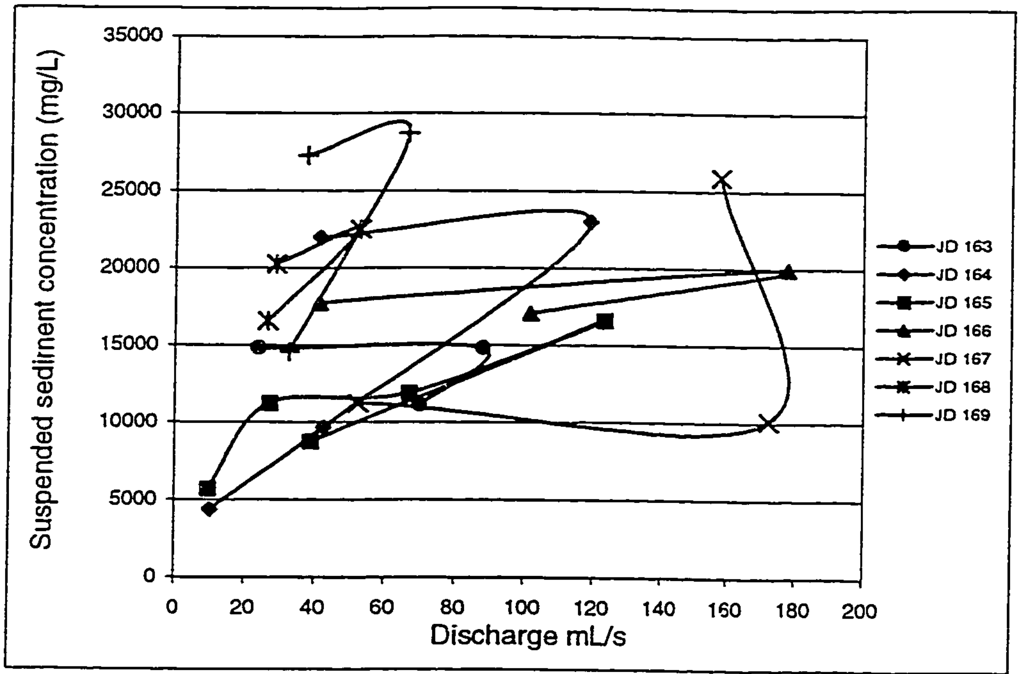

5-17: Diurnal clockwise variability, suspended sediment, A1, 1996.

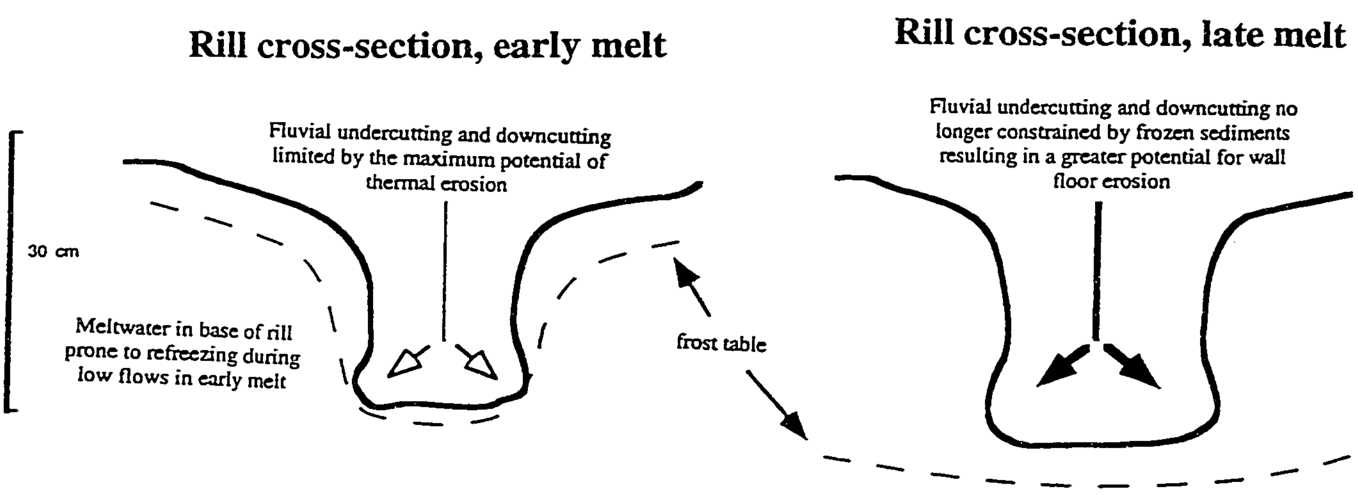

Figure 5-18: The influence of frost table on rill erosion.

maximum potential of thermal erosion. When thaw depths advance below the depth of the rill and meltwater does not refreeze in the rill channel, wall erosion is no longer constrained by frozen slope materials (Figure 5-18). These points are speculative, however they are supported by the extremely high amounts of sediment transport observed by several researchers (Cogley and McCann, 1976) during intense summer rainfall events. Deep rill development and gully initiation were observed at detachment slide scars and unvegetated slopes in August 1997 after a record rainfall event on the Fosheim Peninsula.

The overall trends in suspended sediment concentrations at the fresh detachment slide scars imply that the duration and patterns of snowmelt runoff can influence the total amount of sediment removed from the slope. For example, the snowmelt runoff at A2 was not conducive to maximum erosion by suspended sediment removal, because peak flows occurred on the third day of runoff when flow distance was short and concentrations were still low. The patterns of snowmelt runoff were more conducive to high amounts of suspended sediment removal at A1 (in 1996), when peak flows did not occur until the tenth day of surface runoff and the flowpaths were longer and suspended sediment concentrations therefore were higher (see Figure 5-13).

5.1.2 – Suspended Sediment Analysis

5.1.2.1 – *Coal in Surface and Suspended Sediment Samples*

Percentage of coal in surface sediment ranged between 3 percent in samples from the vegetated portion of A3 to 32 percent at B1 (Appendix C-2). The distribution of coal was not evaluated, but qualitative observations of sediment retained during wet sieving suggest that at some sites (A1, B1) the larger grainsizes (> 1ϕ) consist almost completely of coal.

Coal constitutes between 10 to 20 percent of the total weight of the suspended sediment samples (Appendix C-3). The transportation of coal by surface wash was investigated by plotting coal percentage against instantaneous discharge. Sites A1, A2, B1 and B2 were grouped together because of their comparable hydraulic conditions (similar discharges and rill dimensions). A separate relationship between percentage of coal and discharge was established at A3. Both data sets revealed an inverse relationship between coal percentages and discharge (Figure 5-19 and 5-20). The correlation for the multiple sites ($n = 12$) yielded the equation $y = -0.068x + 19$. At A3, the relationship between the same two variables is described by the equation $y = -0.0049x + 16.77$. This analysis indicates that coal is preferentially transported during low flows.

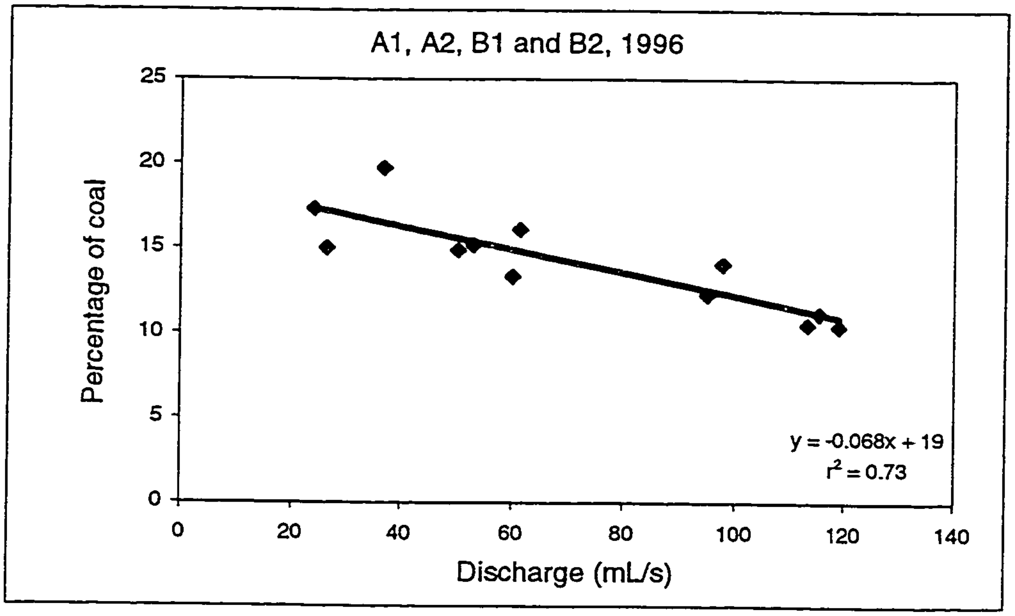

Figure 5-19: Discharge - percentage of coal relationship for A1, A2, B1 and B2.

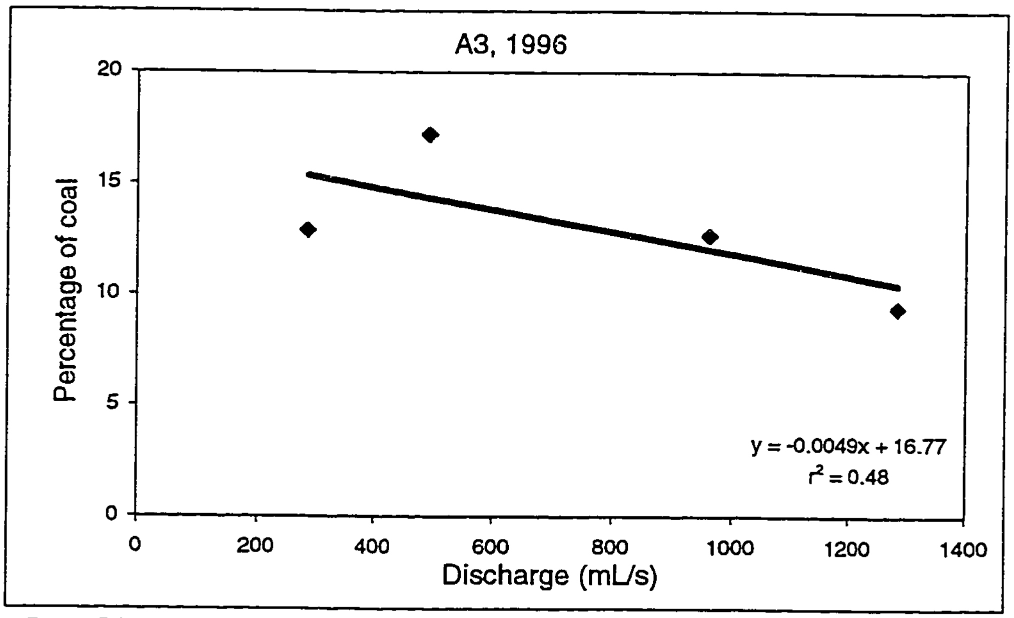

Figure 5-20: Discharge - percentage of coal relationship for A3.

5.1.2.2 – *Grain-Size Analysis of Surface and Suspended Sediment Samples*

For the plot surfaces, the difference between the mean and median grain-sizes for individual samples is minimal (Table 5-2). The differences in mean grain-sizes of surface samples between study plots range between 4.4 ϕ (B4, Transect 4) and 7.5 ϕ (A1, T1). The lower vegetated portion of A3, B3 and B4 are underlain by coarse silt (after Pettijohn *et al.*, 1972) in the 4 ϕ range (Figures 5-21, 5-22 and 5-23), but the dominant grain-sizes at fresh detachment slide scars are classified as medium to very fine silt between 6 ϕ and 8 ϕ (Figure 5-24 and 5-25).

Table 5-2: Grain-size analysis summary table for surface sediment samples.

Site	$M\phi$	$M_z\phi$	$\sigma_G\phi$	SK_G	K_G
A1, T1	7.40	7.50	1.66	2.99	0.93
A1, T3	6.80	6.53	2.48	1.51	1.07
A2, T1	7.40	5.42	2.01	1.67	0.93
A2, vt3	7.40	6.57	1.87	2.28	1.00
A3, T1	4.10	4.50	2.31	1.27	1.13
A3, T3	6.90	6.97	1.91	2.36	0.50
A3, T5	6.00	6.10	2.15	1.79	0.54
A4, T1	6.10	6.23	1.94	2.15	0.56
B1, T1	6.50	6.27	2.96	0.93	1.44
B1, T5	5.90	5.63	3.03	0.86	1.42
B2, T1	4.50	4.93	2.36	1.37	1.03
B2, T3	6.10	6.13	2.14	1.81	0.93
B3, T1	5.70	5.73	2.38	1.56	0.90
B3, T3	4.30	4.92	2.39	1.54	0.90
B4, T1	4.30	4.70	2.26	1.45	1.00
B4, T4	4.10	4.40	3.16	0.77	1.30

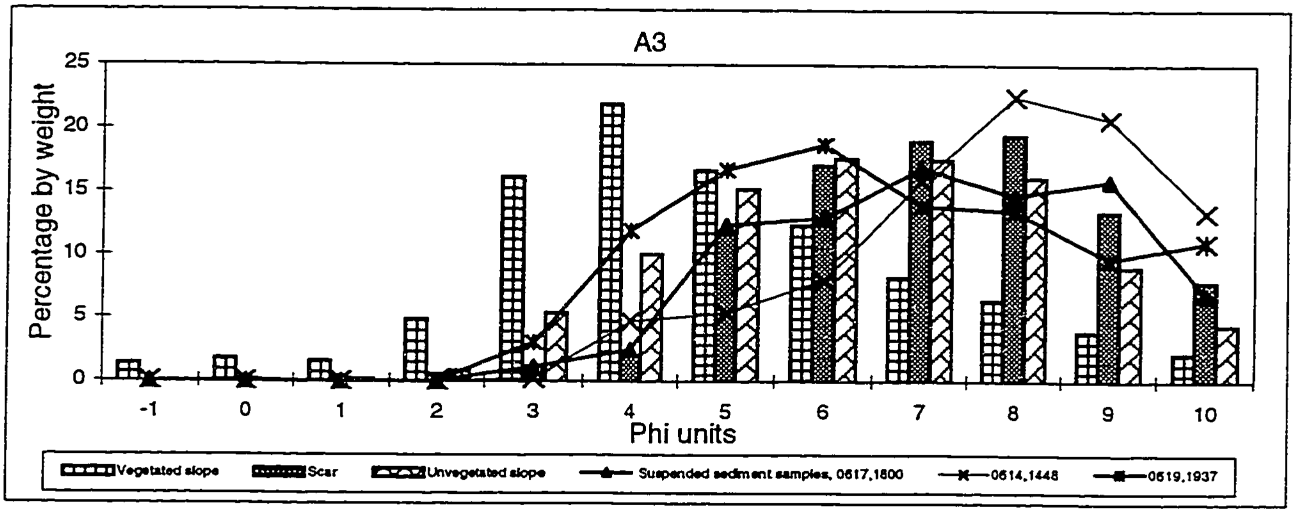

Figure 5-21: Grain-size distributions for surface and suspended sediment samples at A3.

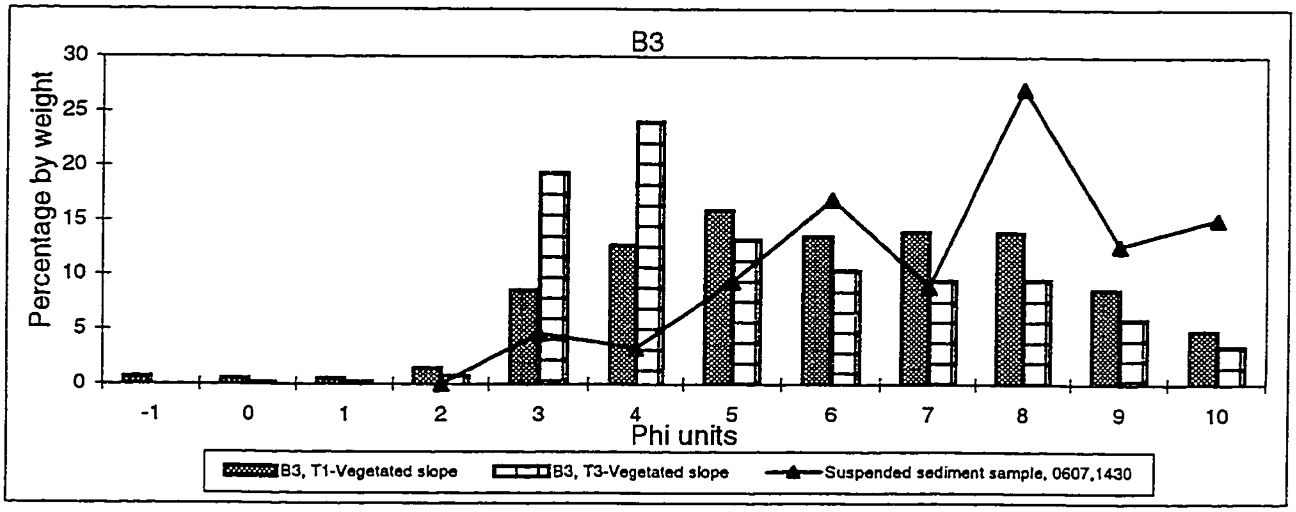

Figure 5-22: Grain-size distributions for surface and suspended sediment samples at B3.

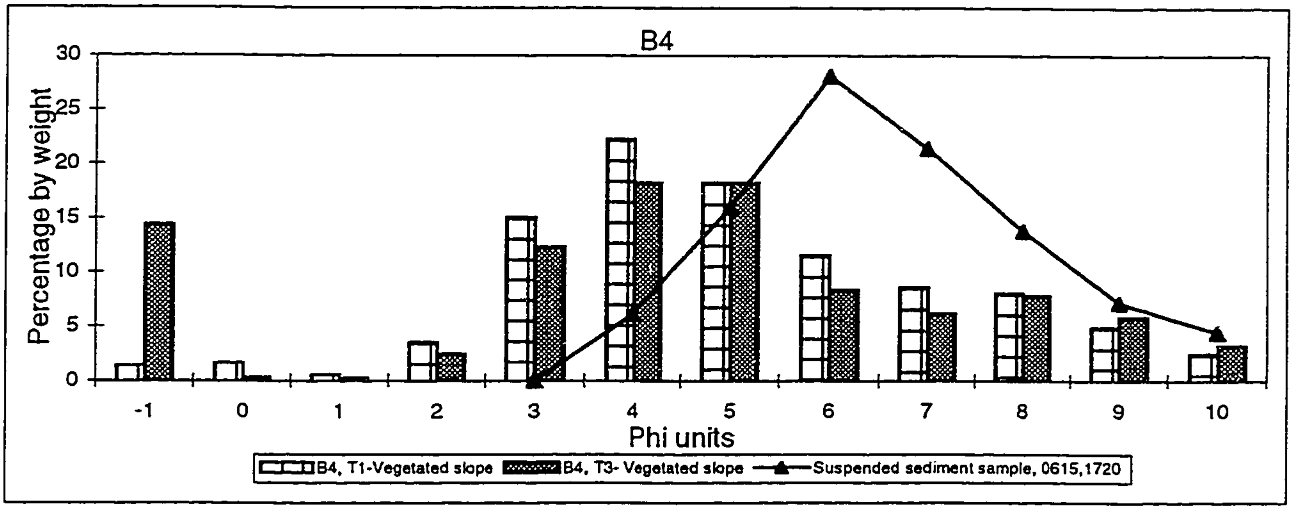

Figure 5-23: Grain-size distributions for surface and suspended sediment samples at B4.

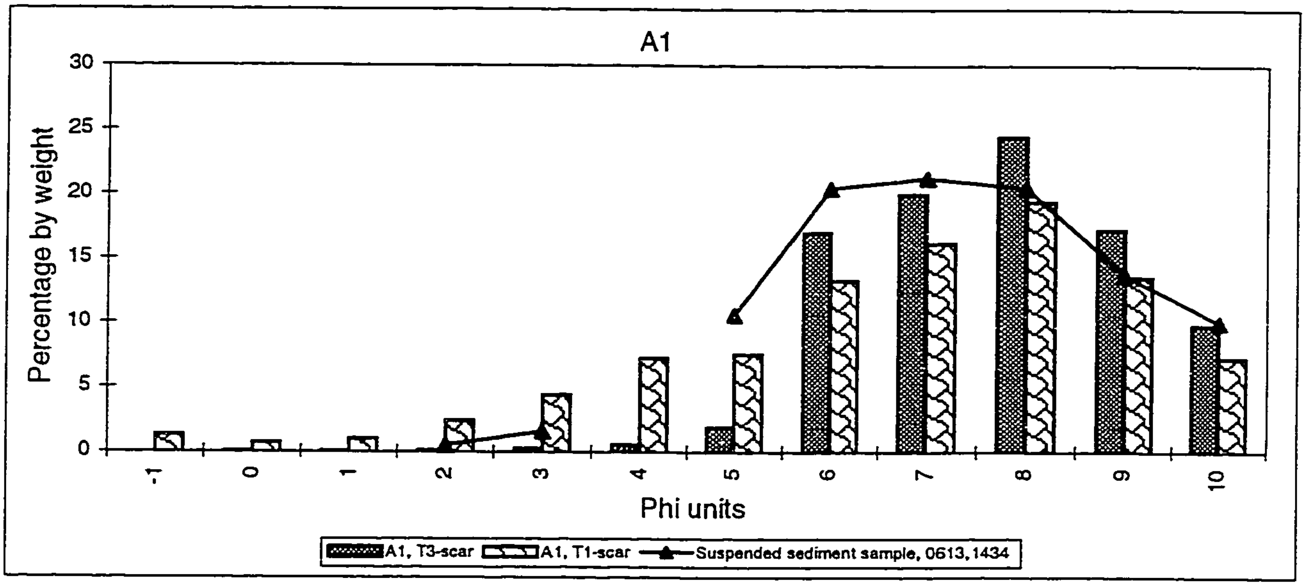

Figure 5-24: Grain-size distributions for surface and suspended sediment samples at A1.

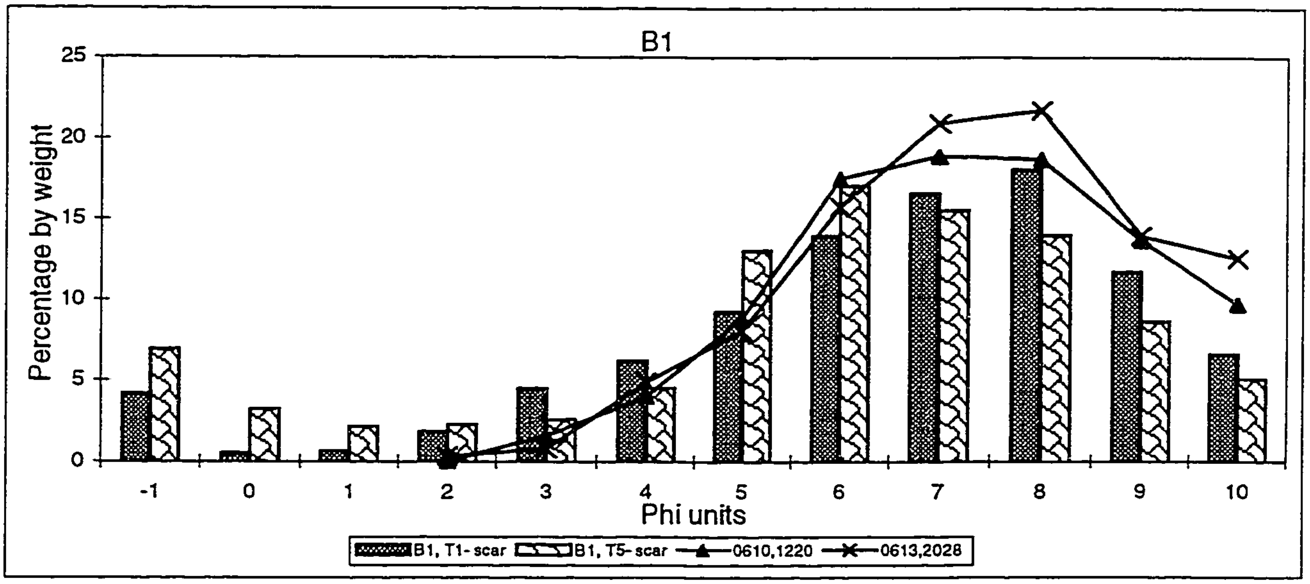

Figure 5-25: Grain-size distributions for surface and suspended sediment samples at B1.

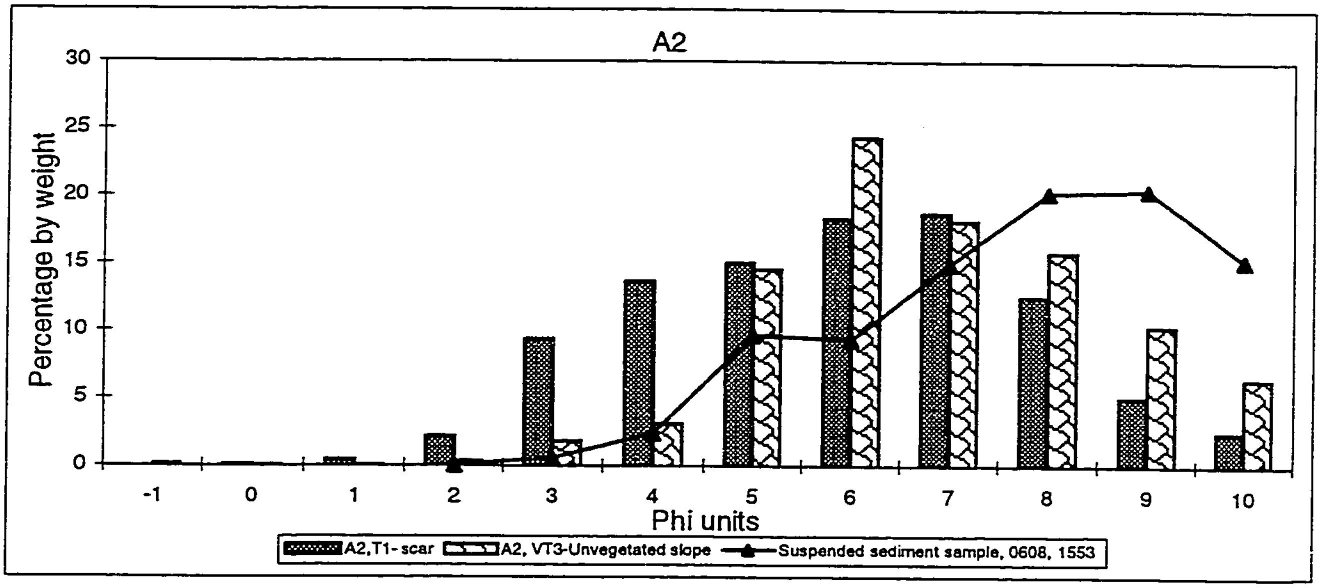

Figure 5-26: Grain-size distributions for surface and suspended sediment samples at A2.

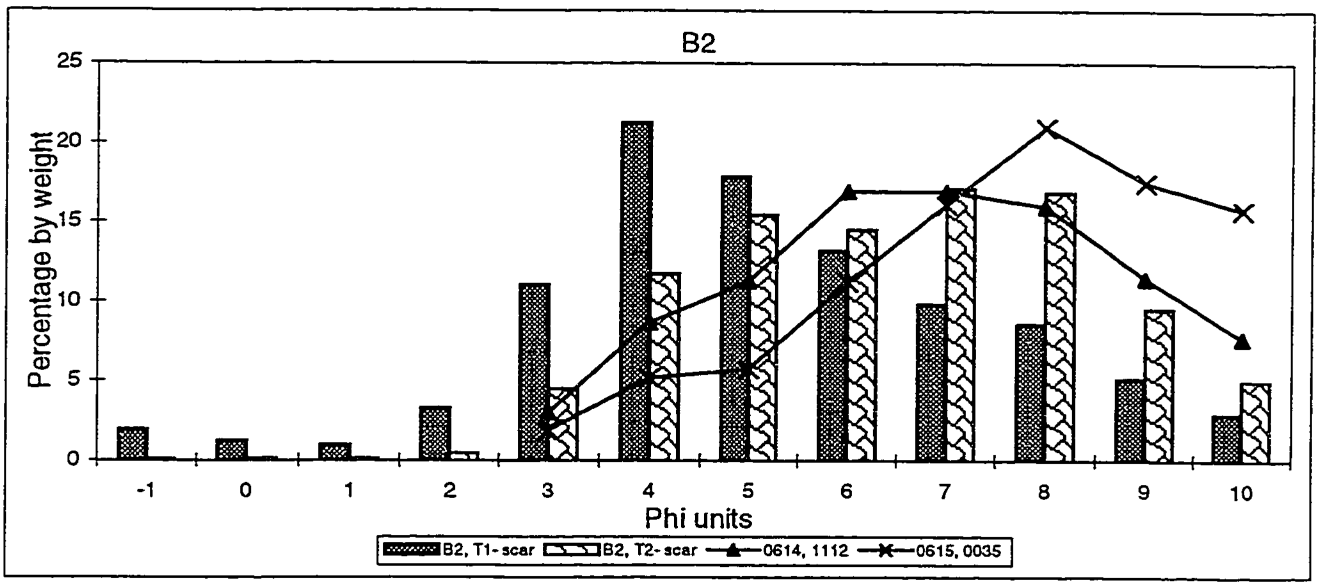

Figure 5-27: Grain-size distributions for surface and suspended sediment samples at B2.

The samples from site A are poorly to very poorly sorted and all samples at site B are very poorly sorted (see Table 5-2). All surface sediment samples are very positively skewed and kurtosis varies from very platykurtic (A3 - T3, A3 - T5, A4 - T1) to leptokurtic (A3, T1, B1- T1, B1 - T5, B4 - T4) (see Table 5-2).

The mean and median grain-sizes of the suspended sediment samples fall between 5.9 and 7.8 ϕ (Figure 5-28). After the coal was burned from each sample, both the mean and median Phi values increased slightly. Sample A3, 0609 1608 was an aberrant case as the median decreased slightly after the removal of the coal. All of the coaled samples were poorly to very poorly sorted. After baking, the degree of sorting improved, and the samples became more positively skewed indicating that most of the larger grain-sizes consisted of coal.

Several inferences can be made by comparing the grain-size distributions of surface samples with those in the wash. The grain-size distributions of the suspended sediment samples at A1 and B1 closely mirror the distributions in the surface samples (see Figures 5-24 and 5-25). At these plots, surface wash does not have the competency to transport significant amounts of grain-sizes larger than about 3 ϕ. Sediment transport appears to be more selective at the old detachment slide scars (Figures 5-26 and 5-27) where particle size distributions in suspended sediment samples are slightly shifted towards the finer grain-sizes, but the surface sediments are less positively skewed than at the fresh detachment slide scars. At vegetated plots, the comparison between surface samples and suspended sediment samples indicates the selective transport of finer grained particles. Despite higher percentages of grain-sizes around 4 ϕ in the surface sediment samples, suspended sediment distributions peak between 6 to 8 ϕ (see Figures 5-22 to 5-

Figure 5-28: A, B, C, D and E: Grain-size summaries for suspended sediment samples with and without coal.

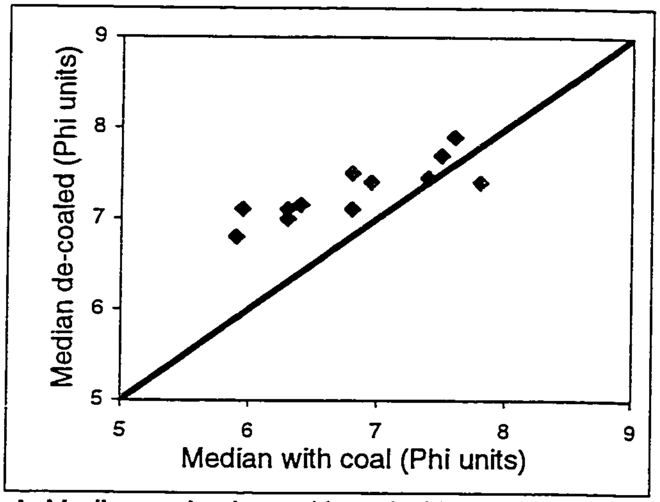

A: Median grain-sizes with and without coal.

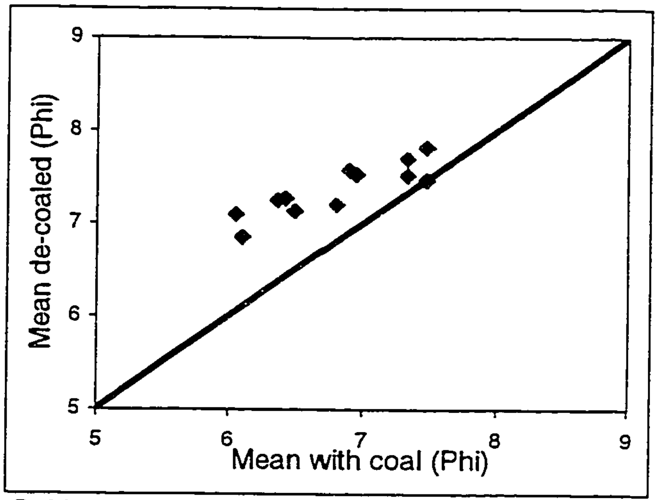

B: Mean grain-sizes with and without coal.

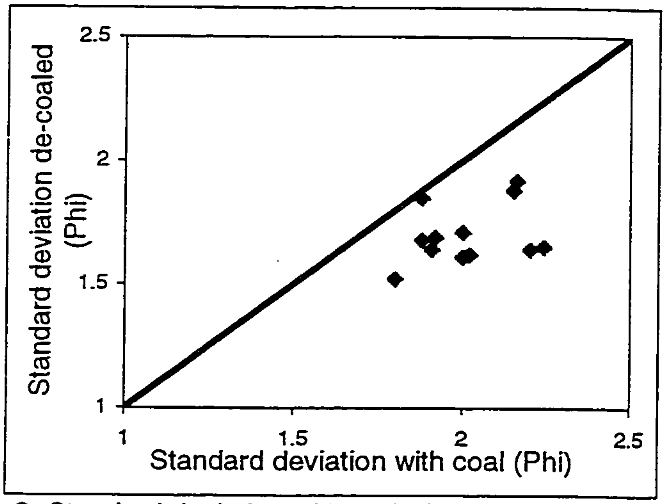

C: Standard deviation with and without coal.

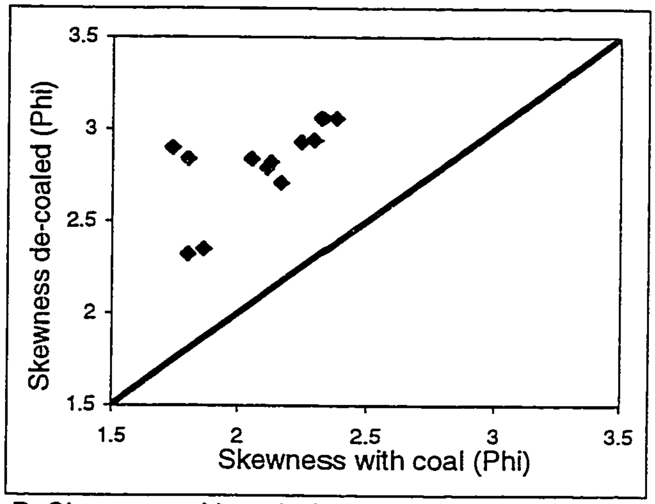

D: Skewness with and without coal.

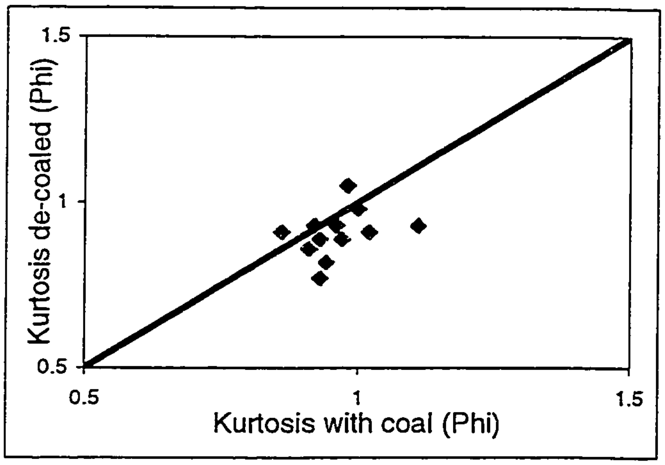

E: Kurtosis with and without coal.

23). This suggests that flows at B3 and B4 do not have the competency to transport materials in the 3 to 4 ϕ range.

Plot A3 (see Figure 5-21) shows variable grain-size distributions in the surface sediments and in the suspended sediment samples. Surface samples from the vegetated portion of the plot mainly consist of coarse silts around 4 ϕ but the grain sizes from the other two samples collected from the central and upper parts of the plot are much finer. The suspended sediment samples are very positively skewed and more closely mirror the particle-size distributions of surface samples collected on the upper parts of the plot. A3-0617,1800 has the highest mean grain-size and is the least positively skewed of any sample. The greater competency of flow associated with higher discharges (1.3 L/s) resulted in the transport of larger particle sizes.

5.1.2.3- *Discussion (Sediment Analysis)*

Low density lignite coal is easily entrained and transported by surface wash. The preferential transport of coal occurs at low flows when energy levels are not high enough to entrain a large portion of the silt and clay particles. Loss on ignition indicates that a substantial proportion of the sediment load (up to 20% by weight during low flows) consists of coal (see Figures 5-19 and 5-20).

Grain-size distributions of coaled and de-coaled samples indicate that the larger particles transported by surface wash consist of coal. The P.S.A. analysis of coaled samples can incorrectly suggest higher energy levels of the transport medium. Therefore, determining the coal distribution in suspended sediment samples is necessary when assessing the fluvial energy environments if coal is present in the wash load.

The largest portion of suspended sediment, fine silt, can be transported under most flow conditions. Local variations in vegetation cover and surface sediment determine the availability of fine materials. Grain-size distributions of surface sediments at most vegetated slopes are less positively skewed than the surface sediments at the fresh and old detachment slide scars (see Table 5-2). However, the suspended sediment samples from the vegetated slopes are very strongly skewed, which suggests surface wash is selectively removing fine particles from the slope. At fresh detachment slide scars, the grain-size distributions of suspended sediment samples closely resemble those from the surface sediment (see Figures 5-24 and 5-25). The suspended sediment distributions at A3 show the greatest amount of variability between samples (see Figure 5-21). This variability is probably due to:

1. The wide range of discharges (from 284 mL/s to 1286 mL/s) at which the samples were obtained.
2. Possible changes in contributory area.

Slopewash appears to have the competency to transport fine silts to clays under most runoff conditions. Surface sediments at fresh detachment slide scars are rich in fines, and these are reflected in the wash load. There is a shift towards slightly coarser surface sediments at the older detachment slide plots, while grain-size distributions for suspended sediment samples remain similar to those at the fresh scars. The surface samples at vegetated slopes are characterized by the coarsest sediments. The trends in grain-size distribution for surface samples show that the finest sediments are found on the youngest slope surfaces, however suspended sediment samples from all plots consist of uniformly fine materials (6 to 8 ϕ range). This suggests that surface wash may preferentially remove the finer particles, resulting in the gradual coarsening of surface sediments over time.

5.1.3 – Suspended Sediment Amounts

The results from sections 5.1.1.2 and 5.1.1.3 indicate that although diurnal variation in suspended sediment concentrations can be significant (up to 60%), the greatest scatter in the suspended sediment concentration - discharge relationships can be attributed to seasonal variation (up to two orders of magnitude). Therefore, to more accurately determine suspended sediment loads, the flow season was separated into a maximum of four different periods of transport: early melt, main melt, recession flow, and rainfall (see Section 3.3.2). Polynomial and linear rating curves were then used to develop relationships between discharge and suspended sediment concentrations so that sediment loads could be more accurately predicted (Figure 5-29 to 5-35). The suspended sediment – discharge rating equations are presented in Appendix C-4.

In 1996 the total suspended sediment loss varied from 0 g/m^2 at A4 and A5 where no surface runoff was generated to 1482 g/m^2 at A1 (Table 5-3). The hypothesized relationship between sediment loss and freshness of scar was present at both the A and B sites where the total plot losses mirror the pattern of average suspended sediment concentrations (compare Tables 5-1, 5-3). There is a progressive decrease in sediment yield from A1 to A2 to A3 to A4, and from B1 to B2 to B4. The mixed plot B3 which has the highest vegetation cover (~30%) had the lowest total suspended sediment load (6.2 g/m^2) of any plot that produced surface runoff.

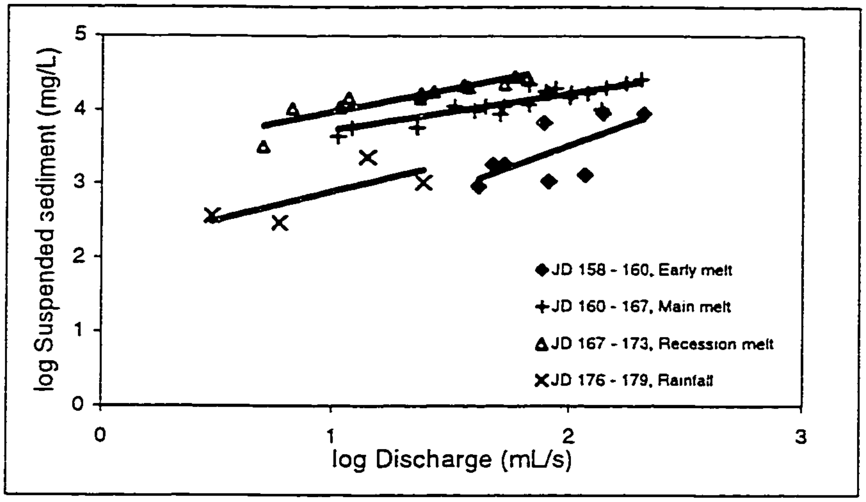

Figure 5-29: A1, 1996.

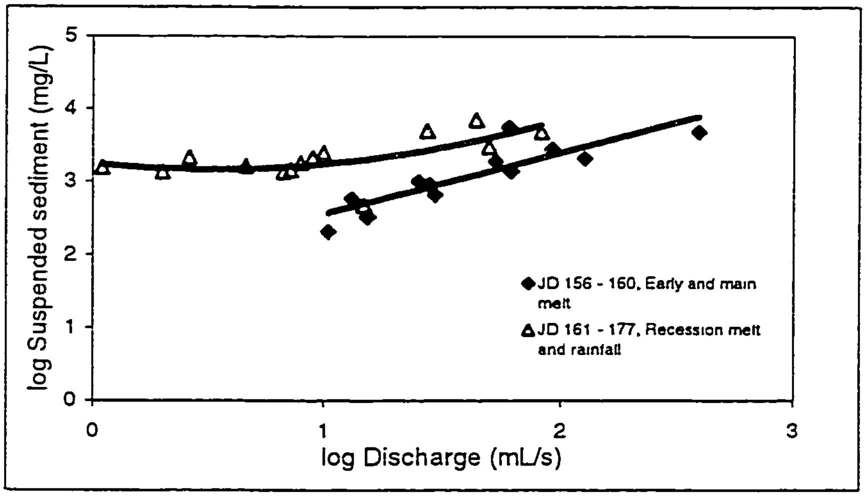

Figure 5-30: A2, 1996.

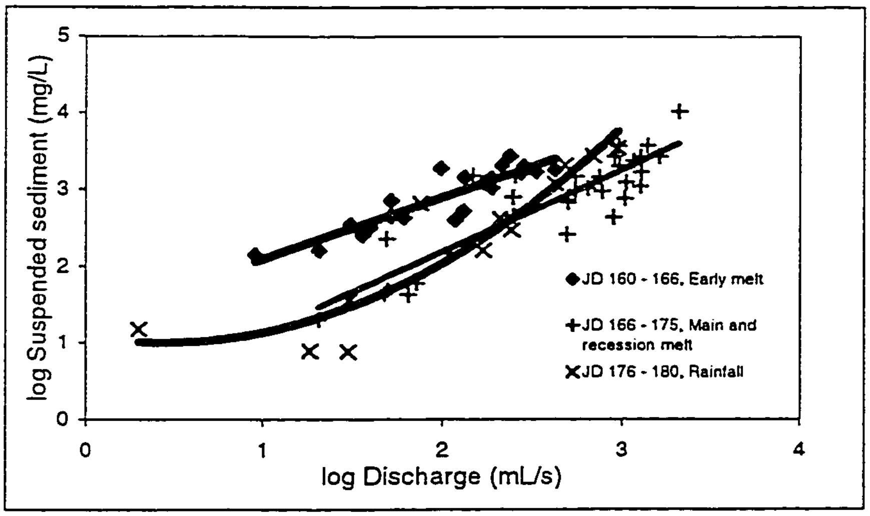

Figure 5-31: A3, 1996.

Figures 5-29 to 5-31: Discharge - suspended sediment rating curves for site A.

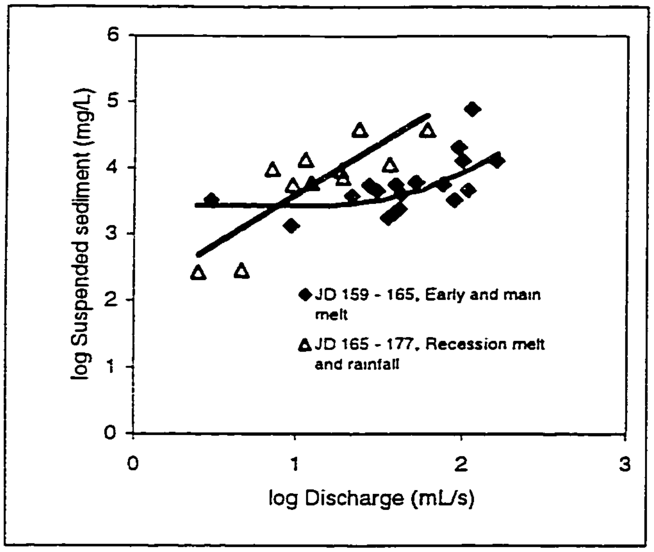

Figure 5-32: B1, 1996.

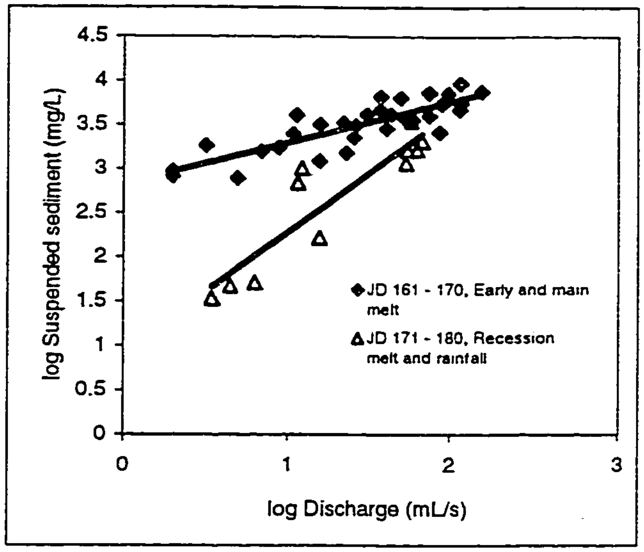

Figure 5-33: B2, 1996.

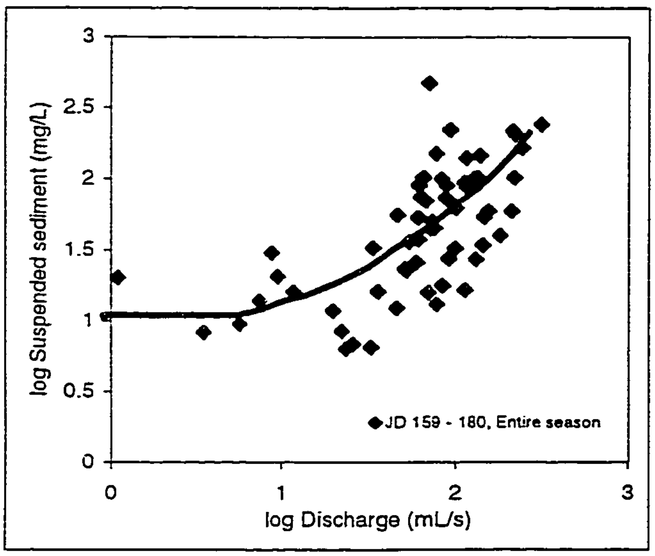

Figure 5-34: B3, 1996.

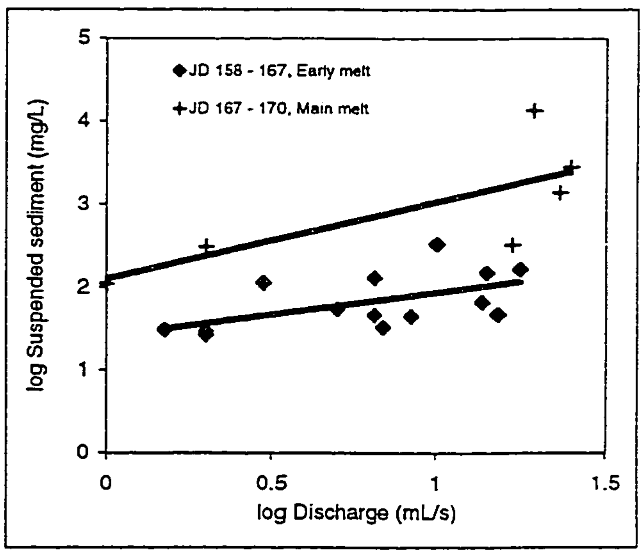

Figure 5-35: B4, 1996.

Figures 5-32 to 5-35: Discharge-suspended sediment rating curves for site B.

The highest amount and relative proportion of suspended sediment removed during rainfall-induced runoff occurred at A3. During rainfall 13% (9.3 g/m^2) of the suspended sediment load was transported by 11% of the total runoff generated at A3. Overall, rainfall events following snowmelt did not remove significant proportions or absolute amounts of sediment from the plots (Table 5-3). This is because only small amounts of runoff were produced at the most erodible plots (A1, B1). Given high suspended sediment concentrations, if substantial amounts of surface runoff were to be generated, unvegetated slopes could be susceptible to large amounts of sediment erosion.

Table 5-3: Suspended sediment yields and aeolian inputs.

Plot	**Suspended sediment yield, removal during snowmelt (g/m^2)**	**Suspended sediment yield, removal during rainfall (g/m^2)**	**Total suspended sediment yield (g/m^2)**	**Aeolian inputs (g/m^2)**
A1	1480.0	1.6	1482.0	156.0
A2	324.0	1.19	325.0	104.0
A3	64.0	9.27	73.3	77.0
A4	0.0	0.0	0.0	81.7
A5	0.0	0.0	0.0	12.5
B1	676.0	10.2	686.0	79.1
B2	244.0	18.7	263.0	59.8
B3	5.85	0.36	6.2	92.3
B4	20.6	0.0	20.6	90.8
A1, 1993	948.0	0.0	948.0	unavailable
A3, 1993	22.8	0.0	22.8	unavailable

A comparison between 1993 and 1996 indicates that suspended sediment losses at A1 and A3 were both lower in the earlier year (Table 5-3). 948 g/m^2 of sediment was removed at plot A1 in 1993. This is 37% less than the total amount removed from the same plot in 1996, although 27% less runoff was generated in 1993. Similarly at A3, 73 g/m^2 of sediment was removed in 1996, but only 22.8 g/m^2 left the plot in 1993. During the earlier year 32% less runoff was produced, most of which was generated from a large snowbank on the lower well-vegetated portion of the slope, resulting in the lower amount of suspended sediment transport.

5.1.3.1 – *Amounts of Coal Transported in the Suspended Sediment Load*

The relationships established in Section 5.1.2.1 between discharge and percentage of coal in suspended sediment load enabled the use of the continuous discharge record to predict coal percentages throughout the runoff season. Using the continuous records of coal percentage and suspended sediment amounts, a continuous record of coal amounts was obtained. The continuous coal records and the discharge records were used to determine coal yields. This method was applied only to plots from which samples were used in establishing the coal percentage-discharge relationships (A1, A3, B1 and B2).

Coal yields from the plots range from 16.4 g/m^2 at A3 to 166.9 g/m^2 at A1. Although the absolute amount was the lowest at A3, this value constitutes over 22% of the total weight of sediment removed from the plot. Lower values were calculated for the other plots (16% at B1, 13.2% at B2 and 11.3 % at A1). The density of silt clay is about 2.5 times the density of low grade lignite coal. Therefore the volume of coal relative to the total volume of sediment removed from the sites ranges from about 30% at A1 to more than 50% of the sediment by volume at A3.

5.1.3.2 – *Aeolian Inputs*

Snow samples were collected prior to snowmelt to determine snow-water equivalents and niveo-aoelian sediment concentrations.

Fifteen samples were evaluated for suspended sediment concentrations which ranged from 3039 mg/L at site A2 to 406 mg/L at B1. The average concentration was 1250 mg/L at the A sites and 748 mg/L at the B sites (Appendix C-5). A t-test for difference of means indicated that the two groups were significantly different at $p < .05$, so that when aeolian sediment inputs were calculated, two separate averages were applied. The average suspended sediment concentrations calculated for 1996 are lower than those measured by Edlund and Woo (1992) at Hot Weather Creek in 1990-91. Bellisario (1993) showed that a late season single wind storm could more than double pre-storm sediment concentrations. Therefore a large degree of seasonal variability in aeolian sediment concentrations can be expected. Considerable spatial variability in sediment concentrations is observed between samples collected in this study (see Appendix C-5).

The maximum solute concentration of snow samples did not exceed 60 mg/L. Solute concentration averages for samples from the two sites were very similar, so an overall average was calculated (26 mg/L, see Appendix C-5) and used for determining total dissolved load in the snowpack at each plot. The dissolved concentrations are up to two orders of magnitude lower than aeolian solute concentrations measured by Bellisario

(1993) at Black Top Creek and at least one order of magnitude lower than suspended sediment concentrations measured in this study.

The average sediment concentrations and dissolved solid concentrations were combined and multiplied by the water equivalent of individual plots so that the total sediment inputs could be determined for each plot. Aeolian inputs were dominated by suspended sediment which made up over 96% of the totals at all of the plots. Total inputs ranged from 156 g/m^2 at A1, to 12.5 g/m^2 at A5 (see Table 5-3). These results are compared with total sediment losses in Section 6.1.1.3.

5.1.3.3 – Discussion (Detachment Sliding, Distribution of Vegetation Cover and Sediment Inputs into the Stream)

The results presented in this chapter indicate that detachment sliding enhances rates of surface wash erosion. Suspended sediment concentrations and rates of sediment erosion measured at fresh detachment slide scars exceeded those at vegetated slopes by two orders of magnitude. Undoubtedly, vegetation plays an important role in reducing surface wash erosion. However, sediment erosion did not take place on the bare undisturbed slope (A5) in 1996, since no surface runoff was generated by the thin snow cover. The high rates of surface erosion at detachment slide scars are related to both the enhanced hydrologic conditions (see Chapter 4) and to the lack of stabilizing vegetation cover in the base of the fresh scar.

On Banks Island, Lewkowicz (1981) found that the wettest areas (those with the highest unit discharge) coincide with those possessing highest vegetation covers. Therefore on slopes where surface runoff is most commonly produced, the presence of higher vegetation cover mitigates high rates of sediment transport. The natural relationship between moisture availability and vegetation cover minimizes runoff generation and sediment removal from undisturbed unvegetated areas. This relationship is present on undisturbed slopes in the study area, but not at the fresh detachment slide scars. High rates of erosion measured at old detachment slide scars indicate that detachment sliding can alter suspended sediment yields for at least several decades.

Vegetation cover has a significant influence on suspended sediment concentrations, but it is apparent that *overall* vegetation cover cannot be used to accurately predict suspended sediment concentrations or total suspended sediment yields.

It is the distribution of vegetation cover that is most important when considering suspended sediment removal from a slope. For example, at A1, the small part of the plot above the detachment slide scar has a vegetation cover of over 50% which increases the overall vegetation cover value for the plot. However, this vegetation has very little effect on the extremely high suspended sediment concentrations measured at the flume. The distribution of vegetation cover at B3 is the opposite. A fresh detachment slide exists at the top of the site, but surface runoff generated from the scar eventually flows over the hummocky, well-vegetated (>50% cover) lower portion of the plot, where flows are slowed and dispersed. Qualitative observations made during the runoff season (the formation of small sediment fans on hummocky sections of the slope and a visible difference in the turbidity of surface runoff between the detachment slide scar and the flume) suggest that the vegetated lower portion of the slope is a zone of sediment deposition. Consequently, very low suspended sediment concentrations were measured at the flume (see Table 5-1). The lower portion of A3 is also well-vegetated with several detachment slide scars present on the upper part of the slope. A3 experienced higher suspended sediment concentrations than B3 (see Table 5-1) because a well-developed rill runs down the centre of the plot. This collects surface wash inputs from both the detachment slide scars and vegetated portions of the plot and effectively transports sediment to the base of the slope.

These observations indicate that suspended sediment removal from slopes is dependent on the distribution of the vegetation cover in relation to the areas of surface runoff generation and sediment production, and on the characteristics of the flow paths. Therefore suspended sediment removal from the detachment slide scars cannot be directly translated into sediment input to the stream. The relationship between surface wash erosion and sediment input to the river is dependent on the linkages between the slope system and the stream system.

5.2 – Dissolved Load

Three or more water samples were collected from each site during snowmelt runoff. Half of each sample was sent for geochemical analysis, and the other half was evaporated to determine the total dissolved solids concentration. The relationship between TDS and conductivity yielded the equation y = 0.60x (Figure 5-36). Solute concentrations in mg/L were estimated by multiplying the specific conductance (μS/cm) by 0.60, a value within the range from 0.55 to 0.75 according to solute types given by Gregory and Walling (1973).

The TDS values were compared to the results of the water geochemistry analysis. TDS for the latter was determined by summing the concentrations of individual ions. There was not enough sample to evaluate bicarbonate concentrations so their values were obtained by calculating the residuals. However, due to the uncertainty of these values they were not included in the comparison between evaporated and analysed samples. Despite this deficit, concentrations determined by evaporation generally yielded lower values (Figure 5-37). This type of error can not easily be explained. The predicted solute concentrations determined by the equation y = 0.60x thus represent minimum values. The continuous conductivity record was used to predict solute concentrations throughout runoff.

Solute concentrations measured at the flume are dependent on the solute content of the snow and the conditions which exist between the snowbank and the flume. The average solute concentration of all snow samples collected in 1996 is 26 mg/L (see Appendix C-5). The average concentrations measured at the sites are at least one order of magnitude higher (Table 5-4). Variables influencing solute concentrations

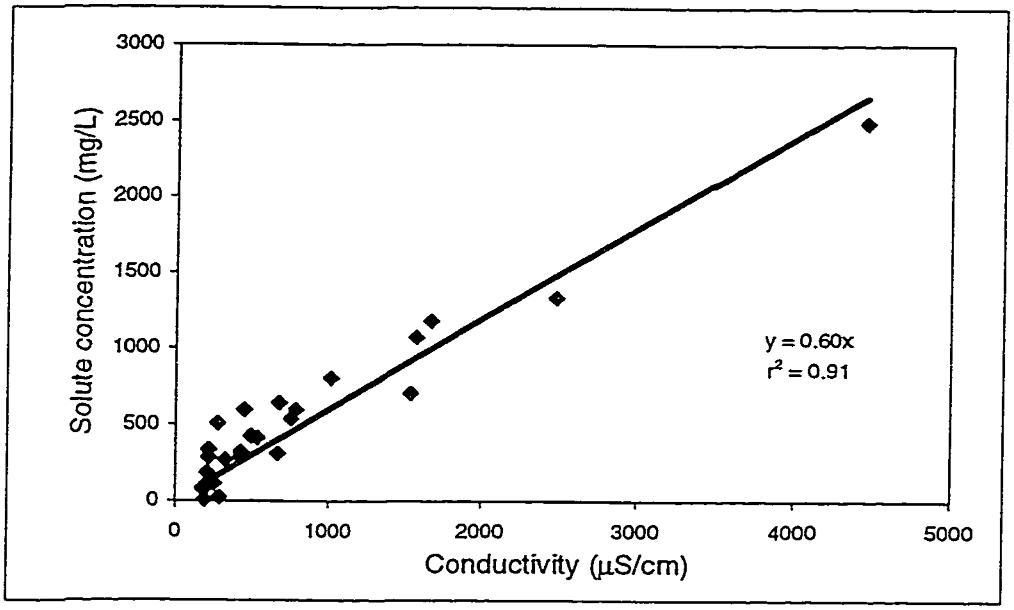

Figure 5-36: Relationship between conductivity and solute concentration. Regression constrained through zero.

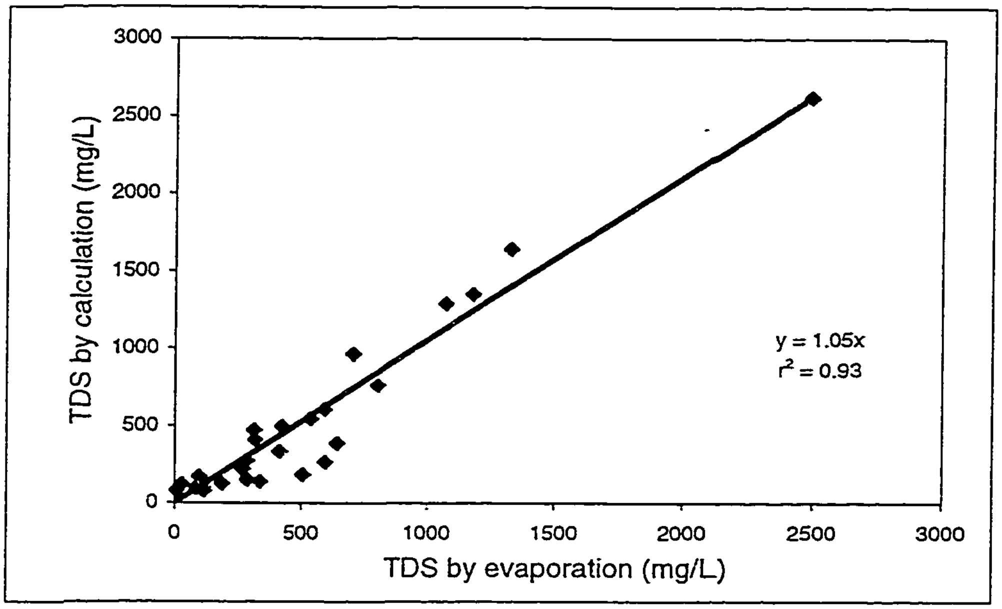

Figure 5-37: Correlation between solute concentration determined by evaporation and by geochemistry.
Regression constrained through zero.

include: a) travel time of the water between the snow edge and the collector, b) degree of flow mixing, c) solubility of the regolith, and d) temperature of the water (Lewkowicz, 1981). Given the heterogeneity of some plots, the duration of the runoff and the occurrence of rainfall-induced runoff, all of the variables changed through time.

5.2.1 – Dissolved Solid Concentrations

5.2.1.1 – Snowmelt (Seasonal Variability)

Solute concentrations during snowmelt ranged from 3673 mg/L at A1 to 40 mg/L at B4 (Table 5-4 and Figures 5-38 to 5-44). The highest average concentrations were measured at the fresh detachment slide scars, A1 and B1 and the lowest were measured at the vegetated undisturbed site, B4 (Table 5-4). Average concentrations decreased from A1 to A2 to A3, and from B1 to B3 to B4. Average solute concentrations at B2 were lower than at B3 during snowmelt (Table 5-4).

The most notable seasonal trend in solute concentrations occurred at B3 where solute concentrations increased with time (Figure 5-43). This reflects increasing residence times which can be attributed to the development of subsurface pathways within the deepening active layer, and to increasing amounts of runoff being generated from a fresh detachment slide scar located on the upper part of the plot. Although average conductivities were greatest at fresh detachment slide scars, their rilled surfaces promoted the rapid removal of meltwater, and the progression of snowmelt had little effect on solute concentrations (Figure 5-38, 5-39, 5-41, 5-42). Contrary to B3, A3

Table 5-4: Average solute concentrations and ranges in solute concentrations. [a]

Plot	Average solute concentrations for runoff season (mg/L)	Range of solute concentrations for runoff season (mg/L)	Average solute concentrations for snowmelt (mg/L)	Range of solute concentrations for snowmelt (mg/L)
A1	1620	129 - 12785	840	120 - 3673
A2	582	49 - 3487	458	49 - 2658
A3	317	70 - 1887	173	70 - 346
B1	720	300 – 2010	630	308 – 2010
B2	650	141 – 3560	352	141 – 2335
B3	605	169 – 1250	526	169 – 1250
B4	160	93 – 241	160	93 – 241

[a] Calculated from conductivity measurements.

experienced a decrease in solute concentrations during snowmelt runoff (Figure 5-40). This is probably due to the decrease in runoff generated from fresh and old detachment scars in the central part of the slope. This trend is expanded upon in section 5.2.2.2 (water geochemistry) and can be observed in suspended sediment concentrations (see 5.1.1.1).

At almost all of the plots, solute concentrations are inversely related to discharge (see figures 5-38, 5-39, 5-41, 5-42 and 5-43). Concentrations generally were diluted by higher flows during snowmelt, indicating that dissolved loads are limited by the availability of soluble ions. Only at A3 during main melt, was the inverse relationship between discharge and conductivity not as evident, probably due to plot heterogeneity (Figure 5-40).

Clockwise hysteresis is observed at most of the plots for several days during snowmelt runoff. Higher solute concentrations on the rising limbs of most diurnal

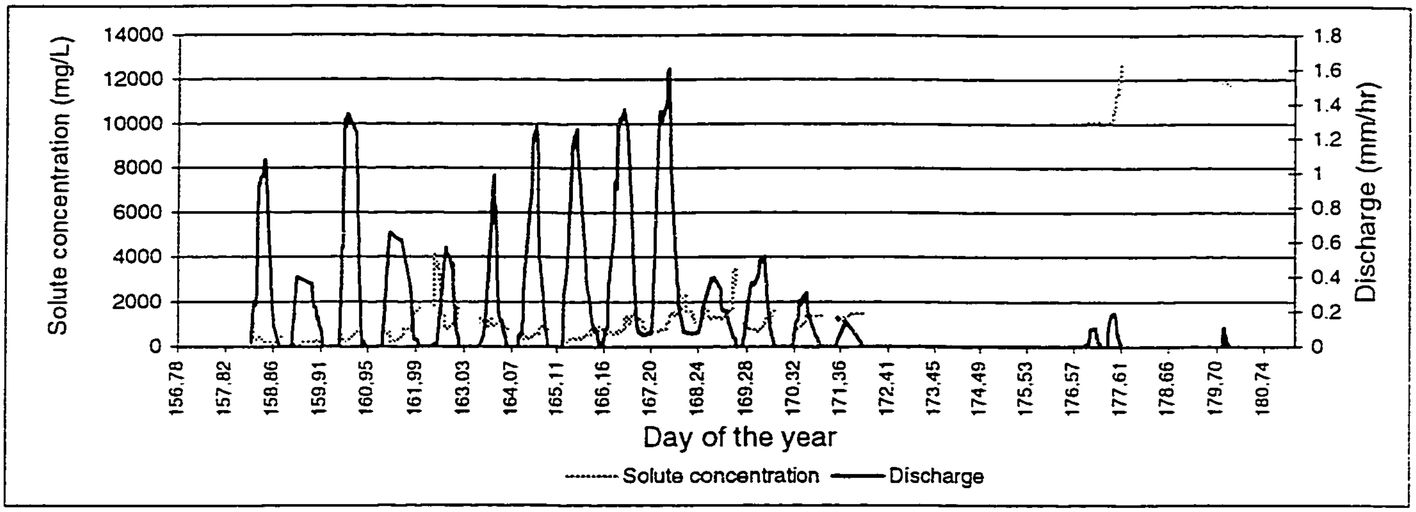

Figure 5-38: A1 1996, discharge and solute concentration.

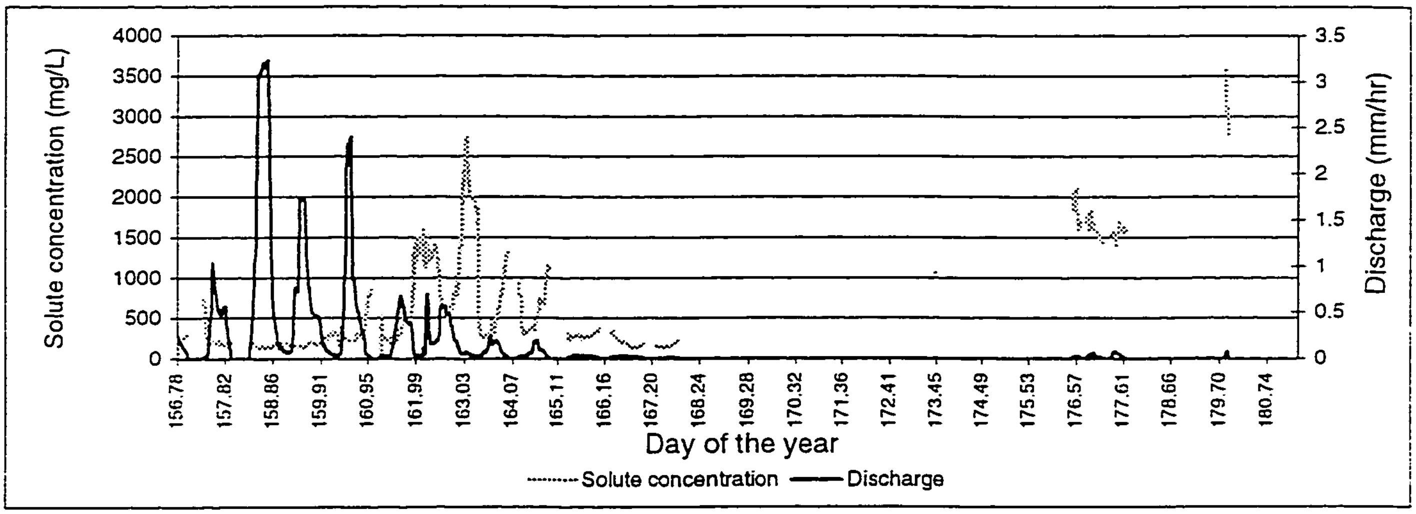

Figure 5-39: A2 1996, discharge and solute concentration.

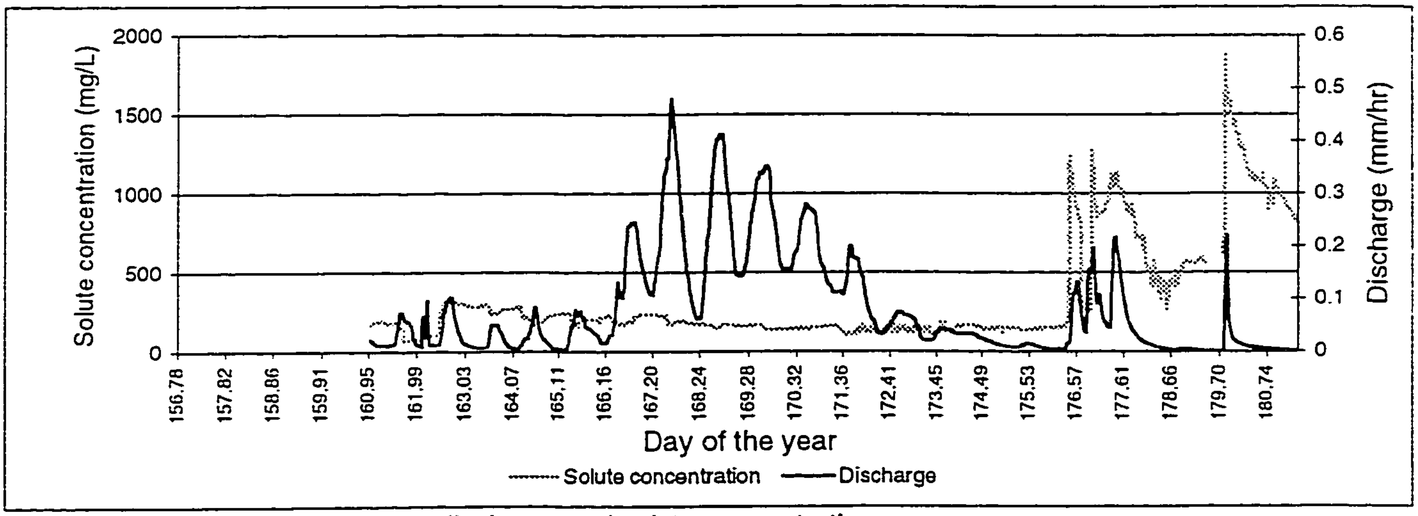

Figure 5-40: A3 1996, discharge and solute concentration.

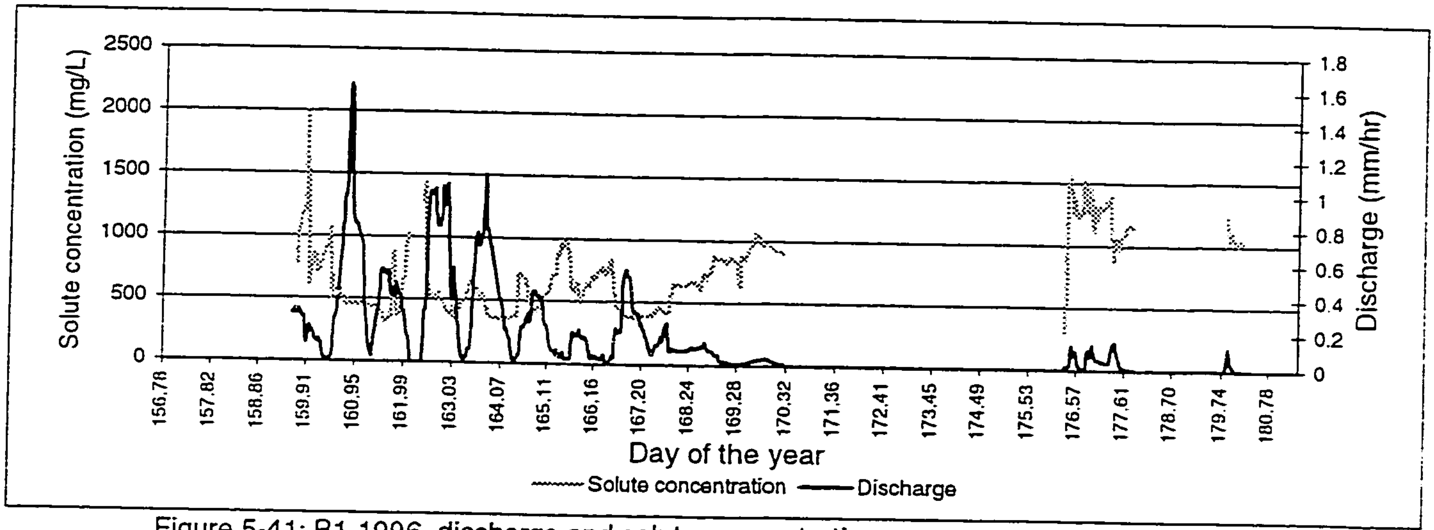

Figure 5-41: B1 1996, discharge and solute concentration.

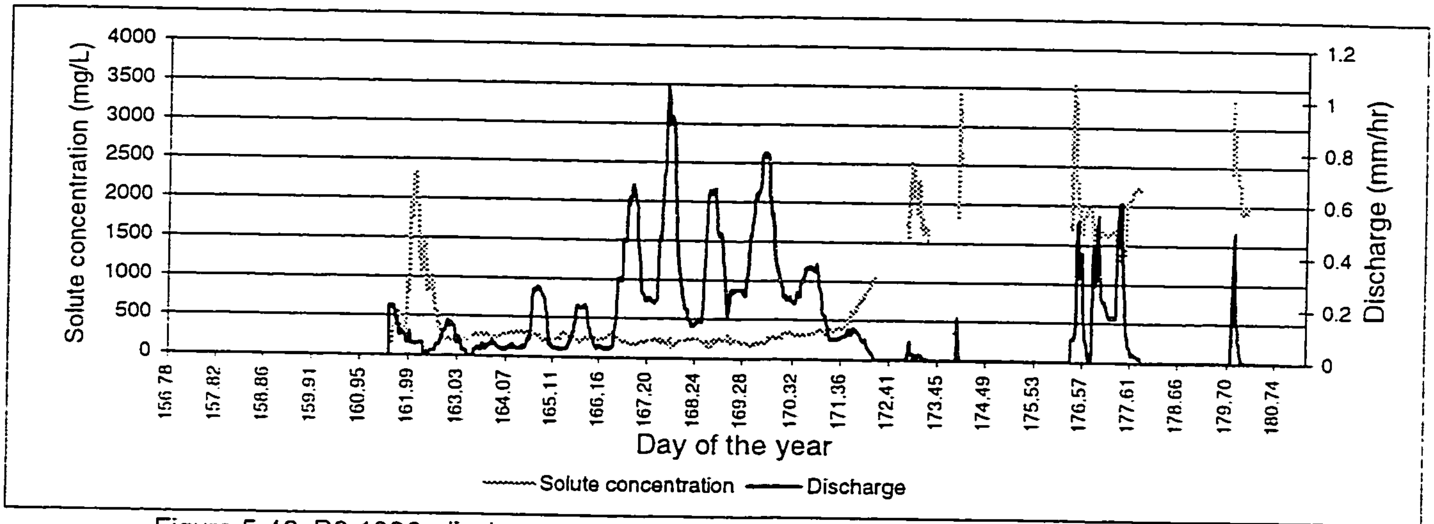

Figure 5-42: B2 1996, discharge and solute concentration.

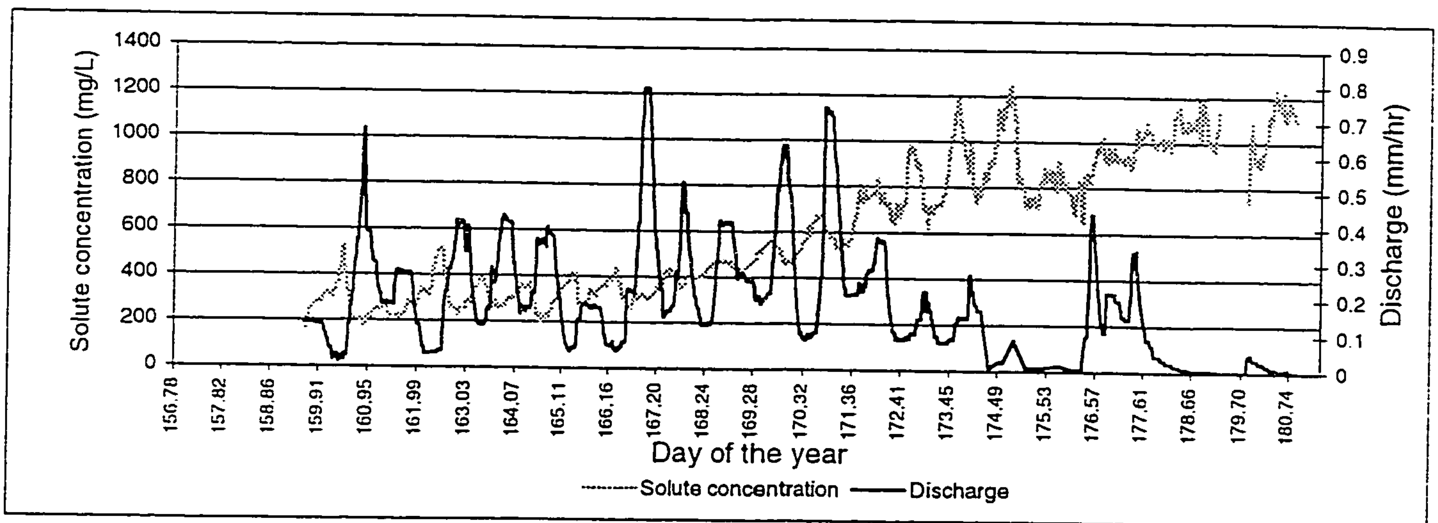

Figure 5-43: B3 1996, discharge and solute concentration.

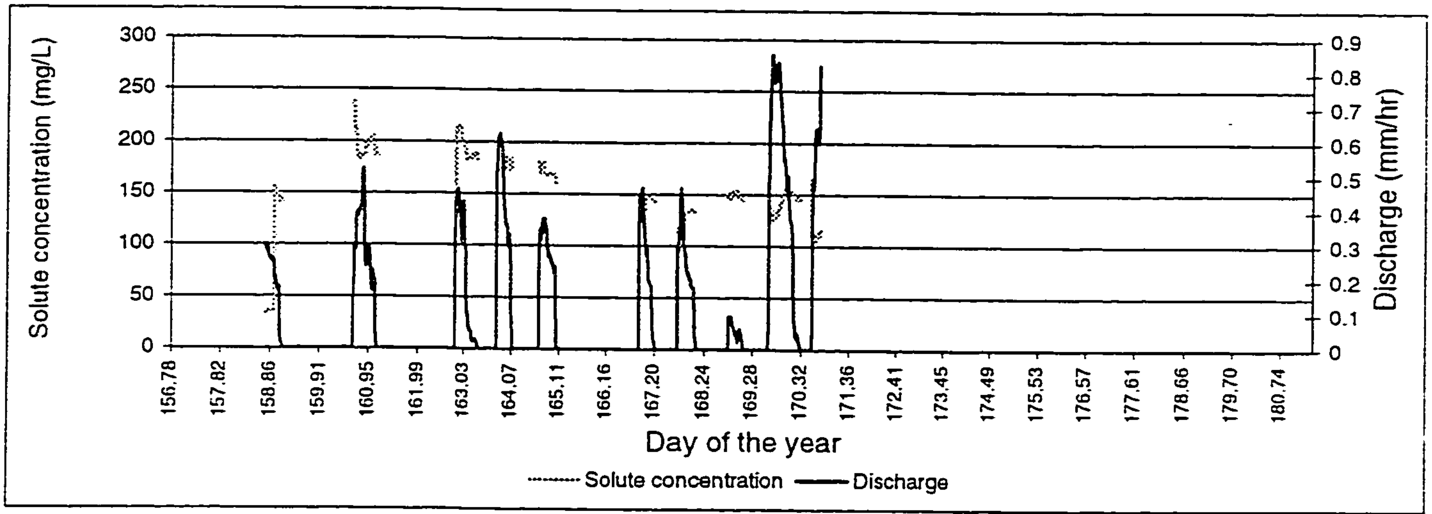

Figure 5-44: B4 1996, discharge and solute concentration.

hydrographs indicate that solutes are flushed from the slope by diurnal rise in discharge (Figures 5-45 and 5-46). Strong diurnal fluctuations in solute concentrations are noted at B3 throughout runoff. Clockwise hysteresis occurred during early melt, but as the melt season progressed counterclockwise hysteresis was observed (Figure 5-47). The stacked hysteresis curves illustrate the overall rise in solute concentrations with the progression of melt. At B3, the diurnal dilution of solute concentrations also developed a lag as the melt season progressed. During early melt, diurnal peaks in solute concentration occurred just prior to hydrograph rise (Figure 5-48). By late melt, peak solute concentrations lagged up to 6 hours behind the diurnal rise in discharge. The displacement of soil water by snow meltwater results in a diurnal flush of solutes. A lag probably develops because of the increase in active layer storage. This was not observed at detachment slide plots.

Diurnal hysteresis was also observed at plot A1, and behaved consistently in a counterclockwise direction during snowmelt runoff (Figure 5-49). This indicates that solute concentrations were higher on the falling limb of diurnal hydrographs. This may be attributed to solute charged subsurface flow collected by the rill system. During periods of discontinuous flow, subsurface discharge will lag behind peak surface discharge (Lewkowicz and French, 1982). Solute rich subsurface flow should constitute a greater proportion of the discharge during hydrograph recession. However, no additional support of this hypothesis can be provided.

A final influence on solute concentrations during snowmelt was from snowfall. A snowfall event on June 7 (JD 159) resulted in peak solute concentrations at B1 and a spike in concentrations at B3 (see Figures 5-41, 5-43). A similar event on June 09 (JD

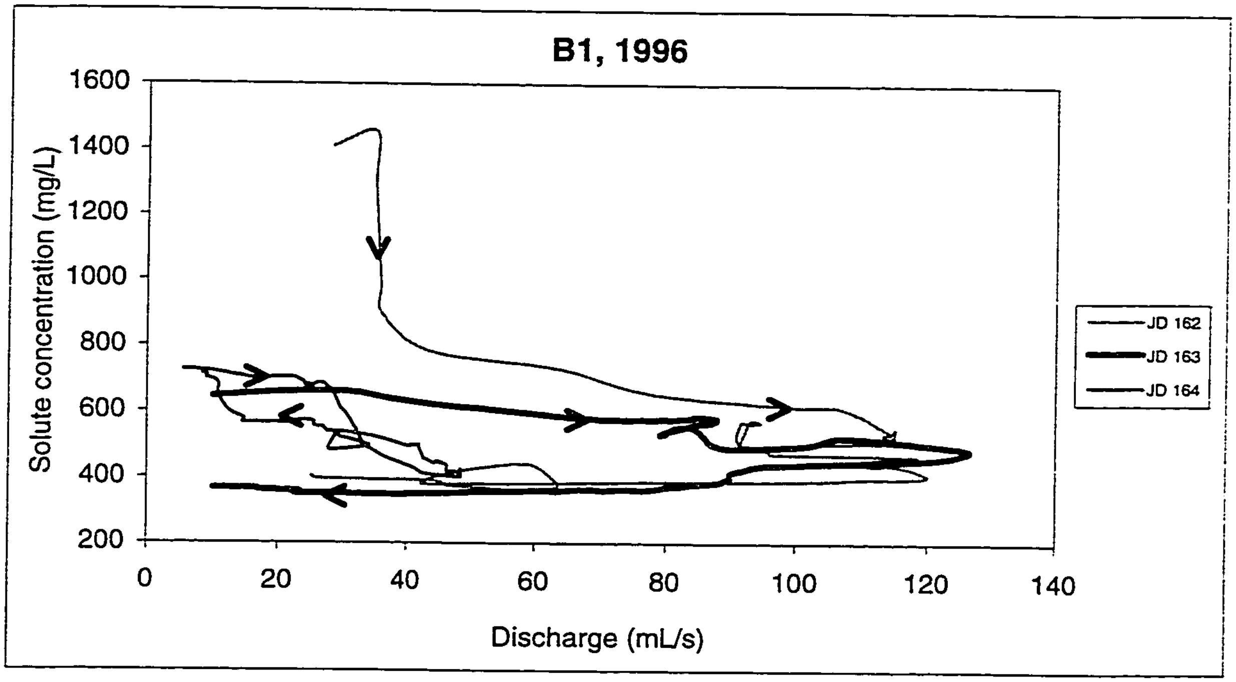

Figure 5-45: Diurnal hysteresis in solute concentrations at B1.

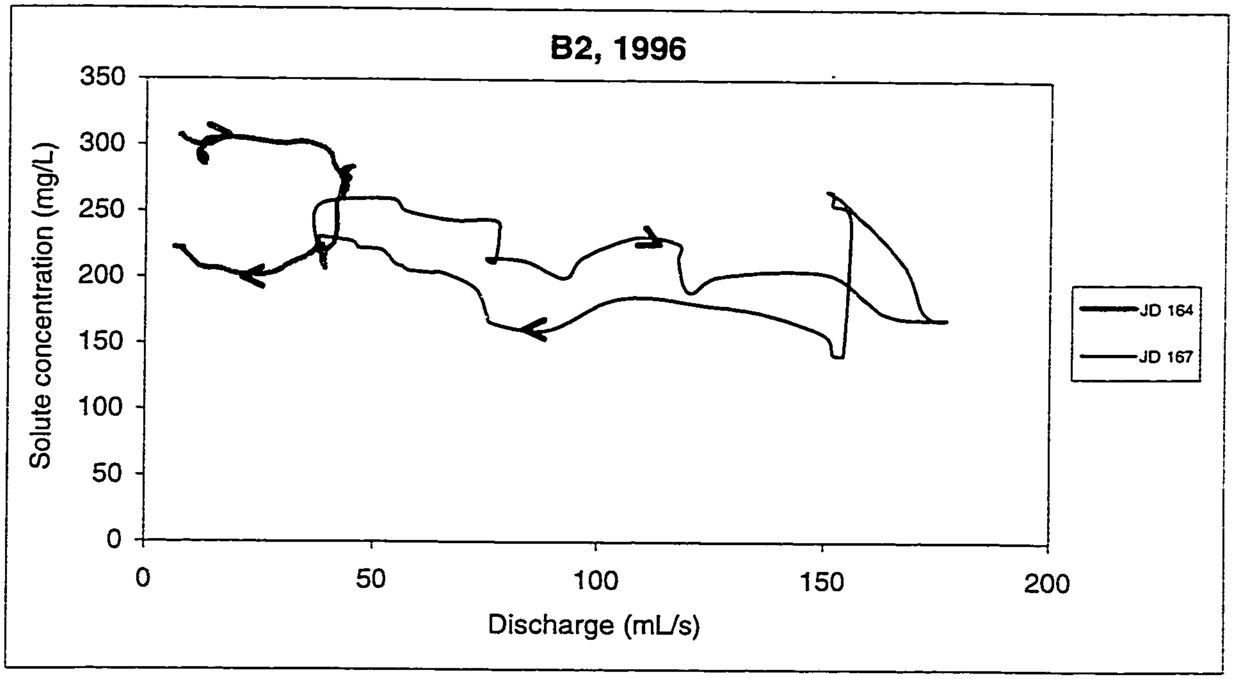

Figure 5-46: Diurnal hysteresis in solute concentrations at B2.

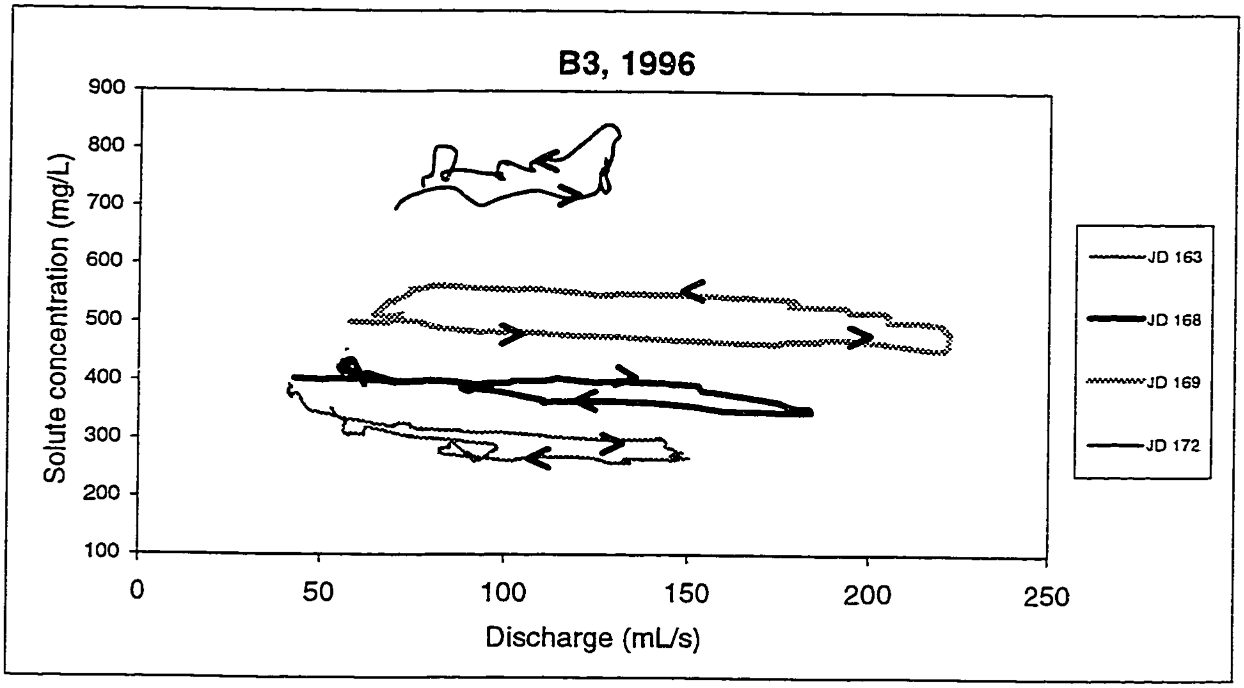

Figure 5-47: Diurnal hysteresis in solute concentrations at B3.

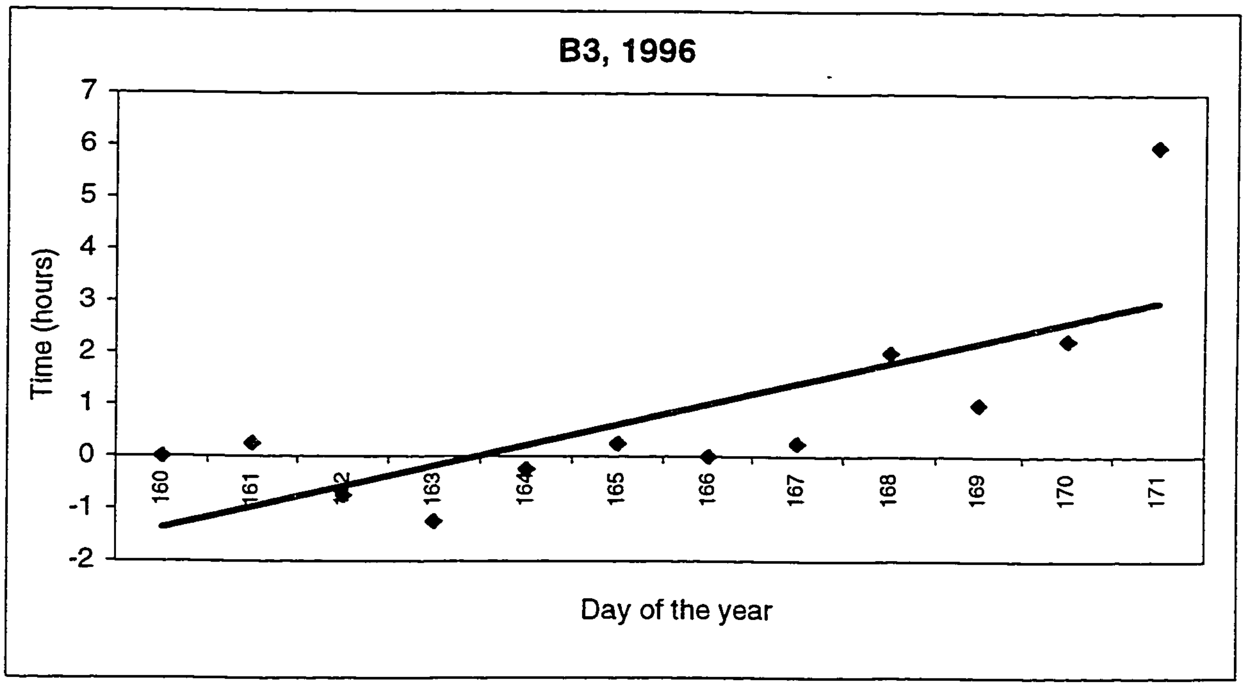

Figure 5-48: Time of peak conductivity in relation to increase in discharge, B3.

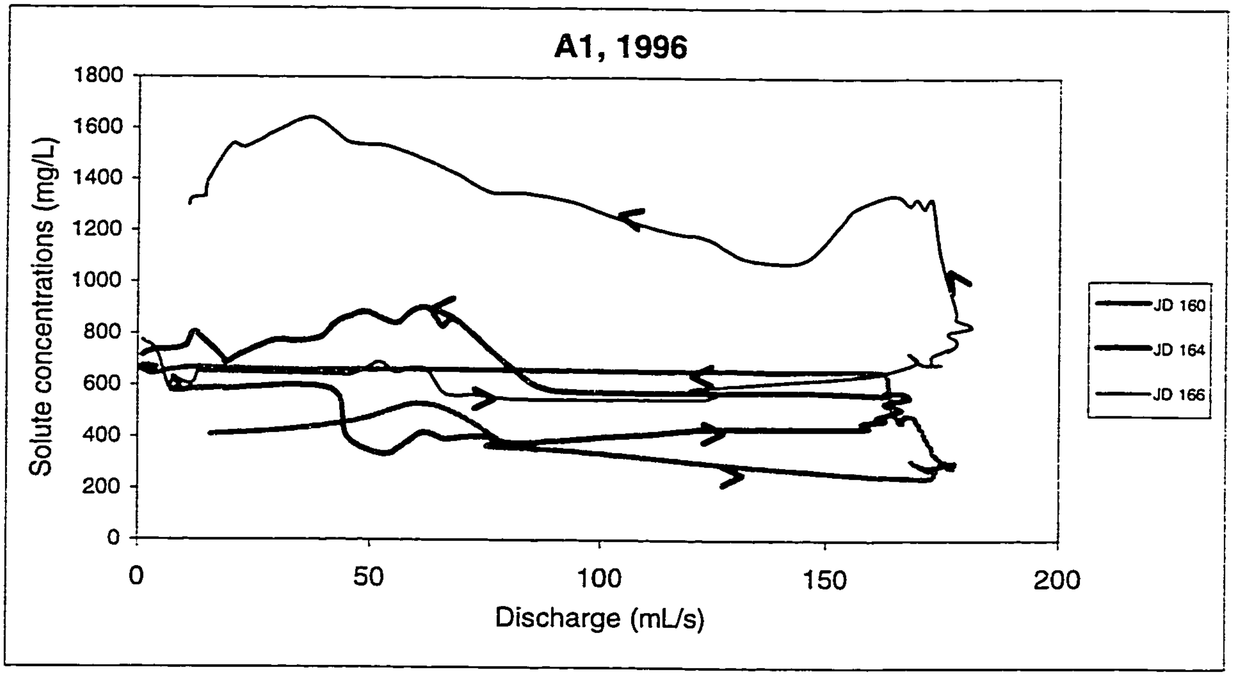

Figure 5-49: Diurnal hysteresis in solute concentrations at A1.

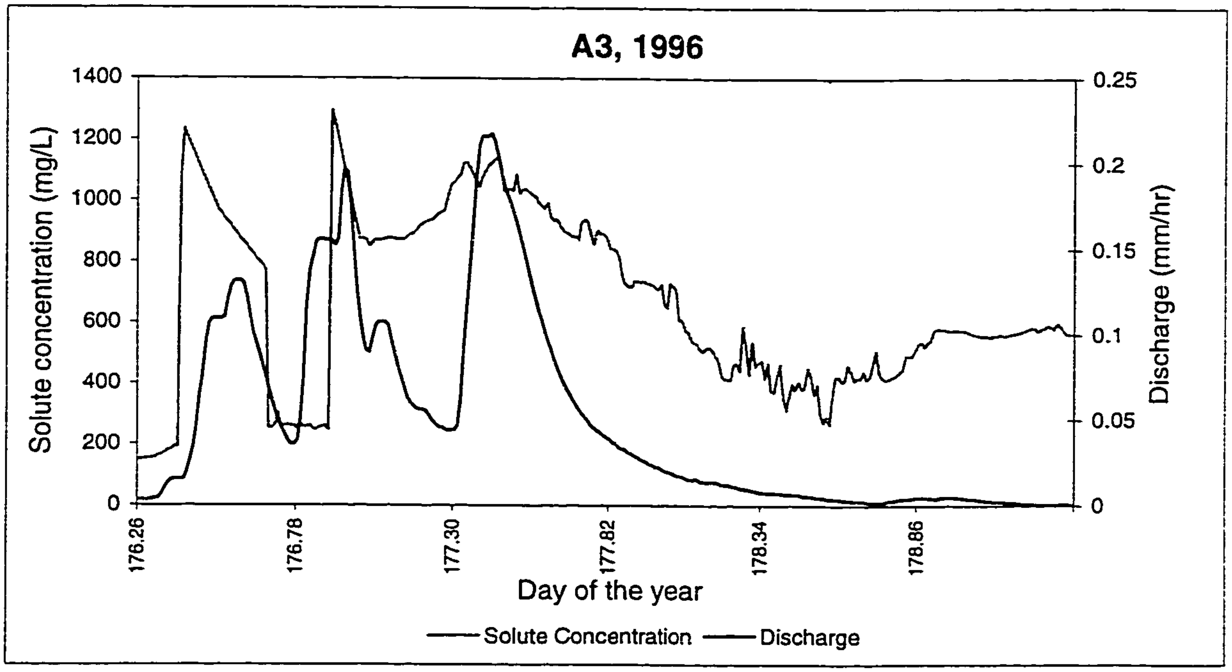

Figure 5-50: Discharge and solute concentration during rainfall-induced runoff.

161) resulted in peak concentrations at A1 and B2, and increases in solute concentrations at A2, B1 and B3 (Figures 5-41 to 5-44). This response is thought to be due to the melting of fresh snow, which results in the flush of surface salts which form due to evaporative processes on the drying snow-free sections of slopes.

5.2.1.2 - Rainfall

At A1, A3 and B2, solute concentrations during rainfall-induced runoff were an order of magnitude greater than during the snowmelt period. The highest solute concentrations during rainfall runoff, >12700 mg/L, occurred at A1. Solute concentrations during rainfall increased from A3 to A2 to A1. This trend was not repeated at site B (see Table 5-5) where peak values of 3560 mg/L occurred at B2, the old detachment slide scar.

Unlike the results from the snowmelt period, there is a positive relationship between runoff and conductivity during rainfall-induced runoff at most of the plots (Figure 5-50). This is probably due to evaporative processes which result in the formation of salt crusts on the scar surface as the slope dries (Figure 5-51), and to the more extensive flow paths associated with rainfall-induced runoff which increase the total area from which solutes may be removed (Figure 5-52). The increases in solute concentrations associated with rainfall-induced runoff are not evident at the vegetated plot B3. After snowmelt runoff, saturated conditions were sustained on this slope, promoting the rapid translocation of rainfall-induced runoff and minimizing the effect of expanding contributory areas on solute concentrations (see Figure 5-52).

Figure 5-51: Salt efflorescences form on the surface of unvegetated scars (A1) as the slope dries following snowmelt.

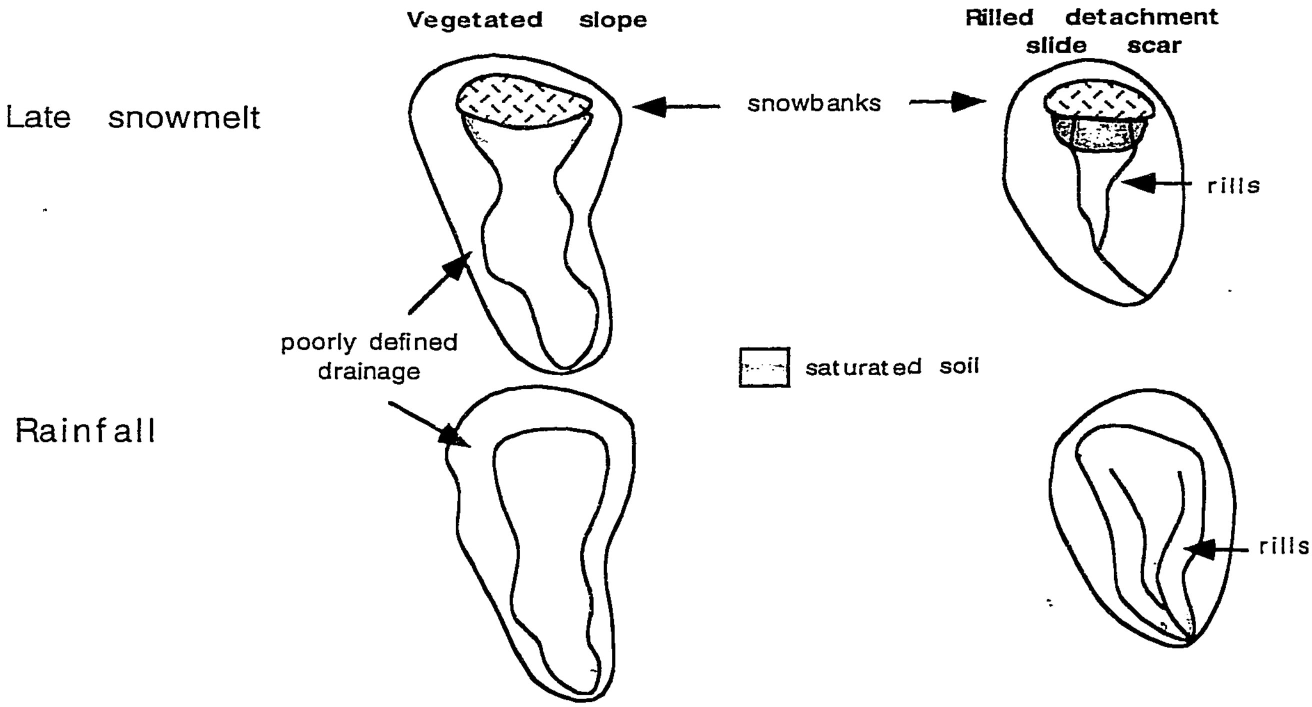

Figure 5-52: Differences in flowpaths during snowmelt and rainfall-induced runoff at a well-vegetated slope and at a rilled detachment slide slope.

Geochemical analyses of soil and surface water were undertaken to better understand the relationship between elevated solute concentrations in surface wash and freshness of scar.

5.2.2 – Geochemistry

5.2.2.1 – Soil Geochemistry

In 1997, five soil pits were dug and soil samples were collected to assess the soil geochemistry at: (1) a 1988 detachment slide scar, A1 (2) an adjacent undisturbed slope, (3) two vegetated undisturbed slopes (A3 and B3) and (4) a pre-1950 detachment slide scar (B2) (Appendix C-6).

At A1, sodium concentrations in the fresh active layer in marine sediments were up to two orders of magnitude greater than concentrations from the adjacent undisturbed slope and the well-vegetated undisturbed slopes at A3 and B3 (Figure 5-53). Concentrations increased with depth in the 1988 scar, in the adjacent slope and at B3. This is probably due to the reduced opportunity for solute removal at depths which thaw for only a short period during late summer, and may not thaw at all during cooler summers. Furthermore, if surface erosion is occurring, the active layer continually advances into the solute rich permafrost, leading to the release of additional ions at depth. At pits B2 and A3, higher Na^{+} concentrations occur near the surface of the active layer. At B2, Na^{+} concentrations in near- surface samples are an order of magnitude greater than at depth. This may be an effect of deposition as sediments are almost certainly being washed into the scar from the adjacent slope. The ions K^{+} and Mg^{++} are also relatively enriched at the fresh detachment slide (Figures 5-54 and 5-55). These

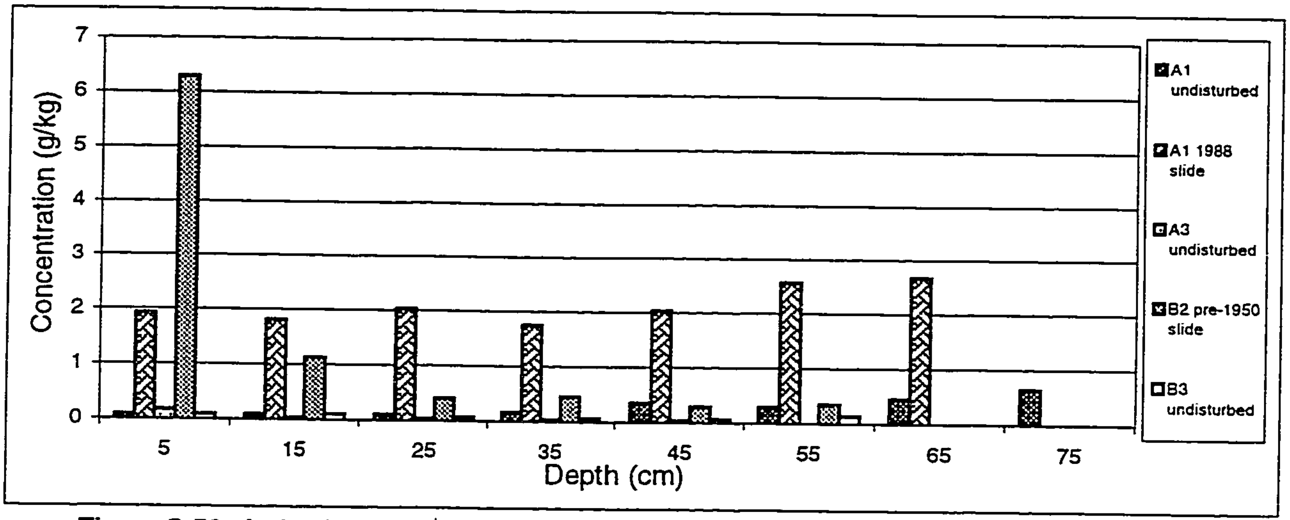

Figure 5-53: Active layer Na^{+} concentrations.

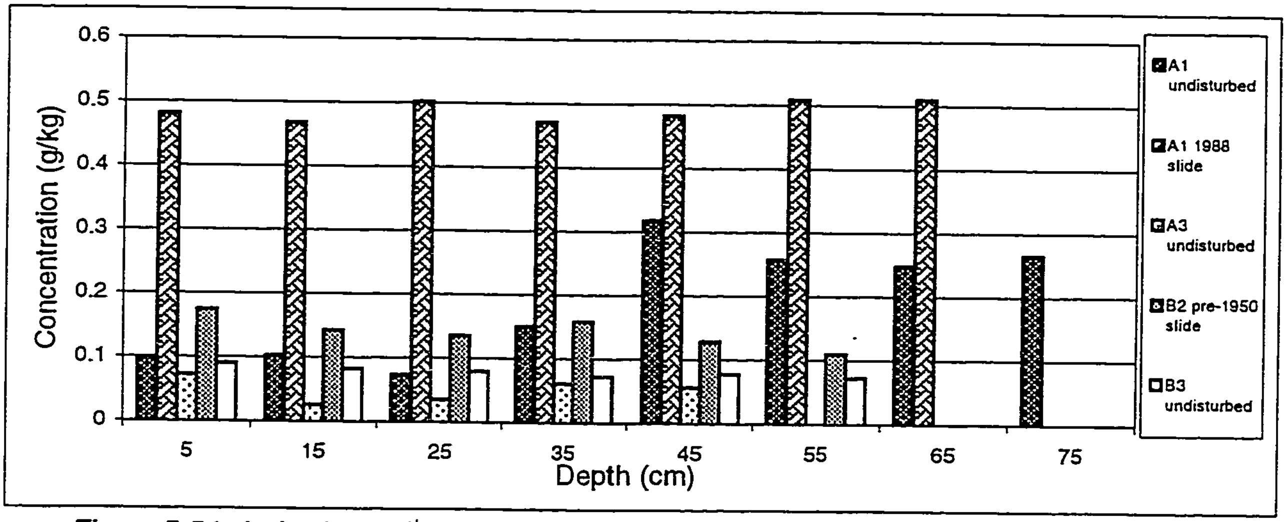

Figure 5-54: Active layer K^{+} concentrations.

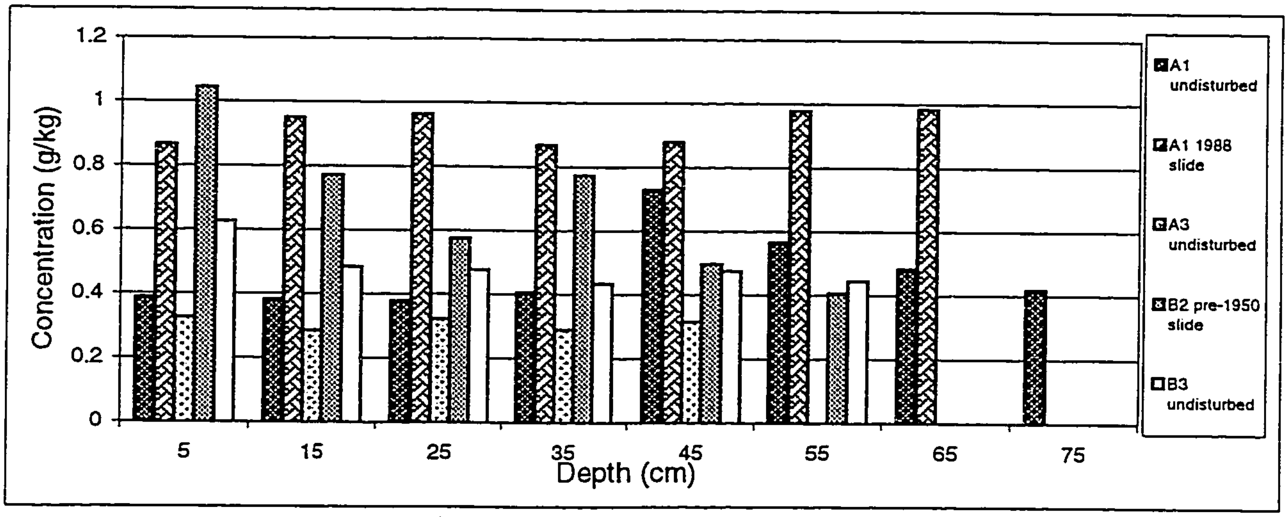

Figure 5-55: Active layer Mg^{++} concentrations.

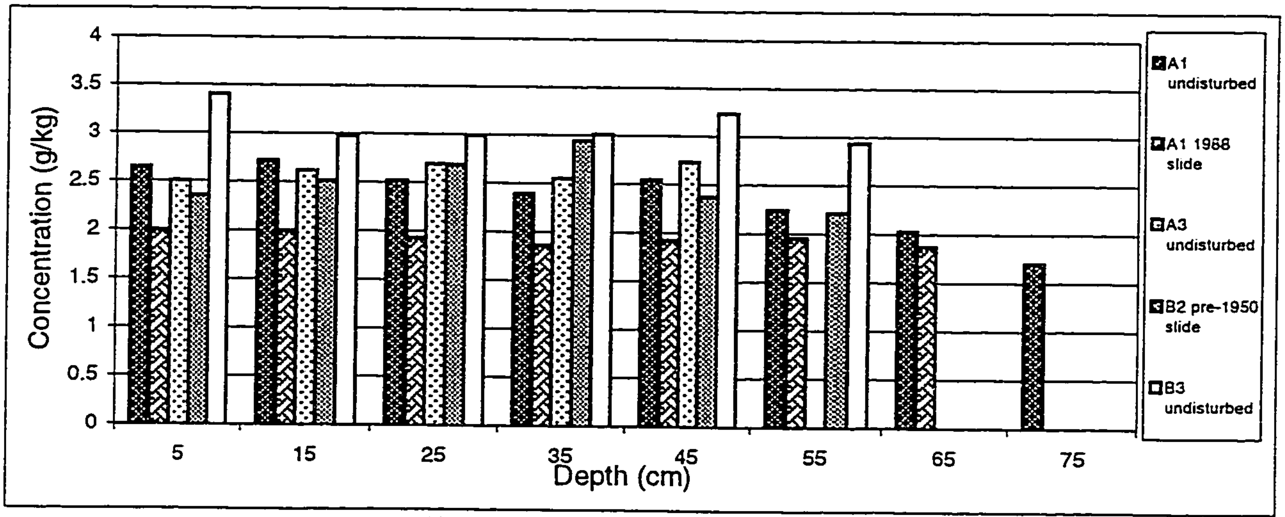

Figure 5-56: Active layer Ca^{++} concentrations.

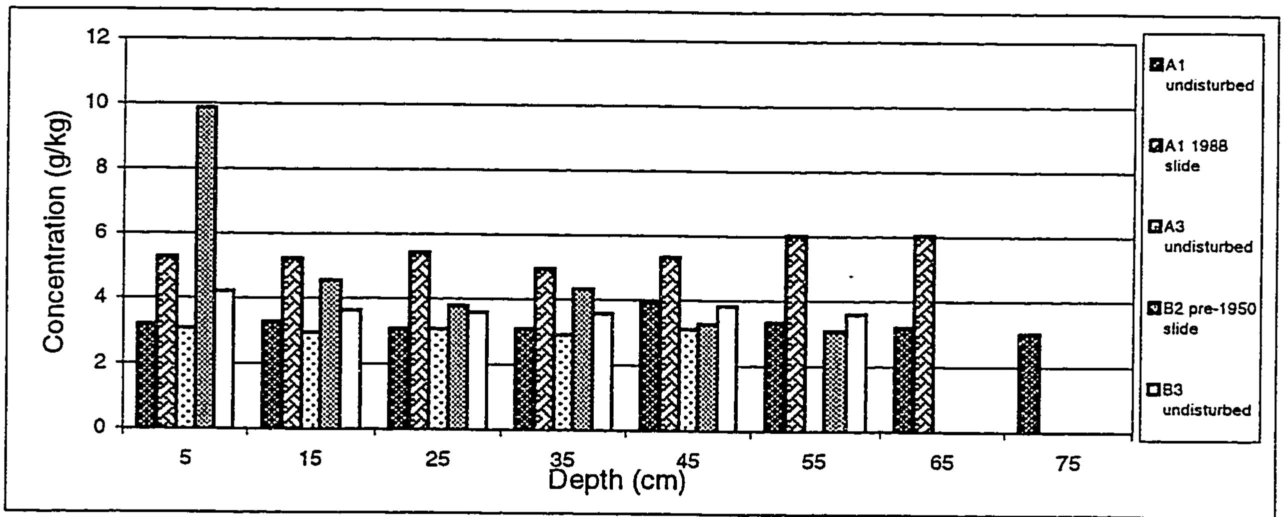

Figure 5-57: Active layer cation concentrations.

results are expected given the marine origin of the sediment. Ca^{++} values are slightly higher at the B sites but there is an indication that undisturbed sites and old slides have higher concentrations (Figure 5-56).

These results indicate that after detachment sliding in marine sediments, Na^{+} concentrations can be up to two orders of magnitude greater than on adjacent undisturbed slopes. Higher concentrations of K^{+} and Mg^{++} can also be expected at fresh scars in marine sediments while concentrations of Ca^{++} decrease. Overall, there is a large surplus of exchangeable cations in samples from the fresh active layer at A1. This suggests that in freshly thawed marine sediments, Na^{+}, K^{+} and Mg^{++} may exist in mineral form. This could account for the apparent differences in the cation exchange capacity of the soil samples from the fresh active layer at A1 and those from the adjacent and nearby undisturbed slopes (Figure 5-57).

At the time of sampling, salt crusts were not observed on the scar surfaces. This is because the samples were collected 4 days after a record rainfall event in 1997. As a result saline soil conditions which usually develop in the near surface sediments were not as pronounced as they would have been prior to the precipitation. The rainfall probably flushed a significant amount of the near surface salts, and may have redistributed Na^{+} within the soil profile.

5.2.2.2 - Water Geochemistry

Water samples were tested for anions (F^{-}, Cl^{-}, NO_2^{-}, Br^{-}, NO_3^{-}, HPO_4^{--}, SO_4^{--}) and cations (Al^{+++}, Ba^{++}, Ca^{++}, Fe^{++}, K^{+}, Li^{+}, Mg^{++}, Mn^{++}, Na^{+}, Sr^{++}). Due to small amounts of sample, bicarbonates (HCO_3^{-}) were determined by calculation. With the exception of

NO_3^-, Cl^-, SO_4^{--}, Ca^{++}, K^+, Mg^{++}, and Na^+ only small amounts of the other ions were measured in the water samples (Appendix C-7) and are not represented in the following graphs.

At plot A1 the relative proportions and absolute amounts of Na^+ and Cl^- increased as snowmelt progressed (Figures 5-58, 5-59) with the exception of the relative proportion of Cl^- which decreased from June 19 (JD 171) to June 20 (JD 172). At A2, relative proportions of Na^+ and Cl^- decreased from June 7 (JD 159) to June 8 (JD 160), but absolute amounts increased. At this time SO_4^{--} increased in both proportion and absolute amount. There was little variation in relative proportions or absolute amounts between the last two samples. At A3, the larger heterogeneous plot, relative proportions and absolute amounts of Na^+ and Cl^- increased from early morning on June 9 (JD 161) to the afternoon of June 10 (JD 162). During an early morning late melt sample on June 20 (JD 172), the relative and absolute importance of Na^+ and Cl^- were the lowest, probably because most of the runoff during this time is derived from a north facing late lying snowbank on the lower vegetated portion of the slope. Conversely, the greatest relative proportions of Na^+ and Cl^- occurred on June 10 (JD 162) near peak daily flow, during early melt, at which time a relatively large proportion of the runoff was being generated from several detachment slide scars on the middle portion of the plot.

At B1, relative proportions and absolute amounts of the major anions and cations showed little variation (Figure 5-60, 5-61). SO_4^{--} constituted over half of the ionic load in each sample, and NO_3^- and Ca^{++} made up a greater proportion of the ions than at any A site. Na^+ and Cl^- constituted only a small portion of the total ions at B1 despite it

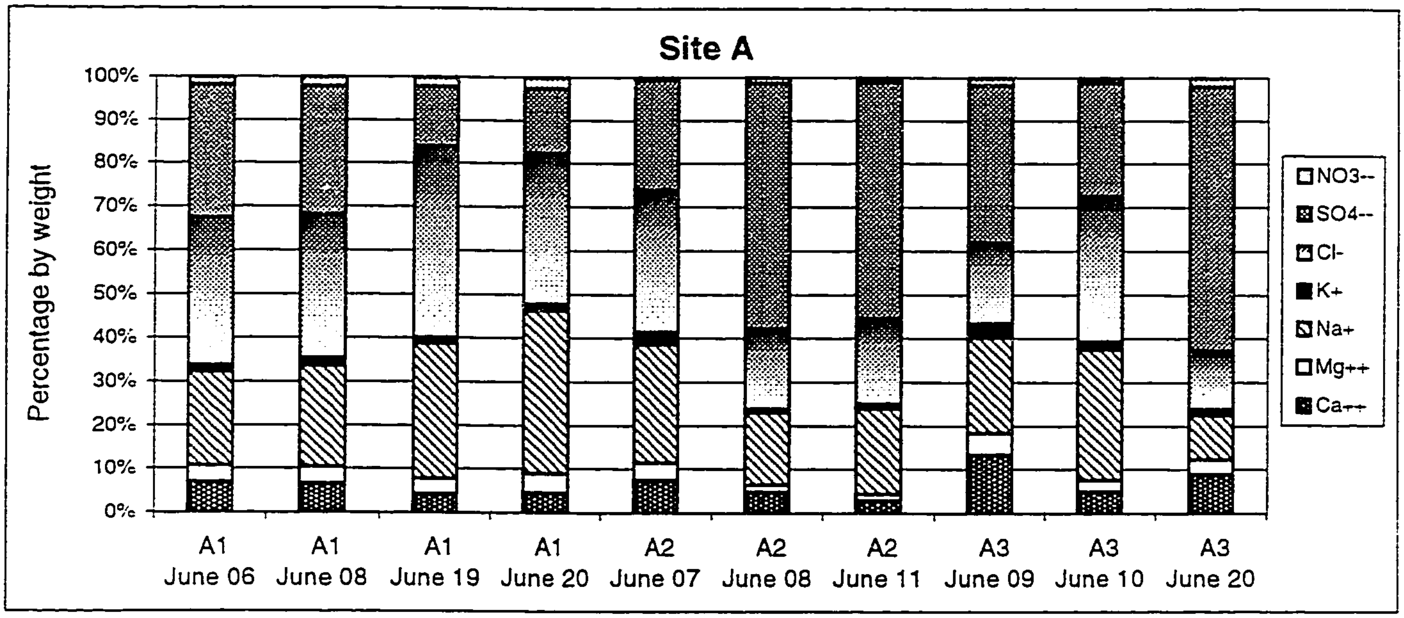

Figure 5-58: Dissolved solids analysis for Site A.

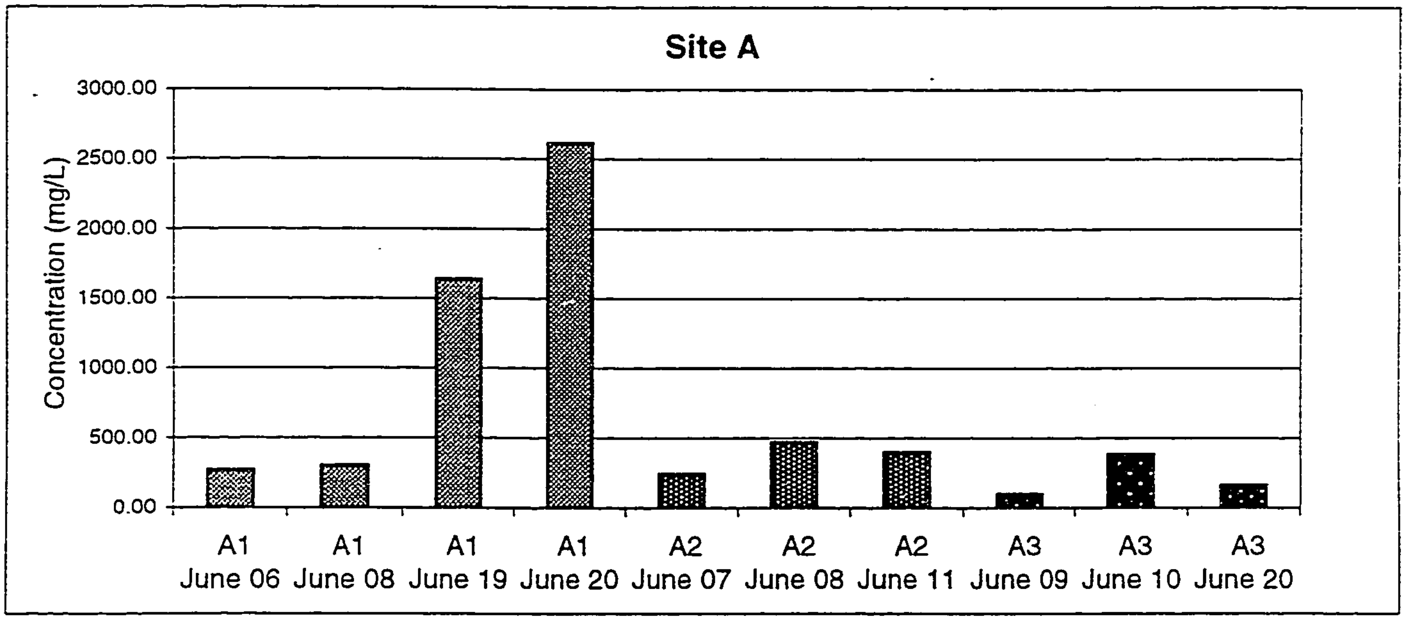

Figure 5-59: Solute concentrations of water chemistry samples for Site A.

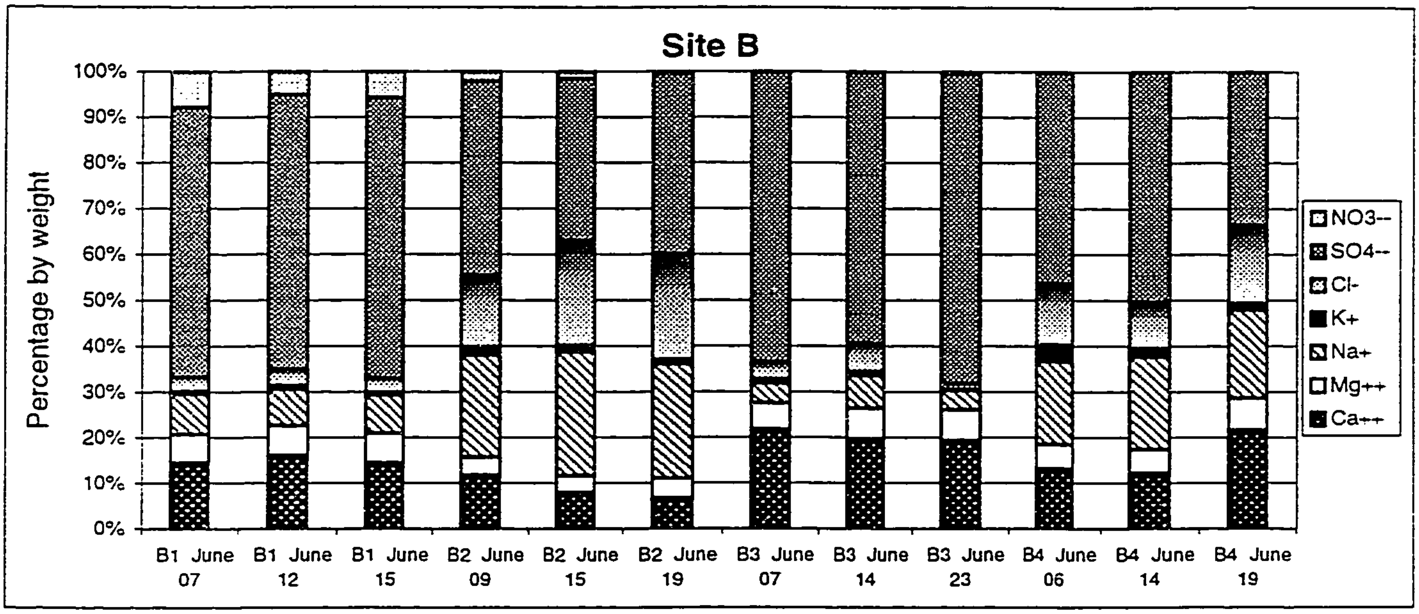

Figure 5-60: Dissolved solids analysis, Site B.

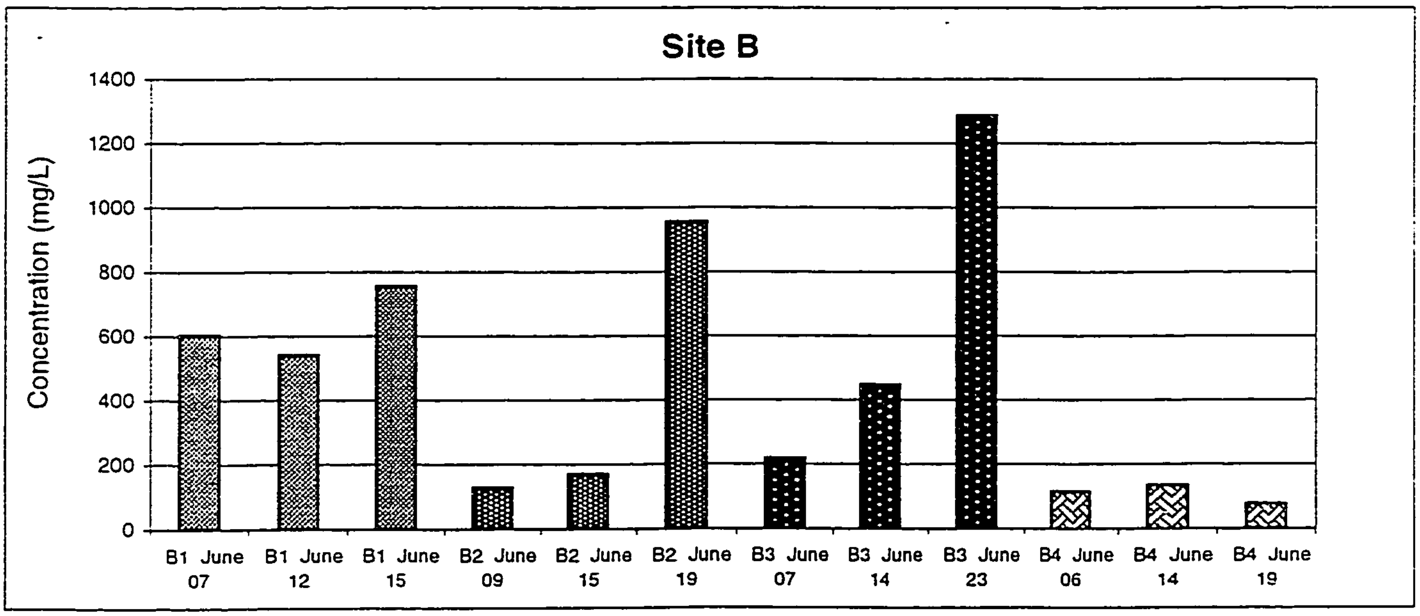

Figure 5-61: Solute concentrations of water chemistry samples for Site B.

being a fresh detachment slide. The difference in solutes transported results from the substrate: at B1, bedrock strata were visible on the scar surface. Ionic proportions at B2 show similar percentages to those at A1 and A2: Na^+ and Cl^- occur in much greater proportions than at any other B site. An unvegetated area of fine-grained silt exists outside the western edge of the plot. The sediments are probably of marine origin as salt effloresences are visible on air photos from 1990 and were observed in the field in 1996. It is possible that these sediments are being transported onto the plot by slopewash or aeolian processes, resulting in elevated Na^+ concentrations in the near surface sediments (see Figure 5-53), and high Na^+ and Cl^- concentrations in the surface runoff. Patterns at B3 are similar to B1. The relative proportions of ions remain the same even though absolute values vary greatly, probably due to greater active layer depths resulting in increasing residence times, and due to snowbank recession over a fresh detachment slide scar (not in marine sediments) on the upper portion of the plot. Relative proportions show slight variation at B4. Proportions of Na^+ and Cl^- were greater than at B1 or B3, however total dissolved solids are low in all of the B4 samples.

The contrasts in water geochemistry in runoff from a fresh scar in marine sediment (A1), and from two plots with fresh scars underlain by a mixture of bedrock and other non-marine deposits (B1 and B3) are illustrated by plotting percentages of SO_4^{--} against Na^+ plus Cl^- (Figure 5-62). Na^+ and Cl^- dominates in runoff from the scar in marine sediments, and SO_4^{--} is dominant in the water samples collected from the plots with fresh scars in non-marine deposits. When the samples from the remaining sites are plotted on the graph, all points fall within the range of A1 and B1 and B3 (Figure 5-62). A3 shows the greatest differences between samples. This probably reflect changes in contributory area, which range from fresh detachment slide scars in marine sediments to vegetated undisturbed slopes.

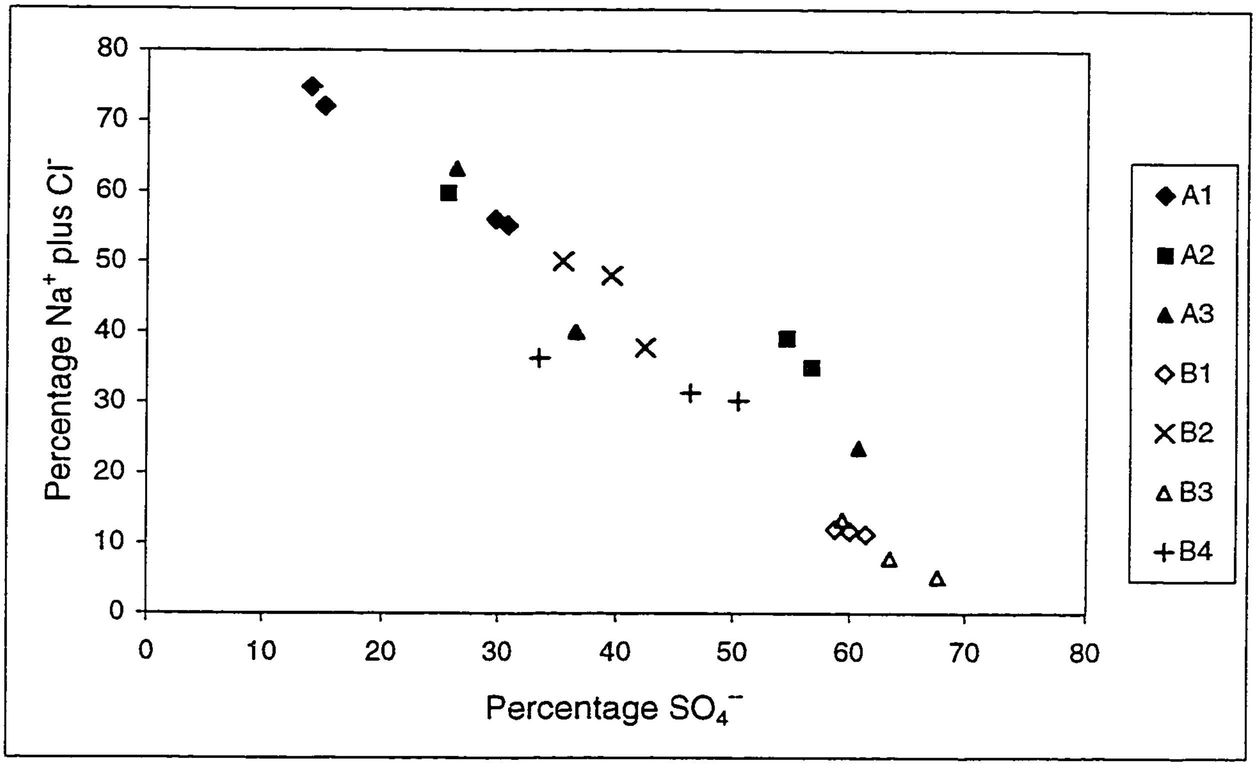

Figure 5-62: Relationship between SO_4^{--} and Na^+ Cl^- percentage in water chemistry samples from Sites A and B.

5.2.2.3 – Discussion (Variability in Solute Production)

Temporal variability in solute production can be attributed to fluctuations in discharges and to changes in contributory area. These factors influence solute concentrations on diurnal and seasonal time scales. Overall, solute concentrations did not show a large amount of variability during snowmelt runoff, with the exception of diurnal fluctuations related to discharge, and snowfall events. B3 is a notable difference where solute concentrations increased with the progression of snowmelt. This is probably due to increases in residence times due to the development of subsurface pathways within the deepening active layer and to increasing amounts of runoff being generated from a fresh detachment slide scar. The rilled surfaces at fresh detachment slide scars promoted the rapid removal of meltwater, and the progression of snowmelt had little effect on the overall trends in solute concentrations.

Extremely high solute concentrations were measured in the rainfall-induced runoff which suggest that relatively small proportions of runoff can transport substantial amounts of solutes from the slope (see Section 5.2.3). Several factors contribute to the efficacy of solute removal by rainfall-induced surface runoff. Rainfall may flush soil water with high residence times (Lewkowicz and Wolfe, 1994). This could explain the initial spike in solute concentrations at the beginning of rainfall events. The higher temperatures of rainwater will increase the rates of chemical reactions, but the slight difference in water temperatures cannot account for the large contrasts in measured solute concentrations. The most probable explanations for high conductivities during rainfall-induced surface runoff are:

1. The dissolution of salt crusts that develop on unvegetated slopes in marine sediments (see Figure 5-51). The crusts form due to capillary water movement and evaporative processes on the snow-free sections of slope.
2. The development of more extensive flow paths which increase the total area from which solutes may be removed (see figure 5-52).
3. The solubility of the regolith. Compared to snowmelt runoff, plots A1, A3 and B2 experienced increases in solute concentrations of an order of magnitude. All three are underlain by marine sediments and have been influenced by detachment sliding (see Section 5.2.2)

5.2.3 - Dissolved Sediment Amounts

Using plot discharge and continuous conductivity records, the total solute load was calculated for each plot. Total weight loss by solution ranged from 82 g/m^2 at A1, to 0 g/m^2 at A4 and A5. There is a relationship between freshness of scar and total solute removal at site A, with increasing yields from A3 to A2 to A1 (Table 5-5). This pattern was only partially present at the site B. Yields increased from B4 to B2 to B1 but higher solute concentrations during snowmelt, and a large amount of runoff produced the highest yield of 44 g/m^2 at B3. It should be noted that a fresh detachment slide occupies the upper part of B3, and is at least partially responsible for the high amount of solute removal from the plot. A slightly lower amount of sediment removal by solution (30 g/m^2) occurred at B2. Low solute concentrations and runoff production resulted in less than 5 g/m^2 of solute removal at the vegetated plot B4.

Table 5-5: Total dissolved loads.

Plot	Solute load, snowmelt (g/m^2)	Solute load, rainfall (g/m^2)	Total (g/m^2)
A1	66.1	15.6	81.7
A2	20.6	1.36	22.0
A3	5.81	4.30	10.1
A4	0.0	0.0	0.0
A5	0.0	0.0	0.0
B1	32.7	2.7	35.4
B2	13.8	16.0	29.8
B3	36.2	7.60	43.8
B4	4.50	0.0	4.50
A1, 1996	49.9	0.0	49.9
A3, 1996	3.76	0.0	3.76

The values presented here include solutes removed during rainfall events after snowmelt runoff, but do not include the substantial solute loads associated with snowfall events which briefly covered the plots and then ablated during the melt period. At B2 over 50% of the solute load (16 g/m^2) was removed during rainfall events which generated only 14 % of the annual runoff at that plot. At A1 over 15 g/m^2 of solutes were removed by 2 mm of rainfall-induced runoff. This translates to 19% of total solute load being transported by only about 2 % of the total runoff. Rainfall- induced runoff removed over 40 % of the annual solute load at A3, however the absolute amount was low. The low amounts of solute removal at A2 and B1 can be attributed to the small amounts of runoff generated at the two plots.

A comparison between 1993 and 1996 indicates that solute losses at A1 and A3 were both lower in the earlier year (see Table 5-5). The total amount of solutes removed at A1 in 1993 was 39% less than in 1996. At plot A3 solute removal in 1993 was 63% less than in 1996. Rainfall-induced runoff removed significant amounts of solutes in 1996. If only snowmelt solute load is considered the differences between the two years are not as marked, (A1 – 25%, A3 - 35%) but are still significant. This can be largely attributed to lower amounts of snowmelt runoff produced in 1993 (A1 – 26% less in 1993, A3 – 23% less in 1993). In 1993 most of the runoff at A3 was generated from a large snowbank on the undisturbed, well-vegetated portion of the slope which also contributed to the lower solute concentrations during that year.

5.2.3.1 – *Discussion (Detachment Sliding and Solute Yields)*

The spatial variability of solute concentrations in runoff from the study plots can be linked to the nature of the underlying substrate. The highest solute concentrations developed in runoff generated from a fresh active layer in marine sediments. Detachment sliding involves translation downslope of the thawed layer and consequently creates an unvegetated depression in the scar zone. A new active layer begins to develop in the scar zone immediately following failure. High solute concentrations at fresh scars are attributable to the abundance of soluble ions in the fresh active layer, particularly in marine sediments (Figure 5-63) (section 5.2.2.1). Total solute losses are enhanced by the large amounts of surface runoff produced at the detachment slide scars.

Figure 5-63: The geochemical effect of detachment sliding in marine sediments.

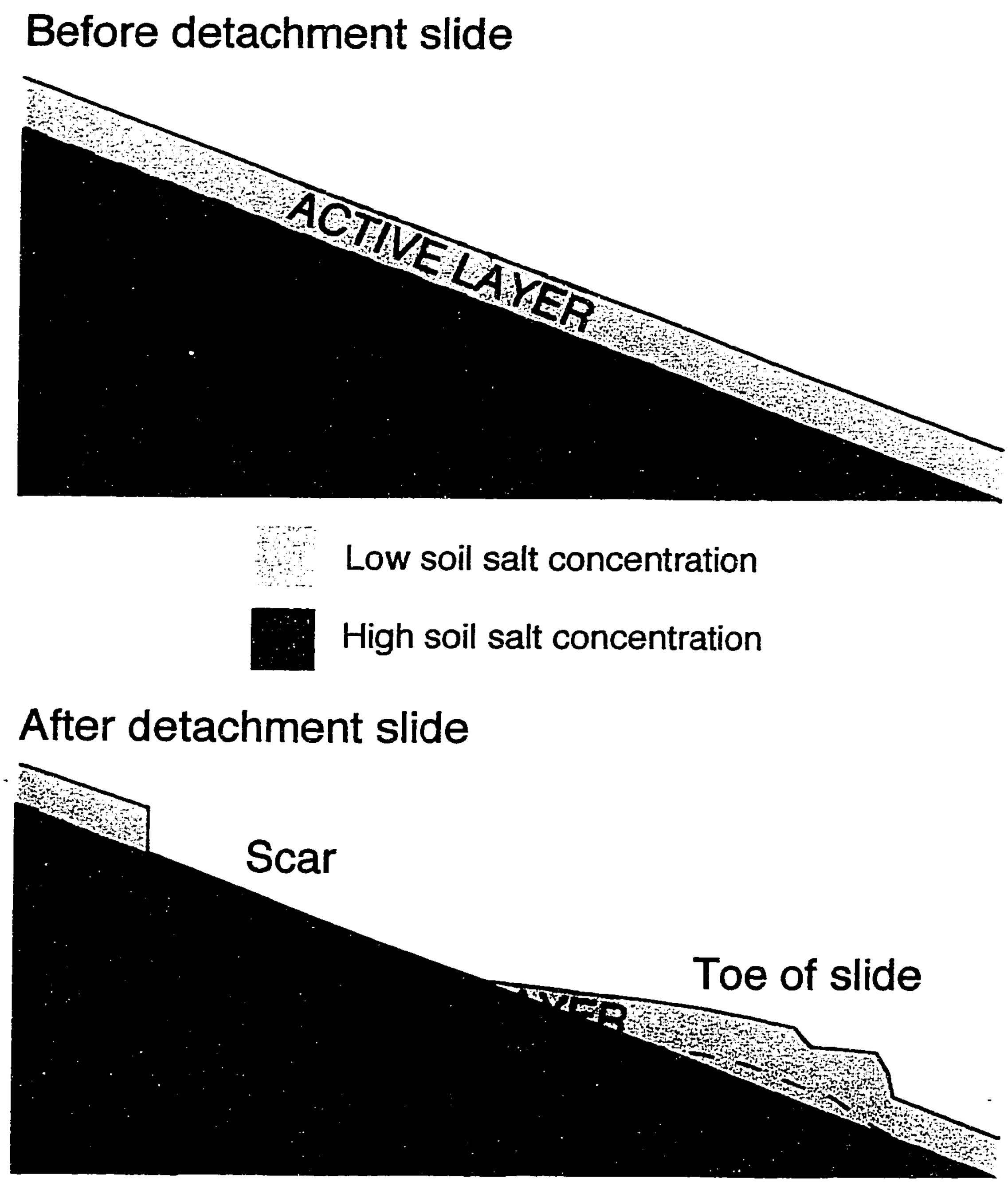

Although this point is speculative, rillwash at detachment slide scars may include contributions from subsurface flow. Throughout much of snowmelt, the depth of the rill is greater than the depth of thaw in adjacent areas. Therefore on laterally concave slopes, the rills will collect a significant portion of subsurface flow. During the snowmelt period, the water moving downslope as subsurface flow is probably only a small portion of the total runoff measured (Lewkowicz and French, 1982a; Woo and Xia, 1995), but because of the greater time of contact between water and regolith, subsurface contributions may exhibit high solute concentrations.

Solute removal at vegetated slopes is restricted by the type of ions present in the active layer (see Figures 5-53 and 5-57) and by the lower amount of surface runoff produced during snowmelt. Total losses at the study plots appear to fit the relationship between freshness of active layer and total solute removal, with the exception of B3 which experienced very high solute yields. However, this is not surprising given that over 30% of B3 consists of a fresh detachment slide scar, and the lower slope is poorly drained, increasing the residence times of runoff. Although suspended sediment generated from the detachment slide scar at B3 is deposited on the lower vegetated portion of the slope (see Section 5.1.3.3), the solute load may be transported from the slope by surface runoff (see Section 5.2.2.2). This indicates that solutes may be removed from slopes which lack the flow-paths required for the effective transport of suspended sediment. This has implications regarding solute inputs into river and lake basins influenced by detachment sliding (see Section 6.1.1.2).

5.2.3.2 – *Cation Liberation and Flushing of Na^+ Following Detachment Slides*

High solute concentrations in the fresh active layer at detachment slide scars may inhibit the revegetation of the scar. For example, some grasses and *Stellaria* sp. have begun to revegetate the 1988 detachment slide scar at B1, but the 1988 detachment slide scar (A1) in marine sediments remains completely unvegetated. The inability of plants to recolonize the fresh scar contributes to a positive feedback resulting in a prolonged period of modified drainage and enhanced erosion. This is especially relevant to detachment slides in marine sediments where Na^+ is found at levels toxic to most arctic plant species. Therefore it is useful to determine the time required for soil Na^+ concentrations to decline to levels tolerated by colonizing plant species. This provides a temporal perspective on the geomorphic and ecological impacts of detachment sliding.

Although samples are limited in number, it is possible to relate the concentration of Na^+ to the conductivity of the surface wash at A1 (Figure 5-64). This graph indicates that concentrations of up to 4600 mg/L of Na^+ were likely present in the surface wash during early summer rainfall events when conductivities reached 21456 µS/cm.

Using the best-fit equation $y = 0.21x$ (Figure 5-64), the continuous conductivity record, and the continuous runoff record, the total amount of sodium removed from plot A1 during the 1996 runoff season was estimated to be 14 kg (Appendix C-8). Assuming that all of this Na^+ was derived from the scar area of the detachment slide within the plot, 37 g/m^2 of Na^+ was removed from the scar by surface wash. Based on the Na^+ concentrations derived from the cation exchange it is estimated that it would take about

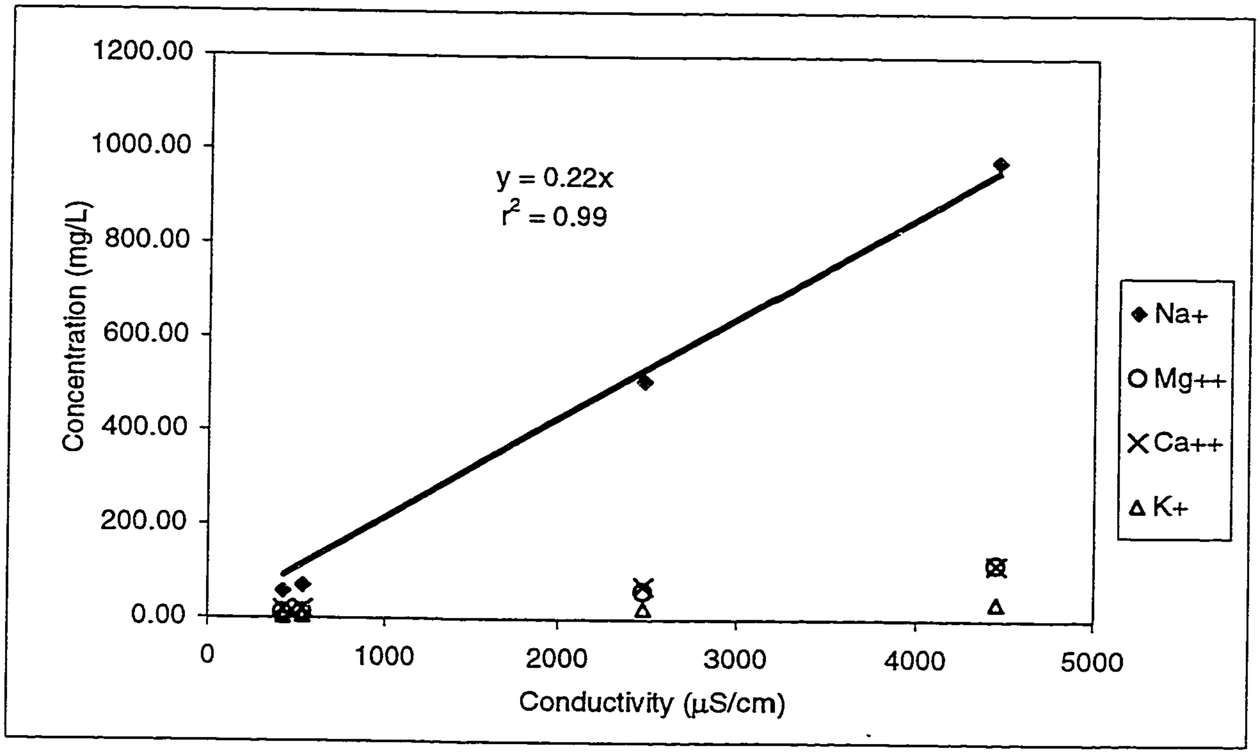

Figure 5-64: Relationship between conductivity and solute concentration.
Best fit line is for Na^+.
Regression line constrained through the origin.

45 years for Na^+ levels to fall from those in the detachment slide scar to those in the adjacent slope.

This is, by necessity, an order of magnitude calculation. Potential error is derived from the following assumptions:

1. That surface wash is the main mode of Na^+ removal from the slope. Snowmelt runoff coefficients for fresh slides are 63 – 81 %, hence subsurface runoff is small in volume but it could have high concentrations of solutes.
2. That the 1996 value of Na^+ removal is representative of the average yearly amount of Na^+ removed from the plot. Snow accumulations were probably above average, and rainfall was greater than normal in 1996.
3. That dissolution rates remain constant at lower Na^+ concentrations.
4. That capillary water movement and evaporative processes sustain high levels of Na^+ near the surface of the active layer even when Na^+ concentrations in the active layer begin to decrease. This may be assisted by the exclusion of solutes during two-sided freezing which could provide another mechanism for the upward movement of soluble salts.
5. That no further inputs of Na^+ occur into the active layer. In fact, rates of erosion are high enough that permafrost table will slowly degrade, allowing further release of Na^+. Based on the rate of erosion in 1996, the surface would be lowered almost 6 cm over 50 years, which would result in the liberation of an additional 166 g/m^2 of Na^+ into the active layer (Appendix C-9). This process is suggested by the pattern of the Na^+ profile on the adjacent "undisturbed" slope (see Figure 5-53). Furthermore it is possible that

ions from the permafrost are transported into the active layer during annual moisture movements in and out of the permafrost (Mackay, 1983).

Despite these assumptions, it is clear that much more than a decade is required for salt concentrations to fall to background levels (nine years have already elapsed since 1988), but given the rates of removal, the duration needed is probably less than a century.

5.2.3.3 – *Discussion (Ecological Implications of Detachment Sliding in Marine Sediments)*

Soil geochemistry suggests that areas underlain by marine sediments are the most sensitive to geomorphic and ecological change following detachment sliding. Sodium levels in the fresh active layer at A1 were up to two orders of magnitude greater than those on adjacent slopes. These elevated salt concentrations may inhibit the revegetation of detachment slide scars (Personal communication, G. Henry, University of British Columbia), and prolong accelerated rates of erosion. High rates of solute removal were measured at the detachment slide plots, particularly during rainfall events. Despite the very high solute concentrations in runoff, elevated sodium levels will take several decades to decrease (see Section 5.2.3.2).

The soil geochemistry and solute concentrations measured in surface runoff can be placed into an ecological context through examining the research conducted by Srivastava and Jefferies on the interaction between salinity and plant growth of salt tolerant graminoids (*Puccinellia phryganodes* and *Carex subspathaces*)(Srivastava and Jefferies, 1995a; Srivastava and Jefferies; 1995b; and Srivastava and Jefferies, 1996).

This research was conducted in the coastal lowlands of southwestern Hudson Bay, but both subject species can be found on Ellesmere Island (Porsild, 1957).

Srivastava's and Jefferies' work showed that increased soil salinity would result in decreased plant growth and increased plant mortality. They also found that applications (10 mL/day) of a saline solution (4 g/mL to 40 g/mL) had detrimental effects on the growth of the two graminoids and that the effects of the treatments were more severe as the salinities were increased. At A1, the high salt concentrations measured throughout the active layer (see Section 5.2.2.1) and the extensive salt crust formation observed after the slopes become snow free indicate that very saline conditions can certainly develop in the near-surface sediments of the fresh scar. Solute concentrations measured in the rainfall runoff from the 1988 detachment slide scar exceeded 12 g/L (hypersaline = Na^+ > 12 g/L in soil water), a level shown to increase mean leaf death rates and significantly decrease mean leaf birth rates in *Puccinellia phryganodes* (Srivastava and Jefferies, 1995b). It can be deduced that the soil salt levels in surface sediments at A1 were greater than the salt concentrations measured in the rainfall-induced runoff. It can be hypothesized that if runoff from fresh detachment slide scars in marine sediments saturated vegetated areas downslope of the scars, or ponded at the base of slopes, the vegetation (most of which is certainly less salt tolerant than *Puccinellia phryganodes* and *Carex subspathacea*) in those areas would be adversely affected.

The redistribution of salts from detachment slide scars and thermokarst terrain by surface runoff is evident from air photos of study site A and surrounding areas (Figure 5-65). Detachment slides and thermokarst areas in marine sediments are identifiable on air

A

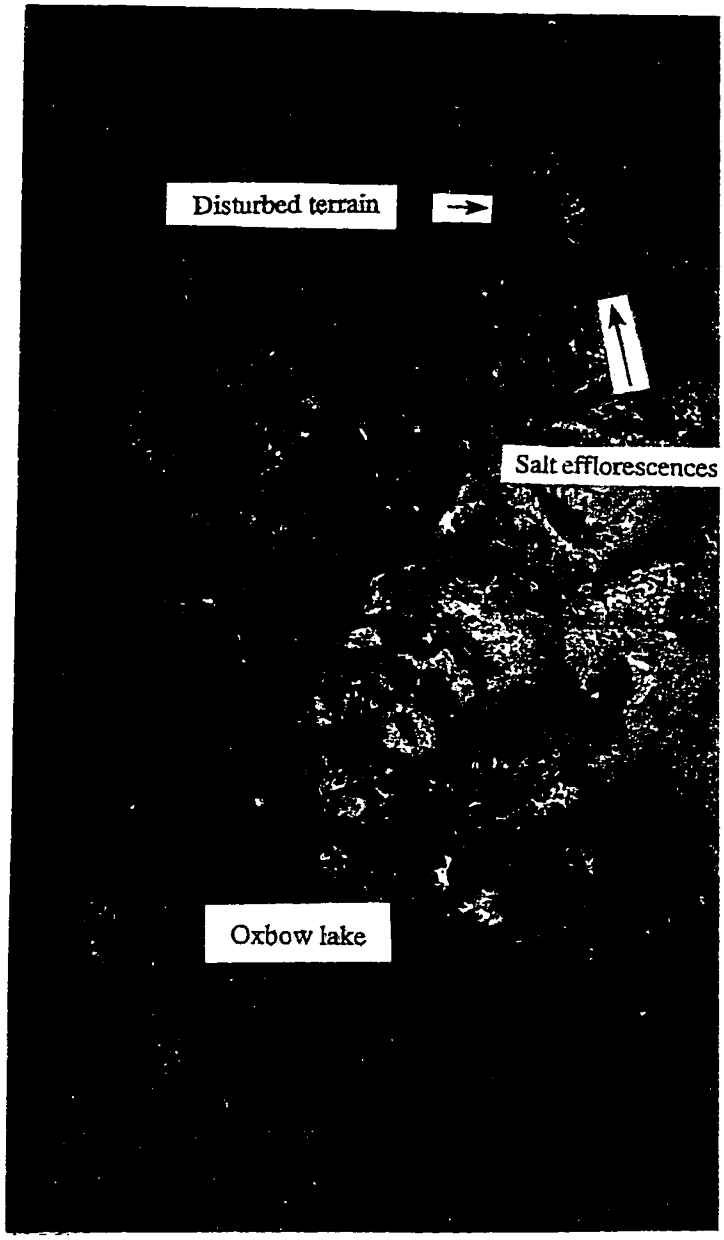

B

Figure 5-65: Aerial photograph A shows fresh detachment slides and areas of salt redistribution in slope depressions and at the valley bottom of study site A. Aerial photograph B is a small basin three kilometers southeast of Hot Weather Creek which has been significantly influenced by thermokarst, thaw slumping and detachment sliding. Salt efflorescences are clearly visible on the disturbed terrain. The drainage network empties into a former oxbow lake basin where salts have been redeposited over most of the old lake bed.

photos by the white color of salt efflorescences which form on the surface of the disturbed terrain. If the drainage networks from these disturbances are traced, often extensive areas of salt redeposition can be located where channel gradient decreases resulting in poor drainage and surface ponding. Despite the high moisture availability in these areas, they are almost completely unvegetated. Four main points are raised from this discussion:

1) Soil salt concentrations in the fresh active layer in marine sediments are high enough to restrict growth and reproduction in terrestrial arctic plant species.
2) Runoff from fresh detachment slide scars (particularly during rainfall events) contains salt concentrations toxic to terrestrial plant species.
3) The influence of detachment sliding in marine sediments has ecological implications which range beyond the area directly affected by the scar. The spatial extent of areas influenced by detachment slides can be assessed through a topographic analysis of the slope and local drainage network.
4) Other natural and anthropogenic terrain disturbances which lead to surface lowering of thawing of permafrost in areas underlain by marine sediments (accelerated surface erosion, thermokarst – thaw slumps, removal of vegetation) can also result in the liberation of salts from the active layer. Such phenomena may have significant impacts on soil geochemistry, water geochemistry of runoff and on the local ecology.

5. 3 - Sorbed Ions

Sorbed ion amounts ranged from 20.2 mg/L at B1 to 0.6 mg/L at B3 (Table 5-6). These concentrations constitute between 0.43 and 1.3% of the total weight of the suspended sediment samples (Table 5-7). The highest concentration of sorbed Na^{+} was measured in a sample from the fresh detachment slide scar in marine sediments (A1) and the highest concentration of sorbed Ca^{++} was measured in samples from B1. The concentrations of Fe^{++}, K^{+} and Mg^{++} were present at low concentrations.

A linear relationship was established between suspended sediment concentrations and sorbed ion concentrations. The relationship was constrained through the origin and yielded the equation y = 0.0053x (Figure 5-66). Because the sorbed cation concentrations depend on suspended sediment concentrations they can be important during periods of peak flows when sediment concentrations are high. However, overall the equation shows that sorbed cations represent only 0.53% of the total suspended sediment load. Total sorbed cation loads ranged from 7.8 g/m^2 at A1 to less than 0.03 g/m^2 at plot B3 (Table 5-7). Although the sorbed ion load is an insignificant portion of the suspended sediment load, the amounts may be significant relative to solute concentrations.

To make the comparisons between sorbed cations and dissolved cations, a relationship was established between conductivity and dissolved cations using values obtained from the geochemical analysis (Figure 5-67). This correlation gave the equation y = 0.27x and was used to predict dissolved cation concentrations. The relative proportions of sorbed cations for the samples ranged from 0.32% at B3, to 10.73% at A3. Using the relationships established above, the maximum sorbed cation concentration at B1 was estimated to be 413 mg/L which is about double the predicted dissolved cation

Table 5-6: Sorbed ion concentrations in mg/L.

Sample	**Ca^{++}**	**Fe^{+}**	**K^{+}**	**Mg^{++}**	**Na^{+}**	**Total cation concentration**
A106071654	4.2	0.0	0.4	0.7	2.0	7.4
A106181420	6.2	0.0	0.9	1.8	5.6	14.6
A206042130	4.8	0.0	0.4	0.8	2.1	8.2
A306111450	5.5	0.0	0.6	0.9	3.8	10.9
A306132030	4.2	0.0	0.4	0.5	1.6	6.7
B106080958	10.1	0.0	0.4	1.1	2.6	14.3
B106081637	13.8	0.0	0.8	1.8	3.8	20.2
B206130200	3.4	0.0	0.4	0.4	2.3	6.5
B206182045	3.2	0.0	0.4	0.5	2.3	6.4
B306150921	0.3	0.0	0.1	0.0	0.2	0.6
B306251245	1.5	0.0	0.2	0.4	0.9	3.0
B406142320	0.5	0.0	0.1	0.1	0.3	1.0

5-7: Suspended sediment and sorbed ion concentrations and total sorbed ion load for runoff season.

	Suspended sediment concentration (mg/L)	Sorbed ion concentration (mg/L)	Percentage of suspended sediment concentration	Total sorbed ion Yield (g/m^2)
A106071654	1778.46	7.43	0.42	**7.80**
A206042130	332.62	4.39	1.32	**1.70**
A306111450	2012.20	11.27	0.56	**0.40**
A306132030	1235.29	6.05	0.49	
B1 06080958	3264.44	14.30	0.44	**3.50**
B1 06081637	3349.29	20.42	0.61	
B206130200	1215.63	6.97	0.57	**1.40**
B206182045	1159.46	6.66	0.57	
B306150921	58.95	0.74	1.25	**0.03**
B306251245	468.78	3.35	0.71	
B406142320	130.30	1.15	0.88	**0.10**

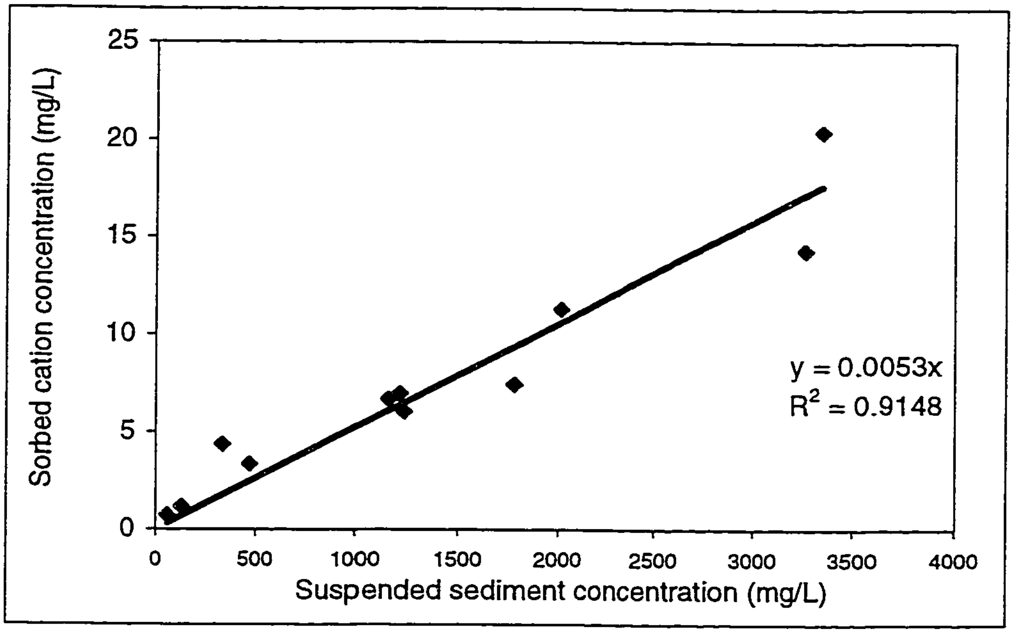

Figure 5-66: Relationship between suspended sediment concentration and sorbed cation concentration.
Regression constrained through the origin.

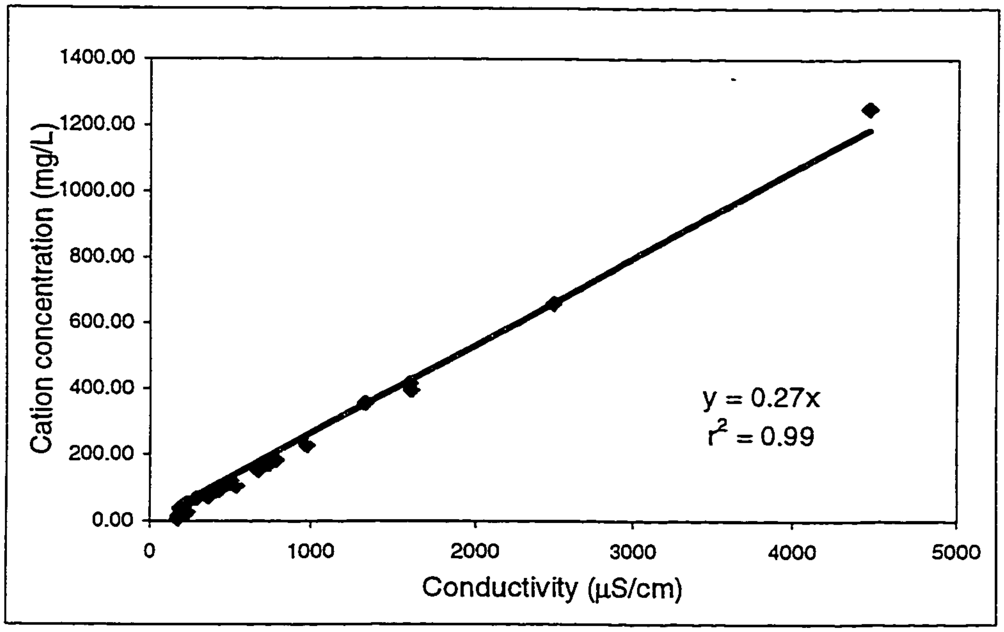

Figure 5-67: Relationship between conductivity and cation concentration.
Regression constrained through the origin.

load (237 mg/L) for the same time. However, the total sorbed cation load was about 80% less than the total dissolved cation load at B1. It should be noted that the maximum suspended sediment concentration of any sample tested for sorbed ions was 3350 mg/L and the relationship established was used to predict the amount of sorbed cations for a suspended sediment concentration over one order of magnitude greater than this value.

Chapter 6 – Sediment Yields, Relative Proportions and Denudation Rates

6.1 – Total Sediment Losses and Relative Proportions

The sediment yields and load proportions are presented in Tables 6-1 and 6-2. As expected the greatest amounts of total sediment removal occurred at the fresh detachment slide scars, where both the suspended sediment and solute concentrations were highest. These plots also produced very high amounts of runoff (see Table 4-1). Total sediment yields were 1564 g/m^2 at A1 and 721 g/m^2 at B1. The extremely high amounts of suspended sediment removal at A1 and B1 overshadowed relatively high rates of solute removal (Table 6-1 and 6-2). Total yields were slightly lower at the old detachment slide scars (Table 6-1) but were still dominated by suspended sediment losses (>82%) at all sites which produced surface runoff. The only exception was the well-vegetated mixed plot, B3 (Table 6-2) where solute transport dominated and only 6.2 g/m^2 of suspended sediment removal took place despite high amounts of runoff. This constituted only 12.4 % of the total sediment removal from the plot. Solute removal would also have been of greater importance at B4 if suspended sediment concentrations had not risen on the last two days of runoff due to the initiation of mudslides near the crest of the slope (see Figure 5-11).

Table 6-1: Total sediment yields

A1, 1996 Runoff: 103.1 mm
Yield: 1563.7 g/m^2

Period	Julian Day	Surface runoff (mm)	Suspended sediment (g/m^2)	Sorbed cations (g/m^2)	Dissolved solids (g/m^2)
Snowmelt:	JD 159 - 171	101.6	1480.0	7.84	66.1
Rainfall	JD 176 - 180	1.5	1.6	0.008	15.6
Totals		103.1			
Yield (g/m^2)			1482.0		81.7

A2, 1996 Runoff: 75.4 mm
Yield: 347.1 g/m^2

Period	Julian Day	Surface runoff (mm)	Suspended sediment (g/m^2)	Sorbed cations (g/m^2)	Dissolved solids (g/m^2)
Snowmelt:	JD 156 - 167	74.4	324.0	1.72	20.6
Rainfall	JD 176 - 180	0.754	1.19	0.006	1.36
Totals		75.2			
Yield (g/m^2)			325		22.0

A3, 1996 Runoff: 39.5 mm
Yield: 83.4 g/m^2

Period	Julian Day	Surface runoff (mm)	Suspended sediment (g/m^2)	Sorbed cations (g/m^2)	Dissolved solids (g/m^2)
Snowmelt:	JD 161 - 176	35.1	64.0	0.339	5.81
Rainfall	JD 176 - 181	4.4	9.27	0.049	4.30
Totals		39.5			
Yield (g/m^2)			73.3		10.1

Note: Suspended sediment totals include sorbed ions.

Table 6-1: continued

B1, 1996 Runoff: 66.5 mm

Yield: 721 g/m^2

Period	Julian day	Surface runoff (mm)	Suspended sediment (g/m^2)	Sorbed cations (g/m^2)	Dissolved solids (g/m^2)
Snowmelt	JD 159 - 170	64.2	676	3.58	32.7
Rainfall	JD 176 - 180	2.26	10.2	0.054	2.70
Totals		66.5			
Yield (g/m^2)			686		35.4

B2, 1996 Runoff: 62.6 mm

Yield: 293 g/m^2

Period	Julian day	Surface runoff (mm)	Suspended sediment (g/m^2)	Sorbed cations (g/m^2)	Dissolved solids (g/m^2)
Snowmelt	JD 161 - 172	53.5	243.8	1.29	13.8
Rainfall	JD 172 - 180	9.10	18.7	0.099	16.0
Totals		62.6			
Yield (g/m^2)			263		29.8

B3, 1996 Runoff: 90.7 mm

Yield: 50.0 g/m^2

Period	Julian d+C43a\	Surface runoff (mm)	Suspended sediment (g/m^2)	Sorbed cations (g/m^2)	Dissolved solids (g/m^2)
Snowmelt	JD 159 - 176	82.7	5.85	0.031	36.2
Rainfall	JD 176 - 180	8.00	0.36	0.002	7.60
Totals		90.7			
Yield (g/m^2)			6.20		43.8

B4, 1996 Runoff: 30 mm

Yield: 25.1 g/m^2

Period	Julian day	Surface runoff (mm)	Suspended sediment (g/m^2)	Sorbed cations (g/m^2)	Dissolved solids (g/m^2)
Snowmelt	JD 158 - 170	30.0	20.6	0.109	4.50
Rainfall	JD 172 - 180				
Totals		30.0			
Yield (g/m^2)			20.6		4.50

Note: Suspended sediment totals include sorbed ions.

Table 6-2. Load proportions 1996.

	A1	A2	A3	B1	B2	B3	B4
Fraction of suspended sediment load (%)							
Snowmelt	99.9	99.6	87.4	98.5	92.9	94.2	100.0
Rainfall	0.1	0.4	12.6	1.5	7.1	5.8	n/a
Proportion of total sediment load	**94.8**	**93.7**	**87.8**	**95.0**	**89.0**	**12.4**	**82.0**
Fraction of solute load (%)							
Snowmelt	80.9	93.8	57.4	92.4	46.3	82.6	100.0
Rainfall	19.1	6.2	42.6	7.6	53.7	17.4	n/a
Proportion of total sediment load	**5.2**	**6.3**	**12.1**	**5.0**	**11.0**	**87.6**	**18.0**

6.1.1 – Spatial Variability of Sediment Losses from the Slope

Sediment yield calculations and the derived denudation rates do not consider the spatial variability of sediment erosion and deposition which occurs on heterogeneous slopes. Sediment yields derived for different terrain units in this study were applied to the respective terrain units on heterogeneous plots to assess the transferability of measured sediment yields and to illustrate the spatial variability of sediment production and removal from heterogeneous slopes. Plots A3 and B3 were divided into three easily distinguishable terrain units: (1) Vegetated undisturbed slopes, (2) unvegetated undisturbed slopes, and (3) detachment slide scars. Each plot was digitized so that total area of each terrain unit could be determined. Then sediment yields for each terrain unit were derived by averaging the sediment yields measured at the smaller homogeneous plots (Appendix D-1). The derived average loss for vegetated slopes was applied to the total area of vegetated slope, and the same was done for bare undisturbed slopes and those influenced by detachment sliding (Appendix D-1).

The suspended sediment patterns at A3 suggest spatial variability in sediment production (see Section 5.1.1.2). Parts of the plot influenced by detachment sliding may experience sediment yields one order of magnitude greater than the total value for the slope, (83.4 g/m^2) (see Appendix D-1) but suspended sediment concentrations and total amounts are lower due to dilution by runoff from vegetated portions of the plot. Total losses calculated for A3 were 94 g/m^2 which is an over-prediction of the measured losses by only 13%.

This estimate of sediment removal demonstrates the use of terrain units and measured results to determine sediment yields for other slopes in the study area. However, such an accurate estimate of sediment removal is possible only because of the strong connectivity of flowpaths from the plot (see Section 5.1.3.3). As a result most of the suspended sediment generated on the upper and middle part of the slope is removed from the plot rather than re-deposited on segments downslope. The same method was used to predict sediment yields at B3 (see Appendix D-1). The plot consists of about 50% vegetated undisturbed slope and about 30% detachment slide scar (located in the upper portion of the slope). Sediment removal was over-predicted by about 450%

because most of the sediment produced from the detachment slide scar on the upper part of the slope was re-deposited on the hummocky, well-vegetated lower part of the slope (see section 5.1.3.3). Based on the predicted values for suspended sediment removal from detachment slides, the scar area at B3 should have produced between 250 to 300 kg of suspended sediment, and if it did, more than 98 percent was re-deposited on the lower parts of the slope. This underlines the importance of slope connectivity in the removal of suspended sediment from the slope, and as discussed in Section 5.1.3.3, suggests that large amounts of sediment removed from detachment slide scars may be re-deposited on the slope system and therefore do not become direct inputs to the stream (Figure 6-1).

6.1.2 – Effect of Detachment Sliding on Solute Inputs into the Stream

A rough calculation was attempted to evaluate the impact of the 1988 landslide event on solute production and inputs into the stream. Lewkowicz (1992) mapped the detachment slides in a 1.5 km stretch of river valley at Hot Weather Creek. The total area influenced by the 1988 detachment slides in this section of valley was about 16500 m^2. Based on amounts of solute removal from fresh detachment slide scars in 1996, the total amount of solutes removed by surface wash for the total area influenced by the 1988 landslides would have been almost 1000 kg (Appendix D-2). By applying the amount of solute losses at the heterogeneous plot A3 to the total area influenced by the 1988 slides, the amounts of solute removal under slope conditions unmodified by the 1988 slides can be estimated. This value is only about 170 kg, which is almost an order of magnitude lower than estimated post-slide transport. Given the low solute yields in Hot Weather Creek, detachment slide events which influence a significant portion of the basin may

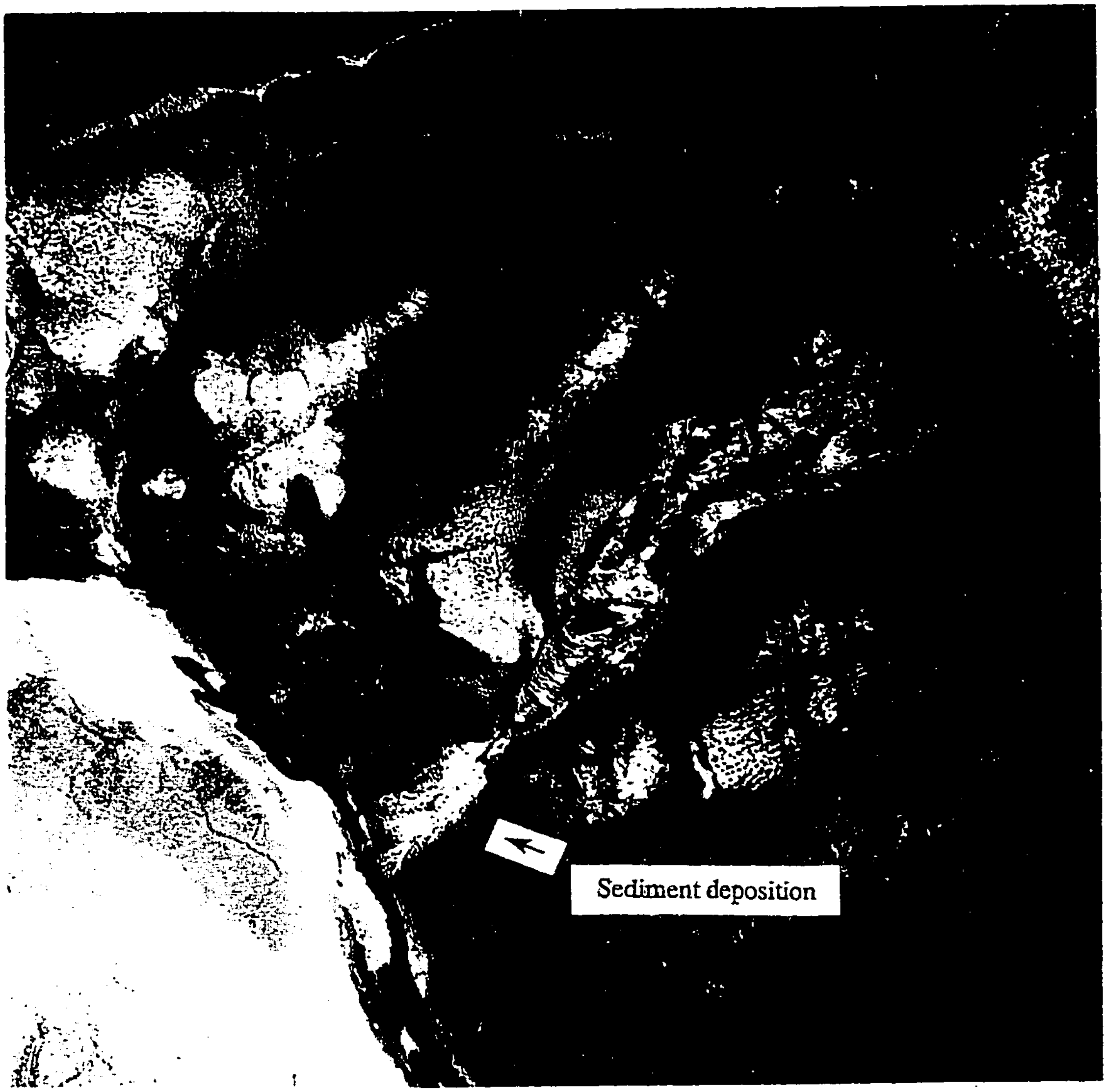

Figure 6-1: If channelized drainage is not present between detachment slide scars and the stream, large amounts of suspended sediment may be redeposited downslope of the scar. Note the large amount of sediment which has been deposited downslope of this detachment slide scar located about 6 km upstream of the study sites.

alter solute loads and stream geochemistry. Increases in solute concentrations in streams may be one result of increased geomorphic activity within the basin.

6.1.1 – <u>Net Losses</u>

Simple calculations indicate that significant amounts of aeolian material can be deposited on slopes in the study area (see section 5.1.3.4). Based on total sediment yields and total niveo-aeolian inputs, net sediment removal was determined for the study plots. Sediment yields exceeded niveo-aeolian inputs at all of the detachment slide sites by about one order of magnitude, (Table 6-3) but at vegetated sites, aeolian inputs exceeded sediment losses in surface wash by up to one order of magnitude. Net gains of 82, 42 and 66 g/m^2 of sediment occurred at A4, B3 and B4. The net losses at A3 were only 6 g/m^2 compared to total losses of 83.4 g/m^2. Based on the calculations in Section 6.1.1.1 it can be inferred that high amounts of erosion are occurring on parts of A3 and B3, but deposition is occurring on the vegetated and unvegetated undisturbed slopes at A3 due to aeolian inputs, and at B3 due to aeolian inputs and wash from the rapidly eroding detachment slide scar located upslope. These results have implications when considering rates of slope denudation and the overall evolution of the landscape.

Table 6-3: 1996 sediment yields.

Plot	Total sediment losses (g/m^2)	Niveo-aeolian inputs (g/m^2)	Net sediment losses (g/m^2)
A1	1570	156	1414
A2	347	104	243
A3	83	77	6
A4	0	82	-82
A5	0	12	-12
B1	722	79	643
B2	292	60	232
B3	50	92	-42
B4	25	91	-66

Note: Negative values indicate sediment gain.

6.2 – Denudation Rates

Values of weight loss by suspended sediment, solution, total loss and net loss can all be converted into denudation rates using a dry bulk density factor for the surface sediments of 1.1 g/cm^3 (from Lewkowicz, 1998) (Table 6-4). Average rates of denudation by suspended sediment range from 1346 mm/1000 yr. at A1 to 6 mm/1000 yr. at B3 (see Table 6-4). Maximum rates by solution were one order of magnitude lower than denudation by suspended sediment at all of the detachment slide sites. Denudation by solution was over 6 times greater than by suspended sediment at B3. Although relative proportions for denudation rates by solution were greater at B3, absolute amounts were in the same range as for most of the other plots. Because of the overall importance of suspended sediment losses at the detachment slide plots, highest total denudation rates occurred there. Average total rates ranged from 1422 mm/1000 yr. at A1 to 23 mm/1000 yr. at B4, to 0 at the plots where no runoff was produced (see Table 6-4). The

Table 6-4: Estimates of suspended sediment, solute, total and net denudation by overland flow in mm/1000yr.

	Denudation estimates by suspended sediment erosion	Denudation estimates by solute erosion	Total denudation estimates	Net denudation estimates
A1	1347	75	1422	1285
A2	296	20	316	221
A3	67	9	76	6
A4	0	0	0	-74
A5	0	0	0	-11
B1	624	32	656	584
B2	239	27	266	211
B3	6	40	45	-38
B4	19	4	23	-60

Note: All denudation rates are based on 1996 sediment yields.

calculation of net yields in Section 6.1.1.2 suggests that despite large amounts of surface runoff at some vegetated slopes, they experience net accumulation of sediment. Niveo-aeolian samples collected in 1996 indicate rates of sediment accumulation of up to 74 mm/1000 yr. at vegetated plots where no surface runoff was generated. Accumulations in the same range were measured on vegetated slopes which produced surface runoff.

Large suspended sediment losses at fresh detachment slide scars result in high denudation rates. Niveo-aeolian inputs will be spatially distributed proportionally to snow accumulations. Greater inputs at detachment slide scars are offset by suspended sediment losses which are in the range of one order of magnitude greater than inputs. However, similar inputs at vegetated slopes, result in the net deposition and accumulation of sediment. Niveo-aeolian deposition further contributes to the contrast between highly erodible slopes and those which experience very low amounts of sediment removal, and in particular vegetated slopes, which tend to accumulate greater snow covers.

6.3 – Comparisons with other Studies

Suspended sediment concentrations at the well-vegetated plots are in the range of those measured by Lewkowicz (1983) on Banks Island. However maximum values at the fresh detachment slide sites exceed any suspended sediment concentrations measured in Arctic slopewash studies (Table 6-5). Maximum values at fresh detachment slide scars are at least double the concentrations measured on unvegetated undisturbed slopes at Black Top Creek by Bellisario (1993).

Sediment loads measured at the fresh and old detachment slide scars also exceed any values measured in the high Arctic (Table 6-5). Values at the old detachment slide scars are similar to the value estimated by Bellisario (1993). Low suspended sediment losses measured at the well- vegetated slopes in this study (Table 6-5) are similar to those measured by Lewkowicz (1983) on Banks Island. As expected, maximum denudation rates for suspended sediment at fresh detachment slide sites (1346 mm/1000 yr.) are more than two orders of magnitude greater than those on vegetated slopes in this study and those calculated by Lewkowicz (1983) on Banks Island.

During snowmelt, average solute concentrations at the mixed plot A3 and at the vegetated plot B4 are in the range of concentrations measured by Lewkowicz (1983) on Banks Island (see Table 6-5). Bellisario (1993) measured solute concentrations between 268 mg/L and 782 mg/L on unvegetated slopes underlain by marine sediments at Black Top Creek. These values are comparable to concentrations during snowmelt at old

Table 6-5: Summary of slope erosion studies undertaken in the high Arctic.

Site	Author(s)	Maximum Discharge (L/min)	Maximum Suspended Solids (mg/L)	Maximum TDS (mg/L)	Denudation $g/m^2/yr$ * Suspended sediment erosion # Solution erosion
Spitsbergen	Jahn (1961)	--	--	--	* 16
Radstock Bay, Devon Island, N.W.T.	Wilkinson and Bunting (1974)	--	130[a]	--	--
Banks Island N.W.T.	Lewkowicz (1983)	SF 10.7 (Plot 1) SF 30 (Plot 3)	21 70	217 210	* 0.1 to 0.4 # 1.2 to 4.8 * 1.7 # 49.6
Black Top Creek, Ellesmere Is.	Bellisario (1993)	SF 28.8	13900	782	* 200
Hot Weather Creek, Ellesmere Is.	Kokelj and Lewkowicz (1996)	SF 12.7 (fresh detachment slide scar, A1) SF 16.7 (well vegetated plot, B3)	28700 470	12700 1240	* 1480 # 89 * 6 # 44

detachment slides in this study. During snowmelt, maximum concentrations at A1, the fresh detachment slide in marine sediments, exceeded Bellisario's values by a factor of five. Maximum values during rainfall events were at least double (A3, B1) and up to 16 times greater (A1) than Bellisario's concentrations for snowmelt runoff.

Solute concentrations and total losses measured at the fresh detachment slide scar (A1) are greater than any values measured in high arctic slopewash studies. Solute losses of 49.6 g/m^2 measured by Lewkowicz at Banks Island exceed values calculated for other plots in this study, however the snowbank site at Banks Island produced five times more runoff than any of the plots at Hot Weather Creek. The average rates of denudation for plots in this study fall into the same range as for Lewkowicz (1983) on Banks Island.

Chapter 7 – Summary and Conclusions

7.1 – Systems Model

A systems model (Figure 7-1) was developed to summarize the findings of this study and help place results into the context of the main research objective: To determine the impact of detachment sliding on rates of surface wash erosion. Figure 7-1 is explained in the following discussion.

Detachment sliding involves the translocation of the active layer resulting in the formation of a scar zone and a toe zone (Lewkowicz, 1992). Several physical changes result from detachment sliding (see Figure 7-1): 1) A topographic depression is created in the scar zone, 2) the vegetation cover is removed, and 3) a new active-layer develops in the previously frozen sediments (Lewkowicz, 1992). 1) is responsible for increasing snow accumulation (see Section 4.1), and 1) and 2) combine to increase amounts of surface runoff production (see Section 4.1), and rates of suspended sediment erosion (see Section 5.1). 3) increases the amount of soluble ions in the active layer (see Section 5.2.2.1) and in combination with 1) and 2) results in increased rates solute removal (see Sections 5.2.1 and 5.2.3).

After detachment sliding the above mentioned physical changes initiate several feedback loops which prevent the revegetation of the scar zone and perpetuate high amounts of surface runoff production and sediment erosion:

1. The high rates of sediment erosion at the fresh detachment slide scars (see Section 6.1.1) inhibit revegetation.
2. The rapid removal of runoff by rilled drainage (see Section 4) decreases moisture availability needed by colonizing plants.

Figure 7-1: Systems model, The effect of detachment slide scar formation on surface wash erosion.

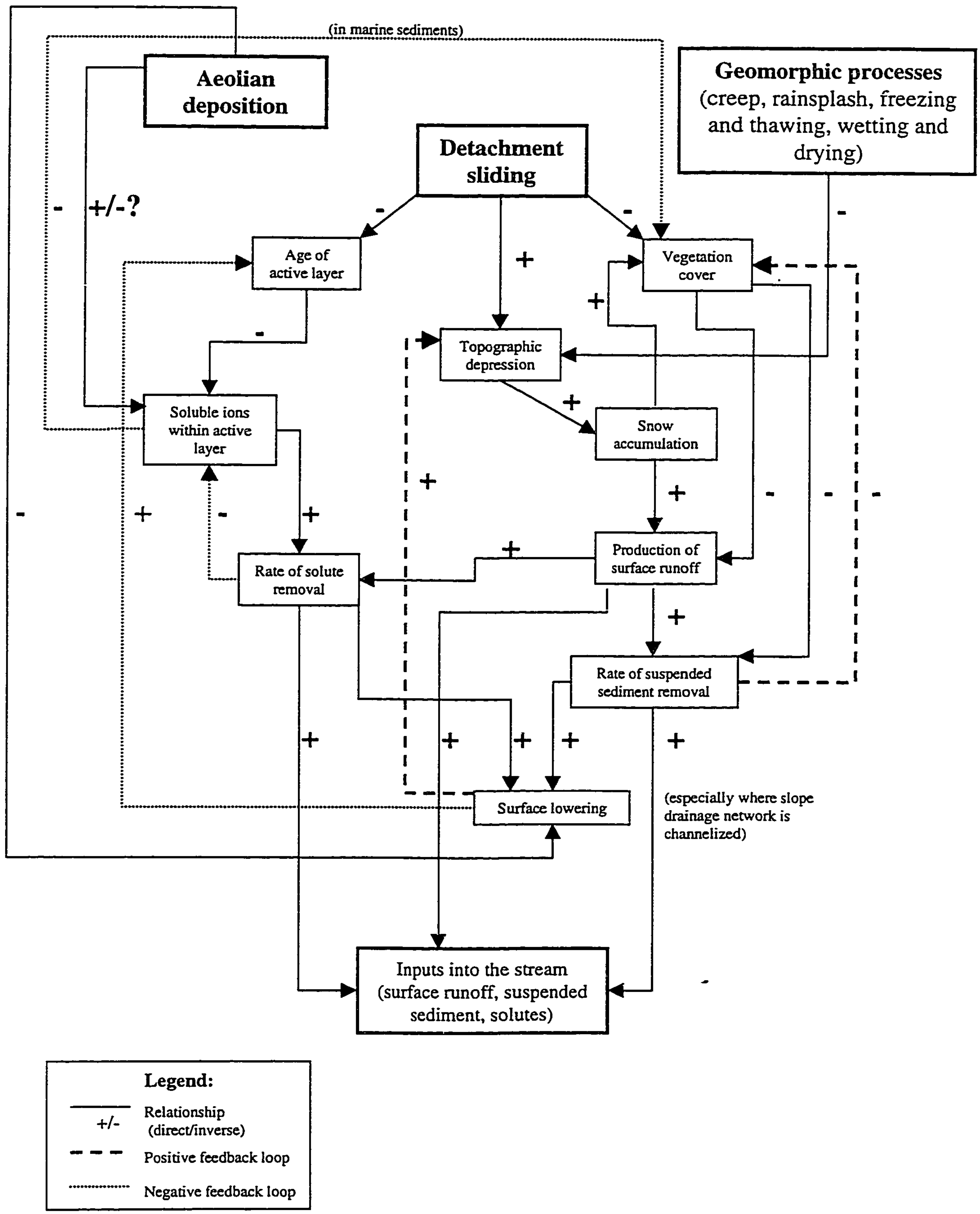

3. Detachment sliding in marine sediments results in the development of a fresh active layer in saline sediments (see Section 5.2.2.1). The high salt content in the fresh active layer will further inhibit the revegetation of the scar zone.
4. The rates of erosion are high enough at the fresh detachment slide scars that permafrost will continue to degrade, allowing for the further release of Na^+ (see Section 5.2.3.2).

Several processes and feedbacks will decrease the effects of detachment sliding on surface wash erosion over time:

1. High solute concentrations in surface runoff will promote the flushing of salts from the active layer of detachment slide scars in marine sediments (see Section 5.2.3.2). It is possible that this runoff may have an adverse affect on the vegetation downslope of the scar (see Section 5.2.3.3) particularly in areas frequently saturated or inundated by the saline runoff.
2. Various geomorphic processes (surface wash, wind action, rainsplash, creep, etc.) result in the weathering of scar ridges and sides, and the toppling of blocks on sides and headwalls, will decrease the definition of the feature and reduce snow accumulation, runoff production and surface wash erosion.
3. A decrease in surface wash erosion on detachment slide scars will slow the rate of surface lowering and decrease Na^+ inputs from the degrading permafrost in marine sediments.

Over time, these feedbacks and processes will modify post-slide soil and erosion conditions so that the slope may revegetate and restabilize. As the plots begin to revegetate and the definition of the scar decreases, lower amounts of runoff can be expected, and suspended sediment yields could decrease by up to two orders of magnitude. However, runoff and sediment yields from the pre-1950 detachment slide scars monitored in this study suggest that conditions conducive to high amounts of runoff and sediment erosion can exist for several decades.

A large increase in the number of detachment slides in a basin will increase the amounts of surface runoff, suspended sediment and solute production on slopes. The transport of high amounts of suspended sediment from detachment slide scars to the stream is dependent on the drainage network between the slope and the stream (see Sections 5.1.3.3 and 6.1.1). Surface runoff and solute yields from detachment slide scars are more likely to reach the river, however the timing and magnitude of the inputs are also dependent on the connectivity of water tracks from the slope to the stream.

7.2 – Conclusions

Several conclusions can be made regarding the effect of detachment sliding on slopewash processes. On undisturbed slopes in the study area:

1. Erosion rates are very low and within the range of those measured by Lewkowicz (1983) on well-vegetated slopes at Banks Island. On well-vegetated slopes in the study area, sediment removal by solution may be more important than sediment removal in suspension.
2. On undisturbed slopes aeolian deposition may exceed surface wash erosion by one order of magnitude.
3. Despite the lack of vegetation cover, low snow accumulations on unvegetated undisturbed slopes result in very low amounts of runoff generation and low rates of sediment erosion.

Detachment sliding results in the modification of hydrologic conditions on the slope:

1. The topographic depression created in the scar zone after detachment sliding does enhance local snow accumulation.
2. The removal of the organic horizon at fresh detachment slide scars decreases the snow water equivalent required to generate surface runoff and the development of a rilled drainage pattern reduces lag times between radiation inputs and meltwater outputs from the plot.

Greater amounts of surface runoff and the removal of vegetation cover enhance rates of suspended sediment erosion on slopes affected by detachment sliding.

1. Rates of suspended sediment erosion at fresh detachment slide scars (A1 – 1480 g/m^2) are two orders of magnitude greater than those on nearby well-vegetated slopes (B3 - 6 g/m^2).
2. Rill erosion is subject to seasonal variation due to the increasing length of flowpaths associated with the upslope recession of snowbanks and to the thawing of the active layer.
3. Inter-annual variation in the amounts and distribution of snow cover will influence total suspended sediment and solute erosion.
4. Suspended sediment generated on slopes influenced by detachment sliding may not be directly translated into inputs to the stream system. The transport of suspended sediment from the scar to the stream is dependent on the slope drainage network. If flowpaths are not channelized, most of the sediment load will be redeposited lower down the slope.

Grain-size, coal and sorbed cations in the wash load were also evaluated:

1. There is an abundance of fine grained materials at fresh detachment slide scars. These grain-sizes are reflected in the wash load. The slightly coarser surficial sediments at vegetated slopes are not reflected in the wash load which is dominated by finer grained sediments. This suggests that surface wash may preferentially remove finer particles, resulting in the gradual coarsening of surficial sediments over time.

2. Coal appears to be preferentially transported during low flows. The total volume of coal relative to the total volume of sediment removed from slopes can be significant (50% at A3).
3. Sorbed cation concentrations depend on suspended sediment concentrations and can be important during periods of peak flows when sediment concentrations are high. However, the relationship established between sorbed cations and suspended sediment concentration shows that sorbed cations represent only a small portion (< 0.53%) of the total suspended load.

Higher rates of solute erosion were measured at the fresh detachment slide scars.

1. Elevated solute concentrations in runoff and high rates of solute removal occur on slopes affected by detachment sliding. Maximum solute concentrations measured at fresh detachment slide scars during snowmelt were up to five times greater (A1 – 3670 mg/L) than any concentrations measured previously in arctic slopewash studies. Concentrations measured during rainfall-induced runoff were over one order of magnitude greater than any values obtained in other studies (A1 – 12700 mg/L).
2. Salt concentrations in the fresh active layer in marine sediments are up to two orders of magnitude greater than on adjacent undisturbed slopes.
3. Despite very high solute concentrations in runoff, high sodium levels in fresh active layers in marine sediments will take several decades to decrease. The amount of time required for fresh active layer salt concentrations to return to residual levels is probably greatest in the polar desert region due to the low amounts of precipitation and surface runoff generation.

The revegetation of detachment slide scars will result in lower rates of suspended sediment erosion.

1. Vegetation cover in the lower part of plots B3 and B4 had a clear effect on overall rates of wash erosion as sediment concentrations were two orders of magnitude lower than at fresh detachment slides.
2. Abiotic conditions at fresh detachment slides (rapid removal of runoff, high rates of suspended sediment erosion, very fine surficial sediments and elevated Na^+ concentrations in fresh active layers in marine sediments) inhibit the revegetation of the scar zone.
3. The results suggest that detachment sliding affects surface wash erosion rates for years to decades. Old detachment slide scars (pre-1950) monitored in this study are sparsely vegetated and experience high rates of sediment removal (> 290 g/m^2).

Detachment sliding appears to have profound effects on the rates of surface wash erosion due to the modification of hydrologic conditions, the removal of the vegetation cover and the formation of a fresh active layer. Rates of suspended sediment erosion at fresh detachments slide scars are at least one order of magnitude greater than any other values measured in the high arctic, and rates of solute erosion are almost double. Physical changes after detachment sliding may inhibit revegetation of the scar area and high rates of surface wash erosion can be sustained for several decades after detachment sliding.

References

Bell, T. (1996). The last glaciation and sea level history of Fosheim Peninsula, Ellesmere Island, Canadian High Arctic. *Canadian Journal of Earth Sciences*, vol 33: 1075-1086.

Bellisario, L.M. (1993). Hydrologic and geomorphic slope processes, Black Top Creek basin, Ellesmere Island, Arctic Canada. N.W.T. unpublished undergraduate thesis, University of Toronto.

Bliss, L.C. (1990). High Arctic Ecosystems: How they develop and are maintained. *In* Canada's Missing Dimension. vol 1. C.R. Harington *ed.* Canadian Museum of Nature. pp 350-384.

Bos, M.G., Replogle, J.A., Aemmens, A.J. (1984). Flow measuring structures for open channel systems. John Wiley and Sons. New York. pp. 148-163

Cogley, J.G., McCann, S.B. (1976). An exceptional storm and its effects in the Canadian high arctic. *Arctic and Alpine Research*, vol 8: 105-110.

Dingman, L. (1984). Physical Hydrology. New York. Macmillan.

Edlund, S.A., Alt, B.T. (1989). Regional Congruence of vegetation and Summer Climate Patterns in the Queen Elizabeth Islands, N.W.T., Canada. *Arctic,* vol 42: 3-23.

Edlund, S.A., Alt, B.T., Young, K.L. (1989). Interaction of climate, vegetation, and soil hydrology at Hot Weather Creek, Fosheim Peninsula, Ellesmere Island, Northwest Territories. *In* Current Research, Part D, Geological Survey of Canada, Paper 89-1D, pp. 125-133.

Edlund, S.A., Woo, M.K. (1992). Eolian deposition on western Fosheim Peninsula, Ellesmere Island, Northwest Territories during the winter of 1990-91. *In* Current Research, Part B, Geological Survey of Canada, Paper 92-1B, pp. 91-96.

Edlund, S.A., Woo, M-K., Young, K., L. (1990). Climate, Hydrology and Vegetation Patterns Hot Weather Creek, Ellesmere Island, Arctic Canada. *Nordic Hydrology.* vol 21: 273-286.

Folk, R.L. (1974). Petrology of Sedimentary Rocks. Austin, Texas. Hemphills.

French, H. M., (1996). The Periglacial Environment. Longman. Essex, England.

French, H.M., Eggington, P.A. (1973). Thermokarst development, Banks Island, Western Canadian Arctic. *In* Permafrost: North American Contribution to the Second International Conference, Yakutsk, U.S.S.R.. National Academy of Sciences, Washington, D.C.: 203-212.

Gardiner, V., Dackombe, R. (1983). Geomorphological Field Manual. George Allen and Unwin. London, England.

Goldsmith, F.B., Harrison, C.M. (1976). Description and Analysis of Vegetation. *In* Methods in Plant Ecology. Chapman *ed.* John Wiley and Sons, Inc., New York.

Gregory, K.J., Walling, D.E. (1973). Drainage Basin Form and Process. Edward Arnold. London, England.

Hodgson, D.A. (1977). A preliminary account of surficial materials, geomorphological processes, terrain sensitivity, and Quaternary history of King Christian and Southern Ellef Ringnes Islands, District of Franklin. – *Report of Activities Part A, Geological Survey of Canada. Paper*, 77-1A: 485-493.

Hodgson, D.A., St-Onge, D.A., Edlund, S.A. (1991). Surficial materials of Hot Weather Creek basin, Ellesmere Island, Northwest Territories. *In* Current Research, Part E: Geological Survey of Canada, Paper 91-1E, pp 157-163.

Jahn, A. (1961). Quantitative analysis of some periglacial processes in Spitsbergen, *Nauka O Ziemi II*, Seria B, vol 5: 3-34.

Kalra, Y.P., Maynard, D.G. (1991). Methods manual for forest soil and plant analysis. Information Report NOR-X-319. Forestry Canada.

Kane, D. L. and Hinzman, L. D. (1988). Permafrost hydrology of a small arctic watershed. *In* Proceedings, Fifth International Conference on Permafrost. *Eds*. Tapir Publishers, Trondheim, pp. 590-595.

Lewkowicz, A.G., (1981). A study of slopewash processes in the continuous permafrost zone, Banks Island, Western Canadian Arctic. Ph. D. thesis. University of Ottawa.

Lewkowicz, A.G. (1983). Erosion by overland flow, central Banks Island, Western Canadian Arctic. *In Permafrost, Proceedings of the Fourth International Conference*. Washington, D.C.: National Academic Press, 701-706.

Lewkowicz, A.G. (1985). Use of an ablatometer to measure short-term ablation of exposed ground ice. *Canadian Journal of Earth Sciences.* vol 22: 1767-1773.

Lewkowicz, A.G. (1987). Nature and importance of thermokarst processes, Sand Hills Moraine, Banks Island, Canada. *Geografiska Annaler*. vol 69: 321-327.

Lewkowicz, A. G. (1988). Slope Processes. *In* Advances in Periglacial Geomorphology. Clark *ed.*, Wiley, Chichester, pp. 325-360.

Lewkowicz, A.G. (1990). Morphology, frequency and magnitude of active-layer detachment slides, Fosheim Peninsula, Ellesmere Island, N.W.T., *In* Permafrost-Canada: Proceedings of the Fifth Canadian Permafrost Conference. Quebec City: Laval, pp. 111-118.

Lewkowicz, A.G. (1992). Factors Influencing the Distribution and Initiation of Active-layer Detachment Slides on Ellesmere Island, Arctic Canada. *In* Periglacial Geomorphology. Dixon, J.C., and Abrahams, A.D., *eds.* The Binghamton Symposia in Geomorphology, International Series no 22, John Wiley and Sons Ltd., Chichester, U.K., pp. 223-250.

Lewkowicz, A.G. (1998). Aeolian Sediment Transport during Winter, Black Top Creek, Fosheim Peninsula, Ellesmere Island, Canadian Arctic. Permafrost and Periglacial Processes. vol 9: 34-46.

Lewkowicz, A.G., Day, T.J., and French, H.M. (1978). Observations on slopewash processes in an Arctic Tundra Environment, Banks Island, District of Franklin. *Scientific and Technical Notes Research*, Part A: Geological Survey of Canada 78-1A, pp. 516-520.

Lewkowicz, A.G., French, H.M. (1982a). The hydrology of small runoff plots in an area of continuous permafrost, Banks Island, N.W.T., *In The Roger J.E. Brown Memorial; Volume, Proceedings of the Fourth Canadian Permafrost Conference*, Calgary, Alberta, March 2-6, 1981. H.M. French *ed.* National Research Council of Canada, Ottawa, pp. 151-162.

Lewkowicz, A.G., French H.M. (1982b). Downslope water movement and solute concentrations within the active layer, Banks Island, N.W.T. *In The Roger J.E. Brown Memorial Volume, Proceedings of the Fourth Canadian Permafrost Conference*, Calgary, Alberta, March 2-6, 1981. H.M. French *ed.* National Research Council of Canada, Ottawa, pp. 163-172.

Lewkowicz, A.G., Wolfe, P.M. (1994). Sediment Transport in Hot Weather Creek, Ellesmere Island, N.W.T., Canada, 1990-1991. *Arctic and Alpine Research.* vol 26: 213-226.

Lewkowicz, A.G., Young, K.L. (1990). Hydrological Processes in a small catchment containing a perennial snowbank, Melville Island, N.W.T. *In* Northern Hydrology : Selected Canadian Perspectives. Proceedings of the Northern Hydrology Symposium, 10-12 July 1990, Saskatoon, Saskatchewan. Prowse, T.D. and Ommanney, C.S.L., *eds.*, National Hydrology Research Institute, Saskatoon, pp. 237-251.

Lorrain, R.D., Souchez, R.A. (1972). Sorption as a factor in the transport of major cations by meltwaters from an alpine glacier. *Quaternary Research.* vol. 2: 253-256.

Mackay, J.R. (1966). Segregated epigenetic ice and slumps in permafrost, Mackenzie Delta area, N.W.T.. *Geogr. Bull.* vol 8: 59-80.

Mackay, J.R. (1983). Oxygen isotope variations in permafrost, Tuktoyaktuk Peninsula area, Northwest Territories. *In* Current research, Part B. Geological Survey of Canada, Paper 83-1B, pp. 67-74.

Mackay, J.R., Mathews, W.H. (1973). Geomorphology and Quaternary history of the Mackenzie River Valley near Fort Good Hope, N.W.T.. *Canadian Journal of Earth Sciences.* vol 10: 26-41.

Marsh, P., Woo, M-K. (1979). Annual water balance of small High Arctic Basins. *In* Proceedings, Canadian Hydrology Symposium: 79- Cold Climate Hydrology. National Research Council of Canada, pp. 536-546.

Marsh, P., Woo, M-K. (1984). Wetting Front Advance and Freezing of Meltwater within a Snow Cover 1. Observations in the Canadian Arctic. *Water Resources Research,* vol 20: 1853-1864.

Mathewson, C.C., Mayer-Cole, T.A. (1984). Development and runout of a detachment slide, Bracebridge Inlet, Bathurst Island, Northwest Territories, Canada. *Bull. Assoc. Engin. Geol.* vol 21: 407-424.

McRoberts, E.C., Morganstern, N.R. (1974). The stability of thawing slopes. *Canadian Geotechnical Journal,* vol 11: 554-573.

Pettijohn, F.J., Potter, P.E., Siever, R. (1972). Sand and sandstone. New York. Springer.

Porsild, A.E. (1957). Illustrated Flora of the Canadian Arctic Archipelago. Department of Northern Affairs and National Resources. Ottawa.

Rudberg, S. (1969). Distribution of small-scale periglacial and glacial geomorphological features on Axel Heiberg Island, N.W.T., *In* The Periglacial Environment. Pewe, T.L., *ed.*, McGill, Queen's University Press., Montreal, Kingston, pp. 129-159.

Ryden, B. E. (1977). Hydrology of Truelove Lowland. *In* Truelove Lowland, Devon Island, Canada. A High Arctic Ecosystem. Bliss *ed.*, University of Alberta Press. Edmonton, Alberta., pp. 107-136.

Sharpe, D.R. (1985). The stratified nature of deposits in streamlined glacial landforms on southern Victoria Island, District of Franklin: Geological Survey of Canada, Paper 85-1A, pp 365-371.

Slaughter, C. W. and Kane, D. L. (1979). Hydrologic role of shallow organic soils in cold climates. In *Proceedings of the Canadian Hydrology Symposium: 79 - Cold Climate Hydrology*, 10-11 May, 1979, Vancouver B.C. Ottawa, National Research Council of Canada, pp. 380-389.

Srivastava, D.R., Jefferies, R.L. (1995a). Mosaics of vegetation and soil salinity: a consequence of goose foraging in an arctic salt marsh. *Canadian Journal of Botany.* vol 73: 75-83.

Srivastava, D.R., Jefferies, R.L. (1995b). The effect of salinity on the leaf and shoot demography of two arctic forage species. *Journal of Ecology.* vol 83: 421-430.

Srivastava, D.R., Jefferies, R.L. (1996). A positive feedback: herbivory, plant growth, salinity, and the desertification of an Arctic salt-marsh. *Journa of Ecology.* vol 84: 31-42.

Stangl, K.O., Roggensack, W.D., Hayley, D.W. (1982). Engineering geology of surficial soils, eastern Melville Island. *In* Proceedings, Fourth Canadian Permafrost Conference, Calgary Alberta, March 1981. H.M. French *ed.* National Research Council of Canada, Ottawa. pp. 136-147.

Steer, P., Woo, M-K. (1983). Measurement of slope runoff in a permafrost region. *Canadian Geotechnical Journal.* vol 20: 361-365.

Stone, D.B., Clarke, G.C., Blake, E.W. (1993). Subglacial measurement of turbidity and electrical conductivity. *Journal of Glaciology.* vol 39: 415-420.

Taylor, A. E., Burgess, M., Judge, A.S., Allen, V.S. (1982). *Canadian Geothermal Data Collection - Northern Wells 1981.* Ottawa: Geothermal Service of Canada.

Washburn, A.L. (1980). Geocryology. John Wiley and Sons. New York. pp. 244.

Wein, R.W., Rencz, A.N. (1976). Plant cover and standing crop sampling procedures for the Canadian High Arctic. *Arctic and Alpine Research*, vol 8: 139-150.

Wilkinson, T.J., Bunting, B.T. (1975). Overland transport of sediment by rill water in a periglacial environment in the Canadian High Arctic. *Geografiska Annaler,* vol 64A: 105-125.

Woo, M.-K. (1982). Snow hydrology of the High Arctic. Western Snow Conference, Reno, Nevada, 20-23

Woo, M.-K. (1993). Northern Hydrology. *In* Canada's Cold Environments. French, H.M., Slaymaker, O., *eds.* McGill, Queen's University Press. Montreal, Kingston., pp. 117-142.

Woo, M-K., Heron, R., Marsh, P., and Steer, P. (1983). Comparison of weather station snowfall with winter snow accumulation in High Arctic basins. *Atmosphere - Ocean*, vol 21: 312-325.

Woo, M.-K., Marsh, P. (1977). Effect of vegetation on limestone solution in a small High Arctic basin. *Canadian Journal of Earth Sciences*, vol 14: 571-581.

Woo, M.K., Marsh, P. (1990). Response of soil moisture change to hydrological processes in a continuous permafrost environment. *Nordic Hydrology*, vol 21:235-252.

Woo, M.-K., Steer, P. (1982). Occurrence of surface flow on arctic slopes, southwestern Cornwallis Island. *Canadian Journal of Earth Sciences*, vol 19: 2368-2377.

Woo, M.-K., Steer, P. (1983). Slope hydrology as influenced by thawing of the active layer, Resolute, N.W.T. Canadian , *Journal of Earth Sciences*, vol 20: 978-986.

Woo, M.K., Steer, P. (1986). Runoff regime of slopes in continuous permafrost areas. *Canadian Water Resources Journal*, vol 11: 58-68

Woo, M.-K., Young, K.L., Edlund, S.A. (1990). 1989 observations of soil, vegetation, and microclimate, and effect on slope hydrology, Hot Weather Creek basin, Ellesmere Island, N.W.T. *Current Research, Part D, Geological Survey of Canada Paper*, 90-1D: 85-93.

Woo, M.-K., Xia, Z. (1995). Suprapermafrost groundwater seepage in gravelly terrain, Resolute, N.W.T., Canada. *Permafrost and Periglacial Processes*, vol 6: 57-72

Young, K. L., Lewkowicz, A., G. (1988). Measurement of outflow from a snowbank with basal ice. *Journal of Glaciology*. vol 34: 358-362.

Young, K. L., Woo, M.-K. and Edlund, S. A. (1997). Influence of local topography, soils, and vegetation on microclimate and hydrology at a high arctic site, Ellesmere Island, Canada. *Arctic and Alpine Research*, **29**, 270-284.

Appendix A-1: Calculation of a snow water conversion factor, 1996.

Plot	Snow depth (cm) *d*	Volume of water (mL) Vw	Volume of snow core (cm^3) Vc = ($\pi * r^2 * d$)	Snow density (Mg/m^3) *c* = (Vw/Vc)
A1	41	160	515	0.31
A1	40	140	503	0.28
A1	64	290	804	0.36
A2	40	203	503	0.40
A2	27	167	339	0.49
A3	75	350	942	0.37
A3	24	85	302	0.28
A3	14	30	176	0.17
A4	40	150	503	0.30
A4	30	105	377	0.28
B1	50	195	628	0.31
B1	39	100	490	0.20
B2	56	260	704	0.37
B3	18	37	226	0.16
B3	36	205	452	0.45
B4	70	335	880	0.38
Average snow density:				0.32

Appendix A-2: Data - logger - discharge rating equations.

Site A

A1, 1. (JD 158) 0606, 1025 to (JD 160) 0608, 2304 note: if DL< 8.39 then discharge = 0	$y = 47.91x^2 - 801.7x + 3353.5$ $r^2 = 0.93$ n = 8
2. (JD 162) 0610, 0830 to (JD 163) 0611, 1744	$y = 3E - 23x^{24.92}$ $r^2 = 0.99$ n = 5
3. (JD 164) 0612, 0740 to (JD 171) 0619, 0207 note: if DL < 8.1 then discharge = 0	$y = 42.69x^2 - 691.9x + 2810.2$ $r^2 = 0.93$ n = 25
4. (JD 176) 0624, 2117 to (JD 177) 0625, 2007	$y = -12.80x^2 + 279.83x - 1457.9$ $r^2 = 0.99$ n = 4
A2, 1. (JD 156) 0604, 1843 to (JD 177) 0625, 0930 note: if DL < 8.16 then discharge = 0	$y = 39.27x^2 - 640.4x + 2613.1$ $r^2 = 0.96$ n = 32
A3, 1. (JD 161) 0609, 0913 to (JD 167) 0615, 0845	$y = 25.10x^2 - 469.2x + 2203$ $r^2 = 0.99$ n = 19
2. (JD 168) 0616, 2322 to (JD 172) 0620, 1513	$y = 44.21x^2 - 1135.4x + 7377.7$ $r^2 = 0.93$ n = 16
3. (JD 173) 0621, 1913 to (JD 181) 0629, 1015 note: if DL < 11.96 then discharge = 0	$y = 22.54x^2 - 539.9x + 3236.5$ $r^2 = 0.98$ n = 19

Site B

B1, 1. (JD 159) 0607, 1445 to (JD 163) 0611, 0817 note: if DL < 7.8 then discharge = 0	$y = 60.19x^2 - 928x + 3579$ $r^2 = 0.98$ $n = 10$
2. (JD 164) 0612, 1701 to (JD 166) 0614, 1952	$y = 14.18x^2 - 134x + 266.2$ $r^2 = 0.94$ $n = 9$
3. (JD 167) 0615, 0020 to (JD 169) 0617, 2028	$y = 21.55x^2 - 269x + 839.2$ $r^2 = 0.72$ $n = 9$
B2, 1. (JD 161) 0609, 1308 to (JD 173) 0621, 1554	$y = 24.48x^2 - 310.7x + 979.4$ $r^2 = 0.90$ $n = 29$
2. (JD 176) 0624, 1155 to (JD 180) 0628, 1225 note: if DL < 7.39 then discharge = 0	$y = 73.69x^2 - 1056.2x + 3780.6$ $r^2 = 0.93$ $n = 9$
B3, 1. (JD 159) 0607, 1345 to (JD 176) 0624, 1139	$y = 20.12x^2 - 47.06x - 2.53$ $r^2 = 0.87$ $n = 38$
2. (JD 176) 0624, 1604 to (JD 180) 0628, 1228	$y = 22.76x^2 - 109.7x - 130.5$ $r^2 = 0.99$ $n = 8$
B4, 1. (JD 158) 0606, 1814 to (JD 170) 0618, 1715 note: if DL < 5.90 then discharge = 0	$y = 22.30x^2 - 259x + 751.8$ $r^2 = 0.77$ $n = 23$

Appendix A-2: Stage - discharge relationships, site A1 and A2.

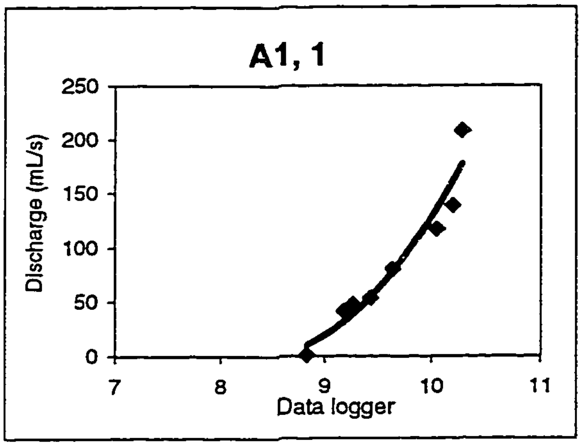

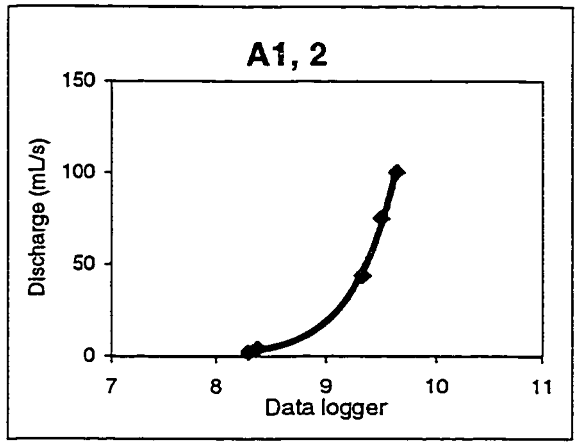

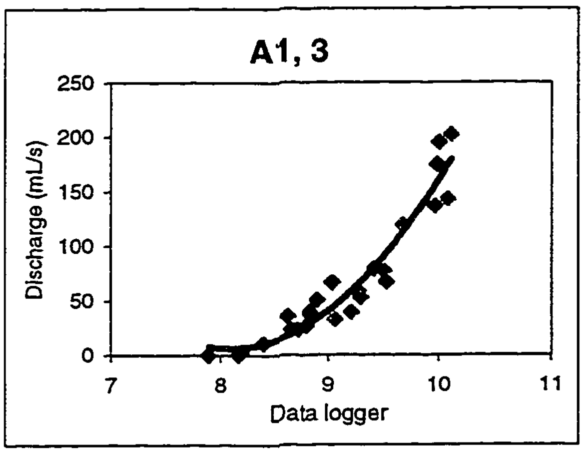

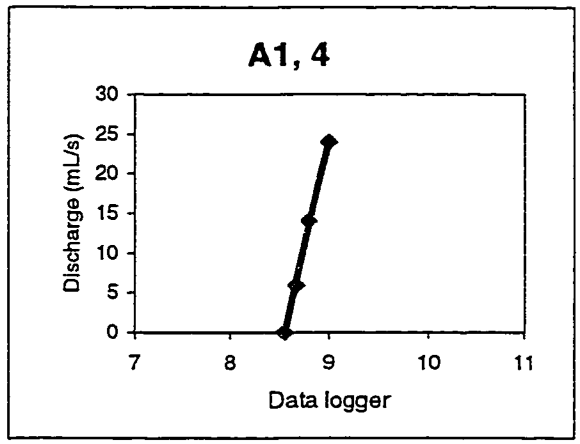

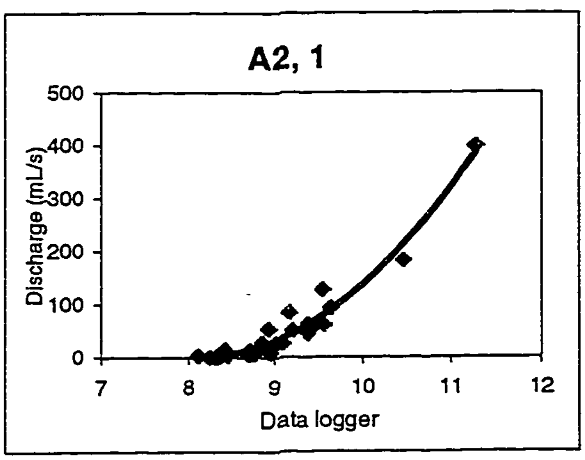

Appendix A-2: Stage - discharge relationships, site A3.

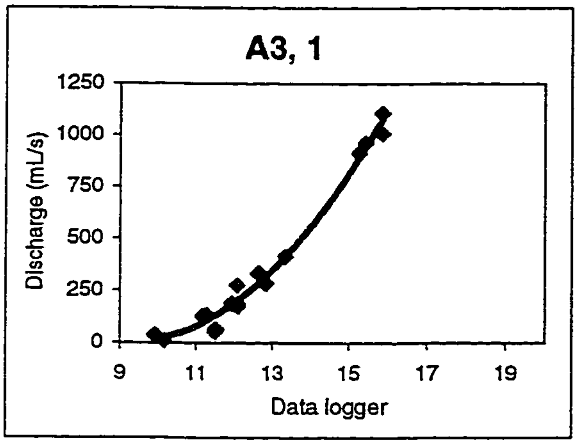

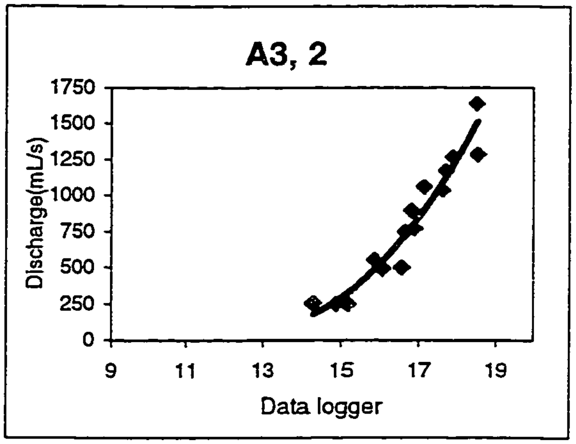

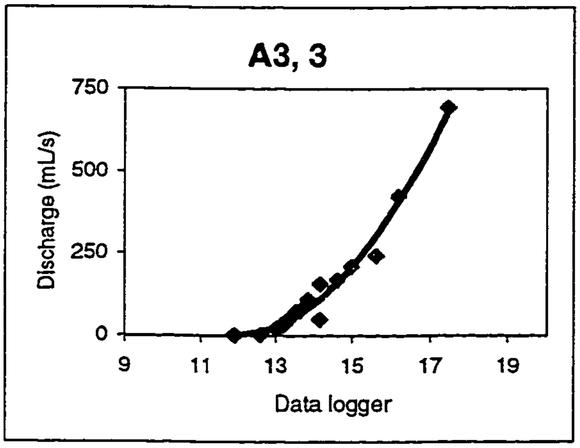

Appendix A-2: Stage - discharge relationships, site B1 and B2.

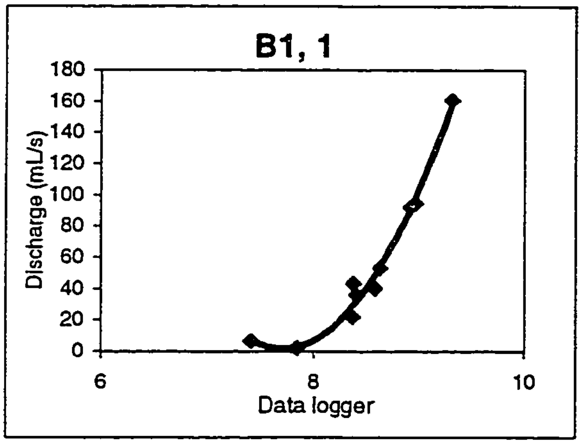

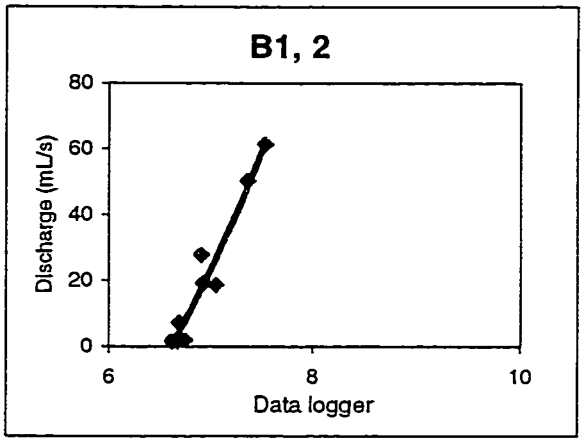

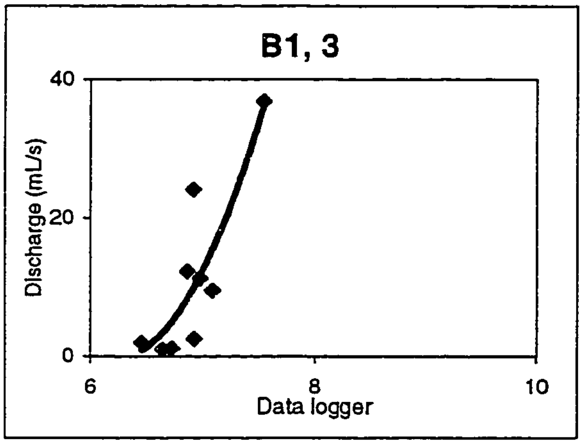

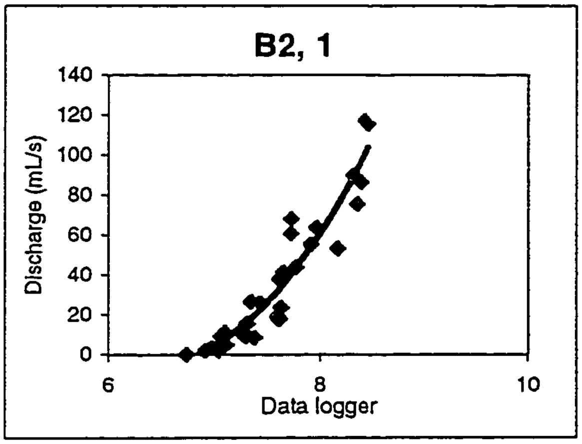

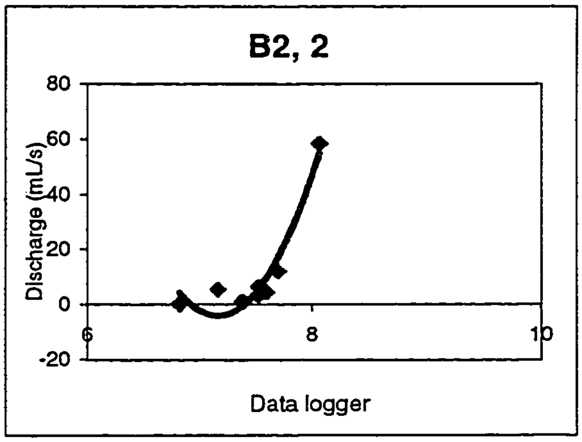

Appendix A-2: Stage - discharge relationships, plots B3 and B4.

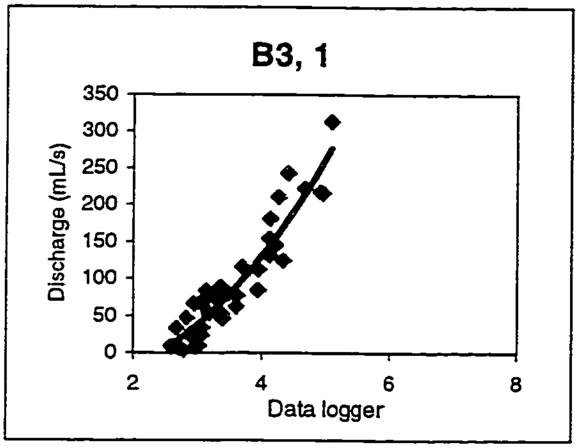

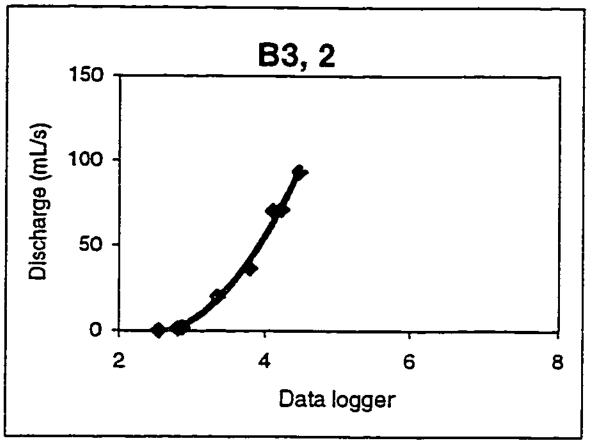

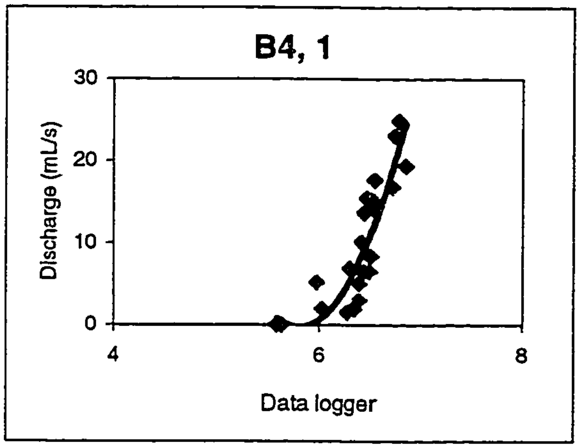

Appendix A-3: Discharge corrections using field notes, net radiation record and hydrographs from adjacent plots.

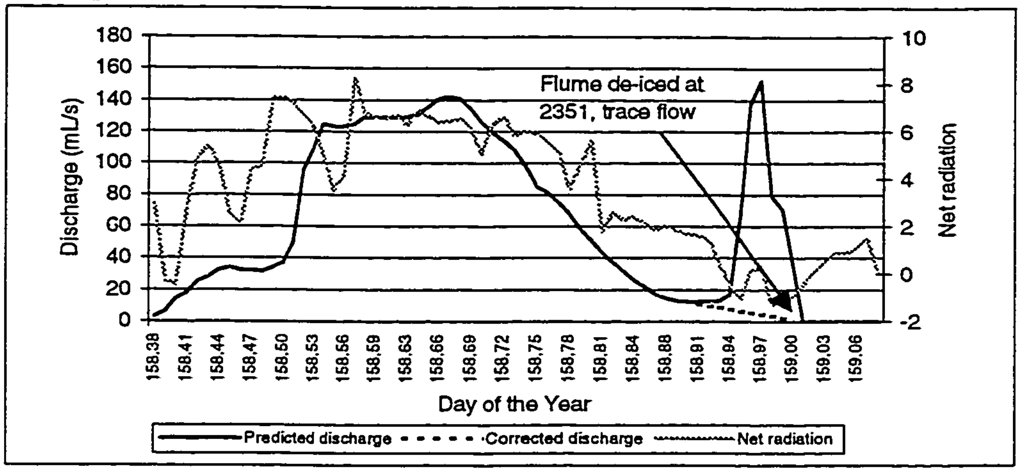

Plot A1, late peak due to icing of the flume during early runoff.

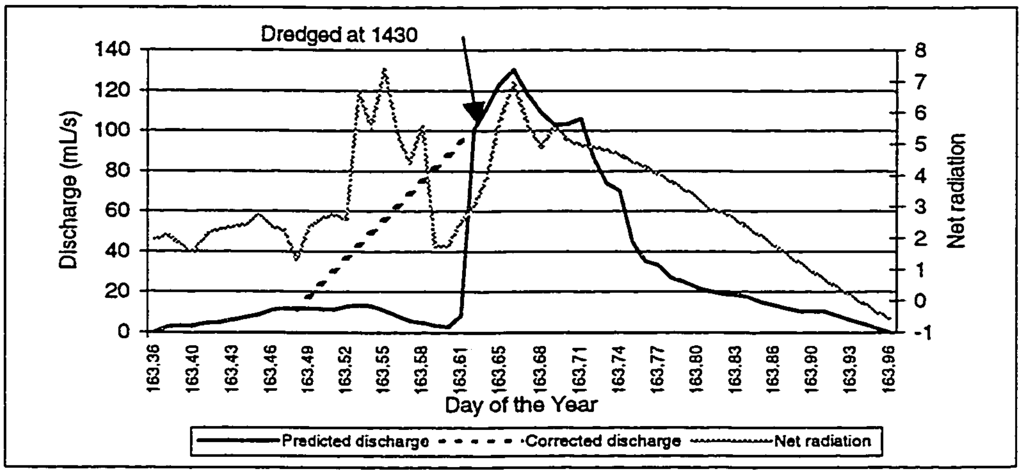

Plot A1, sedimentation of flume during discharge rise.

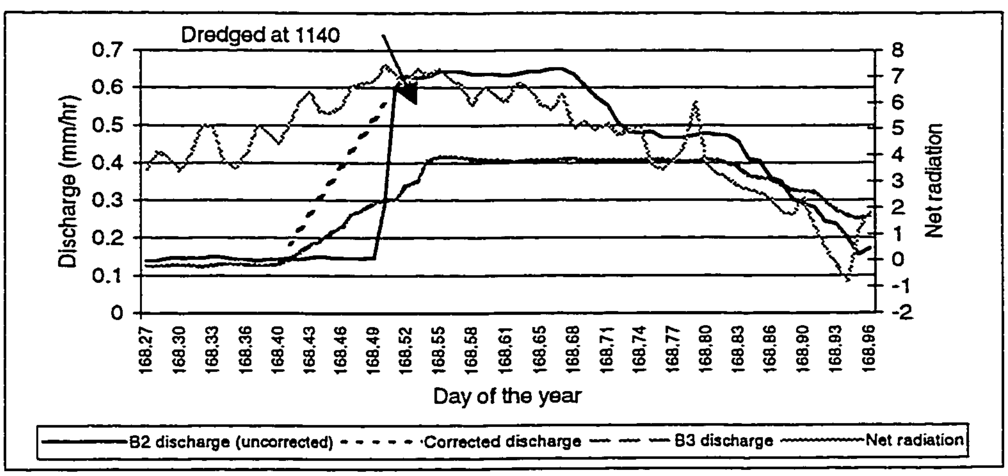

Plot B2, sedimentation of flume during discharge rise.

Appendix A-4: Development of storm hydrographs for A2 and B1.

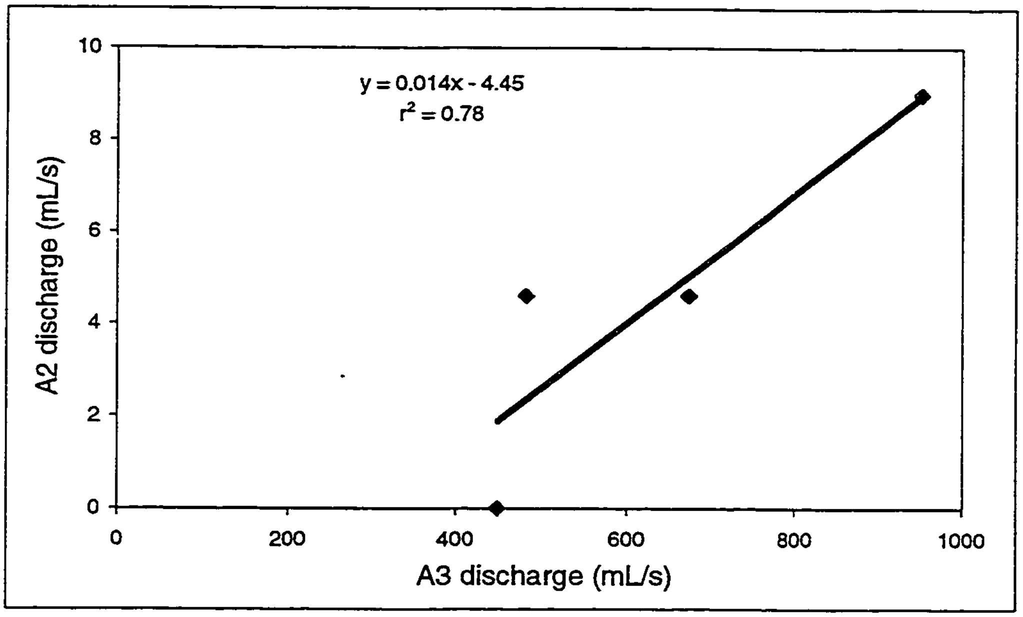

A3 discharge vs A2 discharge during storm events.

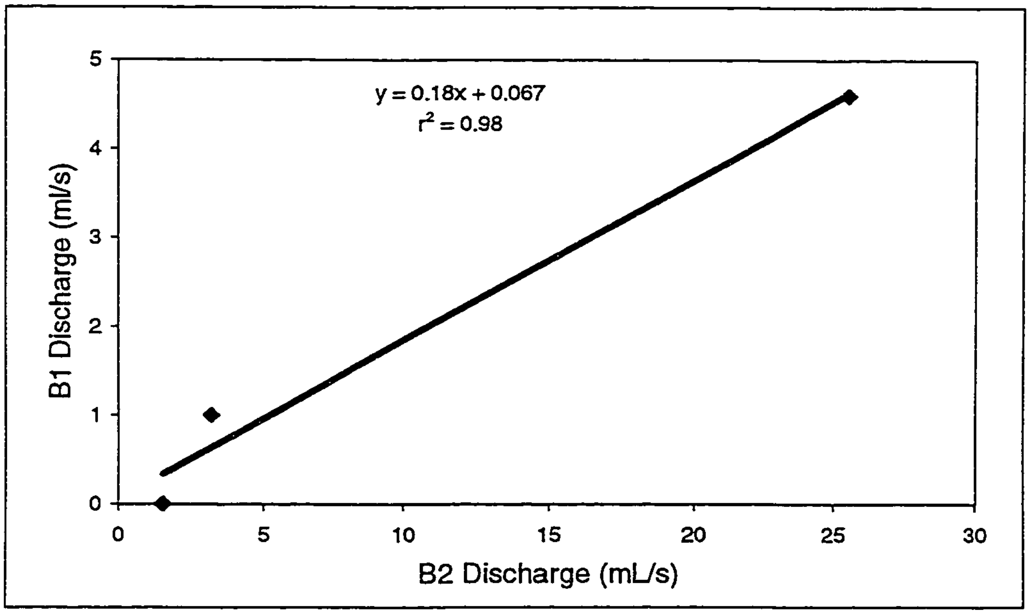

B2 discharge vs B1 discharge during storm events.

Appendix A-5: Site A, a coefficients.

	t1	Cond1 @ t1	t2	Cond2 @ t2	Lt2 - Lt1	Lt1 (t2-R)	Lt2 (t1-R)	(Lt2-Lt1)/(Lt1(t2-25))-(Lt2(t-25))	a in %/°C	sample average
A1, 1	8.7	289.1	14.9	321.7	32.6	-2919.9	-5243.7	0.0140	1.403	1.503
	14.9	321.7	17.7	339	17.3	-2348.4	-3423.9	0.0161	1.609	
	17.7	339	20.7	351.7	12.7	-1457.7	-2567.4	0.0114	1.144	
	20.7	351.7	25.9	388.6	36.9	316.5	-1671.0	0.0186	1.857	
A1, 2	8.1	3288	11	3460	172	-46032.0	-58474.0	0.0138	1.382	1.494
	11	3460	15.7	3777	317	-32178.0	-52878.0	0.0153	1.531	
	15.7	3777	21.2	4151	374	-14352.6	-38604.3	0.0154	1.542	
	21.2	4151	24.8	4392	241	-830.2	-16689.6	0.0152	1.520	
								Average value for a	=	**1.499**

A2, 1	4.8	270.5	9.2	298	27.5	-4273.9	-6019.6	0.0158	1.575	1.649
	9.2	298	11.7	315.7	17.7	-3963.4	-4988.1	0.0173	1.727	
	11.7	315.7	17.5	355.3	39.6	-2367.8	-4725.5	0.0168	1.680	
	17.5	355.3	20.1	375	19.7	-1741.0	-2812.5	0.0184	1.838	
	20.1	375	24.8	402	27	-75.0	-1969.8	0.0142	1.425	
A2, 2	7.8	334	12.3	375.7	41.7	-4241.8	-6462.0	0.0188	1.878	1.964
	12.3	375.7	14.7	396.6	20.9	-3869.7	-5036.8	0.0179	1.791	
	14.7	396.6	18.9	434.2	37.6	-2419.3	-4472.3	0.0183	1.831	
	18.9	434.2	22.9	482	47.8	-911.8	-2940.2	0.0236	2.357	
A2,3	10.1	316.4	16.9	367.7	51.3	-2562.8	-5478.7	0.0176	1.759	2.016
	16.9	367.7	22.1	416.1	48.4	-1066.3	-3370.4	0.0210	2.101	
	22.1	416.1	25	444.3	28.2	0.0	-1288.5	0.0219	2.189	
								Average value for a	=	**1.877**

A3, 1	3.4	133.9	6.7	142.9	9	-2450.4	-3086.6	0.0141	1.414	1.704
	6.7	142.9	8.8	150	7.1	-2315.0	-2745.0	0.0165	1.651	
	8.8	150	14.8	170.8	20.8	-1530.0	-2767.0	0.0168	1.682	
	14.8	170.8	19.1	185.5	14.7	-1007.7	-1892.1	0.0166	1.662	
	19.1	185.5	23.3	204.3	18.8	-315.4	-1205.4	0.0211	2.112	
A3, 2	6	428	10.6	508	80	-6163.2	-9652.0	0.0229	2.293	1.922
	10.6	508	12.8	541	33	-6197.6	-7790.4	0.0207	2.072	
	12.8	541	16.2	572	31	-4760.8	-6978.4	0.0140	1.398	
	16.2	572	20.8	633	61	-2402.4	-5570.4	0.0193	1.926	
A3, 3	6.5	129.6	10.7	145.2	15.6	-1853.3	-2686.2	0.0187	1.873	1.839
	10.7	145.2	13.4	154	8.8	-1684.3	-2202.2	0.0170	1.699	
	13.4	154	19.1	177	23	-908.6	-2053.2	0.0201	2.009	
	19.1	177	22.3	188.5	11.5	-477.9	-1112.2	0.0181	1.813	
	22.3	188.5	25.8	201	12.5	150.8	-542.7	0.0180	1.802	
								Average value for a	=	**1.822**

Appendix A-5: Site B, a coefficients.

	t1	Cond1 @ t1	t2	Cond2 @ t2	Lt2 - Lt1	Lt1 (t2-R)	Lt2 (t1-R)	(Lt2-Lt1)/(Lt1(t2-25))-(Lt2(t1-25))	a in %/°C	sample average
B1, 1	3.5	498	8.3	563	65	-8316.6	-12104.5	0.0172	1.716	1.668
	8.3	563	11.4	604	41	-7656.8	-10086.8	0.0169	1.687	
	11.4	604	15.5	655	51	-5738.0	-8908.0	0.0161	1.609	
	15.5	655	21.4	725	70	-2358.0	-6887.5	0.0155	1.545	
	21.4	725	24.8	772	47	-145.0	-2779.2	0.0178	1.784	
B1, 2	4.3	539	7.8	561	22	-9270.8	-11612.7	0.0094	0.939	1.501
	7.8	561	12.1	613	52	-7236.9	-10543.6	0.0157	1.573	
	12.1	613	15.3	648	35	-5946.1	-8359.2	0.0145	1.450	
	15.3	648	19.3	705	57	-3693.6	-6838.5	0.0181	1.812	
	19.3	705	25.5	789	84	352.5	-4497.3	0.0173	1.732	
B1, 3	10.2	796	12.7	809	13	-9790.8	-11973.2	0.0060	0.596	1.422
	12.7	809	16.3	866	57	-7038.3	-10651.8	0.0158	1.577	
	16.3	866	21.8	981	115	-2771.2	-8534.7	0.0200	1.995	
	21.8	981	24.8	1028	47	-196.2	-3289.6	0.0152	1.519	
								Average value for a	**=**	**1.531**

B2, 1	6.4	167.4	9.3	179.6	12.2	-2628.2	-3340.6	0.0171	1.713	1.845
	9.3	179.6	13.5	194	14.4	-2065.4	-3045.8	0.0147	1.469	
	13.5	194	18	214	20	-1358.0	-2461.0	0.0181	1.813	
	18	214	23.4	247.1	33.1	-342.4	-1729.7	0.0239	2.386	
B2, 2	7.8	203.7	11	217.5	13.8	-2851.8	-3741.0	0.0155	1.552	1.712
	11	217.5	15.6	237.4	19.9	-2044.5	-3323.6	0.0156	1.556	
	15.6	237.4	21.1	267.4	30	-925.9	-2513.6	0.0189	1.890	
	21.1	267.4	25	288.2	20.8	0.0	-1124.0	0.0185	1.851	
B2, 3	6.6	791	10.3	850	59	-11627.7	-15640.0	0.0147	1.470	1.555
	10.3	850	15	922	72	-8500.0	-13553.4	0.0142	1.425	
	15	922	20.2	1016	94	-4425.6	-10160.0	0.0164	1.639	
	20.2	1016	23.9	1085	69	-1117.6	-5208.0	0.0169	1.687	
								Average value for a	**=**	**1.704**

B3, 1	5.1	240	7.7	252.8	12.8	-4152.0	-5030.7	0.0146	1.457	1.588
	7.7	252.8	11.4	271.5	18.7	-3438.1	-4697.0	0.0149	1.485	
	11.4	271.5	15.7	299.4	27.9	-2525.0	-4071.8	0.0180	1.804	
	15.7	299.4	18.5	311.3	11.9	-1946.1	-2895.1	0.0125	1.254	
	18.5	311.3	23.2	343.8	32.5	-560.3	-2234.7	0.0194	1.941	
B3, 2	7.3	448.5	11.4	489	40.5	-6099.6	-8655.3	0.0158	1.585	1.996
	11.4	489	14.2	539	50	-5281.2	-7330.4	0.0244	2.440	
	14.2	539	17.6	588	49	-3988.6	-6350.4	0.0207	2.075	
	17.6	588	22.1	646	58	-1705.2	-4780.4	0.0189	1.886	
B3, 3	4.7	1049	9.9	1142	93	-15839.9	-23182.6	0.0127	1.267	1.764
	9.9	1142	14.8	1298	156	-11648.4	-19599.8	0.0196	1.962	
	14.8	1298	18.6	1385	87	-8307.2	-14127.0	0.0149	1.495	
	18.6	1385	21.1	1480	95	-5401.5	-9472.0	0.0233	2.334	
B3, 4	8.8	1139	11.8	1202	63	-15034.8	-19472.4	0.0142	1.420	1.626
	11.8	1202	16.8	1319	117	-9856.4	-17410.8	0.0155	1.549	
	16.8	1319	20.8	1444	125	-5539.8	-11840.8	0.0198	1.984	
	20.8	1444	24.3	1528	84	-1010.8	-6417.6	0.0155	1.554	
								Average value for a	**=**	**1.744**

B4, 1	4.7	146.3	8.7	152.9	6.6	-2384.7	-3103.9	0.0092	0.918	1.751
	8.7	152.9	10.8	164	11.1	-2171.2	-2673.2	0.0221	2.211	
	10.8	164	16.2	181.6	17.6	-1443.2	-2578.7	0.0155	1.550	
	16.2	181.6	22.6	215.6	34	-435.8	-1897.3	0.0233	2.326	
B4, 2	5.4	148.5	9.4	165.6	17.1	-2316.6	-3245.8	0.0184	1.840	1.856
	9.4	165.6	14.6	191	25.4	-1722.2	-2979.6	0.0202	2.020	
	14.6	191	19.1	214.4	23.4	-1126.9	-2229.8	0.0212	2.122	
	19.1	214.4	23.6	229.6	15.2	-300.2	-1354.6	0.0144	1.441	
B4, 3	6.2	116	10.4	133.9	17.9	-1693.6	-2517.3	0.0217	2.173	1.630
	10.4	133.9	13.4	141.8	7.9	-1553.2	-2070.3	0.0153	1.528	
	13.4	141.8	20.2	167	25.2	-680.6	-1937.2	0.0201	2.005	
	20.2	167	22.6	170.4	3.4	-400.8	-817.9	0.0082	0.815	
								Average value for a	=	**1.746**

Appendix A-6: Air temperature/net radiation – water temperature rating equations.

Site A

A1. Air temperature – water temperature rating curve (JD 158) 0606 to (JD 177) 0625	$y = 0.36x + 0.44$ $y^2 = 0.83$ $n = 33$
A2. Net radiation* – water temperature rating curve (JD 156) 0604 to (JD 177) 0625	$y = 0.69x + 2.18$ $r^2 = 0.44$ $n = 17$
A3, 1. Net radiation* – water temperature rating curve (Snowmelt) (JD 161) 0609 to (JD 175) 0623 **A3, 2.** Net radiation – water temperature rating curve (Rainfall) (JD 176) 0624 to (JD 180) 0628	$y = 0.49x + 0.59$ $r^2 = 0.72$ $n = 34$ $y = 0.60x + 3.47$ $r^2 = 0.57$ $n = 7$

Site B

B1,1. Air temperature – water temperature rating curve (JD 159) 0607 to (JD 162) 0610 **B1,1.** Air temperature – water temperature rating curve (JD 163) 0611 to (JD 177) 0625	$y = 1.25x^2 + 0.43$ $r^2 = 0.82$ $n = 5$ $y = 0.66x^2 + 3.08$ $r^2 = 0.87$ $n = 6$
B2. Air temperature – water temperature rating curve (JD 162) 0610 to (JD 177) 0625	$y = 0.75x + 1.74$ $r^2 = 0.76$ $n = 18$
B3. Air temperature – water temperature rating curve (Snowmelt) (JD 159) 0607 to (JD 177) 0625	$y = 0.87x + 2.09$ $r^2 = 0.75$ $n = 33$
B4. Net radiation* – water temperature rating curve (JD 158) 0606 to (JD 170) 0618	$y = 0.84x + 3.71$ $r^2 = 0.91$ $n = 8$

Note: * indicates net radiation converted to a 30 minute average

Appendix A-6: Air temperature/net radiation - water temperature relationships.

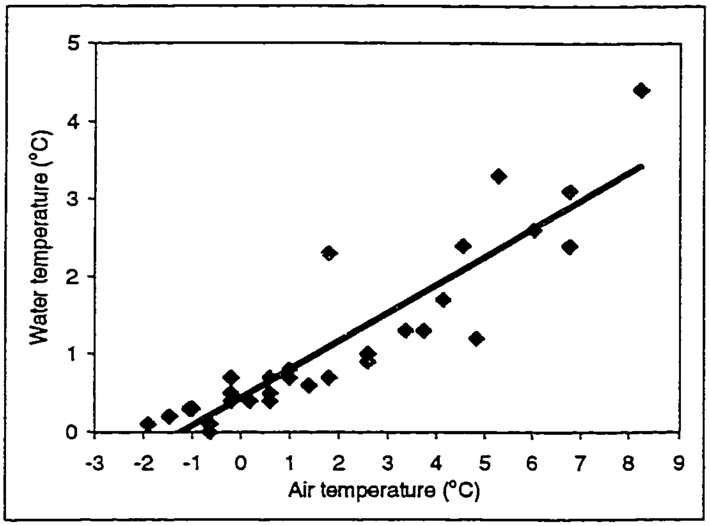

A1: Air temperature - water temperature relationship.

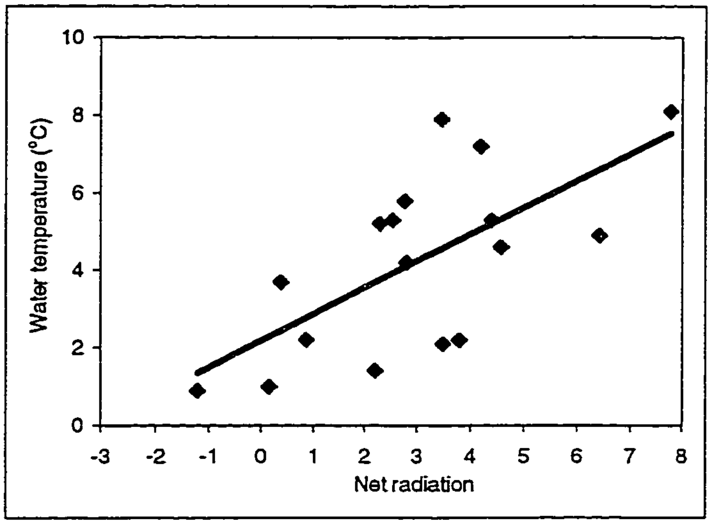

A2: Net radiation - water temperature relationship.

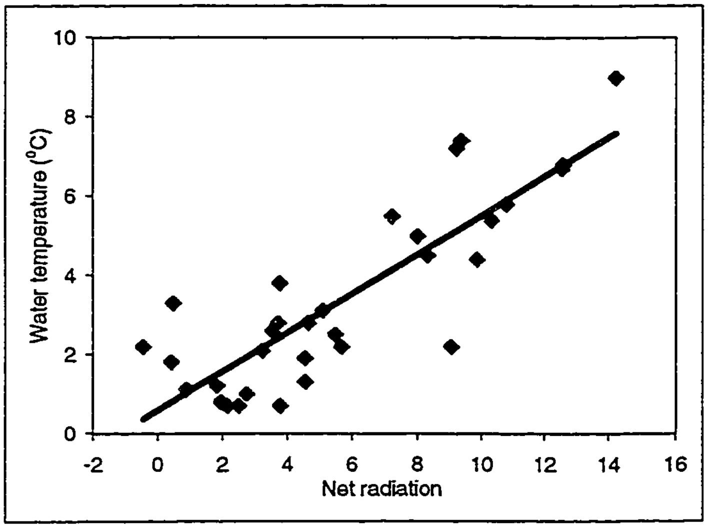

A3, 1: Net radiation - water temperature relationship.

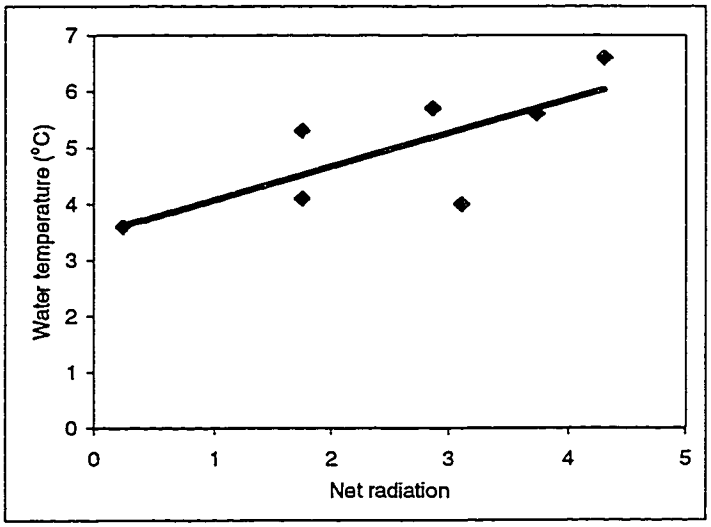

A3, 1: Net radiation - water temperature relationship.

Note: The net radiation values are taken from the uncalibrated data logger record and have not been converted to W/m2.

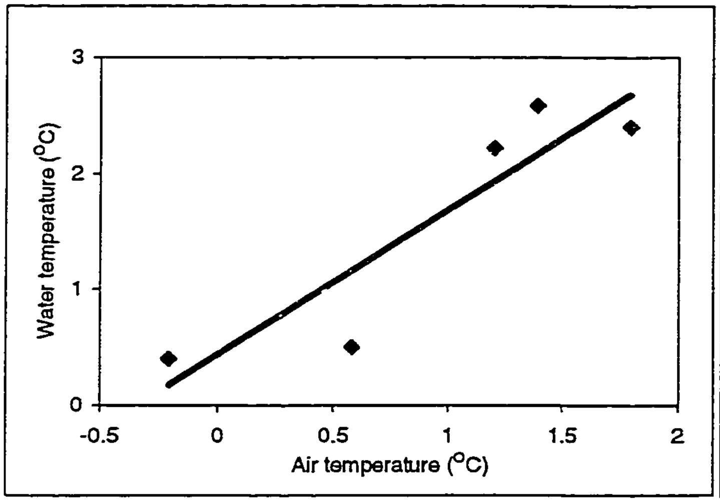

B1, 1: Air temperature - water temperature relationship

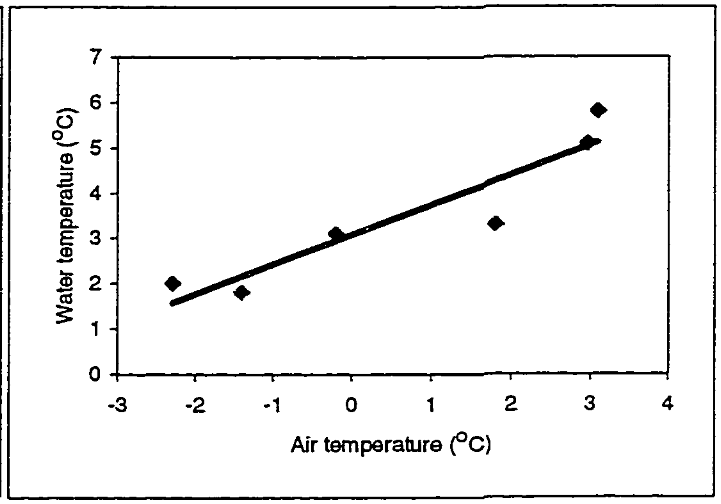

B1, 2: Air temperature - water temperature relationship.

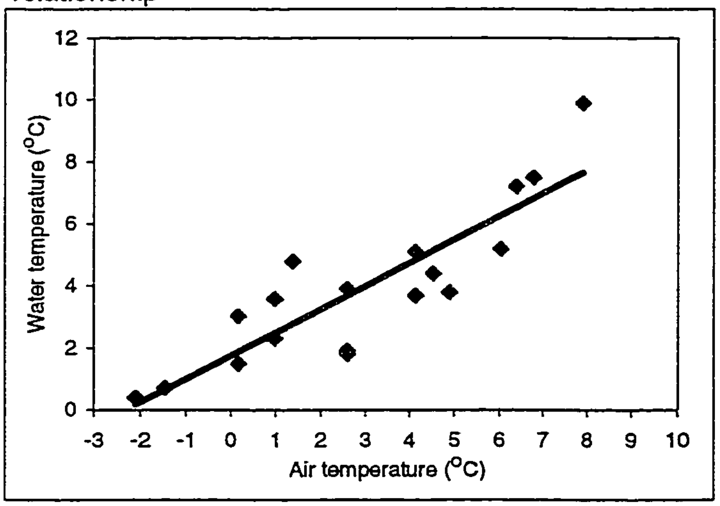

B2: Air temperature - water temperature relationship.

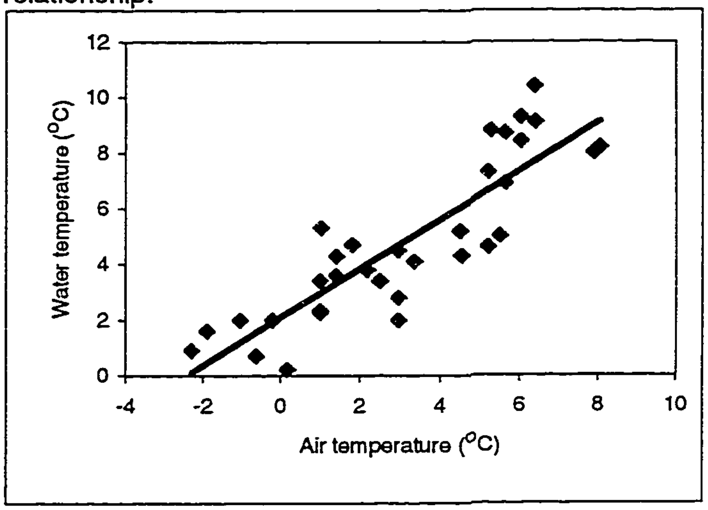

B3: Air temperature - water temperature relationship.

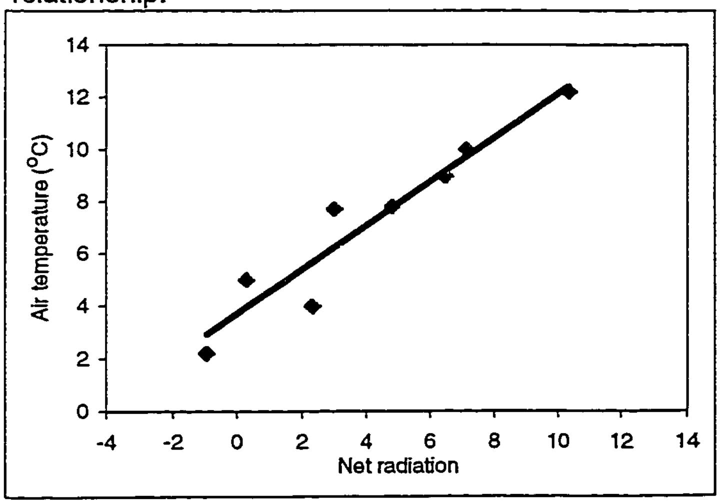

B4: Net radiation - air temperature relationship.

Appendix A-7: Data logger – conductivity rating equations.

Site A

A1	$y = 18716x^{-1.15}$	$r^2 = 0.82$	n = 36
A2	$y = 13729x^{-1.036}$	$r^2 = 0.96$	n = 32
A3	$y = 20947x^{-1.20}$	$r^2 = 0.88$	n = 63

Site B

B1	$y = 42482x^{-1.36}$	$r^2 = 0.72$	n = 27
B2	$y = 21994x^{-1.15}$	$r^2 = 0.93$	n = 45
B3	$y = 74865x^{-1.60}$	$r^2 = 0.92$	n = 60
B4	$y = 6899.6x^{-0.83}$	$r^2 = 0.74$	n = 20

Appendix A-7: Data logger - conductivity relationships.

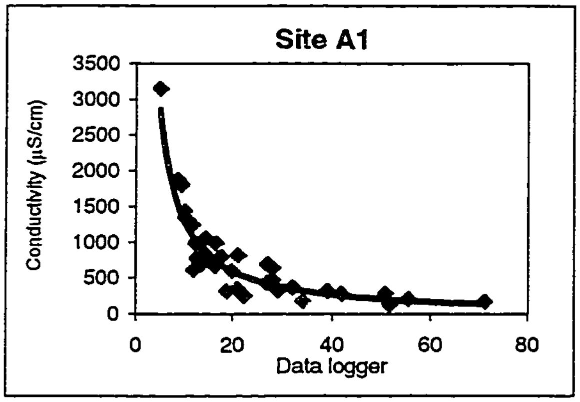

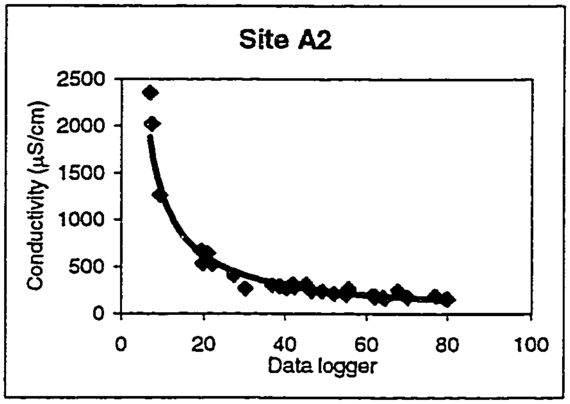

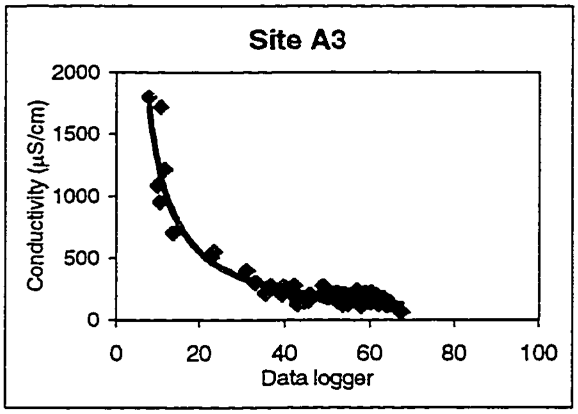

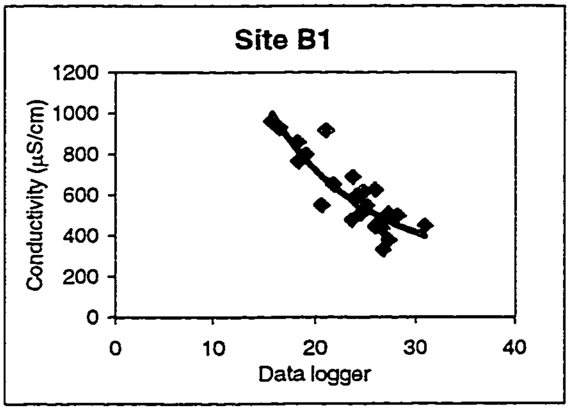

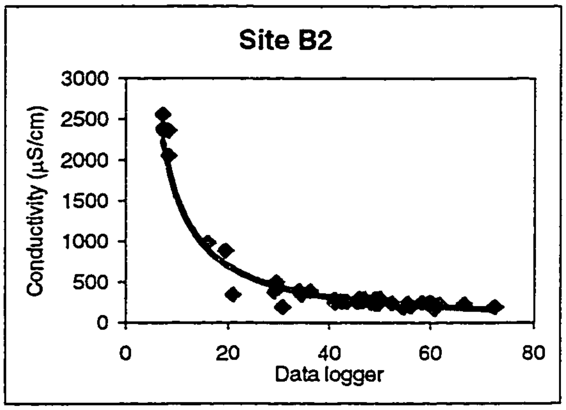

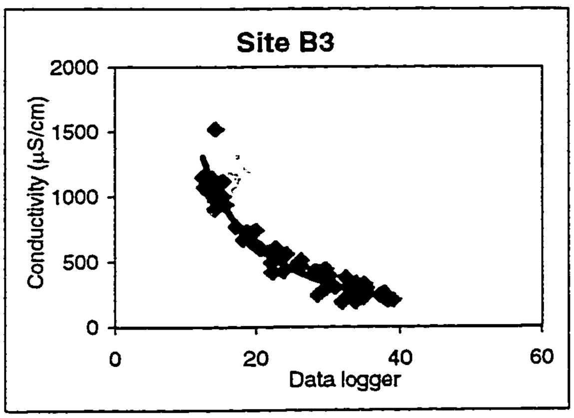

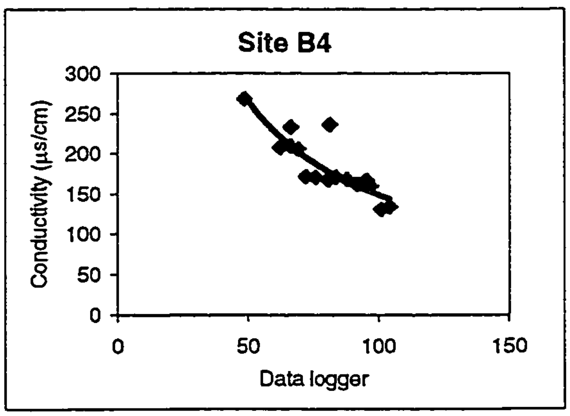

Appendix B-1: Infiltration experiment, fresh detachment slide scar and adjacent slope, 1997.

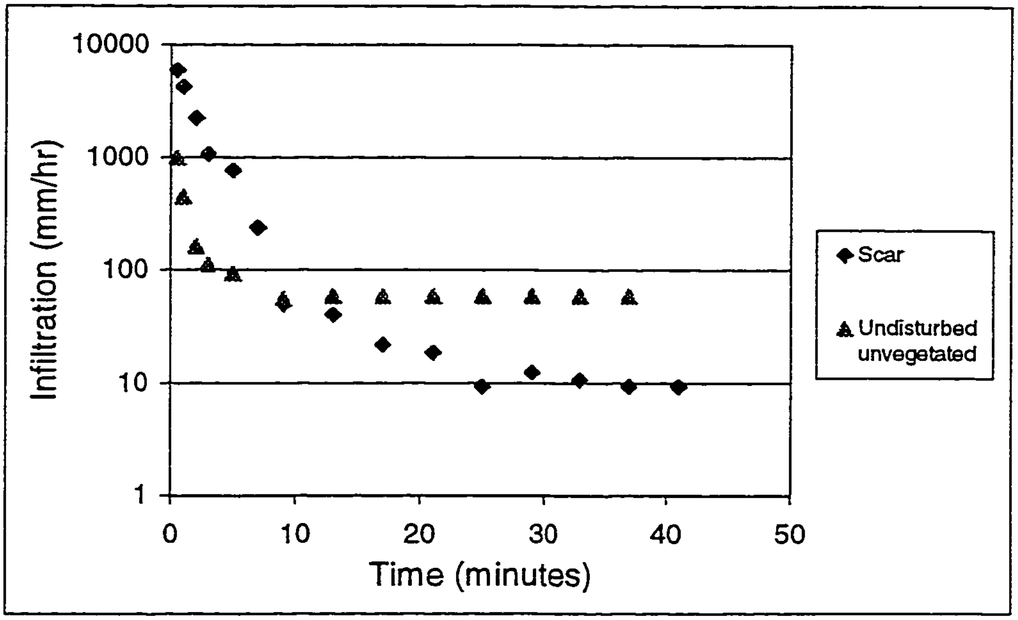

** Initial infiltration rates for an adjacent vegetated undisturbed site exceeded 10000 mm/hr and the experiment could not be continued as the water source was rapidly exhausted.

Appendix C-1: Plots A1, A2 and A3, 1996, discharge and suspended sediment concentrations.

	Sample	Dis. mL/s	SSC mg/L	Sample	Dis. mL/s	SSC mg/L	Sample	Dis. mL/s	SSC mg/L
1	A10606,1041	41.1	910.8	A2 0604,1857	29.4	654.8	A30608,2315	98.4	1885.5
2	A10606,1526	116.7	1303.4	A20604,2130	15.3	332.6	A30609,1003	52.3	713.7
3	A10606,1815	81.4	1066.8	A20605,0957	10.5	208.4	A30609,1608	284.1	2031.3
4	A10607,0906	53.2	1818.3	A20605,1240	126.8	2113.9	A30610,0848	52.6	447.7
5	A10607,1654	47.3	1778.5	A20605,1621	61.9	1407.1	A30610,1821	426	1793.6
6	A10608,0900	77.74	6696.4	A20605,2119	27.9	917.7	A30610,2016	171.9	1230.0
7	A10608,1055	208.3	8885.3	A20606,0958	53	1880.7	A306110907	9.1	139.3
8	A10608,1525	139.2	9056.7	A20606,1508	397.8	4791.4	A30611,1200	31.8	346.5
9	A10609,0925	86.3	19641.4	A20606,2342	13.2	582.1	A30611,1450	214.3	2038.4
10	A10609,1548	81.2	16736.5	A20607,0845	92.1	2806.9	A30611,1800	189.2	1386.1
11	A10610,1144	22.52	5801.7	A20607,2132	25.1	1006.4	A30611,2313	40	325.4
12	A10611,1153	23.9	14790.7	A20608,1553	60.6	5611.8	A30612,1213	239.4	2688.1
13	A10611,1430	100.4	14812.4	A206091526	83.2	4791.5	A30612,1600	188.1	1053.9
14	A10611,1744	43.8	11130.7	A20609,2045	49.7	3018.1	A30612,1832	131.1	523.9
15	A10612,0740	66.7	21968.2	A20610,0820	14.8	475.0	A30612,2038	61.5	428.7
16	A10612,1153	174.6	22988.1	A20610,1438	43.8	7108.0	A30613,0030	21	161.6
17	A10612,1818	39.2	9687.2	A20611,0853	10	2525.3	A30613,0619	36.7	254.8
18	A10612,2038	10.5	4364.3	A20611,1413	27.2	4980.0	A30613,1450	333.9	1704.2
19	A10613,0625	50.6	8785.6	A20611,1734	8	1823.8	A30613,1745	274.7	1640.0
20	A10613,1434	118.8	16596.7	A20612,1522	7.2	1442.9	A30613,2030	172.3	1228.2
21	A10613,1736	66.9	11927.4	A20613,1410	6.7	1360.0	A30614,0005	117.8	402.1
22	A10613,2025	32.4	11266.9	A20614,1411	2.6	2146.2	A30614,0515	132.8	1432.3
23	A10614,0001	12	5707.6	A20614,1820	1.1	1570.6	A30614,1448	962.8	3680.6
24	A10614,0525	79	17727.1	A20615,1414	2	1374.6	A30614,2040	969.6	2005.9
25	A10614,1431	142.6	19950.7	A20624,2047	4.6	1658.8	A30615,0845	912.1	2720.6
26	A10614,1820	101.5	17078.1	A20625,0930	9	2131.4	A30615,1431	2111.6	10475.3
27	A10615,0832	202	25896.3				A30615,1844	1403.5	3770.0
28	A10615,1452	136.2	10137.3				A30615,2238	643.8	1038.4
29	A10615,1830	52.5	11256.2				A30616,0739	551.4	1478.7
30	A10615,2251	10.7	10674.5				A30616,1658	1270	2662.4
31	A10616,0720	37.3	20251.3				A30616,2322	500.8	730.5
32	A10616,1336	52.8	22519.2				A30617,0752	1169	2372.8
33	A10616,2016	23.3	16570.8				A30617,1400	1641	2697.6
34	A10617,0737	66.1	27302.1				A30617,1800	1286	1702.2
35	A10617,1342	58.4	28754.3				A30617,2227	770.4	948.2
36	A10617,1730	23.2	14614.1				A30617,2349	750.2	1465.9
37	A10618,0759	35.5	21762.7				A30618,0814	1057.9	1245.6
38	A10618,1420	26.6	17850.0				A30618,1435	1265.8	1110.0
39	A10619,0730	6.7	10268.6				A30618,0208	500	684.5
40	A10619,1506	11.7	14364.7				A30619,0750	552.3	961.1
41	A10619,1740	5	3206.4				A30618,1804	1036.7	763.5
42	A10624,2117	14	2256.9				A30619,1519	894.8	438.9
43	A10625,0935	24	1025.4				A30619,1937	492.9	261.2
44	A10625,1442	5.9	289.2				A30619,2327	248.4	456.2
45	A10627,2200	3	364.4				A30620,0737	254.6	1516.5
46							A30621,1513	246.5	793.1

47			A30621,2015	148.3	1518.2
48			A30622,0913	49.24	227.4
49			A30622,1456	110.4	147.4
50			A30622,1835	71.7	59.6
51			A30622,2236	50.2	48.5
52			A30623,0909	48.3	43.6
53			A30623,1414	64.5	42.2
54			A30623,2110	20.8	20.0
55			A30624,0930	75.9	662.6
56			A30624,1239	482.6	2063.9
57			A30624,1624	242.7	300.0
58			A30624,2121	692.3	2730.6
59			A30625,0950	952.5	3451.1
60			A30625,1501	423	1198.5
61			A30625,2015	169.2	161.9
62			A30626,0747	31.2	35.6
63			A30626,1530	2	15.0
64			A30627,2155	210	414.6
65			A30628,0912	30.5	7.6
66			A30628,1814	18.7	7.8

Appendix C-1: Plots A1 and A3, 1993, discharge and suspended sediment concentrations.

	Sample	Dis. (mL/s)	SSC (mg/L)	Sample	Dis. (mL/s)	SSC (mg/L)
1	A10529,1500	50	8608	1	120.2	118
2	A10529,1700	40	7712	2	84.5	460
3	A10530,0900	23	6235	3	193	513
4	A10530,1100	79	10138	4	506	1252
5	A10530,1300	82	9896	5	547	924
6	A10530,1500	90	10175	6	598	682
7	A10530,1700	56	7718	7	63.5	248
8	A10531,1140	78	9375	8	90	211
9	A10531,2050	2	624	9	224	245
10	A10601,1130	158	9314	10	365	462
11	A10601,1530	116	12670	11	452	879
12	A10601,2025	33	7799	12	439	557
13	A10602,0656	28	9530	13	325	680
14	A10602,0855	104	14667	14	193	638
15	A10602,1100	130	14299	15	95	510
16	A10602,1310	92	10123	16	201	358
17	A10602,1510	100	10188	17	515	914
18	A10602,1705	36	6560	18	624	1232
19	A10602,1905	10	2914	19	798	1291
20	A10603,1150	123	19421	20	535	839
21	A10604,1100	151	19915	21	240	413
22	A10604,1430	105	21352	22	628	1497
23	A10605,1115	149	20972	23	823	1979
24	A10606,2105	12	7660	24	894	2705
25	A10607,1305	48	21484	25	897	3065
26	A10608,1255	41	21653	26	410	665
27	A10608,1420	40	17832	27	934	2179
28	A10610,1237	18	16509	28	676	1423
29	A10611,1545	9	2444	29	541	999
30				30	1136	468
31				31	342	664
32				32	753	644
33				33	380	165
34				34	551	361
35				35	506	193
36				36	258	380

Appendix C-1: Plots B1 and B2, 1996, discharge and suspended sediment concentrations.

	Sample	Dis (mL/s)	SSC (mg/L)	Sample	Dis (mg/L)	SSC (mg/L)
1	B10607,1445	36.1	1804.2	B20610,1200	3.2	1810.0
2	B10607,2046	22.0	3765.9	B20610,1702	15.7	3148.3
3	B1608,0958	3	3264.4	B20610,1919	25.7	2264.0
4	B10608,1324	31	4550.3	B20611,0001	5	774.4
5	B10608,1441	40.3	5642.1	B20611,0845	2	938.7
6	B10608,1841	160.8	12943.1	B20611,1645	7	1568.4
7	B10609,1141	53.4	6052.8	B20611,2206	2	815.9
8	B10609,1835	43.5	4085.5	B20612,1047	8.9	1744.2
9	B10610,1139	94.9	20560.8	B20612,1714	43.8	4155.5
10	B10610,1220	113.2	78861.0	B20613,0020	15.6	1221.3
11	B10610,1852	100	13020.0	B20613,1115	11.33	4047.7
12	B10610,1958	108	4654.4	B20613,1232	10.8	2460.0
13	B10611,0007	42.4	2415.6	B20613,1608	37.7	4631.2
14	B10611,1637	89.6	3349.3	B20613,2042	31.1	4110.6
15	B10611,2154	76.7	5705.7	B20613,2123	22.2	3302.7
16	B10612,1033	9.3	1332.6	B20614,1112	26.4	3110.3
17	B10612,1701	27.8	5528.3	B20614,1301	50.3	6335.8
18	B10613,0012	39.7	2152.7	B20614,1746	74.9	7295.2
19	B10613,1558	19.2	7323.1	B20614,2010	115.4	9423.8
20	B10613,2028	18.6	9245.1	B20614,2310	97.7	7209.6
21	B10614,1250	7.2	9651.7	B20615,0035	53	3728.0
22	B10614,1952	61.4	38315.9	B20615,0757	41	2873.2
23	B10615,0020	36.8	11701.9	B20615,0931	37.67	6585.5
24	B10615,1658	24.1	39309.0	B20615,1712	155.67	7522.5
25	B10615,1909	12.3	6117.8	B20615,1925	89	5407.1
26	B10616,1135	11.3	13423.0	B20616,1149	117	5539.3
27	B10616,1645	9.5	5580.0	B20616,1654	75	3993.1
28	B10616,2234	2.5	266.5	B20616,2223	23	1505.3
29	B10625,1210	4.6	287.6	B20617,0749	60	3558.1
30				B20617,1526	114.5	4736.0
31				B20617,2034	86.5	2568.0
32				B20618,0020	55	1632.6
33				B20618,1134	68.1	2037.1
34				B20618,1741	63.4	1659.5
35				B20618,2045	54.1	1159.5
36				B20619,0250	11.5	687.8
37				B20619,1358	15.6	165.0
38				B20624,1155	58.4	3480.6
39				B20624,1627	6.4	51.7
40				B20625,1155	12.2	1013.7
41				B20625,1555	3.5	34.1
42				B20627,2230	4.5	47.3
43						
44						
45						
46						

Appendix C-1: Plots B3 and B4, 1996, discharge and suspended sediment concentrations.

	Sample	Dis. (mL/s)	Dis. (mg/L)	Sample	Dis. (mL/s)	SSC (mg/L)
1	B30607,1430	64.1	74.6	B40606,1822	4.99	54.5
2	B30607,2102	34.3	32.7	B40606,2225	2	26.7
3	B30608,0958	8.85	30.2	B40608,1500	6.9	33.2
4	B30608,1334	67.85	70.3	B40608,1914	15.26	47.0
5	B30608,1856	210.5	59.3	B40608,2357	1.5	30.6
6	B30608,2351	128	100.7	B40610,1945	8.4	44.2
7	B30609,1156	62	53.4	B40610,2353	2	29.5
8	B30609,1848	76.7	45.6	B40611,2143	6.5	45.9
9	B30610,1130	33.4	6.5	B40612,1727	13.7	65.5
10	B30610,1650	100	32.4	B40614,2025	14.2	150.0
11	B30610,1928	181	40.0	B40614,2320	6.5	130.3
12	B30611,0013	113	16.5	B40615,0030	3	112.6
13	B30611,0801	23.6	6.3	B40615,1720	17.7	164.7
14	B30611,1603	88.8	74.3	B40615,1915	10.1	332.5
15	B30611,2145	154.4	59.6	B40616,1705	2	309.3
16	B30612,1025	89.2	90.0	B40617,1534	23.1	1402.8
17	B30612,1653	112.2	94.2	B40617,2044	16.8	327.0
18	B30612,1918	135.3	102.3	B40618,0005	1	110.3
19	B30613,0007	91.4	27.6	B40618,1715	24.9	2848.2
20	B30613,1058	65.8	102.9	B40618,2036	19.4	13695.6
21	B30613,1239	83.96	100.0			
22	B30613,1553	62.4	90.0			
23	B30613,2015	72.36	44.7			
24	B30613,2117	60.2	25.7			
25	B30614,1058	47.04	56.0			
26	B30614,1255	78	151.0			
27	B30614,1740	101	62.5			
28	B30614,1940	242.74	165.8			
29	B30614,2258	313.75	241.1			
30	B30615,0045	218	102.0			
31	B30615,0743	52	23.3			
32	B30615,0921	55	36.1			
33	B30615,1656	115	140.0			
34	B30615,1932	144.3	34.3			
35	B30616,1130	96.7	66.8			
36	B30616,1630	131.4	27.1			
37	B30616,2241	62.1	37.5			
38	B30617,0740	46.5	12.3			
39	B30617,1512	74	50.4			
40	B30617,2020	221.7	205.4			
41	B30618,0030	124.7	89.5			
42	B30618,1120	26.2	6.8			
43	B30618,1725	139.1	145.5			
44	B30618,2054	215.8	218.5			
45	B30619,0300	84.4	17.8			
46	B30619,1406	78.9	13.1			

47	B30619,1836	88.8	
48	B30621,1608	22.6	
49	B30622,1221	20.5	
50	B30622,1402	13.7	
51	B30622,1930	8.4	
52	B30623,1130	8.2	
53	B30623,1818	9.5	
54	B30624,1139	54.0	
55	B30624,1604	15.8	
56	B30625,1141	222.5	
57	B30625,1245	468.8	
58	B30625,1545	16.1	
59	B30625,1951	11.8	
60	B30626,1939	20.0	
61	B30627,2225	15.9	

Appendix C-2: Loss on ignition results for surface sediment samples.

Sample	**Weight difference after 6 hr**	**Percentage coal**	**Weight difference after 8 hr**	**Percentage coal**
A1, T1	1.3092	**9.5**	1.2937	**9.4**
A2, T1	0.7418	**5.8**	0.7472	**5.8**
A2, vt3	0.9842	9.0		
A3, T1	0.4906	**3.2**	0.5135	**3.4**
A3, T3	1.31	10.3		
A3, T5	0.8346	8.1		
A4, T1	0.8954	9.1		
B1, T1	2.652	**16.3**	2.6496	**16.3**
B1, T5	3.4109	32.4		
B2, T1	1.9641	**12.1**	1.9878	**12.2**
B2, T3	1.3026	9.7		
B3, T1	2.2637	**14.5**	2.277	**14.5**
B3, T3	1.3126	6.7		
B4, T1	1.3281	10.6		
B4T4	0.6609	6.0		
B4MF	1	5.5		

Appendix C-3: Refiltering and loss on ignition results for suspended sediment samples.

Sample	Sample weight (mg/L)	Percentage of weight retained after refiltering	Coal percentage
A10607,0906	0.3582	55	-
A10613,1434	2.9926	80	10.3
A20608,1553	0.6173	81	11.8
A20611,1734	0.2918	49	-
A30609,1608	0.3047	82	12.9
A30614,1448	0.6257	75	12.7
A30617,1800	0.3915	74	11.9
A30619,1937	0.0834	74	17.2
B10610,1220	8.2804	84	10.5
B10610,1139	2.4673	90	12.3
B10614,1958	5.5558	64	16.1
B10615,1658	5.6998	99	17.3
B10615,0020	1.8723	90	19.7
B20614,1112	0.451	73	15.0
B20614,1301	1.0454	74	14.9
B20614,2010	1.5078	87	11.2
B20614,2310	0.9012	79	14.1
B20615,0035	0.6524	41	15.2
B20617,0749	0.5693	74	13.3
B30607,1430	0.0235	29	-
B30625,1141	0.0534	37	-
B406151720	0.1361	22	-

Note: Samples from B3 and B4 were too small to subdivide for the evaluation of coal.

Appendix C-4: Discharge – suspended sediment concentration rating equations.

Site A

A1. Early melt (JD 158 to JD 160)	$y = 1.16x + 1.19$ $r^2 = 0.46$ $n = 8$
Main melt (JD 160 to JD 167)	$y = 0.19x^2 - 0.19x + 3.83$ $r^2 = 0.65$ $n = 21$
Recession (JD 167 to JD 173)	$y = 0.63x + 3.34$ $r^2 = 0.82$ $n = 12$
Rainfall (JD 176 to JD 179)	$y = 0.78x + 2.11$ $r^2 = 0.57$ $n = 4$
A2. Early and main melt (JD 156 to JD 160)	$y = 0.84x + 1.72$ $r^2 = 0.75$ $n = 12$
Recession and rainfall (JD 161 to JD 177)	$y = 0.31x^2 - 0.32x + 3.25$ $r^2 = 0.43$ $n = 14$
A3. Early melt (JD 160 to JD 166)	$y = 0.80x + 1.29$ $r^2 = 0.81$ $n = 22$
Main melt and recession (JD 166 to 175)	$y = 1.07x + 0.06$ $r^2 = 0.78$ $n = 32$
Rainfall (JD 176 to JD 180)	$y = 0.43 x^2 - 0.39x + 1.09$ $r^2 = 0.86$ $n = 12$

Appendix C-4: Discharge – suspended sediment concentration rating equations.

Site B

B1. Early and main melt (JD 159 to JD 165)	$y = 0.67x^2 - 1.30x + 3.94$ $r^2 = 0.48$ n = 19
Recession and rainfall (JD 165 to JD 177)	$y = 1.53x + 2.07$ $r^2 = 0.71$ n = 10
B2. Early and main melt (JD 161 to JD 170)	$y = 0.47 + 2.82$ $r^2 = 0.71$ n = 31
Recession and rainfall (JD 171 to JD 180)	$y = 1.35x + 0.92$ $r^2 = 0.82$ n = 11
B3. Snowmelt and rainfall (JD 159 to JD 180)	$y = 0.38x^2 - 0.49x + 1.22$ $r^2 = 0.48$ n = 61
B4. Early melt (JD 158 to JD 167)	$y = 0.53x + 1.40$ $r^2 = 0.31$ n = 14
Main melt up to mudslide (JD 167 to JD 170)	$y = 0.93x + 2.10$ $r^2 = 0.56$ n = 6

Appendix C-5: Niveo-aeolian sediment and dissolved solid concentrations of 1996 snow samples.

Sample	Sediment concentration (mg/L)	Dissolved solids (mg/L)
A1,T1,0529	1130.0	11.97
A1,T3,0529	604.0	N
A1,T5,0529	800.7	N
A2,T2,0529	988.7	31.64
A2,T1,0529	X	33.84
A2,T3,0529	3039.5	28.51
A3,T1,0529	515.1	17.91
A3,T3,0529	1143.5	54.85
A4,T1,0529	1136.0	13.82
A4,T2,0529	1897.1	25.10
A average	**1250**	**27.2**
B1,T2,0530	411.3	18.16
B1,T4,0530	406.5	20.75
B2,T2,0529	475.8	12.66
B3,T1,0530	2289.2	60.52
B3,T3,0530	433.2	21.76
B4,T2,0529	473.7	10.74
B average	**748**	**24.1**
Overall average	**1050**	**25.8**

Note: X – sample was lost.
N – conductivity measurement was not taken.

Appendix C-6: Soil geochemistry results.

Sample	*a* - Sample weight (g)	*b* - Soil geochmisty results, in mg/L (ion concentrations in exchange solution)				*c* - Soil geochemistry in g/sample weight (= *b* /volume of exchange solution - 100 mL)				g of cations/kg of soil (=*c* /*a* *10^-3)				Total cations
		Ca	K	Mg	Na	Ca	K	Mg	Na	Ca	K	Mg	Na	
A1-1 5cm	20,629	546,7	20,13	79,97	16,39	0,05467	0,00201	0,007997	0,0016	2,6502	0,0976	0,3877	0,0795	3,2148
A1-1 15cm	20,184	548,9	20,79	77,176	19,14	0,05489	0,00208	0,007718	0,0019	2,7195	0,103	0,3824	0,0948	3,2997
A1-1 25cm	20,628	520,3	15,18	78,133	22,88	0,05203	0,00152	0,007813	0,0023	2,5223	0,0736	0,3788	0,1109	3,0856
A1-1 35cm	20,24	485,1	30,47	82,17	33,99	0,04851	0,00305	0,008217	0,0034	2,3967	0,1505	0,406	0,1679	3,1212
A1-1 45cm	18,764	478,5	59,73	136,73	66,99	0,04785	0,00597	0,013673	0,0067	2,5501	0,3183	0,7287	0,357	3,9541
A1-1 55cm	19,99	447,7	51,59	112,97	58,85	0,04477	0,00516	0,011297	0,0059	2,2396	0,2581	0,5651	0,2944	3,3572
A1-1 65cm	20,33	412,5	50,6	98,252	92,84	0,04125	0,00506	0,009825	0,0093	2,029	0,2489	0,4833	0,4567	3,2179
A1-1 75cm	20,05	341	53,35	83,776	129,8	0,0341	0,00534	0,008378	0,013	1,7007	0,2661	0,4178	0,6474	3,032
A1-2 5cm	19,99	399,3	96,25	173,03	387,2	0,03993	0,00963	0,017303	0,0387	1,9975	0,4815	0,8656	1,937	5,2815
A1-2 15cm	20,08	400,4	94,16	191,015	364,1	0,04004	0,00942	0,019102	0,0364	1,994	0,4689	0,9513	1,8132	5,2275
A1-2 25cm	19,967	385	100,21	192,17	407	0,0385	0,01002	0,019217	0,0407	1,9282	0,5019	0,9624	2,0384	5,4309
A1-2 35cm	19,996	372,9	94,38	173,69	350,9	0,03729	0,00944	0,017369	0,0351	1,8649	0,472	0,8686	1,7549	4,9603
A1-2 45cm	20,039	386,1	96,69	176	409,2	0,03861	0,00967	0,0176	0,0409	1,9267	0,4825	0,8783	2,042	5,3296
A1-2 55cm	20,016	391,6	101,97	196,02	515,9	0,03916	0,0102	0,019602	0,0516	1,9564	0,5094	0,9793	2,5774	6,0226
A1-2 65cm	20,019	374	102,08	196,9	539	0,0374	0,01021	0,01969	0,0539	1,8682	0,5099	0,9836	2,6924	6,0541
A3 5cm	20,06	503,8	14,52	65,472	34,98	0,05038	0,00145	0,006547	0,0035	2,5115	0,0724	0,3264	0,1744	3,0846
A3 15cm	20,04	525,8	5,258	57,211	7,557	0,05258	0,00053	0,005721	0,0008	2,6238	0,0262	0,2855	0,0377	2,9732
A3 25cm	20	539	7,051	64,284	7,007	0,0539	0,00071	0,006428	0,0007	2,695	0,0353	0,3214	0,035	3,0867
A3 35cm	19,987	510,4	12,386	57,948	7,04	0,05104	0,00124	0,005795	0,0007	2,5537	0,062	0,2899	0,0352	2,9408
A3 45cm	20	546,7	11,33	63,294	6,611	0,05467	0,00113	0,006329	0,0007	2,7335	0,0567	0,3165	0,0331	3,1397
B2 5cm	16,769	394,9	29,37	175,34	1056	0,03949	0,00294	0,017534	0,1056	2,3549	0,1751	1,0456	6,2973	9,873
B2 15cm	20,002	502,7	28,49	154,44	226,6	0,05027	0,00285	0,015444	0,0227	2,5132	0,1424	0,7721	1,1329	4,5607
B2 25cm	19,999	537,9	27,17	115,28	82,94	0,05379	0,00272	0,011528	0,0083	2,6896	0,1359	0,5764	0,4147	3,8166
B2 35cm	20,01	589,6	31,79	154,77	91,41	0,05896	0,00318	0,015477	0,0091	2,9465	0,1589	0,7735	0,4568	4,3357
B2 45cm	19,995	475,2	25,74	99,473	58,52	0,04752	0,00257	0,009947	0,0059	2,3766	0,1287	0,4975	0,2927	3,2955
B2 55cm	20,009	443,3	22	81,235	70,84	0,04433	0,0022	0,008124	0,0071	2,2155	0,11	0,406	0,354	3,0855
B3 5cm	19,964	680,9	18,227	125,18	19,47	0,06809	0,00182	0,012518	0,0019	3,4106	0,0913	0,627	0,0975	4,2265
B3 15cm	20,002	596,2	16,599	96,943	21,12	0,05962	0,00166	0,009694	0,0021	2,9807	0,083	0,4847	0,1056	3,6539
B3 25cm	20,018	599,5	15,983	95,469	13,244	0,05995	0,0016	0,009547	0,0013	2,9948	0,0798	0,4769	0,0662	3.6177
B3 35cm	20,024	603,35	14,4815	87,1805	11,9405	0,06034	0,00145	0,008718	0,0012	3,0131	0,0723	0,4354	0,0596	3.5805
B3 45cm	19,999	647,9	15,521	94,831	12,584	0,06479	0,00155	0,009483	0,0013	3,2397	0,0776	0,4742	0,0629	3,8544
B3 55cm	19,999	588,5	14,465	89,1	27,94	0,05885	0,00145	0,00891	0,0028	2,9426	0,0723	0,4455	0,1397	3,6002

Appendix C-7: Water geochemistry results in mg/L.

Sample	an dil	cat dil	Cl	NO_2	NO_3	HPO_4	SO_4	HCO_3*	Al	B	Ba	Ca	Fe	K	Li	Mg	Mn	Na	Si	Sr
A10606 1528C	21	4	90.7	<0.5	4.7	<5	83.0	-19.9	0.84	0.00	0.216	18.6	0.44	3.85	0.000	10.54	0.000	58.0	0.96	0.101
A10608 1525C	21	5	105.5	<0.5	6.2	<5	94.8	16.9	1.60	0.25	0.275	21.0	0.86	6.53	0.020	12.37	0.000	80.9	0.90	0.120
A10619 1506C	21	5	718.4	<0.5	33.5	<5	228.6	286.3	0.00	0.35	0.265	70.8	0.39	22.83	0.020	58.27	0.035	508.0	0.30	0.450
A10620 0740C	21	5	906.3	<0.5	64.6	<5	394.6	1415.4	1.80	0.34	0.225	118.8	0.14	36.77	0.030	118.26	0.000	979.2	0.25	0.756
A20607 1621C	21	5	77.6	<0.5	2.0	<5	61.1	52.9	2.94	0.29	0.193	18.1	1.92	6.67	0.01	9.29	0.03	65.0	4.09	0.10
A20608 1553C	21	5	86.7	<0.5	5.3	14.9	267.9	-255.9	1.81	0.20	0.425	22.8	1.40	3.64	0.01	7.75	0.00	78.9	2.34	0.07
A20611 1413C	21	4	77.9	<0.5	3.3	<5	217.2	-203.9	2.67	0.19	0.344	12.0	2.01	3.92	0.016	5.66	0.000	78.3	4.64	0.038
A30609 0915A	21	2	17.5	<0.5	<0.5	<5	34.9	37.3	2.33	0.10	0.126	12.8	1.28	3.20	0.00	4.80	0.00	20.8	3.93	0.06
A30610 1526C	21	4	127.4	<0.5	3.9	<5	100.8	43.0	1.15	0.24	0.234	19.2	0.70	6.70	0.01	10.11	0.00	114.8	1.52	0.10
A30620 0724C	21	4	21.8	<0.5	3.2	<5	99.5	-76.8	1.96	0.07	0.144	14.7	1.14	2.10	0.000	5.49	0.000	16.9	3.28	0.062
B10607 1445C	21	2	19.2	<0.5	47.3	<5	355.3	2.0	0.54	0.13	0.105	88.7	0.16	3.59	0.02	37.58	0.00	53.1	0.41	0.13
B10612 1901C	21	2	19.5	<0.5	26.5	<5	325.0	10.4	0.00	0.12	0.128	87.9	0.03	3.90	0.008	34.95	0.006	43.8	0.55	0.127
B10615 1909C	21	2	21.5	<0.5	42.8	5.80	464.2	-24.4	0.65	0.11	0.108	109.6	0.04	4.66	0.006	49.42	0.010	63.4	0.63	0.156
B20609 1315C	21	2	20.1	<0.5	2.5	<5	52.6	32.1	3.39	0.07	0.221	15.0	2.34	2.41	0.00	5.19	0.00	28.6	5.29	0.04
B20615·1712C	21	4	38.8	<0.5	2.5	<5	60.2	35.3	3.01	0.22	0.136	13.7	2.34	2.22	0.032	6.18	0.000	46.2	4.36	0.029
B20619 1815C	21	2	219.7	<0.5	2.7	5.61	377.4	70.4	0.34	0.08	0.098	64.6	0.07	9.72	0.016	41.26	0.000	239.6	0.81	0.161
B30607 1430C	21	2	7.8	<0.5	<0.5	<5	139.7	-7.7	0.24	0.04	0.094	46.1	0.39	2.04	0.01	12.25	0.00	9.3	0.60	0.07
B30614 1740C	21	2	27.4	<0.5	<0.5	18.44	266.1	37.9	0.00	0.05	0.056	88.1	0.03	3.31	0.004	30.24	0.000	32.6	0.79	0.142
B30623 1930C	21	2	14.2	<0.5	3.6	<5	872.5	-79.3	0.00	0.09	0.086	250.6	0.04	4.52	0.012	85.77	0.000	54.1	1.47	0.336
B40606 1822C	21	2	15.1	<0.5	<0.5	<5	52.4	27.1	3.55	0.18	0.128	14.9	2.08	4.10	0.01	6.17	0.00	20.5	6.93	0.04
B40614 2025C	21	2	13.5	<0.5	0.0	<5	67.6	29.4	4.16	0.24	0.082	16.5	1.90	2.48	0.008	7.02	0.008	27.1	7.94	0.036
B40619 1345C	21	5	13.0	<0.5	<0.5	<5	25.5	54.5	0.56	0.11	0.185	16.5	0.49	1.06	0.010	5.40	0.000	14.7	2.35	0.054

Note: F and B were below detection limits in all samples and are not included in the summary table.

*Note: HCO_3 was calcuated using the following balance equation,

HCO_3 = {[(Na/atomic wieght)+(Mg/atomic weight)+(K/atomic weight)+(Ca/atomic weight)] - [(Cl/atomic weight)+(SO_4/atomic weight)]}

* atomic weight of HCO_3

Appendix C-8: Calculation of time for Na^+ levels to reach residual values following detachment sliding.

Total Na^+ removed by surface runoff in 1996 = 14 kg, or 37 g/m^2/yr

This rate of removal is compared with the total amount of available sodium in the soil at the fresh detachment slide, and the amount in the adjacent undisturbed slope, in order to estimate the time required for sodium levels to reach residual values following detachment sliding.

Available Na^+ in fresh active layer = (Ds*d*s)*a_s
= 1930 g/m^2

Available Na^+ in old active layer = (Ds*d*s)*a_u
= 251 g/m^2

where:

Ds	- density of soil	= 1.3 g/cm^3
d	- maximum active layer depth (ave.)	= 0.7 m
s	- area of the scar	= 375 m^2
a_s	- Na^+ soil conversion factor for fresh active layer	= 0.00212
a_u	- Na^+ soil conversion factor for adjacent slope	= 0.00028

Time required for soil Na^+ to fall to residual levels = (1930 – 251)/37
= approximately 45 years

Appendix C-9: Amount of surface lowering in 45 years, and amount of Na^+ released through the thawing of permafrost.

Net rate of surface lowering at A1= 1.339 mm/yr
surface lowering in 45 years = 1.339 * 45
= 60 mm

For this calculation it is assumed that the amount of permafrost thawed is equal to the amount of surface lowering. Using the same soil densities and soil salt concentrations as in Appendix C-8 the amount of Na^+ released over 45 years due to the thawing of 60 mm of permafrost is:

$$= (Ds*d*s)*a_s$$
$$= 166.0 \text{ g/m}^2$$
$$\text{or} = 3.7 \text{ g/m}^2\text{/yr}$$

where:

Ds	- density of soil	= 1.3 g/cm^3
d	- depth of thawed permafrost = amount of surface lowering	= 60 mm
s	- area of the scar	= 375 m^2
a_s	- Na^+ soil conversion factor for fresh active layer	= 0.00212

Appendix D-1: Calculation of sediment yields by terrain unit for plots A3 and B3.

Plot A3	Area (m^2) (a)	Percentage of plot area	Plots used to derive sediment yields	Average sediment load (g/m^2) (*Asl*)	total (g) =(*Asl**a)	Predicted load for entire plot (g)	Total (g/m^2)	Overprediction of measured sediment load (%)
vegetated slope	7684	48.5	=(A4+B4)/2	12.55	96436	1493664	94.2	12.9
scar	1911	12.2	=(A1+A2+B1+B2)/4	731	1397228			
unvegetated undisturbed slope	6170	39.4	= A5	0	0			
Plot B3								
vegetated slope	706	55.6	=(A4+B4)/2	12.55	8862	300370	236.5	473.0
scar	399	31.4	=(A1+A2+B1+B2)/4	731	291508			
unvegetated undisturbed slope	165	13.0	= A5	0	0			

Note: Values of sediment loss for different terrain units are derived from sediment yields measured in this study.

Appendix D-2: Predicted solute removal from total area influenced by fresh detachment slides (16500 m^2) along a 1.5 km stretch of river valley at Hot Weather Creek.

	Plots used to derive solute yields	Average solute load (*Asl*)	Total predicted solute load =(*Asl**16500) (g)	Total predicted solute load (kg)
Predicted solute load from 1988 detachment slide scars	=(A1+B1)/2	58.55	966075	966
Predicted solute load for the same slope area undisturbed by 1988 detachment slide scars	= A3	10.1	166650	167

IMAGE EVALUATION TEST TARGET (QA-3)

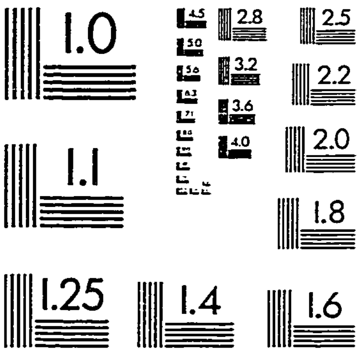

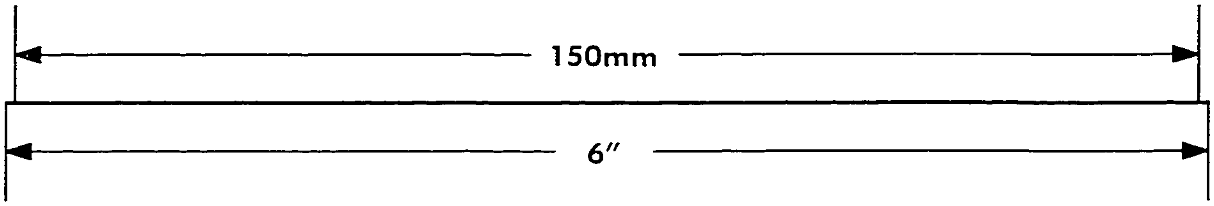

APPLIED IMAGE, Inc
1653 East Main Street
Rochester, NY 14609 USA
Phone: 716/482-0300
Fax: 716/288-5989